

FATIGUE CHARACTERIZATION OF RISERS AND PIPELINES  
UNDER REALISTIC VARIABLE AMPLITUDE LOADING AND THE  
INFLUENCE OF COMPRESSIVE STRESS CYCLES

by

Mohammad Iranpour

Submitted in partial fulfilment of the requirements  
for the degree of Doctor of Philosophy

at

Dalhousie University  
Halifax, Nova Scotia  
January 2013

© Copyright by Mohammad Iranpour, 2013

DALHOUSIE UNIVERSITY  
DEPARTMENT OF CIVIL AND RESOURCE ENGINEERING

The undersigned hereby certify that they have read and recommend to the Faculty of Graduate Studies for acceptance a thesis entitled “FATIGUE CHARACTERIZATION OF RISERS AND PIPELINES UNDER REALISTIC VARIABLE AMPLITUDE LOADING AND THE INFLUENCE OF COMPRESSIVE STRESS CYCLES” by Mohammad Iranpour in partial fulfilment of the requirements for the degree of Doctor of Philosophy.

Dated:                    January 11, 2013

External Examiner: \_\_\_\_\_

Research Co-supervisors: \_\_\_\_\_

\_\_\_\_\_

Examining Committee: \_\_\_\_\_

\_\_\_\_\_

Departmental Representative: \_\_\_\_\_

DALHOUSIE UNIVERSITY

DATE: January 11, 2013

AUTHOR: Mohammad Iranpour

TITLE: FATIGUE CHARACTERIZATION OF RISERS AND PIPELINES  
UNDER REALISTIC VARIABLE AMPLITUDE LOADING AND THE  
INFLUENCE OF COMPRESSIVE STRESS CYCLES

DEPARTMENT: Department of Civil and Resource Engineering

DEGREE: Ph.D. CONVOCATION: May YEAR: 2013

Permission is herewith granted to Dalhousie University to circulate and to have copied for non-commercial purposes, at its discretion, the above title upon the request of individuals or institutions. I understand that my thesis will be electronically available to the public.

The author reserves other publication rights, and neither the thesis nor extensive extracts from it may be printed or otherwise reproduced without the author's written permission.

The author attests that permission has been obtained for the use of any copyrighted material appearing in the thesis (other than the brief excerpts requiring only proper acknowledgement in scholarly writing), and that all such use is clearly acknowledged.

---

Signature of Author

*I dedicate this dissertation to my dear family, and  
ordinary people with extraordinary determination*



## Table of Contents

<b>List of Tables.....</b>	<b>xi</b>
<b>List of Figures.....</b>	<b>xii</b>
<b>Abstract.....</b>	<b>xx</b>
<b>List of Abbreviations and Symbols Used.....</b>	<b>xxi</b>
<b>Acknowledgements.....</b>	<b>xxvii</b>
<b>Chapter 1 Introduction.....</b>	<b>1</b>
1.1 Offshore Oil and Gas Risers and Pipelines.....	1
1.2 Thesis Objectives.....	2
1.3 Thesis Layout.....	3
<b>Chapter 2 Literature Review, State-of-the-Art on Risers’ Fatigue and Influence of Compressive Stress Cycles.....</b>	<b>9</b>
2.1 Introduction.....	9
2.2 Main Sources of Riser’s Fatigue.....	10
2.2.1 First order Floating Platform Motions.....	10
2.2.2 Second Order Floating Platform Motions.....	11
2.2.3 Vortex-induced Vibration.....	11
2.3 VIV-induced Fatigue Analysis.....	12
2.3.1 The Det Norske Veritas (DNV).....	13
2.3.2 The American Petroleum Institute (API).....	15
2.3.3 The Vandiver’s Approach.....	16
2.3.4 The Marintek Approach.....	17
2.3.5 The Torres-Siqueira Method.....	17
2.3.6 The Baarholm Model.....	18
2.3.7 The Maher-Finn Model.....	18
2.3.8 The Ferrari-Bearman Model.....	19

2.3.9	Fracture Mechanics Approach.....	19
2.4	The Influence of Compressive Stresses.....	24
2.4.1	Two Parameter Driving Force.....	32
2.4.2	Fatigue Crack Closure.....	35
2.5	Summary and Conclusion	38
<b>Chapter 3</b>	<b>A Study on Crack Front Shape and the Correlation between the Stress Intensity Factors of a Pipe Subject to Bending and a Plate Subject to Tension.....</b>	<b>40</b>
3.1	Abstract.....	40
3.2	Introduction.....	41
3.3	Plate under Pure Tension.....	43
3.4	Pipe under Pure Bending Moment.....	45
3.5	Finite Element Analysis .....	46
3.6	Dimensionless Stress Intensity Factor Ratio.....	51
3.7	Shape of the Crack Front.....	58
3.8	Computational Simulation of Crack Front Shape.....	62
3.9	Experimental Investigation.....	67
3.10	Summary and Discussion.....	71
3.11	Conclusions.....	74
3.12	Acknowledgements.....	75
<b>Chapter 4</b>	<b>Structural Life Assessment of Oil and Gas Risers under Vortex-induced Vibration.....</b>	<b>76</b>
4.1	Abstract.....	76
4.2	Introduction.....	77
4.3	Long Flexile Tensioned Risers in Deep Waters.....	80
4.4	Experimental Set up.....	84
4.4.1	Loading (stress-time) History.....	86
4.4.2	Material Selection.....	88
4.4.3	Equivalency Testing Preamble.....	91
4.4.4	Testing Apparatus.....	92

4.5	Experimental Results and Discussion.....	96
4.5.1	Actual VIV-Induced Stress-Time History.....	97
4.5.2	Influence of the Third Harmonic.....	98
4.6	Analytical Simulation of Crack Growth.....	102
4.7	Equivalent Constant Amplitude Load.....	107
4.8	Summary and Conclusions.....	110
4.9	Acknowledgements.....	112
<b>Chapter 5</b>	<b>Applicability of Equivalent Constant Amplitude Loading for Assessing the Fatigue Life of Pipelines and Risers and the Influence of Compressive Stress Cycles...</b>	<b>113</b>
5.1	Abstract.....	113
5.2	Introduction.....	114
5.3	Motivation and Problem Definition.....	117
5.4	Experimental VIV Data.....	117
5.4.1	Acceleration-time History.....	120
5.4.2	Stress-time History.....	122
5.5	Experimental Setup.....	126
5.6	Experimental Results and Discussion.....	129
5.6.1	Analytical Estimation of Crack Growth.....	131
5.6.2	Influence of Compressive Stresses.....	134
5.6.3	Tests with the Equivalent Constant Amplitude Load.....	136
5.7	Summary and Conclusions.....	140
5.8	Acknowledgements.....	142
<b>Chapter 6</b>	<b>On the Effect of Stress Intensity Factor in Evaluating the Fatigue Crack Growth Rate of Aluminum Alloy under the Influence of Compressive Stress Cycles.....</b>	<b>143</b>
6.1	Abstract.....	143
6.2	Introduction.....	144
6.3	Problem Definition and Objectives.....	148
6.4	VAL Stress-time History.....	149

6.5	Tests with Various Levels of Compressive Stress cycles.....	151
6.6	Test Setup and Material.....	154
6.7	Experimental Observations and Results.....	156
6.7.1	Results of Test Series No. 1.....	156
6.7.2	Results of Test Series No. 2.....	156
6.7.3	Results of Test Series No. 3.....	160
6.7.4	Results of Test Series No. 4.....	163
6.8	Roughness-induced Crack Closure.....	164
6.9	Summary and Conclusions.....	169
6.10	Acknowledgements.....	171
<b>Chapter 7</b>	<b>Analytical and Computational Investigations of the Influence of the Compressive Stress Cycles on Crack Growth under Variable Amplitude Loading using CTOD.....</b>	<b>172</b>
7.1	Abstract.....	172
7.2	Introduction.....	173
7.3	Finite Element Analysis.....	175
7.3.1	Finite Element Mesh .....	175
7.3.2	Loading Scenarios.....	177
7.3.3	Material Model and Crack Tip Singularity .....	178
7.3.4	Modeling of Crack Surface Interaction.....	179
7.4	Finite Element Analysis Results .....	180
7.4.1	Effect of CSC on the Crack Front Stresses.....	180
7.4.2	Effect of CSC on CTOD.....	183
7.5	Further Discussion .....	187
7.5.1	CTOD Related Relationships.....	187
7.5.2	The use of Stress Intensity Factor for Estimation of FCG.....	189
7.5.3	The use of CTOD for Estimation of FCG.....	193
7.6	Application of some Analytical Models for Estimation of FCG.....	197
7.6.1	Variable Amplitude Loading FCG Estimation.....	197

7.6.2	Evaluation of Crack Growth Retardation due to Tensile Overloads.....	199
7.7	Summary and Conclusions.....	203
7.8	Acknowledgements.....	204
<b>Chapter 8</b>	<b>Influence of the Peak Tensile Overload Cycles and Clipping Level on the Fatigue Crack Growth of Aluminum Alloy under Spectrum Loading.....</b>	<b>205</b>
8.1	Abstract.....	205
8.2	Introduction.....	206
8.3	Problem Definition and Objectives.....	209
8.4	VAL Stress-time History.....	209
8.5	Tests with Various Maximum Tensile Stress Levels.....	211
8.6	Test Setup and Material.....	213
8.7	Experimental Observations.....	216
8.7.1	Test Series No. 1.....	216
8.7.2	Test Series No. 2.....	217
8.8	Analytical Analysis and Discussion.....	223
8.9	Summary and Conclusion.....	230
8.10	Acknowledgements.....	232
<b>Chapter 9</b>	<b>Summary and Conclusion.....</b>	<b>233</b>
9.1	Summary.....	233
9.2	Conclusions.....	234
9.3	Recommendations for Future Works.....	236
<b>Bibliography</b>	<b>.....</b>	<b>238</b>
<b>Appendix A</b>	<b>Copyright Agreement Forms.....</b>	<b>253</b>
A.1	Copyright Agreement Form for Chapter 2.....	253
A.2	Copyright Agreement Form for Chapter 3.....	255
A.3	Copyright Agreement Form for Chapter 4.....	262

A.4	Copyright Agreement Form for Chapter 5 .....	268
A.5	Copyright Agreement Form for Chapter 6 .....	269
A.6	Copyright Agreement Form for Chapter 7 .....	276
A.7	Copyright Agreement Form for Chapter 8 .....	277

## List of Tables

Table 3.1	Typical characteristics of coarse, moderate and fine meshes used in the solid region of the finite element model.....	48
Table 3.2	Material property used in the computational simulation of crack growth.....	65
Table 4.1	Material and physical properties of the carbon-glass fiber-reinforced composite riser (Vandiver <i>et al.</i> 2006).....	82
Table 5.1	Main properties of the model and the prototype riser.....	119
Table 5.2	Compositions (%) of the 6061-T651 aluminum alloy.....	129
Table 5.3	Mechanical properties of the 6061-T651 aluminum alloy.....	129
Table 6.1	Summary of the various test series and their descriptions.....	153
Table 6.2	Mechanical properties of the 6061-T651 aluminum alloy.....	155
Table 6.3	Compositions (%) of the 6061-T651 aluminum alloy.....	155
Table 7.1	Mechanical properties of the 6061-T651 aluminum alloy.....	177
Table 8.1	The summary of various test series and their descriptions.....	212
Table 8.2	Mechanical properties of the 6061-T651 aluminum alloy.....	216
Table 8.3	Compositions (%) of the 6061-T651 aluminum alloy.....	216

## List of Figures

Figure 2.1	Basic definitions for two-slope S-N curve (DNV-OS-F201 2001).....	14
Figure 2.2	The three modes of fracture (Lyons et al. 1994).....	20
Figure 2.3	Influence of OLR on the a-versus-N Curve at stress ratio $R = 0.1$ (Rushton and Taheri, 2003).....	23
Figure 2.4	Schematic illustration of tension overload and compression underload (Hudson 1981).....	27
Figure 2.5.	A typical crack growth behavior for (a) tension overload, (b) compression underload followed by tension overload, (c) tension overload followed by compression underload, and (d) compression underload (Hudson 1981).....	27
Figure 2.6	Formation of the crack tip plastic zone (Rushton and Taheri 2003).....	28
Figure 2.7.	The crack tip under cyclic compressive loading (Shabanov 2005).....	29
Figure 2.8.	Schematic illustration of threshold variations with load ratio (Vasudevan and Sadananda 2001).....	32
Figure 2.9.	Schematic illustration of (a) variation of $da/dN$ versus $K_{\max}$ with decreasing load ratio $R$ , and (b) variation of $da/dN$ versus $\Delta K$ with increasing load ratio $R$ (Vasudevan and Sadananda 2001).....	33
Figure 2.10	Schematic illustration of four crack-closure mechanisms (Barsom and Rolfe 1999).....	36
Figure 2.11	The roughness values for tests with ( $R = -1$ ) and without compression ( $R = 0$ ) for the same $K_{\max}$ (Silva 2005).....	37



Figure 3.1	Stress intensity parameters for an elliptical surface flaw in a plate subject to tensile stresses .....	44
Figure 3.2	Two parameter model of the crack front (Carpinteri et al. 1998)	46
Figure 3.3	The finite element model.....	49
Figure 3.4	Stress singularity at the crack tip for coarse, moderate and fine meshes at the crack front region.....	50
Figure 3.5	Comparison between the dimensionless stress intensity factors obtained from the finite element analysis and those reported by Carpinteri <i>et al.</i> (1998).....	51
Figure 3.6	Variation of $K_{I,Plate}^* / K_{I,Pipe}^*$ as a function of the crack depth ratio, $a/t$ , and ellipse diameter ratios, $a/b$ , for $R/t = 10.0$ , a) depth crack, b) surface crack.....	52
Figure 3.7	Variation of $K_{I,Plate}^* / K_{I,Pipe}^*$ as a function of the crack depth ratio, $a/t$ , and ellipse diameter ratios, $a/b$ , for $R/t = 1.0$ , a) depth crack, b) surface crack.....	53
Figure 3.8	Comparison between the stress intensity factor ratio, $K_{I,Plate}^* / K_{I,Pipe}^*$ , between a plate and a pipe with an elliptical crack with different penetration ratio trough wall thickness (pipe radius/wall thickness = 1.0).....	56
Figure 3.9	Comparison between the stress intensity factor ratio, $K_{I,Plate}^* / K_{I,Pipe}^*$ , between a plate and a pipe with an elliptical crack with different penetration ratio trough wall thickness (pipe radius/wall thickness = 10.0).....	57
Figure 3.10	The relation between diameter aspect ratio and crack depth ratio for a plate with circular initial flaw under the action of pure tension (Song <i>et al.</i> 2002).....	60

Figure 3.11	Computational monitoring of a typical surface flaw during its propagation through the wall thickness of a pipe.....	64
Figure 3.12	Variation of ellipse diameter ratio, $a/b$ , as a function of crack depth ratio (a) for a rectangular plate subject to tensile load, (b) for a pipe with $R/t = 1.0$ under pure bending and (c) for a pipe with $R/t = 10.0$ under pure bending.....	66
Figure 3.13	Test apparatus.....	67
Figure 3.14	Typical normalized applied load.....	69
Figure 3.15	Fracture surface showing two beach-marked bands on the cross section of the pipe.....	70
Figure 3.16	Beach-marks under Scanning Electron Microscope (SEM).....	70
Figure 3.17	Comparison of the dimensionless stress intensity factor ratio of plates and pipes with an elliptical crack with different penetration ratio through the wall thickness.....	72
Figure 3.18	Variation of stress intensity factor ratio, $K_{I,Plate}^* / K_{I,Pipe}^*$ , at the center of a circular crack front as a function of crack depth ratio $a/t$ for various $R/t$ and $a/b$ ratios.....	73
Figure 4.1	Schematics of the VIV test (from Vandiver <i>et al.</i> 2005).....	81
Figure 4.2	Cross-flow strain-time history for the 485.3 foot long model riser.....	83
Figure 4.3	Power spectral density of the cross-flow strain time history of a 485.3 foot long model riser.....	84
Figure 4.4	A typical crack surface of a pipe under VIV-induced stress-time history.....	92
Figure 4.5	Test setup.....	93
Figure 4.6	Specimen layout and dimension.....	94

Figure 4.7	Typical crack growth versus the number of VIV-induced stress blocks.....	97
Figure 4.8	Crack length versus the number of applied VIV-induced stress blocks (note: each block consists of 2,000 cycles).....	98
Figure 4.9	Crack length versus the number of applied VIV-induced stress blocks (stresses multiplied by 2.25).....	99
Figure 4.10	Cross-flow strain time history of the filtered data.....	100
Figure 4.11	Power spectral density of the cross-flow filtered strain time history.....	100
Figure 4.12	Crack length versus the number of applied VIV-induced stress blocks for both filtered and unfiltered data (stresses multiplied by 2.25).....	101
Figure 4.13	Crack length versus the number of applied VIV- induced stress blocks (for actual VIV-induced stress-time history with un-factored stresses).....	105
Figure 4.14	Crack length versus the number of applied VIV-induced stress blocks (stresses multiplied by 2.25).....	106
Figure 4.15	Crack length versus the number of applied VIV-induced stress blocks (stresses multiplied by 2.25).....	109
Figure 5.1	Cross-flow acceleration-time history of the 8.5m long model riser at the riser's mid-span, associated with a pretension force of 600N.....	121
Figure 5.2	Stress-time history applied to the test specimen.....	126
Figure 5.3	Test setup.....	128
Figure 5.4	Specimen layout and dimensions.....	128
Figure 5.5	Crack length versus the number of applied VIV-induced stress blocks.....	130

Figure 5.6	Crack length versus the number of applied VIV-induced stress blocks.....	133
Figure 5.7	Power spectral density of the cross-flow stress-time history....	134
Figure 5.8	Stress-time history applied to the test specimen with the compression portion omitted.....	135
Figure 5.9	Comparison of the fatigue crack growth rates under tension-compression and tension-tension VIV-induced stress-time histories.....	136
Figure 5.10	Comparison between the fatigue crack growth under variable amplitude VIV-induced stress-time history and the equivalent constant amplitude load.....	139
Figure 6.1	The VAL stress-time history <i>block</i> and its 9 <i>sub-blocks</i> .....	150
Figure 6.2	The VAL stress-time history (one <i>block</i> ) with all the original values of its CSCs Scaled by 30% (for test Mult-0.3).....	152
Figure 6.3	(a) Specimen configuration and dimensions, (b) test set up.....	155
Figure 6.4	Crack length versus the number of applied VAL stress-time history blocks (the blocks include all the original CSCs).....	156
Figure 6.5	Comparison of the FCGR under the compression-tension and zero-tension stress-time history.....	158
Figure 6.6	Comparison of FCG under compression-tension VAL with various multipliers on the compressive portion of the stress-time history (each curve is the average of at least three tests)...	159
Figure 6.7	Plot of the number of the applied VAL blocks to failure versus the scale multiplier applied to the compressive portion of the stress-time history (Test Series No. 3).....	159
Figure 6.8	Comparison of the FCG for three loading scenarios.....	161

Figure 6.9	Further illustration of the influence of the presence of the CSCs within a VAL time-history.....	162
Figure 6.10	Evidence of the pronounced influence of the maximum compressive stress spike within the VAL <i>block</i> .....	164
Figure 6.11	Comparison of the fracture surfaces for cases with (Tests Mult-1.0 at top) and without (test Mult-0.0 at bottom) the CSC.....	166
Figure 6.12	A typical 3D roughness profile of the fracture surface.....	166
Figure 6.13	Typical roughness profile along the fracture surface: a) roughness measured along two parallel lines (purple and orange lines); b) roughness profile of the purple line.....	167
Figure 6.14	Typical roughness profile of the fracture surface.....	168
Figure 7.1	The VAL stress-time history <i>block</i> and its 9 <i>sub-block</i> .....	174
Figure 7.2	Specimen configuration and dimensions.....	176
Figure 7.3	Finite element model of the test specimen.....	177
Figure 7.4	Distribution of the longitudinal residual stress at the crack front for various scales of compressive stress cycles (the crack tip is at location 15.0 mm).....	181
Figure 7.5	Variation of the von Mises residual stresses at the crack front for various scales of CSC (the crack length is at location 15.0 mm).....	182
Figure 7.6	Variation of the CTOD along the crack surface for various scales of CSC after unloading (the crack length is at location 15.0 mm).....	185
Figure 7.7	Plot of the CTOD versus the compressive stress multiplier at various distances (in mm) ahead of the crack tip (as identified in the legend).....	186

Figure 7.8	Length of the plastic region ahead of the crack tip.....	187
Figure 7.9	A comparison of the variation of the CTOD and fatigue life of the component as a function of the compressive stress multiplier.....	188
Figure 7.10	Comparison of the experimental and numerical/analytical results (using the point-by-point approach of Walker Model combined with Willenborg Retardation Model).....	202
Figure 8.1	A typical compression-tension VAL stress-time history observed in pipelines, risers, helicopters or airplane components.....	210
Figure 8.2	The zero-tension VAL stress-time history used in this study ( <i>one block</i> ).....	210
Figure 8.3	The VAL stress-time history of test series with a clipping level of 0.55.....	212
Figure 8.4	Test set up.....	214
Figure 8.5	Test specimen configuration and dimensions (drawing not to scale).....	214
Figure 8.6	Crack length versus the number of applied VAL stress-time history blocks.....	217
Figure 8.7	Comparison of the fatigue crack growth rates of the base-VAL with test series with a clipping level of 0.85.....	218
Figure 8.8	Comparison of the fatigue crack growth rates of the original 'BASE-VAL' with test results from various clipping levels.....	219
Figure 8.9	Fatigue crack growth rate versus the clipping level.....	221
Figure 8.10	The VAL stress-time history of: (a) the original BASE-VAL, (b) and after application of clipping level of 0.55.....	221

Figure 8.11	A comparison between the exceedances for clipping levels of 1.0 and 0.55.....	222
Figure 8.12	Comparison of the fatigue life of the alloy subjected to the original BASE-VAL with test results with the clipping level of 0.70 and the full compression-tension stress-time history.....	223
Figure 8.13	Comparison of the fatigue crack growth results predicted analytically for the original BASE-VAL load history and the load history clipped at 0.70 level and the experimental results...	228
Figure 8.14	Comparison of the fatigue crack growth rate obtained experimentally and analytically.....	229

## **Abstract**

One of the most prominent factors affecting the performance and longevity of risers is vortex induced vibration (VIV), which can cause severe fatigue damage, especially in risers used in deep waters. The available approaches for analyzing VIV induced fatigue in risers mainly focus on the VIV aspect of the problem; indeed less attention has been paid on the effect of VIV on a riser's fatigue life and in prediction of fatigue life using various models.

This dissertation first demonstrates how one can characterize fatigue of pipes and risers using an equivalent plate specimen as opposed to using a pipe specimen, thereby simplifying the task, yet obtaining good accuracy. Actual variable amplitude loadings (VAL) are used to study the fatigue crack growth in risers' material with a focus on the various influencing parameters. Extensive experimental investigations are performed, followed by analytical and computational nonlinear finite element analyses. It is shown that the higher harmonics do cause significant fatigue damage, thus their influence should not be ignored. The influence of load interaction effects is also investigated, focusing on the fatigue crack growth retardation effects due to tension overloads, as well as the acceleration effects due to compression underloads. The crack closure concept is then used to explore into both the fatigue retardation and acceleration effects within a VAL scenario. An effective method for calculation of the stress intensity factor is proposed, which considers only the tensile portion of the stress range, while proposing another effective approach for accounting for the influence of compressive stress cycles.

Moreover, a two-parameter approach is used in this dissertation, relating the fatigue crack growth rate (FCGR) to the crack tip opening displacement (CTOD). It is shown that the CTOD provides adequate information for calculating the FCGR under VAL, and it can be effectively used to account for the influence of the compressive stress cycles. The experimental investigation also considers the retardation effect resulting from the applied peak tensile overload cycles (TOLC) and the influence of various so-called "clipping" levels, demonstrating the significant influence of the TOLC on crack growth retardation in VAL.



## List of Abbreviations and Symbols Used

### Greeks

$\alpha$	yield offset
$\beta$	shutoff overload ratio
$\Delta CTOD$	cyclic crack tip opening displacement
$\Delta K$	stress intensity factor range
$\Delta K_{eff}$	effective stress intensity factor range
$\Delta K_I$	stress intensity factor range
$\Delta K_{I,th}$	threshold stress intensity factor range in mode $I$
$\Delta K_{nom}$	nominal stress intensity factor range
$\Delta K_{rms}$	root-mean-square value of stress intensity factor range
$\Delta K_{th}$	threshold stress intensity factor range
$\Delta S_{rms}$	nominal root-mean-square stress range
$\Delta S_i$	nominal stress range in the $i^{\text{th}}$ cycle
$\Delta \delta_i$	CTOD range
$\Delta \sigma$	stress range
$\delta_M$	stretch in the crack tip due to the applied maximum load
$\delta_{max}$	maximum CTOD
$\delta_{min}$	minimum CTOD
$\delta_R$	crack tip residual stress due to the minimum load
$\varepsilon$	strain
$\phi$	dimensionless geometric parameter
$\phi$	Willenborg's model parameter
$\varphi$	angle of orientation of the point along the crack front
$\lambda$	material constants for Paris equation
$\theta_R$	non-dimensional constant to satisfy certain self-consistency conditions
$\omega$	natural angular frequency of the vibration

$\omega_n$	natural angular frequency of the vibration for mode $n$
$\sigma$	stress
$\sigma_c$	far-field stress
$\sigma_0$	characteristic stress
$\sigma_M$	maximum bending stress at the outer layer of the pipe
$\sigma_{\max}$	maximum stress
$\sigma_{\min}$	minimum stress
$\sigma_o$	yield stress
$\sigma_T$	far field tensile stress
$\sigma_U$	tensile ultimate stress
$\sigma_y$	tensile yield stress
$\sigma_{Z,M}$	opening normal stress

### Romans

$A$	material constants for Paris equation
$a$	crack depth or crack length
$\bar{a}$	material constant
$a_{ol}$	crack length due to overload
$C_{Depth}$	Paris equation coefficients along the depth
$C_{Surface}$	Paris equation coefficients along the surface
$c$	speed of transverse waves
$D_i$	fatigue damage ratio for each loading phase
$D_F$	fatigue damage
$D_{fat}$	accumulated fatigue damage
$D_n$	fatigue damage
$DFF$	design fatigue factor

$da / dN$	crack growth rates for into the depth direction
$db / dN$	crack growth rates for into the surface direction
$E$	modulus of elasticity
$F$	function of crack shape characteristics
$F_{pt}$	geometry factor
$f_n$	natural frequency of the $n^{\text{th}}$ mode
$g$	geometry factor
$I$	area moment of inertia of cross section
$K$	stress intensity factor
$K_{eff}$	effective stress intensity factor
$K_{I,C}$	fracture toughness
$K_{I,M}$	stress intensity factor for bending
$K_{I,M}^*$	dimensionless stress intensity factor for a pipe under bending moment
$K_{I,Plate}^*$	dimensionless stress intensity factor for mode I in a plate under tension
$K_{I,Pipe}^*$	dimensionless stress intensity factor for a pipe under bending moment
$K_{I,T}$	stress intensity factor for mode one
$K_{max}$	maximum stress intensity factor
$K_{max,eff}$	maximum effective stress intensity factor
$K_{max,ol}$	maximum stress intensity factor
$K_{min,eff}$	minimum effective stress intensity factor
$K_{req}$	stress intensity factor necessary to produce a plastic crack zone
$K_{op}$	opening threshold stress intensity factor
$k$	wave number
$L$	length of the riser
$l_m$	reference length
$M$	bending moment

$m$	mass per unit length, material constant for Paris equation
$N$	total number of cycles or number of cycles required to failure
$N(S)$	number of cycles to failure at stress amplitude $S$
$N_{cg}$	number of stress cycles related to a critical crack size
$N_i^{(k)}$	number of cycles to failure for element $i$
$N_{tot}$	total number of applied stress cycles
$NFREQ$	total number of frequencies in the response analysis
$n$	mode number, material constants or stress hardening exponent
$n_s$	number of cycles
$Q$	function of crack shape characteristics
$R$	radius or stress ratio
$R_a$	arithmetic mean deviation of the roughness profile
$R_e$	Reynolds number
$R_{y,ol}$	size of the yield zone due to an OL
$S$	nominal stress normal to the crack or stress range
$S_{\max(i)}$	maximum stresses of each cycle
$S_{\min(i)}$	minimum stresses of each cycle
$SF_i$	safety factor
$T$	Tension or time
$T_L$	design life of the riser
$t$	thickness
$u$	coordinate transverse to the longitudinal axis of the pipe
$W$	width
$z$	value of surface profile

## Abbreviations

API	American Petroleum Institute
ASTM	American Society of Testing and Materials
CAL	Constant Amplitude Loading
CF	Cross-flow
CSC	Compressive Stress Cycle
CTOD	Crack Tip Opening Displacement
DIN	Deutsches Institut für Normung
DNV	Det Norske Veritas
EDM	Electric Discharge Machine
EICC	Environmentally-induced Crack Closure
FCG	Fatigue Crack Growth
FCGR	Fatigue Crack Growth Rate
FEA	Finite Element Analysis
FEM	Finite Element Method
IL	In-line
LEFM	Linear Elastic Fracture Mechanics
LSY	Large Scale Yielding
MIT	Massachusetts Institute of Technology
MII-ICC	Mode II-induced Crack Closure
MUN	Memorial University of Newfoundland
NSERC	Natural Sciences and Engineering Council of Canada
OL	Overload
PD	Potential Drop

PICC	Plastic-induced Crack Closure
PSD	Power Spectral Density
RICC	Roughness-induced Crack Closure
RMS	Root Mean Square
SCR	Steel Catenary Riser
SEM	Scanning Electron Microscope
SIF	Stress Intensity Factor
SSY	Small Scale Yielding
TDP	Touch-down Point
TOLC	Tensile Overload Cycle
TSC	Tensile Stress Cycle
UL	Underload
VAL	Variable Amplitude Loading
VIV	Vortex Induced Vibration

## **Acknowledgements**

First of all, I would like to thank my dear parents, my brother and my sisters. Their emotional support is greatly appreciated. I would like to express my deep gratitude to Dr. Farid Taheri. He provided me with financial support throughout my Ph.D. studies and wisely supervised me, enabling me to liberally pursue my scholarly interests. Without his guidance and constant support in every respect, this attaining degree would have been indeed impossible. I also like to thank my supervisory committee members, Dr. J. Kim Vandiver, Dr. Neil Pegg and Dr. George Jarjoura. I also thank Dr. Rajamohan Ganesan, the external examiner.

The financial support of Natural Sciences and Engineering Council of Canada (NSERC) in the form of a partnership agreement grant is gratefully acknowledged. My thanks extend to all my friends and colleagues at Dalhousie University, Massachusetts Institute of Technology (MIT), University of New Brunswick (UNB) and Memorial University of Newfoundland (MUN). I cherish all the good times and beautiful memories I had with them.

# **Chapter 1**

## **Introduction**

### **1.1. Offshore Oil and Gas Risers and Pipelines**

Vortex Induced Vibration (VIV) can cause significant fatigue damage in risers used in offshore oil and gas platforms. In deep waters, where oil and gas exploration and production have been taking place in recent years, VIV-induced fatigue becomes even more critical. Extensive research works have been done to investigate VIV response of risers, and several methods have been proposed for the fatigue life estimation of these structures.

This research program first briefly reviews the available methods for VIV analyses of risers, followed by investigating the integrity of some widely used methods for assessing their fatigue life. Extensive experimental fatigue tests have been performed during the course of the research using various VIV data from different sources, and the results are compared with analytical and computational methods. Different aspects of fatigue life estimation and fracture mechanics are studied in detail, which helped the author gain an in-depth and fundamental insight into VIV analysis, fatigue and fracture mechanics. The results presented in this dissertation are the outcome of about 4,200 hours of fatigue test data in the form of various stress-time histories, followed by many analytical and computational nonlinear finite element calculations. Many recommendations are provided for more accurate fatigue life assessment of materials under various loading scenarios, focusing on Variable Amplitude Loading (VAL) stress-time histories.



## 1.2. Thesis Objectives

Many researchers have worked on theoretical and experimental aspects of VIV analyses and the resulting fatigue damages in subsea pipelines and risers. As it is later explained in Chapter Two, the major focuses have been on either developing new methods or advancing the existing methods for predicting the VIV response of such structural components. Once the VIV-induced stresses are calculated, a general purpose fatigue model is usually used to estimate the fatigue life.

This research program focuses on the fatigue life estimation of pipelines and risers, rather than focusing on the VIV response of such components. Both field and lab VIV data has been used to perform the experimental and analytical investigations leading to a more effective fatigue life estimation under VAL loading scenarios. Such data are used to investigate the influence of various parameters, such as the second VIV harmonic, compressive stress cycles, tensile overloads and clipping level.

In summary, the objectives of this research program are:

1. To focus on the fatigue life estimation of risers and pipelines using various parameters.
2. To study the influence of the second VIV harmonic on fatigue life of pipelines and risers due to actual current profiles.
3. To study the detrimental influence of Compressive Stress Cycles (CSC) on FCGR, with focus on their magnitude and number of cycles in the load spectrum.
4. To examine the stress distribution in the vicinity of the crack tip.
5. To investigate the influence of various scales of CSC on the crack tip opening displacement (CTOD).
6. To study the retardation effect of the Tensile Overload Cycles (TOLC) on material's fatigue crack growth rate, and determine the optimum clipping level.

7. To evaluate the effectiveness of some of the widely-used fatigue models for calculating the fatigue crack growth rate of the material under real VIV-induced VAL obtained from various sources.

### **1.3. Thesis Layout**

This dissertation essentially consists of six journals and one conference paper, either published, conditionally accepted or under review for publication at present. It is noted that some parts of the published papers have later been slightly revised for use in this dissertation based on the suggestions provided to the author by the supervising committee and the external examiner during the thesis defense proceedings. All such revisions are of explanatory nature, providing more clarifications by the author, and have no influence on the outcomes and conclusions of any of the papers by any means.

The present chapter gives an overview of the overall dissertation, introducing the main topics included in the subsequent chapters. Chapter Two is the literature survey, and includes the main portion of the conference paper which focused on the significant issues that constituted the preliminary steps of this research program. Chapters Three to Eight, each present a journal paper, and each is a stand-alone document consisting of introduction, literature review, main body, summary and conclusions. The main body of each paper explains the experimental test, analytical methods and computational approaches used to conduct the research. Chapter Nine includes the overall summary of this dissertation, the conclusions and recommendations for future works.

In Chapter Two, some of the available methods for VIV-induced fatigue life estimation of risers are briefly studied, focusing on their main underlying assumptions. The main focus is on the influence of direct action of currents on risers. It is observed that fatigue life of risers is greatly dependent on the different parameters used in calculating the VIV-induced stress-time history of risers. It will be shown that any minor change in these parameters would significantly influence the predicted fatigue life. It is also illustrated that the available approaches for analyzing VIV-induced fatigue of risers mainly have focused on the VIV portion of the task, and have paid less attention to the

actual fatigue life analysis using various fatigue models. These observations motivated the present research. As it will be explained later in detail, to avoid any uncertainties in fatigue life estimation, the author used ‘real’ field and laboratory test data. The real-life VIV data was obtained through experts in the field.

Chapter Three studies the concept of using a simple rectangular plate subject to tension as an equivalent substitute for a pipe subject to bending. In other words, whether a simple fractured plate could be used to mimic the response of a fractured riser (pipe) under bending is examined in detail. This approach has been tried by a few researchers to avoid the complexity, associated expense and need for sophisticated monitoring instruments usually involved with experimental crack growth investigations of pipes hosting initial surface flaws. This chapter studies the validity of this approach using both the finite element and experimental methods, and also evaluates the ranges of the crack depth ratio and elliptical crack diameter ratios for which this approach would be admissible. A series of finite element analyses are carried out to verify both the values of the stress intensity factors reported in the literature, as well as the results of the interpolation function used in the computational simulation in this research. A series of experimental investigations was performed to verify the validity of the proposed computational simulation. The results show the rationality and admissibility of the proposed approach.

In Chapter Four, the field data on multimodal vibration of a long flexible riser is used to conduct a series of experimental tests for fatigue life estimation of risers. The VIV field tests (the input required for the fatigue tests performed by the author) were collected by the Massachusetts Institute of Technology (MIT) researchers in the Gulf of Mexico; the author also participated in these field tests. It is shown that VIV imposes a Variable Amplitude Loading (VAL) on risers, thus adding complexity to fatigue life estimation.

Long risers in deep waters undergo multimodal vibration with two different harmonics clearly illustrated by the Power Spectral Density (PSD) of the field data. The prototype riser tested in the field was instrumented by strain gauges at its four quadrants around the circumference. The measured strains are directly transformed to stress and then applied to a number of specimens to investigate the Fatigue Crack Growth Rate

(FCGR). Moreover, the influence of load interaction effects is also investigated through experimental tests, by studying the combined effect of tensile overloads and compressive underloads present in a VAL scenario. The study on the load interaction effect has been continued throughout the subsequent chapters of this dissertation by revising the load spectrum as discussed in detail in each chapter. The changes in the base load spectrum were accomplished by altering the tensile or compressive cyclic portions of the base VAL stress-time history, with focus on the magnitude of the stresses and the number of applied cycles. The influence of different frequency harmonics of the VIV-induced time-history is studied. The experimental results from this study indicate that the higher harmonics cause significant fatigue damage and should not be ignored.

According to design standards (e.g, DNV-OS-F201, 2001), the riser material and its girth welds shall have adequate safety due to unstable fracture for a representative part or through-wall crack during the service life of the riser. In order to avoid brittle fracture, a material with sufficient ductility should be used, along with nondestructive testing (NDT) evaluation during its fabrication. This is to ensure that only acceptable defects would be present in the riser system after its fabrication. Moreover, due to limited accessibility for in-service inspection, a larger design safety factor against fatigue should be used for welds (DNV-RP-C203, 2001). For one- side girth welds, the lack of potential penetration defect would be difficult to detect, even for crack depth of about 1 to 2 mm (DNV-OS-F201, 2001). Therefore, it would be unrealistic to assume a flaw free weld and an initiation fatigue life for the weld. It is recognized that a defect size of up to 5.0 mm may be present without being detected, even with a careful examination of the root of a tubular joint (DNV-RP-C203, 2001). Therefore, weld in risers and similar structural components cannot be assumed as defect-free, even in cases where no defect has been detected during the inspection. This makes the fatigue life estimation of risers even more challenging, as the defects may be overlooked during inspections. In other words, defects are assumed to exist in both the riser parent material and its welds, thus requiring the designer to perform a fatigue crack growth calculation based on the concepts of fracture mechanics (DNV-OS-F201, 2001). Therefore, the focus of this dissertation has been on the parent material, and the weld material has not been considered within this research project.

Chapter Four also describes the reasons for the choice of 6061-T651 aluminum alloy as the test material in this research project. It is recognized that risers are typically made of steel (mostly stainless steel). The corrosive environment of sea water, the VAL nature of the VIV-induced stress-time history and the near-threshold fatigue crack growth in riser structures impact the endurance limit of steel. Therefore, due to limitations imposed by the availability of the test facility for the required time, as a mean to mimic such effect on the actual riser materials, the author decided to use 6061-T651 aluminum alloy. This is because this alloy does not have any endurance limit and the influence of every single stress cycle in the VIV-induced VAL stress-time history could be taken into account, thereby responding similar to the way the steel material used in risers is impacted by the noted parameters.

Chapter Five first briefly studies the available methods widely used by the offshore industry for fatigue life estimation of pipelines and risers. Such models have basically been developed for constant amplitude loading scenarios. However, the VIV-induced stress-time history has a variable amplitude nature, which may create significant under/overestimation of the fatigue life of such components.

In this chapter, ‘real’ VIV-induced variable amplitude loading test data are used to perform a series of fatigue tests. The VIV laboratory tests (the input required for the fatigue tests performed by the author) were collected by the Memorial University of Newfoundland (MUN). The VIV-induced accelerations were then transformed to stresses, and were then directly used in this research program to conduct the experiments on FCG of material. The fatigue test results were then compared with analytical fatigue models commonly used by the offshore industry. It is observed that the fatigue models currently used by the industry produce significant underestimation of the fatigue damage. In addition, the influence of the Compressive Stress Cycles (CSC) of the stress-time history on the fatigue life is studied experimentally. It is shown that the compressive stress has a significant influence on the fatigue crack growth of risers, and should not be ignored. These findings promoted further understanding of the underlying mechanism of the damaging influence of compressive stresses in the next stages of this research project.

In Chapter Six, a VAL stress-time history is used to study the fatigue response of 6061-T651 aluminum alloy, with a focus on the influence of the compressive portion of the stress-time history. An experimental investigation is conducted to assess the influence of VAL, in particular, the influence of the CSC on FCG of the material. In the tests, the tensile portion of the stress-time history is kept unchanged, while the compressive portion of the stress-time history is multiplied by various scaling factors. The experimental results demonstrate that the compressive stress portion of the applied load has a significant influence on the overall fatigue life of the material, thus should not be ignored. It is observed that even introducing a few number of small CSC into the stress-time history can significantly decrease the fatigue life of the material. In addition, the influence of the CSC is also examined by means of a microscopic evaluation of crack surfaces' roughness. The results of the experimental investigations explained in this chapter provides a fundamental insight into the application of stress intensity factor for calculating the damaging effect of compressive portion of VAL stress-time history. As it is later explained in Chapter Six, the use of a new approach for establishing the stress intensity factor range should be explored, so that the influence of the compressive stresses could be more effectively accounted for.

Chapter Seven studies the FCGR of 6061-T651 aluminum alloy subject to the VAL, using a coupled analytical/computational approach. This chapter uses the experimental results presented in Chapter Six. The analytical approach uses the Willenborg's retardation model in conjunction with the Walker FCG model, with several of the parameters used in the models obtained through nonlinear finite element analyses. A two-parameter approach is used in this chapter to relate the FCGR of the material resulting from a VAL stress-time history to the Crack Tip Opening Displacement (CTOD). In addition, the nonlinear finite element method is used to further assess the FCGR of the material, particularly under the influence of the compressive underloads and tensile overloads. More specifically, the crack closure concept is used to explore the retardation effect of the tensile overloads, as well as the detrimental influence of the compressive underloads. The finite element analysis results are compared to the experimental results discussed in Chapter Six. It is observed that the CTOD provides us with adequate information for calculating the FCGR under the VAL stress-time history

applied to a material. The results further demonstrate both the influence of FCG retardation effects due to the tensile overloads, and the acceleration effect due to the applied compressive underloads of a VAL stress-time history.

Chapter Eight discusses the structural life assessment and damage-tolerant analysis of structural components (such as aircrafts, risers and offshore pipelines) which are in direct contact with a fluid. It is noted that water is not a compressible fluid, while air is a compressible fluid. However, both water and air create vortices around the moving object, which in turn causes VIV-induced fatigue in the component.

In previous chapters, the focus was on the FCG accelerating effect due to CSC. Therefore, Chapter Eight only focuses on the crack growth retardation effect from the tensile overloads by revising the tensile portion of the VAL stress-time history applied to the test specimens. In this chapter, a VAL stress-time history is used to study the fatigue life of 6061-T651 aluminum alloy, with focus on the retardation effect resulting from the applied peak Tensile Overload Cycles (TOLC). It is understood that airspace industry uses aluminum alloy grades 2000 and 7000, and not grade 6000. The reason for using grade 6000 for the tests performed in Chapter Eight is to use the same material throughout the entire research project so that the results from different chapters can be compared with each other.

In Chapter Eight, various so-called “clipping” levels are tested, and the results are compared with those obtained through an analytical approach, using the Willenborg retardation method, in conjunction with the Walker fatigue crack growth model. The results demonstrated the significant influence of the TOLC present within VAL scenarios on retarding the FCGR of the material. This chapter also investigates the influence of various clipping levels on the fatigue response of the material, highlighting the limitations of the analytical approach in estimating the resulting FCGR. It is observed that the analytical method predicts a higher fatigue life for the material subjected to VAL, which is non-conservative for design purposes. Some suggestions are provided for better fatigue life estimation of the material when subjected to VAL scenarios.

Chapter Nine presents a brief summary of this research program, as well as the conclusions and recommendation for future work.

## **Chapter 2**

### **Literature Review, State-of-the-Art on Risers' Fatigue and Influence of Compressive Stress Cycles**

#### **2.1. Introduction**

As a safety limit state, a riser system is required to exhibit adequate safety against repeated loading cycles within its design service life against all imposed cyclic loadings. Fatigue assessment is usually performed at the latter stages of the design process. There exist several different sources that could impose major influence on the riser fatigue response, one of the most prominent ones is the phenomenon of Vortex Induced Vibration (VIV).

In this chapter, some of the methods available in literature for predicting the fatigue life of risers' subject to VIV are briefly reviewed, and their capabilities are compared. There are other methods that practicing engineers use for fatigue life prediction of risers; and, the review of the pertinent literature could not lead to any one unified method. In fact, the industry tends to keep their adopted methodologies as proprietary. Several parametric studies are also reviewed in order to better understand the influence of different parameters on the fatigue response of materials. The above review revealed that the available methods used for riser VIV fatigue life assessment provide significant overestimation of the fatigue damage, which is not desirable for design purposes. Moreover, due to the complex nature of fluid-structure interaction, the riser VIV-induced fatigue life becomes greatly dependent on several contributing parameters and any small variation in these parameters could significantly influence the predicted fatigue life. It will also be discussed that most of the researches on the influence of VIV on fatigue of



risers have indeed focused on the VIV analysis as opposed to considering the actual fatigue issue itself (Iranpour and Taheri, 2006a)<sup>1</sup>.

In this chapter, some of the available fatigue life estimation methods are studied. The parameters that could result into under/over estimation of fatigue life are briefly investigated, mainly focusing on the more prominent ones that are later used in the experimental segments of this dissertation. The influences of tension overload and compression underload are briefly discussed, followed by an introduction to the two parameters, which are the driving forces that affect the fatigue response. As explained earlier, each chapter of this dissertation is a paper that has been published or is currently under review for publication. Therefore, each chapter is a stand-alone document, outlining the overall objectives followed by a detailed problem definition and literature review, technical investigation and discussion of the results.

## **2.2. Main Sources of Riser's Fatigue**

Literature survey indicates that four major phenomena contribute and promote riser's fatigue damage due to dynamic cyclic loads. These are the wave forces and the resulting platform motions, vortex induced vibration due to currents, thermal and pressure-induced stress cycles, and finally collisions with other risers or external objects (DNV-OS-F201 2001; Bai 2001). Among these, the flow-induced forces (described below), are known to have the greatest effects on risers (Bai 2001). The above sources are briefly described in the following section.

### **2.2.1. First Order Floating Platform Motions**

Fatigue damage from all sea-states could be taken into account using the linearization of a riser's response by assuming a statistical distribution (Bai 2001). This type of analysis must consider wave height, period and offset representative of the window so that the

---

<sup>1</sup> Certain sentences mentioned and/or used in this chapter are taken verbatim from author's own paper, published by ASME, titled "The State-of-the-Art Review of Risers' VIV Fatigue," by Mohammad Iranpour and Farid Taheri, Paper No. OMAE2006-92636.

importance of the first order motions on the touch-down point (TDP) and the fatigue damage distribution can be considered (Jensen 1999). To account for nonlinearities, a random time domain analysis is performed and fatigue damage from each sea-state is determined using the total stress transfer function. Assuming a Rayleigh distribution for stress peaks, Miner's rule is widely used to obtain the cumulative damage (Jensen 1999; Bai 2001).

### **2.2.2. Second Order Floating Platform Motions**

To consider the second order floating platform motions, a Rayleigh distribution (for low frequency stresses) is applied to each scatter diagram window for each sea-state. This considers a conservative representative root mean square (RMS) drift offset and drift motion mean crossing period for each window (Bai 2001). Having each sea-state fatigue damage, the total fatigue damage could then be calculated. This second order motion analysis is usually based on a static analysis of floating platform motion, without considering the effects of waves or currents (Bai 2001).

### **2.2.3. Vortex-induced Vibration**

Vortex-induced vibration has been known as the most important design issue for riser structures, especially for environments with high current profile. Riser high frequency vibrations generate severe cyclic stresses, which in turn would create significant fatigue damage rates. In deeper waters, the riser natural frequency decreases, which lowers the magnitude of the current required to induce vibration (Bai 2001).

When fluid flows around a solid object, vortex shedding creates both in-line and cross-flow vibrations. Any structure with a sufficiently bluff trailing edge sheds vortices in the flow. As the flow velocity is increased or decreased, the shedding frequency approaches the natural frequency of the structure and suddenly "locks" into the structure frequency. The locked-in resonant oscillations of the near wake input energy to the structure and large amplitude vibrations can be produced. The broad response peaks of

the vibration amplitude versus fluid velocity diagrams are indicative of locked-in vortex shedding resonances.

The literature survey indicates that most of the available approaches for VIV induced fatigue prediction only consider the lock-in vibration in uniform flows, which may lead to an overestimation of fatigue damage. In a more realistic approach, the methods should consider a multimodal vibration in sheared flow. Factoring each sea-state based on their frequency of occurrence, the total VIV fatigue damage is calculated as the sum of damage from each sea-state (Bai 2001). The analysis is usually conducted for both in-plane and normal currents to risers; however, the most severe form of VIV response is known to be due to the cross-flow vibration.

Many research works have been conducted in consideration of fatigue of risers (Vandiver *et al.* 2006, Maher and Finn 2000; Serta *et al.* 2000; Larsen *et al.* 2000). Most of the studies are concerned with the VIV-induced fatigue, which is considered to be the most severe source of damage. It will be shown that most of the reported methods focus on the VIV analysis aspect, rather than focusing on the performance of the various available fatigue life prediction models (Iranpour and Taheri 2006a). This encouraged the author to focus on the fatigue life estimation of risers and pipelines using various fatigue parameters and real VIV-induced stress-time history field and lab data.

### **2.3. VIV-induced Fatigue Analysis**

As stated earlier, risers are very sensitive to both platform motions and direct effects of currents. Most of the available fatigue models only consider one source of damage; that is, either fatigue due to waves or currents. There exist only a few analytical procedures that account for both waves and currents. The following sections present a brief review of the methods available for VIV-induced fatigue life prediction of risers.

### 2.3.1. The Det Norske Veritas (DNV)

DNV considers the contribution of fatigue from three different sources: the wave-induced, the low-frequency, and VIV-induced stress cycles. If the fatigue damage is calculated to be within the tolerable limit, a simplified VIV analysis is assumed to be sufficient (DNV-OS-F201 2001). The dominant mode shapes and natural frequencies are determined and the vibration amplitude and the corresponding stress range are calculated for each current velocity (Sarpkaya 1979). The fatigue damage is then assessed based on the S-N curve approach (DNV-OS-F201 2001), by:

$$D_F = \frac{f_n T_L}{\bar{a}} S^m \quad (2.1)$$

where  $f_n$  is the frequency of the relevant mode,  $T_L$  is the design life of the riser,  $S$  is the stress range (including both axial and bending stresses) and  $m$  and  $\bar{a}$  are empirical constants that define the S-N curve. In cases with serious VIV-induced fatigue damage, a multimodal response analysis should be performed based on empirical or semi-empirical values of hydrodynamic coefficients. DNV recommends solving the full Navier-Stokes equation for a series of two dimensional cross sections along the riser length, which makes the method time consuming, costly and relatively difficult for everyday design purposes (DNV-OS-F201 2001).

The S-N curve approach fatigue damage criterion is introduced as:

$$D_{fat} \times DFF \leq 1.0 \quad (2.2)$$

where  $D_{fat}$  is the accumulated fatigue damage and  $DFF$  is the design fatigue factor, varying between 3.0 to 10.0 for low to high safety classes, respectively. The S-N curve expresses the number of cycles required for the failure of the material and is expressed by (DNV-OS-F201 2001):

$$N = \bar{a} S^{-m} \quad (2.3)$$

where the empirical constants  $\bar{a}$  and  $m$  are found from experimental data. The fatigue damage stress range is calculated using the stress concentration and a thickness correction

factor (DNV-OS-F201 2001). In some cases, a bilinear S-N curve, like the one illustrated in Figure 2.1, may be used for modeling the experimental fatigue response.

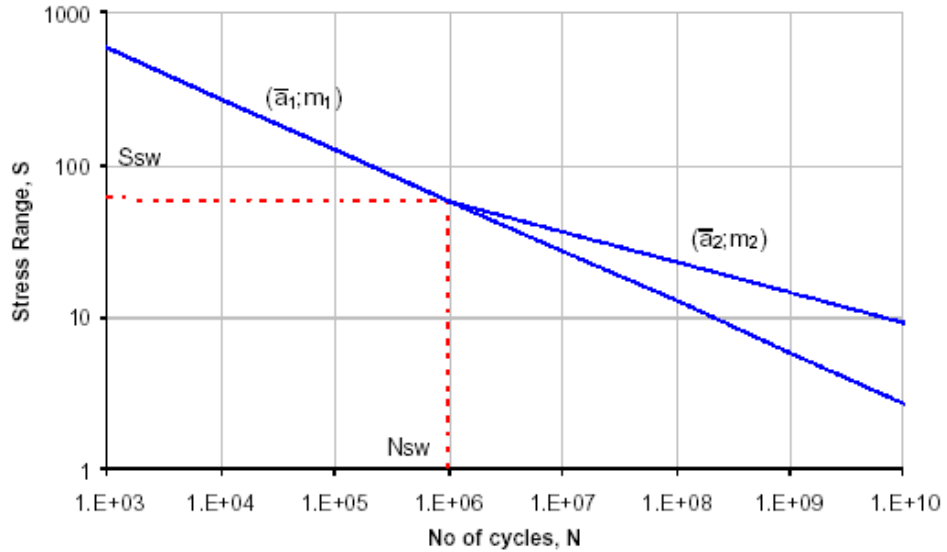


**Figure 2.1.** Basic definitions for two-slope S-N curve (DNV-OS-F201 2001)

To estimate fatigue crack growth life and establish an effective inspection criteria, DNV recommends another approach, which is based on fatigue crack propagation and is expressed by (DNV-RP-C203 2001):

$$\frac{N_{tot}}{N_{cg}} \times DFF \leq 1.0 \quad (2.4)$$

where  $N_{tot}$  is the total number of applied stress cycles,  $N_{cg}$  is the number of stress cycles related to a critical crack size and  $DFF$  is the design fatigue factor explained above. This above approach does not include the crack initiation portion of fatigue, and therefore shorter fatigue life is anticipated. In this approach, only the stress components normal to the propagation plane are considered and the effect of compressive stresses are ignored. As in most other guidelines, DNV uses Paris' equation to predict the crack propagation (DNV-RP-C203 2001), where the rate of crack growth is predicted by:

$$\frac{da}{dN} = C(\Delta K)^m \quad (2.5)$$

where  $\Delta K = K_{\max} - K_{\min}$ , is the range of stress intensity factor corresponding to the stress intensity factors resulting from the maximum and minimum applied stress within the cycles,  $a$  is the crack depth, and  $C$  and  $m$  are material parameters obtained from fatigue test data. The stress intensity factor  $K$  can be approximated by:

$$K = \sigma g \sqrt{\pi a} \quad (2.6)$$

where  $\sigma$  is the nominal stress normal to the crack and  $g$  is a factor depending on the geometry of the member and the crack.

### 2.3.2. The American Petroleum Institute (API)

The general approach of API is, in its fundamentals, similar to DNV's. The design fatigue life is required to be at least three times the service life. The fatigue damage should satisfy the following relation (API RP - 2RD 1998):

$$\sum_i SF_i D_i \leq 1.0 \quad (2.7)$$

where  $D_i$  is the fatigue damage ratio for each loading phase and  $SF_i$  is the safety factor. To consider the effect of the mean stress on fatigue damage, the Goodman mean stress correction method can be used, which incorporates the effect of stress concentration. The fatigue crack growth assessment in this standard is performed based on Paris' equation, which is applicable to constant amplitude loading (API RP - 2RD 1998). To consider variable amplitude loading scenarios, the Miner cumulative damage summation may be used. The total damage is assumed to not be affected by the sequence of the applied load and any minor changes in the stress range or the stress amplification factor would result in large changes in the predicted fatigue life. These can be considered as one of the main disadvantages of the S-N curve approach, which could explain the reason for the imposition of large safety factors used for the estimation of the fatigue life of risers.

### 2.3.3. The Vandiver Approach

The VIV studies done by Vandiver goes back to the 1970s, when a series of field experiments was conducted to investigate the flow-induced vibration of long slender cylinders (Vandiver, 1993). A theoretical model was developed by Vandiver and Chung (1988) to predict the vortex-induced vibration of a cylinder in sheared flow. Those studies resulted in developing a computer program at MIT, named SHEAR, for predicting the vortex-induced vibration response of beams and cables in non-uniform flow with linearly varying tension (Vandiver and Li 2005). Recent versions of this program are entirely new and are based on mode superposition, identifying which modes are likely to be excited. This program estimates the cross-low VIV response in steady, uniform or sheared flows (Vandiver and Li 2005).

SHEAR calculates the natural frequencies, mode shapes, and response of cables and beams with linearly varying tension using a variety of boundary conditions. For a period of one year, the fatigue damage is calculated as (Vandiver and Li 2005):

$$D_n = \int_0^{\infty} \frac{n(S)}{N(S)} ds \quad (2.8)$$

where  $N(S)$  is the number of cycles to failure at stress amplitude  $S$ . The parameter  $n_s$  is the number of cycles at stress amplitude between  $S$  and  $S + dS$  in one year, and is calculated as (Vandiver and Li 2005):

$$n_s = \frac{T p(S)}{2\pi / \omega_n} = \frac{\omega_n T}{2\pi} p(S) \quad (2.9)$$

where  $T$  is the number of seconds in one year ( $T = 365 \times 24 \times 3600$ ),  $\omega_n$  is the frequency for the mode number  $n_s$  and  $p(S)$  is the probability density function for the stress amplitude process. The frequency  $\omega_n$  can be viewed as an expected frequency of narrow-banded process.

### 2.3.4. The Marintek Approach

After calculating each element's vortex induced forces and the resultant stress amplitude distribution for all frequencies, the accumulative fatigue damage is calculated as follow (Larsen *et al.* 2000):

$$AFD_i = \sum_{k=1}^{NFREQ} \frac{n_i^{(k)}}{N_i^{(k)}} \quad (2.10)$$

where  $n_i^{(k)} = f^{(k)} \times 365 \times 24 \times 60 \times 60$  is the number of cycles per year for each element  $i$ ,  $N_i^{(k)} = C \cdot (2 \cdot \sigma_i^{(k)})^m$  is number of cycles to failure for element  $i$ ,  $\sigma$  is the applied stress, and  $NFREQ$  is the total number of frequencies in the response analysis (Larsen *et al.* 2000). Constants  $C$  and  $m$  are the S-N curve constants.

### 2.3.5. The Torres-Siqueira Method

More accurate approaches other than the deterministic one, are two random VIV fatigue analysis approaches proposed by Torres and Siqueira: the frequency domain and the time domain (Torres *et al.* 2001; Torres *et al.*, 1997). Fluid load nonlinearities and the interaction with risers are considered using a time-simulation method. In the frequency approach, the dynamic response is calculated through a direct integration (Torres *et al.*, 1997), and the fatigue damage is then calculated for each sea-state using the S-N curve approach and Miner's rule. In the time-domain approach, the member forces are increased based on the stress concentration factors and the hot-spot time histories are generated including the axial force and bending moment effects. The Rainflow algorithm is then used to identify and count each stress cycle to calculate the damage from each seastate using Equation 2.9 (Torres *et al.* 2001; Torres *et al.*, 1997).

In a study on a Steel Catenary Riser (SCR) connected to semi-submersible platform in a water depth of 770 meters, the fatigue life predicted by the time-domain approach was calculated to be 3-5 times greater than that calculated by the frequency-domain approach. The observed differences were reported to be mostly due to linearization of hydrodynamic loading.



As observed, the method used for the calculation of the VIV response of the riser has a significant influence on the estimated fatigue life. This is one of the main reasons that the author decided to use real field and lab produced VIV data to perform the fatigue tests, rather than focusing on calculating the VIV-induced stress-time history using numerical and analytical approaches.

### **2.3.6. The Baarholm Model**

This model predicts the riser fatigue damage without the need for performing a dynamic analysis, but produces conservative results. In this method, an effective current velocity and excitation length are introduced to identify the cross-flow response frequencies and displacements. The effects of all cross-flow eigen-frequencies within a certain frequency bandwidth around the primary cross-flow response frequency are taken into account. By assuming that the in-line response frequency is twice the cross-flow frequency, the relevant response RMS could then be calculated based on the cross-flow RMS value. Using the S-N curve approach, fatigue damage could then be estimated from the stress RMS values found from mode shape curvatures (Baarholm et al. 2004).

### **2.3.7. The Maher-Finn Model**

The combined time-frequency domain approach of the Maher-Finn model has been developed to estimate the fatigue life of risers subject to heave-induced vortex induced vibration, where a regular sinusoidal displacement is imposed at the top of the riser that induces non-repeating out-of-plane displacement (Maher and Finn 2000).

In this approach, the combination of platform and environment type induces a significant influence on the fatigue life of the riser. Heave-induced VIV phenomenon becomes more significant under the action of larger events; this rare condition should be accounted for in the fatigue analysis. One of the advantages of this model is that it can account for the varying nature of displacement amplitude, thus resulting in a more realistic prediction of the riser fatigue life (Maher and Finn 2000).

### **2.3.8. The Ferrari-Bearman Model**

As a rational approach towards the fatigue life prediction of riser structures, the VIV-induced fatigue damage should be combined with damage caused by all other sources. However, the methods for combining the fatigue damages caused by various sources are not clearly specified in design standards. From a practical point of view, two approaches are being used for calculating the VIV and wave induced fatigue damage in risers (Serta *et al.* 2000):

In the first approach, fatigue damage from each source is calculated separately and then superimposed to establish the total fatigue damage. In this approach, all loads are assumed to be totally uncoupled, which does not seem to be a realistic assumption. In the second approach, fatigue damage is calculated directly from the resultant stresses of all cyclic loads.

In the conventional riser fatigue analysis, the VIV analysis is a different step in the design process. Direct action of waves is then taken into account and its related fatigue damage is calculated using a commonly used method. This simplified approach may overestimate the VIV fatigue damage. In such an approach, neither of the above-mentioned strategies is used (Serta *et al.* 2000). In the approach proposed by Ferrari and Bearman, the in-line and cross-flow forces are simultaneously taken into account for the calculation of the applied forces by using the modified Morison's equation (Serta *et al.* 2000). Using such approach, VIV analysis becomes an integral part of the fatigue analysis as opposed to being a separate step in the design process. The results from this model have been reported to be in good agreement with those from the SHEAR program explained earlier, and has shown a good potential for fatigue calculation of riser structures.

### **2.3.9. Fracture Mechanics Approach**

The fracture mechanics approach is based on modeling the crack propagation of a surface flaw as it gradually progresses through the thickness. Figure 2.2 shows three modes of fracture, from which, mode-I would be the most significant and probable mode in riser

structures. In this approach, the stress at the crack tip cannot exceed over a certain value, which corresponds to the plastic deformation of the material. The crack is assumed to start extending through the material when stresses and strains at the crack tip reach a threshold value  $K_{th}$ . Brittle fracture is expected when  $K_I$  reaches the fracture toughness of the material (Lyons *et al.* 1994):

$$K_{Ic} = \sigma_c \sqrt{\pi a} \quad (2.11)$$

where  $a$  is the crack half length and the fracture stress  $\sigma_c$  is the far-field stress.

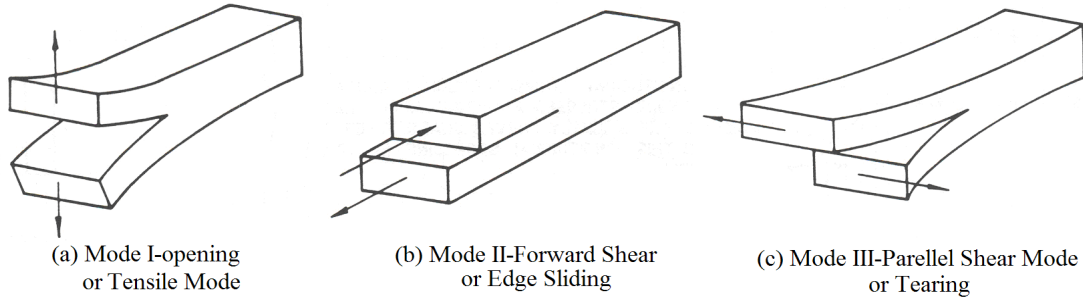


**Figure 2.2.** The three modes of fracture (Lyons *et al.* 1994)

For cases with constant amplitude loading scenarios, both the fatigue and crack growth rate are dependent on the range of the stress intensity factor  $\Delta K = K_{max} - K_{min}$  (Lyons *et al.* 1994). In such loading scenarios, the central portion of the graph of the fatigue crack growth rate versus  $\Delta K$  would be significant, thus describable by the Paris equation as presented earlier.

For a fracture mechanics analysis, an equivalent surface flaw may be used as the basic assumption for the crack's geometry. This would usually be in the form of a part-through circumferential crack originating from the outer diameter of the riser. The stress intensity factor calculation should consider both the tensile and bending stresses. However, for cases where the type of stress is not specified, this factor may be calculated by (Landes *et al.* 2001):

$$K = \sigma \sqrt{\pi a} F_{pt}(a/c, a/t) \quad (2.12)$$

where  $\sigma$  is the combined tension and bending stress and  $F_{pt}$  is a geometry factor. This tension solution formulation has been proposed assuming that a crack propagates due to an initial defect at the outer diameter of the riser. This approach has been used for calculating the fatigue of a typical riser, assuming an initial defect depth varying from 0.05 to 0.1 inches and applying one cycle at a time and evaluating the expected crack growth. This growth has been calculated at the deepest point of the crack and at the surface extremes for the surface flaws. Adding the growth to the existing crack size would result in new crack depth and surface length. Based on the new calibration factors and the stress cycle,  $\Delta K$  would then be recalculated and crack length and shape would be modified accordingly. This is an iterative procedure conducted for all cycles to come up with the riser's fatigue life, which is taken at the condition when the riser leaks (Landes *et al.* 2001). A study was conducted to investigate a total of four crack growth rates, the calculation of the associated failure time, weld geometry mismatch and the sequence of the application of loads, leading to the following conclusions (Landes *et al.* 2001):

1. The initial defect size greatly affects the fatigue life. This influence can be more than an order of magnitude when the defect size is increased by a factor of two.
2. In many cases, the actual data are extrapolated, which may result in incorrect fatigue life prediction. Using  $\Delta K_{th}$  has been shown to be more beneficial for small initial defect sizes than that for large defect sizes.
3. Unlike the loading history, the sequence of the loading cycle does not make much difference on the fatigue life when the growth is accumulated following a linear trend. More research is required to study the influence of loading sequence for cases where the delay in crack growth from an overload is considered.

Due to the existence of a wide range of parameters influencing crack growth, and the associated difficulties in accounting for such parameters, the fracture mechanics approach is not widely used by design engineers for fatigue life prediction of riser structures. The use of the finite element method has been suggested for predicting the fatigue life of those welded joints that do not follow existing S-N curves (such as the cases with weld discontinuity or parent material component containing a flaw).

Due to the changes in environmental conditions and the uncertainties in VIV phenomenon, variable amplitude loading scenarios seem to be a more realistic assumption for fatigue life prediction of risers. In a study conducted by Taheri *et al.* (2002), various methods for fatigue crack growth under both constant and variable amplitude loadings were studied and the results were verified against experimental test results. It was concluded that the rainflow counting method could effectively represent the crack growth behavior.

As briefly studied earlier, the Paris model, which is widely used for fatigue life prediction of riser structures, is only valid for the middle range portion of the fatigue crack growth diagram, and does not consider the effect of stress ratio. In other words, a family of straight lines parallel to each other should be produced for various stress ratios (Taheri *et al.* 2002). In some of the commonly used fatigue models that account for the stress ratio (e.g. the Foreman model), the influence of variable amplitude load interactions is not accounted for. Such models are, however, used to determine the average fatigue crack growth rate by introducing an equivalent constant amplitude loading resulting from the variable amplitude one, resulting in a reasonably accurate predictions for a large number of closely spaced random cycles (Taheri *et al.* 2002).

Moreover, Rushton and Taheri (2003) also investigated the effects of tension overload or compression under-load, under which a considerable influence on the fatigue crack growth rate was observed. In their investigation, the over-loads were applied at a specified crack length. Figure 2.3 shows the difference between the fatigue rate curves for constant and variable amplitude loading scenarios, compared against the typical distribution of experimental test results (Ruston and Taheri, 2003). It was observed that the variable amplitude fatigue crack growth rate showed a sudden increase due to the application of the over-loads, and then the rate would decrease by an amount dependent on the magnitude of the over-load. The figure also illustrates a significant phenomenon in the crack growth rate due to application of the over-loads. The observed retardation is of particular interest, especially with regard to the varying nature of loading conditions that are imposed on riser structures from the environment. The considerable resultant magnitude of tension over-load and/or compression under-load significantly affects the fatigue life of the system.

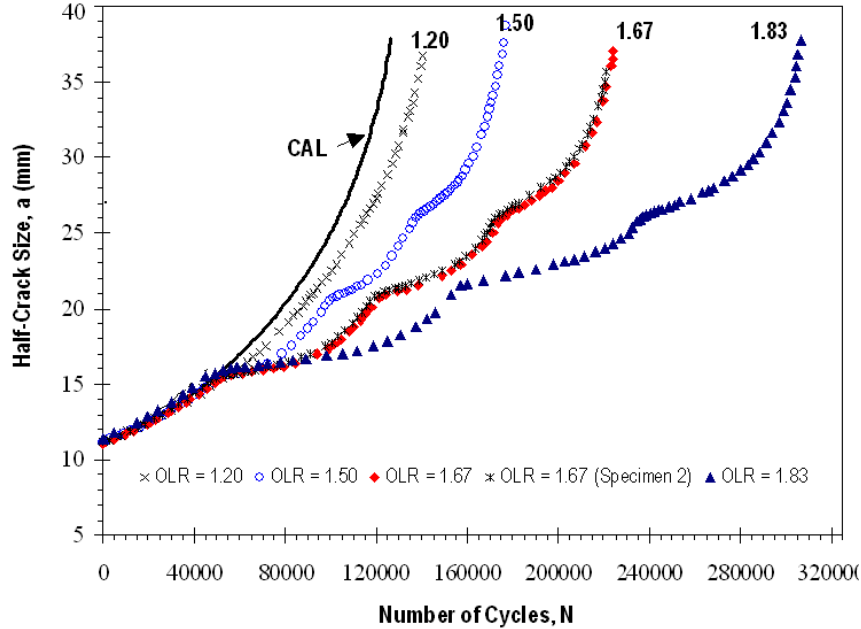


**Figure 2.3.** Influence of OLR on the a-versus-N Curve at stress ratio  $R = 0.1$  (Rushton and Taheri, 2003)

It was also shown that the use of a constant amplitude model could not adequately predict the crack growth rate even due to application of a single tensile over-load. The error margin increases as the number and magnitude of the over-load increase (Taheri *et al.* 2002).

While crack growth retardation increases exponentially with increasing over-load ratio, the application of compressive under-load accelerates the crack growth rate, with a trend that is usually less than the retardation due to an equivalent tensile overload. Since the overload-induced retardation dominates crack growth behavior, the underload-induced acceleration is usually neglected. Rushton and Taheri (2003) observed that when the tensile over-load is followed by a compressive under-load, the retardation rate would increase, but would not eliminate the crack growth. Moreover, the retardation would be almost negligible when the tensile over-load is followed by an immediate under-load. The ratio between the over-load and under-load could be used to quantify this retardation,

with greater retardation for higher ratios (Rushton and Taheri 2003). More recently, Yuen and Taheri (2005) proposed a number of modifications to the Wheeler fatigue crack retardation model. The modifications allow the model to account for the delay in retardation due to applied overloads, the initial crack growth acceleration immediately following an overload, the overload interaction and the net section yielding effect observed in the fatigue crack growth retardation behavior of many materials.

Since the riser structure is under the action of different environmental forces, the varying nature of the load becomes more pronounced. In other words, any sudden change in the VIV characteristics due to surrounding current profile may cause significant changes in the loading history, which in turn creates significant errors in the predicted fatigue life. This shows the importance of the need for an in-depth study on the fatigue response of riser structures under more realistic loading conditions, thereby focusing on the examination of the performance of the available various fatigue models applicable to random loading. A more rational approach for assessing fatigue life of riser structures should also consider random fatigue analysis models; however, the computational time and effort that is required for such analysis may prevent its application to every-day design purposes.

## **2.4. The Influence of Compressive Stresses**

The fatigue crack growth rate of a material depends on many factors such as the stress amplitude, the stress ratio and the nature of the applied load. Most models have been developed for a specific application and incorporate certain main parameters. One of the major influencing parameters is the load history. The early tests on fatigue of materials have been done for Constant Amplitude Loading (CAL) scenarios, and there exist many fatigue models for predicting the fatigue life of a structural component under such loading conditions. In a CAL, the loading is applied as a sinusoidal stress-time history pattern of constant amplitude and fixed frequency. In recent decades, however, more tests have been done on fatigue life of materials under VAL scenarios.

One of the frequent approaches for conducting fatigue tests on materials under VAL is to add a few tensile overload or compressive underload stress spikes to the CAL. This approach has helped the researchers gain fundamental understanding of how stress fluctuation in a VAL affect the fatigue life of materials. It has been demonstrated that any sudden change in the stress intensity factor range could result in substantial changes in the FCGR of materials. The early research in this area goes back to the 1970s, when tensile overloads were observed to result in significant retardation in crack growth rate (Jones and Wei 1971). It is now well-understood that the application of a tensile overload creates residual compressive stresses in a region just beyond the crack tip, which retards the crack growth (Taheri *et al.* 2002; Yuen and Taheri 2005). The compressive stresses, on the other hand, accelerate the fatigue crack growth by limiting the influence of residual compressive stresses created by the tensile overload (Taheri *et al.* 2002; Rushton and Taheri, 2003 and Yuen and Taheri, 2005).

In the classical theory of fracture mechanics and fatigue, the influence of the compressive portion of the stress-time history is completely ignored. In other words, the compressive stress cycles (CSC) are assumed to have no influence on the fatigue crack growth rate (FCGR) of materials. This theory is based on the fact that under a compressive loading cycle, the crack is fully closed and no stress concentration occurs at the crack tip. Therefore, the crack is believed not to grow when it is subjected to a compressive stress. As also explained earlier, the crack growth retardation imposed due to a tension overload is usually larger than the acceleration produced by a compression underload. Since the tension overloads usually dominates the crack growth behavior, the presence of compression underloads is usually ignored.

Ignoring the compressive portion of the stress-time history is widely accepted in both academia and industry. Once the compressive portion of the stress-time history is ignored, one may use any appropriate fatigue model to calculate the fatigue life of the component. Based on such an approach, the stress intensity factor range is considered to only cover the tensile portion of the stress-time history. In other words, the stress intensity factor range is assumed to be equal to the maximum stress intensity factor for each cycle (applicable for  $R \leq 0$ ).

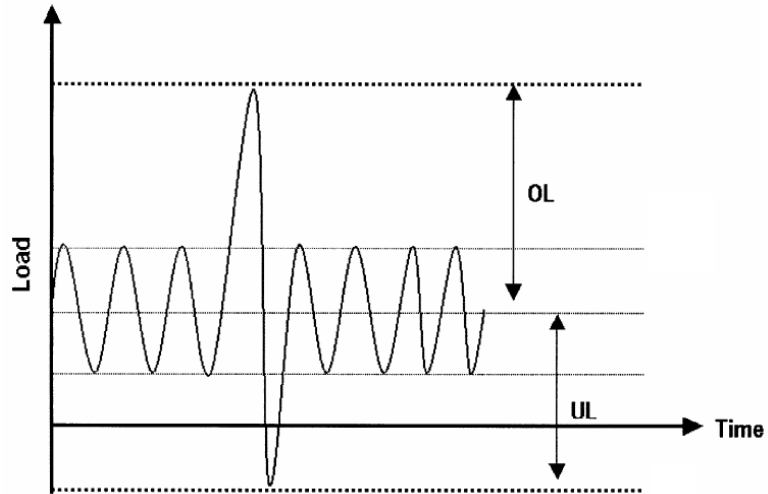


Ignoring the presence of the CSC is even recommended by many design guidelines and standards. For example, ASTM E647-95a suggests that the compression portion of the stress cycles could be ignored. The presence of such recommendations in design guidelines has motivated the designers to completely ignore the presence of the compressive portion of stress-time histories when evaluating the FCG of engineering components.

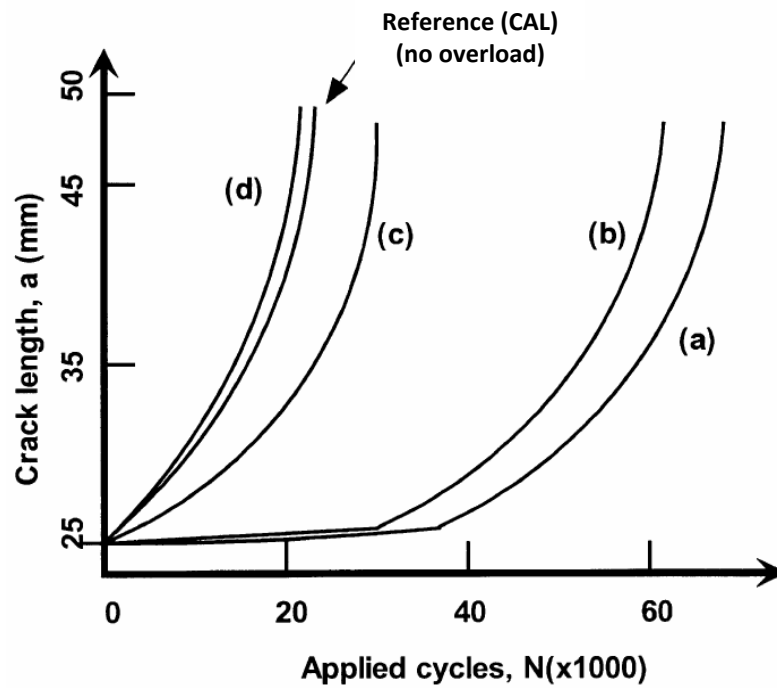
Although the influence of CSC on FCGR of materials have been demonstrated since a few decades ago (e.g. Suresh 1985; Fleck *et al.* 1985), the research in this area has not received much attention. It should be noted that only a few recent works address this issue and present the data that clearly demonstrate the substantial influence of CSC on the crack growth rate (Silva 2005; Shabanov 2005 and Silva 2004).

Figure 2.4 shows a schematic load history with a tension overload and compression underload. Figure 2.5 shows the typical influence of different combination of tension overloads and compression underload on the fatigue crack growth of materials. Five different cases are presented in this figure:

1. Reference Case: a CAL is applied to the specimen (without any tension overload or compressive underload,
2. Case a: a tension overload is applied within CAL,
3. Case b: a compression underload is applied followed by a tension overload within CAL,
4. Case c: a tension overload is applied followed by a compression underload within CAL,
5. Case d: a compression underload is applied within CAL.



**Figure 2.4.** Schematic illustration of tension overload and compression underload (Hudson 1981)



**Figure 2.5.** A typical crack growth behavior for (a) tension overload, (b) compression underload followed by tension overload, (c) tension overload followed by compression underload, and (d) compression underload (Hudson 1981)

As observed in this figure, the application of a tension overload significantly increases the fatigue life of the material (compare Case 'a' with the Reference Case), while a compression underload decreases its fatigue life (compare Case 'd' with the Reference Case). It was also demonstrated that the compressive underloads immediately following a tensile overload has a significant influence on reducing the amount of crack growth retardation due to the tensile overload. Such variation in the crack growth rate is due to crack tip plasticity, residual stresses, and inverse yielding at the crack tip (Broek, 1988). The tensile overload increases the extent of residual stress and the size of the plastic zone ahead of the crack tip. This is usually quantified using the Overload Ratio (OLR), which is the ratio of the peak overload stress to peak stress as measured from the mean stress under 'normal' conditions.

Figure 2.6 shows the formation of the overload-induced plastic zone ahead of the crack tip. The dashed lines show the limits of bean-shaped Irwin plastic zone and the von Mises plastic stress.

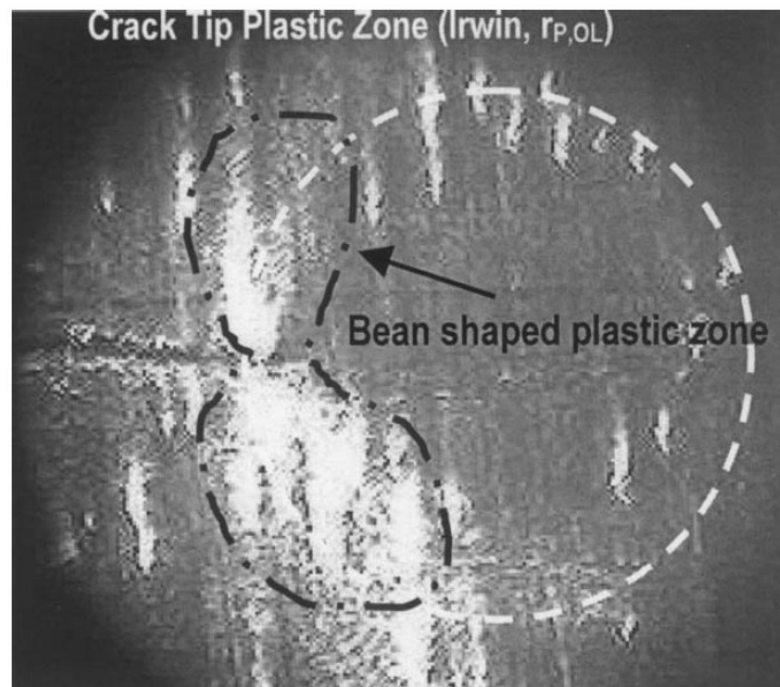


**Figure 2.6.** Formation of the crack tip plastic zone (Rushton and Taheri 2003)

Experimental data has demonstrated that the crack growth retardation increases exponentially with increasing overload ratio (Rushton and Taheri 2003). If the compression underload is followed by a tension overload, the increase in the fatigue life is slightly lower than the case where only a tension overload is applied. It is also observed that the relative ‘position’ of tension overload and compression underload (e.g. which one is applied first) has a significant influence on the crack growth rate of the material. This is shown by Cases b and c in Figure 2.6.

The crack growth acceleration mechanism due to compression underload is illustrated in Figure 2.7, which shows the crack tip under cyclic compressive loading. The solid line in this figure shows the crack at the end of the application of compressive stresses of the cycle, when a plastic zone is formed at the crack tip. The dashed line shows the crack at the end of the unloading stage, when the compressive stresses are removed. At the end of this unloading stage, the size of the plastic zone is reduced, and the material inside this zone is in tension. In the next loading cycle, the plastic zone is shifted (in the direction of crack propagation) and restores to its original size at the end of the loading stage of the previous loading cycle. The dotted line shows the crack at the end of the loading stage of the next cycle, when the crack tip reaches point 2 (Shabanov 2005).

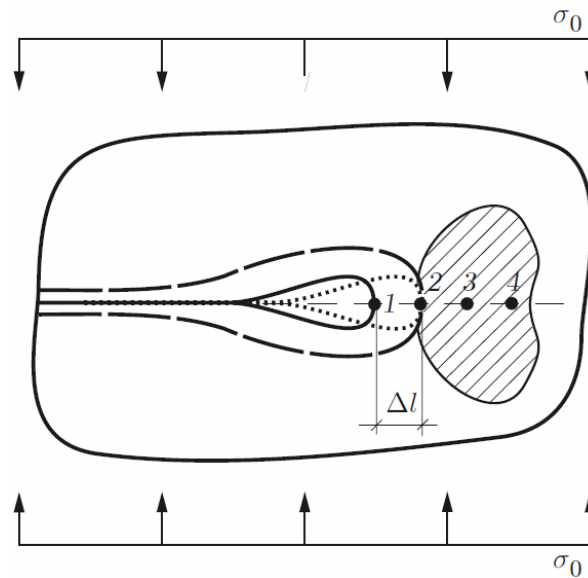


**Figure 2.7.** The crack tip under cyclic compressive loading (Shabanov 2005)

The scarcity of experimental data in relation to the influence of compressive stresses on the crack growth rate of materials has prompted the researchers to pay more attention to the presence of compressive stress in a given cyclic loading scenario. Several researchers have studied the influence of single tensile overload or compressive underload stress spikes on the FCG of materials (Sadananda *et al.* 1999; Taheri *et al.* 2002). Different materials have been tested by different researchers, and it is demonstrated that the influence of the compressive loadings is different from one material to the other (Silva 2005). Moreover, it has been demonstrated that even under fully compressive alternating external loading conditions, a fatigue crack could be initiated and grow nearly to failure (Newman *et al.* 2005; Kasaba *et al.* 1998; Hermann 1994; Vasudevan and Sadananda 2001). This is believed to be due to the tensile residual stress field that could be produced by the application of excessive compressive pre-loads. In such cases, the crack would grow under full compressive load, with a decreasing trend in the growth rate, until crack arrest occurs.

It has also been observed that under a VAL scenario, the crack growth is a function of the stress amplitude, the stress ratio and the nature of the stress-time history (Iranpour *et al.* 2008). This complexity has resulted in the development of numerous models over the past decades; however, there exists no universal model that could predict the FCG under such realistic loading scenarios. Indeed, most of the available models have been mainly developed for a specific case or application, incorporating some of the main influencing parameters (see for example Taheri *et al.* 2002). Furthermore, a majority of the available studies have focused on understanding the fundamentals of the crack growth retardation or acceleration mechanism resulting from the application of a single (or a few) tensile overload(s) and compressive underload(s). A real life VAL usually contains a large number of tensile or compressive stress peaks (see Iranpour *et al.* 2008). Even a ball-bearing, which is generally considered as the best example of a component under a constant amplitude loading scenario, would be essentially subject to a variable amplitude stress-time history during its service life. Therefore, it would be more realistic to study the influence of compressive underloads by conducting experiments on specimens under a VAL stress-time history.

The major reasons that the focus of the previous studies has been basically on CAL with inclusion of a few single tensile overloads or compressive underloads are:

1. In general, a CAL scenario with only a few stress spikes provides the researcher with a very convincing set of data by which the influence of a stress spike can be easily highlighted. This also facilitates the understanding of the underlying physics of the crack growth and the associated retardation/acceleration mechanisms.
2. Furthermore, in comparison to VAL scenarios, conducting an experiment with a CAL scenario is much easier, and the test results can be easily analyzed and interpreted. Moreover, subjecting a specimen to tension-tension loading cycles require no anti-buckling device, which in turn makes the test setup simpler. In addition, there would be less chance of slippage or misalignment in a test with tension-tension CAL. The other factor that has basically confined researchers to CAL tests is the requirement for specialized software for controlling the test machines, in order to impose VAL loading scenarios (often an expensive option).

The influence of a single overload or an underload stress spike is well documented for a wide range of materials. However, some researchers have demonstrated that the retardation effect experienced after a number of consecutive tensile overloads would be larger than that observed after only a single overload. This has been explained to be due to the adaptation of material's yield surface to the tensile overloads (Prommier, 2003). In general, however, the combined effect of the overload and underload on the subsequent stress spikes generates a complex influence on the crack growth rate, mainly depending on their sequence and other dominant mechanisms. It should also be noted that almost all the available studies investigating such an influence have mainly considered CAL scenarios with positive stress ratios (Silva 2005; Taheri *et al.* 2002); in other words, there is a clear lack of data in consideration of the influence of overload/underloads and the CSC in loading scenarios with negative stress ratios. As a result, more works on this area have been pursued in recent years (see for example, Silva 2005; Shabanov 2005; Iranpour and Taheri 2007.)

In this research program, several VAL stress-time histories are used to study the influence of compressive stresses on fatigue crack growth. The scenario is typical of the loading scenario that is experienced by a structural component that is subjected to flow of air or fluid (such as pipelines under ocean current profiles or wings of an aircraft). Some recommendations are offered for improving the accuracy of fatigue life prediction of components under VAL scenarios, by focusing on the CSC.

### 2.4.1. Two Parameter Driving Force

It has been shown by many researchers that the fatigue damage of materials can be calculated using a two parameter driving force (Noroozi et al. 2005; Vasudevan and Sadananda 2001). These driving forces are the stress intensity factor range,  $\Delta K$ , and maximum stress intensity factor,  $K_{\max}$ , explained earlier. For a fatigue crack to grow through the material, these two driving forces need to act simultaneously. As shown in Figure 2.8, there exist two threshold values, namely  $K_{\max}^*$  and  $\Delta K_{th}^*$ , which represent the upper and lower limits, respectively. In this figure, the plateaus show the critical threshold values for both  $K_{\max}^*$  and  $\Delta K_{th}^*$ . Therefore, the total crack-tip driving force for both  $\Delta K$  and  $K_{\max}$  must exceed the threshold values of the two parameters in order for a crack to advance. The load ratio,  $R$ , is calculated as  $R = K_{\min} / K_{\max}$ .

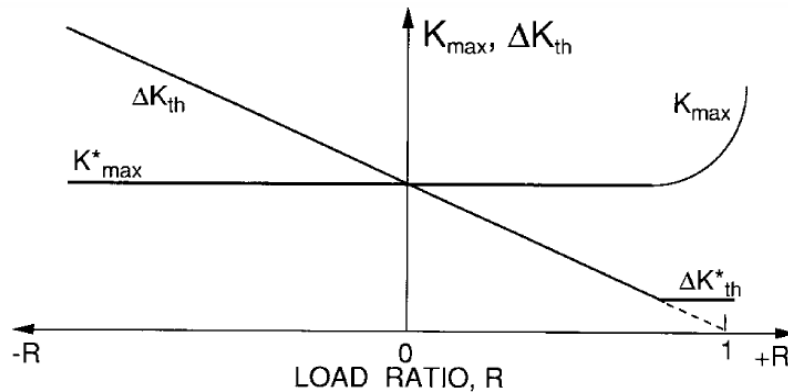


**Figure 2.8.** Schematic illustration of threshold variations with load ratio (Vasudevan and Sadananda 2001)

Figure 2.9 shows the typical variation of  $da/dN$  versus  $K_{max}$  and  $\Delta K$ , for decreasing and increasing load ratios, respectively. As observed, the crack growth rate merges at the lower and upper end of load ratio,  $R$ , which shows the limiting condition of the two driving forces. Such trends are a result of the internal stresses and due to their additional contribution to the driving force,  $K_{max}$ , which either retards or accelerates the crack.

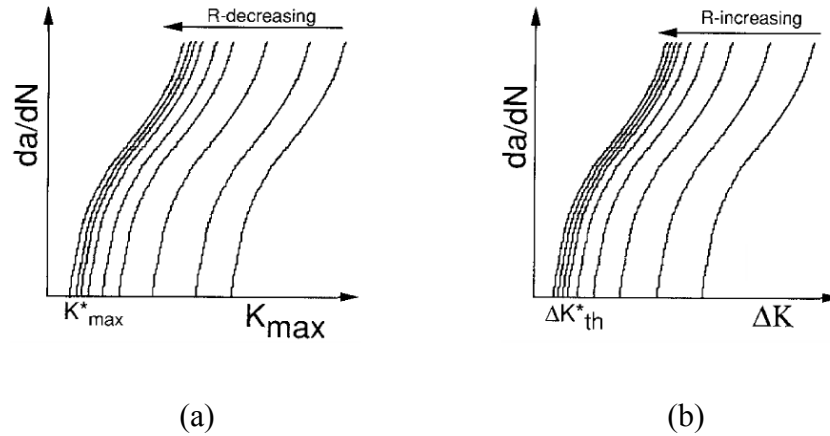


**Figure 2.9.** Schematic illustration of (a) variation of  $da/dN$  versus  $K_{max}$  with decreasing load ratio  $R$ , and (b) variation of  $da/dN$  versus  $\Delta K$  with increasing load ratio  $R$  (Vasudevan and Sadananda 2001)

Noroozi *et al.* (2005) studied the influence of the mean stress and applied compressive stress on FCG using an elastic-plastic crack tip stress-strain history. Their study demonstrated that the FCG was controlled by a two parameter driving force, which was a function of the total maximum stress intensity factor and total stress intensity range. In their investigation, the difference in the stress-strain concentration at the crack tip associated with the compressive part of the loading cycle was taken into account. This was done using two different approaches; one accounting for the tensile part and the other accounting for the compressive part of the load history. This was done based on the assumption that the stress response at the crack tip to a tensile loading cycle (with no contact between the crack surfaces) would be different from that experienced under compression (Noroozi *et al.* 2005). In a recent study on aluminum alloy 7075-T6, Noroozi *et al.* (2008) demonstrated that the detrimental effect of the compressive part of



a loading cycle can be taken into account using a two-parameter driving force, combining the effects of the maximum stress intensity factor and the stress intensity range.

Mikheevskiy and Glinka (2009) studied the load-interaction effect under variable amplitude loading scenarios, focusing on the residual compressive stresses produced by the reverse plastic deformation in the crack tip region. It was observed that the FCG rate depended on both the residual stresses produced by the previous loading cycle and all the stress fields generated by the previous loading history. Their study suggested a procedure for combining the residual stress fields generated by all the preceding loading cycles into a single resultant minimum stress field, which would affect the current fatigue crack growth rate. Their experimental results supported their proposed fatigue model for simulating the load–interaction effect for a variety of variable amplitude loading spectra.

In a study by Kujawski and Stoychev (2010), it was shown that the compressive loads decreased the fatigue life of their test specimens by about 300%, and that the influence of the compressive loads was just as important as that of the tensile overloads. Their study demonstrated that the influence of the compressive loads in a load spectrum on the fatigue life was equivalent to a 34% increase in the applied load. Their study concluded that the role of compressive stress cycles are very important when considering spectrum loading, and that the resulting effect cannot be accounted for using the ASTM recommendation for treating constant amplitude loading, by which the stress intensity factor range is assumed to equal the maximum stress intensity factor due to the positive load ratios.

The two-parameter approach stated above has also been applied and verified by several researchers. For instance, in a study conducted by Toribio and Kharin (2009), it was demonstrated that the influence of loading on FCG (including crack closure), can be related solely to the stress-strain field ahead of the crack tip, with no contribution from that present behind the crack. The stress-time history applied to a material affects the internal stress under either tension or compression loading. This concept is later used in this research program to calibrate the finite element analyses results with those from experiment to further investigate the stress field around the crack tip.

### 2.4.2. Fatigue Crack Closure

Since Elber (1970) explained the importance of crack closure on the crack growth rate, many investigators have conducted research in this area with the aim of better understanding the crack closure phenomenon and its influence on fatigue of materials. Elber noted that the fatigue crack surfaces interfere with one another through a closure mechanism. This closure mechanism may be altered by different factors such as the roughness of the crack surface or the presence of residual plastic deformation left behind the crack tip. In general, four major crack closure mechanisms have been introduced (Barsom and Rolfe 1999):

1. Plastically-induced crack closure (PICC), resulting from the presence of residual plastic deformation left in the wake of the crack
2. Roughness-induced crack closure (RICC), resulting from deviations of the crack trajectory associated with micro-structural characteristics of the material such as grain size and inter-lamellar spacing
3. Mode II-induced crack closure (MII-ICC), caused by the displacement of the crack tip along the shear planes, which prevents a perfect match of the fatigue-crack surfaces features left behind the propagating crack, and
4. Environmentally-induced crack closure (EICC), resulting from corrosion products within the crack surfaces that wedge the surfaces

Figure 2.10 shows a schematic illustration of the four crack-closure mechanisms.

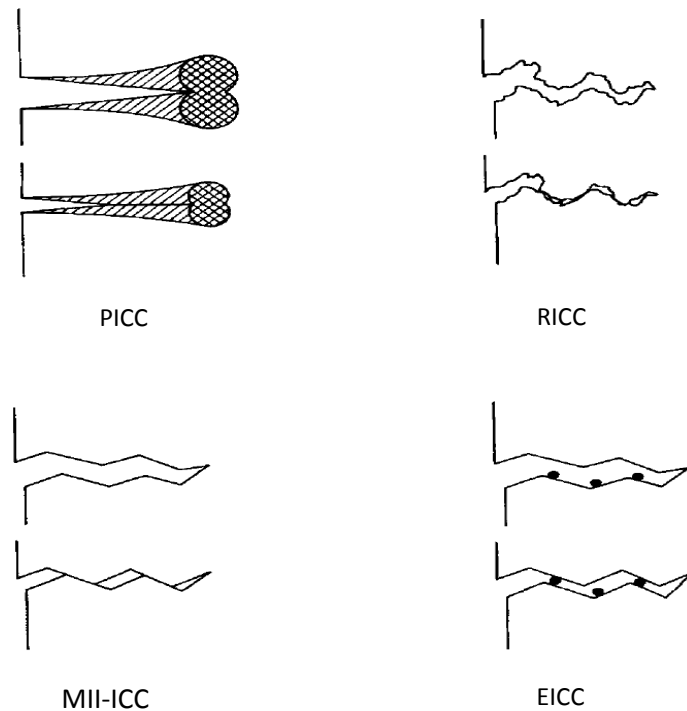


**Figure 2.10.** Schematic illustration of four crack-closure mechanisms  
(Barsom and Rolfe 1999)

The crack closure concept studies the fatigue process based on what happens behind the crack tip. In recent years, researchers have studied the relationship between the influence of CSC and the crack growth rates, with focus on the closure effects (Pommier 2003; Silva 2004 and 2005). Among all the mechanisms resulting from crack closure studied earlier, the PICC and RICC are known to be most important in explaining the influence of CSC on the crack growth rate of materials (Silva 2005). The influence of RICC was first noted by Walker and Bevers (1979). The influence of the load interaction effects and plastic-induced compressive stresses was first studied by Schijve (1962) and later by Jacoby (1966). Their work demonstrated that FCG retardation (or acceleration) was governed by the compressive stress gradient ahead of the crack tip.

In this research, the influence of RICC on FCGR of aluminum alloy 6061-T651 was studied, as will be explained in subsequent chapters. The roughness measurements were done according to standard DIN 4768, using laser profilometry and 3D microscopy

techniques. The Arithmetic Mean Deviation of the roughness profile,  $R_a$ , is usually calculated to quantify the roughness of the fracture surface by the following equation:

$$R_a = \frac{1}{l_m} \int_0^{l_m} z dx \quad (2.13)$$

where  $z$  is the value of surface profile and  $l_m$  is the reference length.

Silva (2005) studied different materials to show their FCGR sensitivities to surface roughness. The materials studied were low carbon steel Ck45, aluminum alloy Al7175 and titanium alloy Ti6Al4V. Figure 2.11 shows the roughness values for tests with ( $R = -1$ ) and without compression ( $R = 0$ ) for the same  $K_{max}$ . In general, FCG in aluminum alloys and titanium alloys are considered to be sensitive to RICC, while that of steel alloys is more dependent on the PICC (Silva 2005). It has been demonstrated by Silva (2005) that the closure concept is not adequate to properly describe the FCGR at negative stress ratios ( $R < 0$ ). The influence of the closure concept is studied in this research in subsequent chapters, and the findings from experimental results on an aluminum alloy are discussed in detail.

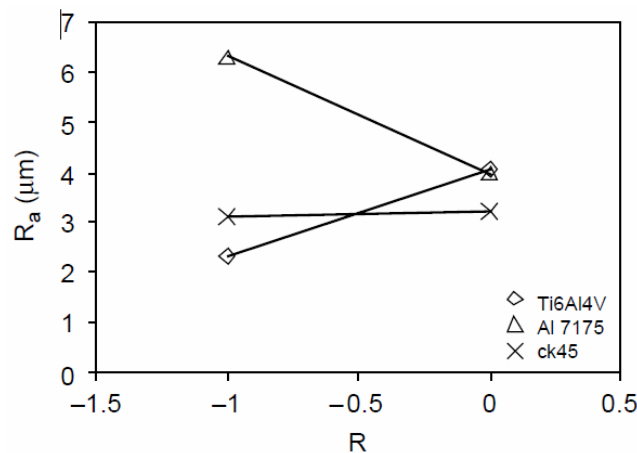


**Figure 2.11.** The roughness values for tests with ( $R = -1$ ) and without compression ( $R = 0$ ) for the same  $K_{max}$  (Silva 2005)

As it is explained in the subsequent chapters of this research, the increase in the crack growth rate due to introducing the compressive stresses (for Aluminum alloy 6-61-T651) is not because of the decreases in the surface toughness and RICC. This verifies with the results reported by other researchers, demonstrating that in stress-time histories that include CSC, roughness effect is not the dominant mechanism resulting from the crack closure (Chen and Lawrence 1997; Silva 2005).

## **2.5. Summary and Conclusion**

This chapter provided a brief insight into the overall direction of this dissertation and a review of the literature. Some of the methods available in literature for predicting the fatigue life of risers subject to VIV were briefly reviewed, and their capabilities were compared. As explained in detail, most of the researches done on the fatigue characterization of pipelines and risers have focused on the VIV analyses of the task, and less attention has been paid to the fatigue life estimation using various models once the VIV-induced stress-time history is known.

During the initial stages on this research project, it was observed that most of the differences in the fatigue life estimation of pipelines and risers were a result of using different approaches for calculating the VIV-induced stress-time history. Therefore, the author decided to use real VIV-induced stress-time histories for all the fatigue studies performed during this research project. As it is explained later in Chapters Two and Three, the input VIV data were obtained from external sources (MIT and MUN). This approach eliminated any uncertainties in the outcome of this research project that could otherwise have been raised from using numerical or computational methods to calculate the VIV-induced stresses.

As explained earlier, each chapter of this dissertation is a paper that has been published or is currently under review for publication. Therefore, each chapter is a stand-alone document, which explains its overall objectives followed by a detailed problem definition and literature review. The reader is encouraged to refer to each chapter for an

in-depth review of the literature associated with the specific topic covered by each chapter.

## **Chapter 3**

### **A Study on Crack Front Shape and the Correlation between the Stress Intensity Factors of a Pipe Subject to Bending and a Plate Subject to Tension**

Mohammad Iranpour and Farid Taheri

Department of Civil and Resource Engineering, Dalhousie University, 1360 Barrington Street, Halifax, Nova Scotia B3J 1Z1, Canada

Published in the Journal of Marine Structures, 2006, vol. 19, pp. 193-216

#### **3.1. Abstract**

The use of a pipe subject to bending moment with an equivalent plate subject to tension has been tried by a few researchers to avoid the complexity usually involved with experimental crack growth investigations of pipes with initial surface flaws. This approach also minimizes the use of more sophisticated monitoring instruments, thereby offering significant cost savings. This equivalency has been done for both experimental and finite element investigations. This paper studies the validity of this approach and evaluates the ranges of the crack depth ratio and elliptical crack diameter ratio for which this approach would be admissible. A series of finite element analysis was carried out to both verify the values of the stress intensity factors reported in the literature, and verify the results of the interpolation function used in the computational simulation in this research. Based on the computational simulations and demonstrating that the crack front follows a semi-circular shape during its growth, a dimensionless relationship between the stress intensity factor of a pipe under bending moment and that of a plate under pure tension has been introduced. A series of experimental investigation was performed to verify the validity of the proposed computational simulation. The results show the

rationality and admissibility of this approach when considering the fatigue crack growth of pipes under bending.

**Keywords:** equivalent stress intensity factor, semi-circular crack, simplified method, finite element analysis.

### **3.2. Introduction**

As a part of widely used experimental test setup for fatigue crack growth studies of a plate under axial load, most researchers use a traveling microscope to measure the incremental fatigue crack growth. Using this technique, the crack tip propagation can be monitored during the test. However, monitoring the fatigue crack propagation of pipes under any type of loading conditions requires more advanced techniques and sophisticated and expensive instruments. The complications arise from the three dimensional nature of the part-through surface cracks (Cai and Shin 2005). The electromagnetic monitoring technique has shown to be accurate within  $0.03 - 0.17\text{mm}$  (Saka *et al.*, 1997). More sophisticated methods, such as the Confocal Scanning Laser Microscopy, are able to measure cracks as small as  $10 - 100\mu\text{m}$  (Varvani-Farahani and Topper, 1997). Methods based on Potential Drop (PD) use the direct and reversing currents to give real time measurements. However, different crack shapes and crack depths may produce the same potential drops. Therefore, multiple probe sites are required to monitor the crack front propagation, which makes it even more expensive and susceptible to electromagnetic and other interferences (Cai and Shin, 2005). Moreover, it is often difficult to place the instrumentation in the small region surrounding the initial flaw. In recent years, many researchers have used Crack Microgauges to monitor the growth of the fatigue crack during the experimental tests (Lugg, 1992; Bian and Taheri, 2006). However, the cost of such an instrument is high. Therefore, the researchers have been encouraged to seek simplified, yet accurate alternative test procedures. One such approach has been testing a plate under axial load in place of a pipe under bending moment (Chen and Lambert, 2005).



In this research, the admissibility of testing a plate under the action of pure axial force in place of a pipe under the action of pure bending moment is investigated. Consideration has been given to the fact that the bending moment causes equivalent, but varying axial stresses in the pipe's wall thickness. This equivalency is based on the stress intensity factor concept, by which the crack tip condition can be characterized in linear elastic materials. A comparison between the stress intensity factor of a pipe under bending moment and a plate under tension would reveal the validity of the approach. In this study, the focus is on the surface cracks with a crack plane normal to the internal stresses resulting from the externally applied loads. As supported by the finite element analysis results, the fatigue crack in a pipe under pure bending and a plate under tension will only grow under mode I. That is because the mode II and III stress intensity factors would be zero. The following relation between stress,  $S$ , and stress intensity factor,  $K$ , shows that a cyclic variation in stress would result in a variation in the stress intensity factor:

$$K = S\phi\sqrt{\pi a} \quad (3.1)$$

where  $S$  is the nominal stress normal to the crack,  $\phi$  is a dimensionless geometric parameter, (i.e. function crack length to specimen width ratio); and  $a$  is the crack depth. Based on the similarity rule, different combinations of the applied stress and crack lengths could result in the same amount of crack propagation if the magnitude of the stress intensity factor is equal for the different combinations of loading and geometry (Liu 1998). In other words, having the same magnitude of stress intensity would guarantee that a specimen with a short crack subjected to high stress levels would show the same crack growth as a specimen with a long crack under low stress levels. This would indicate that the stress intensity factor at crack tip is the controlling parameter for the rate of fatigue crack growth.

These facts were the motivation for conducting a comprehensive experimental and computational investigation for comparing the stress intensity factors of pipes subject to pure bending moment and plates subject to pure tension, in which various crack depth and width were studied. In this paper, the main focus would be on the surface cracks with an elliptical shape, which have been shown to be a common crack type in pipes that are

subjected to bending moments. This comparison has been based on either an analytical approach and/or finite element results that are available in literature. To verify the accuracy of the computational simulation that has been used to monitor the crack front shape during its propagation, a series of experimental investigations were conducted and the results were compared with those from the computational simulation. The outcomes show the validity of replacing a pipe subject to bending moment and a plate subject to tensile loads, and the conditions under which this approach would be admissible.

### 3.3. Plate under Pure Tension

Analytical expressions for stress intensity factors of plates with part-through elliptical cracks, as a function of the plate geometry and applied axial and/or bending stresses, are available in literature (Anderson, 1991). Several experiments have been conducted to establish the integrity of such analytical expressions. The expressions have also been verified by the finite elements method (Raju and Newman, 1979). In a study done by Lei (2004), a cracked plate was modeled and its J-integral was evaluated by built-in counter integration function of ABAQUS on 15 contours around the crack tip. The average of the J-integral values obtained on the 2<sup>nd</sup> to 15<sup>th</sup> contours was used to obtain the crack tip stress intensity factor. The results from this study verified the stress intensity factor solutions given by other researchers (Lei, 2004). The dimensionless expressions for calculating stress intensity factor for mode one elliptical surface flaw in a plate under tension is given by (Anderson, 1991):

$$K_{I,Plate}^* = K_{I,T}^* = \frac{K_{I,T}}{\sigma_T \sqrt{\pi a / Q}} F\left(\frac{a}{t}, \frac{a}{b}, \frac{b}{W}, \varphi\right) \quad (3.2)$$

where  $K_{I,Plate}^* = K_{I,T}^*$  is the dimensionless stress intensity factor of a plate under the action of pure tension,  $K_{I,T}$  is the stress intensity factor for mode one,  $a$  is the crack depth length at the deepest location of the surface flaw and  $\sigma_T$  is the far field tensile

stress. The terms  $Q\left(\frac{a}{b}\right)$  and  $F\left(\frac{a}{t}, \frac{a}{b}, \frac{b}{W}, \varphi\right)$  are introduced as a function of crack shape characteristics. The angle  $\varphi$  represents the orientation of the point along the crack front where the dimensionless stress intensity factor is being calculated. Other parameters are schematically shown in Figure 3.1. In this paper,  $a/b$  and  $a/t$  are referred to as the ellipse diameter ratio and the crack depth ratio, respectively.

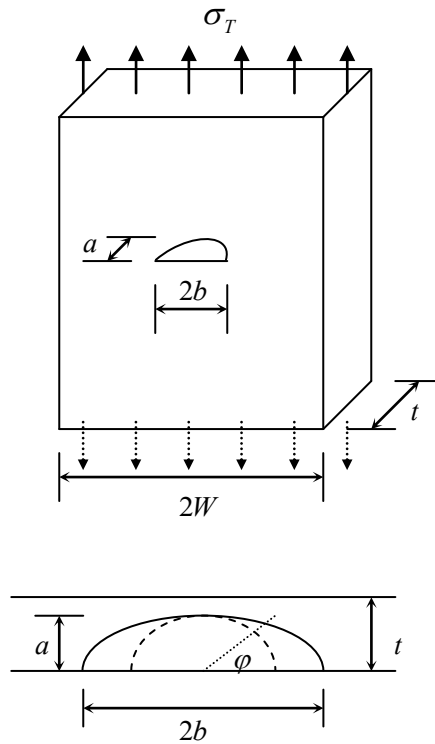


**Figure 3.1.** Stress intensity parameters for an elliptical surface flaw in a plate subject to tensile stresses

Using this formulation, the stress intensity factors were calculated for a wide range of ellipse diameter ratios and crack depth ratios. The results were further post-processed by a computer program and compared with those of an elliptical surface flaw of a pipe under the action of bending moment.

### 3.4. Pipe under Pure Bending Moment

Experimental studies have validated that an actual part-through crack in a wall thickness of a pipe may be replaced by an equivalent elliptical arc crack front. Although a great number of studies have been conducted in consideration of plates and solid bars having elliptical cracks, hollow circular cross sections require more attention. Several investigations have obtained numerical solutions for certain geometries of the cracked cylinders using either the finite element methods or boundary integral solutions (Tan and Shim, 1986). Such solutions require relatively large effort for the generation of the finite element mesh, as well as the solution. In later investigations, axisymmetrical through thickness stress distribution and global bending stresses with respect to two perpendicular axes in the prospective crack plane were also studied (Bergman, 1995; Carpinteri *et al.*, 2000). In a study performed by Carpinteri *et al.* in 1998, a series of three dimensional finite element analyses were carried out. They also proposed a two parameter theoretical model for calculating the stress intensity factor of hollow pipes under the action of bending moment.

Using the above theoretical model and the Paris-Erdogan law, it will be shown that different flaws in pipes with different geometries and initial crack configurations tend to follow a certain trend when considering the ratio of crack depth and pipe wall thickness. The finite element method will be used to validate the approach. Twenty-node isoparametric solid elements will be used for modeling the system, with the crack-tip stress square-root singularity modeled by shifting the midside nodes to quarter point of the element side and near to the crack front. Figure 3.2 shows the two parameter model for the crack front. The values for dimensionless stress intensity factor have been calculated and presented for two different ratios of 1.0 and 10.0 for pipe inner radius and wall thickness, based on the expressions developed by Carpinteri *et al.* (1998):

$$K_{I, Pipe}^* = K_{I, M}^* = \frac{K_{I, M}}{\sigma_M \sqrt{\pi a}} \quad (3.3)$$

where  $K_{I, Pipe}^* = K_{I, M}^*$  is the dimensionless stress intensity factor for a pipe under pure bending moment,  $K_{I, M} = \sigma_{Z, M} \sqrt{2\pi r}$  is the stress intensity factor for bending, where  $\sigma_{Z, M}$

is the opening normal stress at the distance  $r$  evaluated perpendicular to the crack front. When the distance  $r$  approaches zero, the maximum bending stress at the outer layer of the pipe can be calculated by (Carpinteri *et al.*, 1998):

$$\sigma_M = \frac{4M(R+t)}{\pi((R+t)^4 - R^4)} \quad (3.4)$$

where  $R$  and  $t$  are inner radius and thickness of the pipe, respectively.

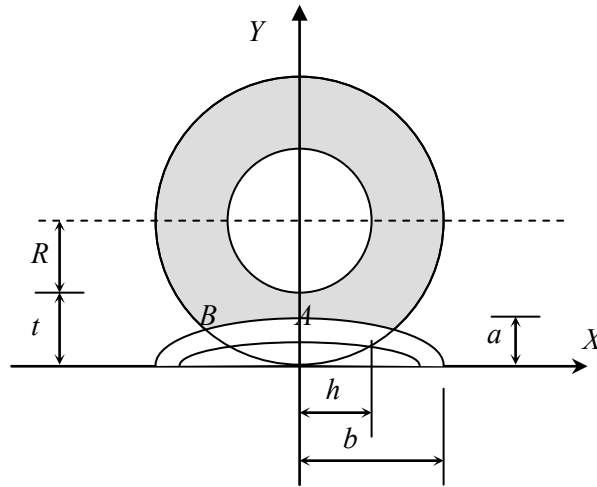


**Figure 3.2.** Two parameter model of the crack front (Carpinteri *et al.* 1998)

### 3.5. Finite Element Analysis

The dimensionless stress intensity factor for a pipe subject to bending moment has been reported in literature based on finite element analysis results (e.g. Carpinteri *et al.* 1998). These values are reported for specific  $a/b$  and  $a/t$  ratios, and one needs to use an interpolation technique to calculate the magnitudes of the dimensionless stress intensity factor for other desired combination of  $a/b$  and  $a/t$  ratios. In this research, a finite element analysis was therefore carried out to both verify the values of the stress intensity factors reported in the literature, and verify the integrity of those evaluated by interpolating the results reported by Carpinteri *et al.* 1998.

The finite element analysis was performed by the commercial ABAQUS code. Several contour integral evaluations are possible at each location along a crack front, each thought of as the virtual motion of a block of material surrounding the crack tip. This code automatically finds the elements that form each ring from the regions designated as the crack front. In cases where the crack is considered as a sharp one, the large strain zone at the crack tip is much localized and a small-strain assumption at the cracked component is applicable, thus reducing the computation time.

To model the crack-tip strain singularity, one may use linear elasticity, perfect plasticity, and power-law hardening models. Note that the results for pure power-law nonlinear elastic materials in a body under traction loading are proportional to the load by some multiplier. Therefore, the fracture parameters in one geometry under a particular load can be scaled for other loads, as long as the resulting loading distribution is the same. To simulate the singularity field, 20-node brick elements with a collapsed face were used. To obtain the maximum accuracy when meshing the model, the planes of the three-dimensional elements perpendicular to the crack line were kept planar. This action prevents the element's Jacobian from becoming negative at some integration points when the midside nodes are moved to the 1/4 points (ABAQUS, 2005). The midside nodes were moved to the 1/4 points and the nodes on the collapsed face of the element were allowed to move independently.

To maximize the accuracy of the contour integrals, the size of the crack-tip elements were kept small (see Table 3.1), especially in the radial dimension of the elements from the crack tip. To reduce the number of elements while maintaining a fine mesh in the vicinity of the crack front, a quarter of the pipe was modeled with a large portion of the pipe modeled by shell elements (see Figure 3.3). The cracked region of the pipe was modeled by 20-node quadratic brick elements. The midside nodes of the element surrounding the crack tip were moved to the 1/4 points to impose singularity. A surface-based shell-to-solid coupling was introduced in the model to allow for a transition from shell element modeling to solid element modeling. This modeling feature does not require any alignment between the elements in solid and shell meshes and automatically selects the coupling nodes located on a solid surface lying within the coupled regions. A set of multipoint coupling constraints was used to couple the nodes along the edge of the

shell elements interacting with the solid surface (ABAQUS, 2006). Shell edge nodes should be centrally located with respect to the wall thickness direction of the solid and at least two solid elements should be included through the thickness at a shell-to-solid interface. This smoothens the curvature and stress gradient along the shell-to-solid coupling region. The coupling interface should be placed at least a distance more than the shell thickness away from the region of interest in the solid mesh where the stress and strain fields are calculated (ABAQUS, 2006). This has been further verified by a set of trial and error runs, so that the introduced coupling interaction does not affect the calculated stress intensity factors.

**Table 3.1.** Typical characteristics of coarse, moderate and fine meshes used in the solid region of the finite element model

Mesh	Element dimension at crack tip (percent of crack depth)	Total number of elements in the solid region	Number of contours
Coarse	0.5	2050	4
Moderate	0.10	4120	6
Fine	0.05	6500	9

Figure 3.3 shows the isometric view of the quarter symmetry model of the pipe. The quarter model of the pipe consists of 6500 quadratic elements in the solid region and 300 elements in the shell region. Using the shell elements for modeling a large portion of the pipe significantly decreased the computational time, making it convenient to use a very fine mesh at the crack tip region in the solid part, thus improving the accuracy of the results.

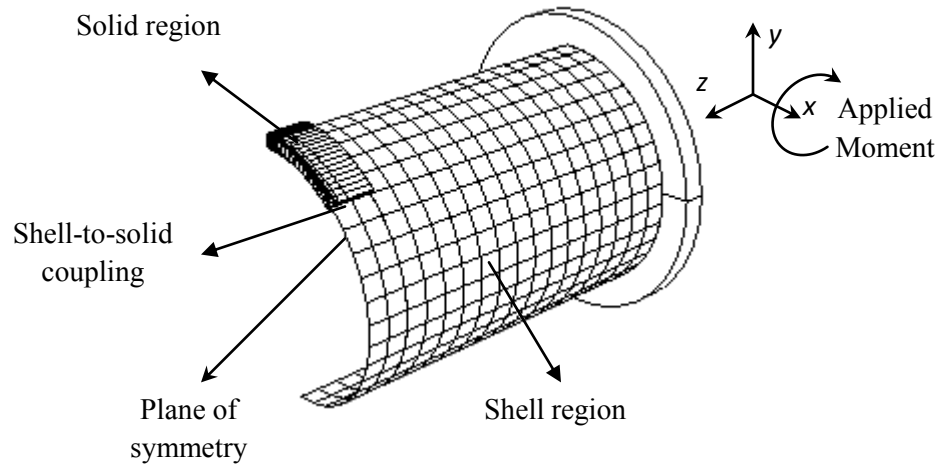


**Figure 3.3.** The Finite Element Model

Due to the stress concentration at the crack tip, the stress gradient is relatively large at the region near the crack front. Although a path dependent  $J$ -integral is an indication of a coarse mesh, it cannot be concluded that the mesh is fine enough if the  $J$ -integral is observed to be path independent. Therefore, a mesh convergence study was performed. Figure 3.4 shows the variation of stress in the radial direction (in the Y-direction shown in Figures 3.2 and 3.3), starting from the outer surface of the pipe towards the inner surface. As illustrated in this figure, the crack tip singularity can be traced using a fine mesh. Moreover, the calculated values of the stress intensity factor does not differ significantly in models with a “moderate” or “fine” mesh (see Table 3.1 for specifications of “moderate” and “fine” mesh in this study). Therefore, to reduce the computational costs of the finite element analysis, the attributes corresponding to a “moderate” mesh were applied to all cases for which stress intensity factors were calculated. In other words, the solid region was meshed such that its elements surrounding the crack tip vicinity had a dimension of about 0.1 percent of the crack depth at that region. Table 3.1 shows the characteristics of different mesh levels used in this research.



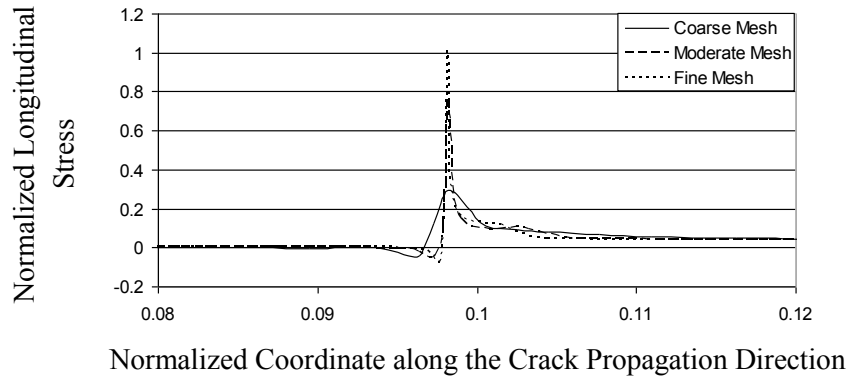


**Figure 3.4.** Stress singularity at the crack tip for coarse, moderate and fine meshes at the crack front region

The results of the finite element analysis were compared with those reported by Carpinteri *et al.* (1998). As stated, the reported values for the stress intensity factors available in the literature are reported for specific combinations of  $a/b$  and  $a/t$  ratios. To find the values of the stress intensity factor for any desired combination of  $a/b$  and  $a/t$  ratios not in the report, one may use an interpolation function. To verify the outcomes of such an interpolation, the results of the finite element analysis of this research was compared with those calculated based on interpolating the values reported by Carpinteri *et al.* (1998). Figure 3.5 shows a comparison between the dimensionless stress intensity factor calculated for a pipe with  $R/t=10.0$ , having an elliptical crack front with  $a/t=0.1$  and  $a/b=0.1$ . As seen, interpolating the values of stress intensity factor reported by Carpinteri *et al.* (1998) between  $a/b=0.0$  and  $a/b=0.2$ , agrees well to those calculated in this research by the finite element analysis.

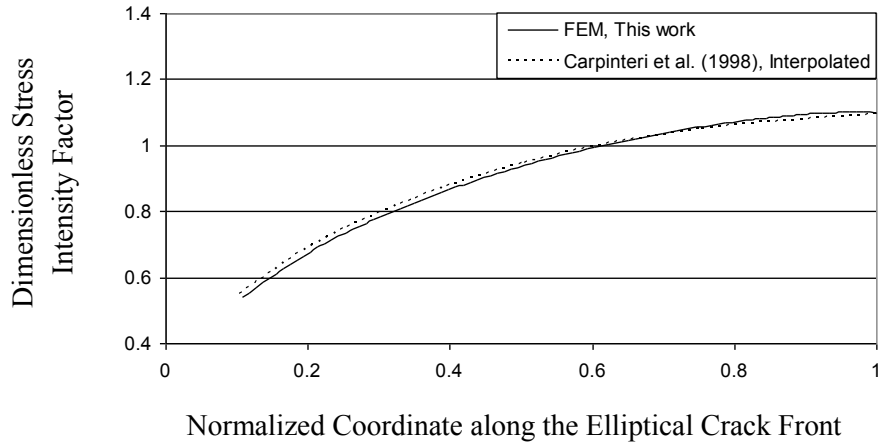
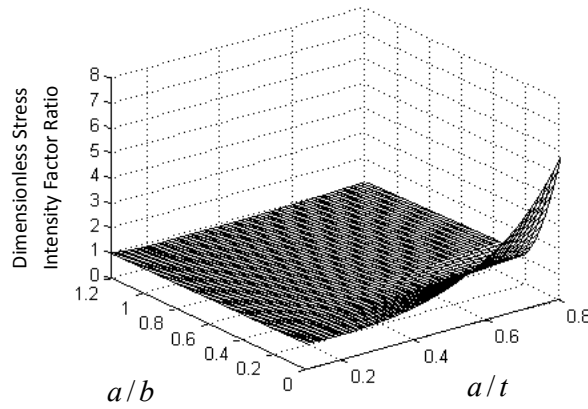


**Figure 3.5.** Comparison between the dimensionless stress intensity factors obtained from the finite element analysis and those reported by Carpinteri *et al.* (1998)

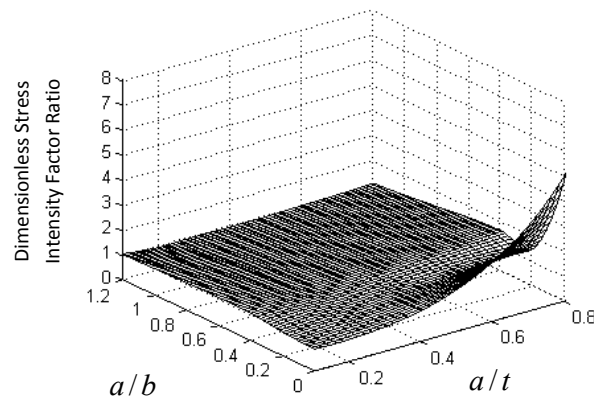
### 3.6. Dimensionless Stress Intensity Factor Ratio

After establishing the dimensionless stress intensity factors, the ratio of dimensionless stress intensity factors were compared for the two structural components under different loading configurations. Figures 3.6 and 3.7 show the variation of the dimensionless stress intensity factor ratios as a function of crack depth (the deepest point along the crack front) and crack length (the two ends of the crack front). In this paper, the deepest location along the crack front (point A in Figure 3.2) is referred to as the “crack depth”, and the location growing on the outside surface of the pipe (point B in Figure 3.2) is referred to as the “surface crack”. These graphs are presented for thin and thick wall pipes, having  $R/t$  values of 10.0 and 1.0, respectively, where  $R$  is the internal radius of the pipe and  $t$  is the wall thickness. The flaw aspect ratio is introduced as the ratio of the small and large diameter of the ellipse,  $a/b$ , and has been varied from 0.2 to 1.2. The crack depth ratio,  $a/t$ , that is the ratio of the crack depth to the wall thickness of the pipe, has been varied from 0.2 to 0.8. As illustrated in these figures, the dimensionless stress intensity factor ratio,  $K_{I,Plate}^* / K_{I,Pipe}^*$ , shows considerable variations for deep cracks with the diameter ratios smaller than 0.4. For diameter ratios higher than 0.4, the

dimensionless stress intensity factor ratio seems to maintain a constant value as the crack propagates through the thickness of the material. This trend seems to be the same for both thin and thick wall pipes with  $R/t$  values of 10.0 and 1.0, respectively.



(a)



(b)

**Figure 3.6 (a and b):** Variation of  $K_{I,Plate}^* / K_{I,Pipe}^*$  as a function of the crack depth ratio,  $a/t$ , and ellipse diameter ratios,  $a/b$ , for  $R/t = 10.0$ , a) depth crack, b) surface crack

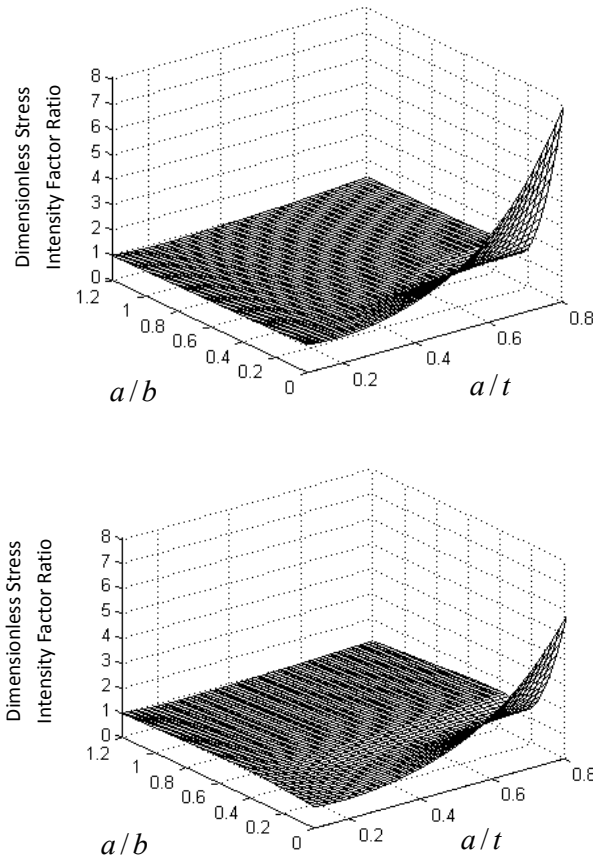


**Figure 3.7 (a and b):** Variation of  $K_{I,Plate}^* / K_{I,Pipe}^*$  as a function of the crack depth ratio,  $a/t$ , and ellipse diameter ratios,  $a/b$ , for  $R/t = 1.0$ , a) depth crack, b) surface crack

To further examine the variation of the dimensionless stress intensity factor ratio,  $K_{I,Plate}^* / K_{I,Pipe}^*$ , a series of graphs are presented in Figures 3.8 and 3.9. In these graphs, the magnitudes of dimensionless stress intensity factors is presented as a function of the normalized coordinate along the crack front for different diameter ratios and crack depth ratios.

Figure 3.8 shows the ratio between the dimensionless stress intensity factor of pipe and plate,  $K_{I,Plate}^* / K_{I,Pipe}^*$ , for a  $R/t$  value of pipe equal to 1.0. Such a low value of  $R/t$  mostly applies to pressure vessels rather than pipelines, where high levels of stresses are to be tolerated by the material. As observed from the figure, the ratio varies from 0.85 up to 1.60 for different crack depth ratio; the higher the crack depth ratio, the

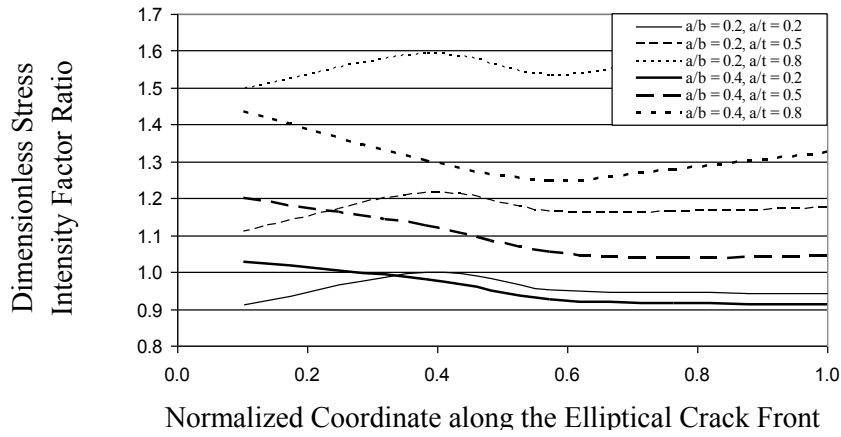
higher the dimensionless stress intensity factors ratio  $K_{I,Plate}^* / K_{I,Pipe}^*$ . Moreover, as the diameter ratio,  $a/b$ , increases, the dimensionless stress intensity factor ratio decreases. For crack fronts with a diameter ratio,  $a/b$ , of 0.8 to 1.2, where elliptical crack front has changed its shape closer to a semi-circular form, the crack depth ratio does not seem to play a significant role on the dimensionless stress intensity factors ratio. For such range of diameter ratio,  $a/b$ , the deviation between the dimensionless stress intensity factor along the crack front of pipe and plate is lower. The difference between dimensionless stress intensity factor of a plate subject to pure tension and a pipe subject to pure bending moment becomes negligible at the middle portion of the elliptical crack front, which is the deepest region of the crack through the wall thickness of a pipe or a plate. The values of dimensionless stress intensity factors ratio,  $K_{I,Plate}^* / K_{I,Pipe}^*$ , changes between 0.90 up to 1.60 for wide ellipses; however, this limit reduces to 0.85 to 1.25 when the crack front shape changes from a wide ellipse to a semi-circular shape. In other words, the closer the crack front shape to a circular form, the lower and more constant the values of dimensionless stress intensity factors ratio  $K_{I,Plate}^* / K_{I,Pipe}^*$  along the crack front.

As it is illustrated in Figures 3.8b and 3.8c, the stress intensity factors ratio,  $K_{I,Plate}^* / K_{I,Pipe}^*$ , becomes constant for the middle region of the crack front, that is the region with a normalized coordinate greater than 0.50. Along this region of the crack front and for high ellipse diameter ratios, the dimensionless stress intensity factors ratio,  $K_{I,Plate}^* / K_{I,Pipe}^*$ , has a constant value depending on the relative depth of the crack front to the pipe wall thickness,  $a/t$ . For cases with an ellipse diameter ratio greater than 0.6, where the crack front shape is circular rather than elliptical, the dimensionless stress intensity factors ratio is illustrated to show no dependency on the ellipse diameter ratio.

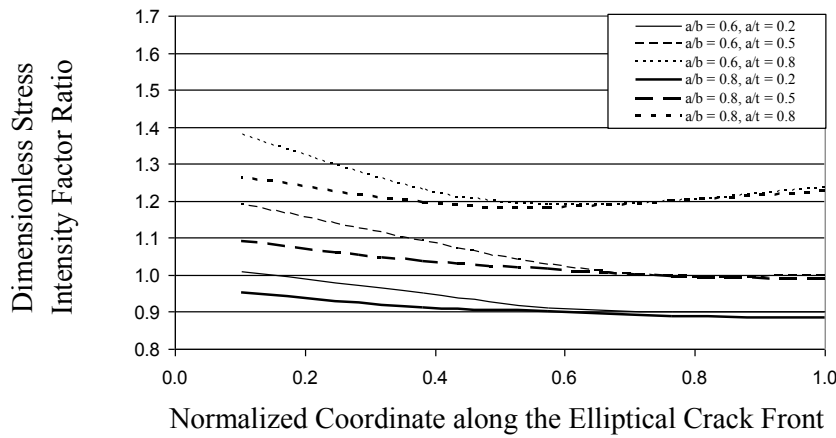
Figure 3.9 shows the ratio between the dimensionless stress intensity factor of pipe and plate,  $K_{I,Plate}^* / K_{I,Pipe}^*$ , for a  $R/t$  value of pipe equal to 10.0. This case is applicable to pipelines, where the wall thickness is small compared to the pipe diameter. Figure 3.9 illustrates that the ratio between the dimensionless stress intensity factor,  $K_{I,Plate}^* / K_{I,Pipe}^*$ , varies from 0.85 to 1.55, along the crack front. The limits of this variation become lower

for points closer to the center of the crack front, which have a deeper crack tip through the wall thickness of the pipe or plate. As in pipes with lower  $R/t$  ratio, the dimensionless stress intensity factor ratio decreases as the ellipse diameter ratio,  $a/b$ , increases. Moreover, in cases with lower  $R/t$  ratio and a semi-circular crack front shape, the ratio of crack depth to pipe wall thickness does not seem to play a significant role on the ratio of the dimensionless stress intensity factor  $K_{I,Plate}^* / K_{I,Pipe}^*$ . The only cases that do not follow this trend are those with very high ellipse diameter ratios and low crack depth ratios. At the middle region of the crack, the dimensionless stress intensity factor ratio shows less dependency on the ellipse diameter ratio,  $a/b$ , for semi-circular cracks. The length of this region increases as the ellipse diameter ratio,  $a/b$ , increases. The deviation in the magnitude of the stress intensity factors ratio,  $K_{I,Plate}^* / K_{I,Pipe}^*$ , is as low as five percent for semi-circular cracks along a long region of the crack front. Compared to the thicker pipes, the region of the crack front with a constant stress intensity factors ratio,  $K_{I,Plate}^* / K_{I,Pipe}^*$ , is longer for pipes with higher  $R/t$  ratio.

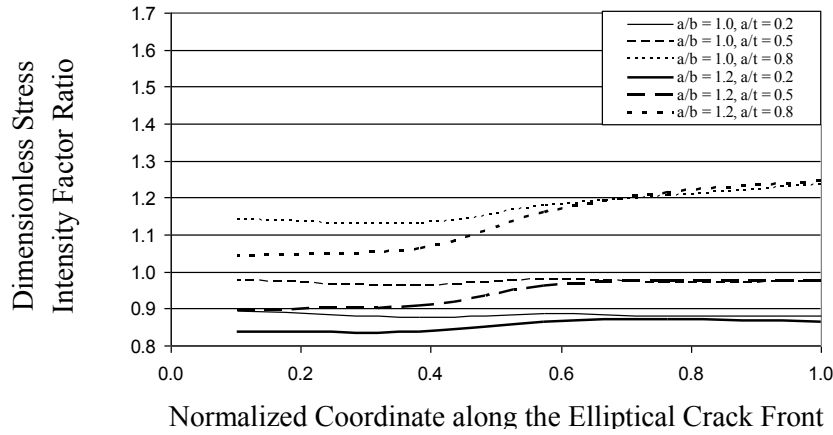
As illustrated in these figures, the dimensionless stress intensity factor ratio varies considerably for different crack depth ratio and ellipse diameter ratios. However, for certain values of these ratios, the changes in the dimensionless stress intensity factor become smaller and seem to follow a similar trend. This interesting characteristic is usually observed in cases where the diameter ratio changes between the values 0.7 to 1.2. In other words, the shape of the crack front is observed to have a strong influence on magnitude of the dimensionless stress intensity factor ratio of a pipe under bending moment and a plate under tension. Therefore, the assessment of the influence of variation of both the shape and size of a surface crack during its propagation on the dimensionless stress intensity factor ratio is an essential concept in structural integrity prediction. The next section explains the procedure used for tracing the shape change of a surface flaw as it propagates through the thickness of the material. The findings were further supported by a computational parametric study using a numerical procedure written in MATLAB code.



(a)

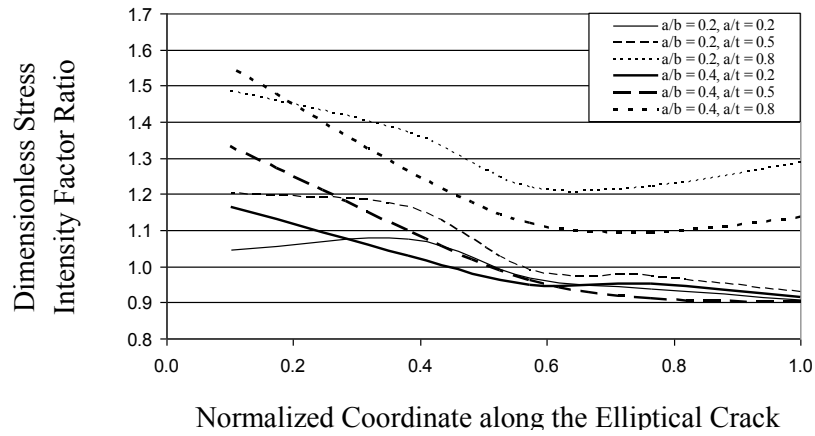


(b)

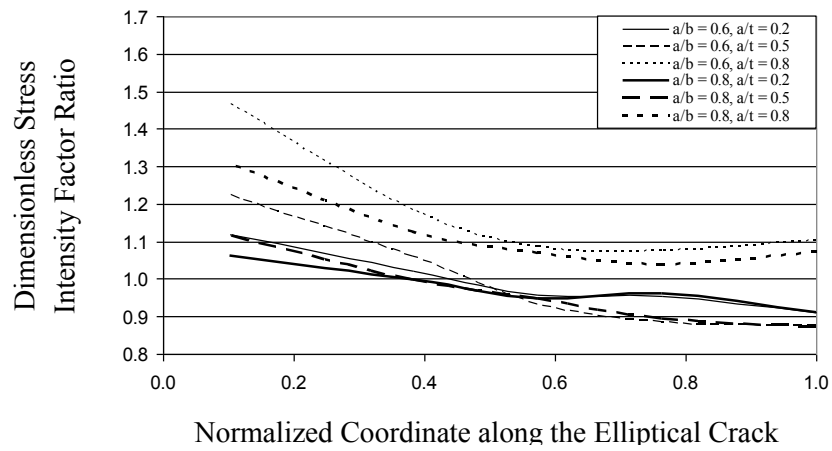


(c)

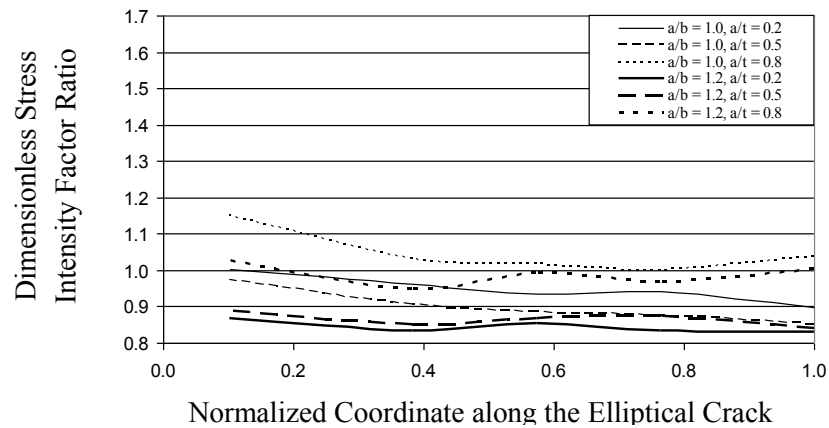
**Figure 3.8 (a, b and c).** Comparison between the stress intensity factor ratio,  $K_{I,Plate}^* / K_{I,Pipe}^*$ , between a plate and a pipe with an elliptical crack with different penetration ratio trough wall thickness (pipe radius/wall thickness = 1.0)



(a)



(b)



(c)

**Figure 3.9 (a, b and c).** Comparison between the stress intensity factor ratio,  $K_{I,Plate}^* / K_{I,Pipe}^*$ , between a plate and a pipe with an elliptical crack with different penetration ratio trough wall thickness (pipe radius/wall thickness = 10.0)



### 3.7. Shape of the Crack Front

Various classical solutions have been presented for evaluating the stress intensity factors of elliptical surface flaws in a pipe under the action of pure bending moment and for plates under the action of pure tension. Unlike the cases with a through-the-thickness crack with a straight crack front, part-through cracks do not have a constant geometry factor, and therefore, do not present a constant stress intensity factor along the crack front. In the cases with low ellipse diameter ratio,  $a/b$ , the maximum value of the stress intensity factor is at the center of the crack front, which is the deepest point of the crack through the wall thickness of a pipe or plate with an elliptical crack front. When the value of the stress intensity factor becomes equal or greater than the fracture toughness anywhere along the crack front, fracture would occur at that point. Considering the fact that a through-the-thickness crack is constrained by the thickness of the material, the plane strain fracture toughness criterion would be admissible.

Moreover, when the crack tip has a circular shape, the stress intensity factor is the same everywhere along the crack front, and the fracture occurs simultaneously along the crack tip. However, in cases with low ellipse diameter ratio,  $a/b$ , the stress intensity at the end of the crack tip is considerably lower than that at the center of the crack front. This could lead to the conclusion that the fracture may be postponed, and this conclusion has been supported by some experimental data. Therefore, as long as the stress intensity factor attains its largest value at the center on the crack front, more growth would occur in a certain cycle at the deepest location along the crack front (point A in Figure 3.2) rather than elsewhere along the crack front (e.g. points B and C). This would gradually force the crack front to change its shape closer to a circular form; that is, an ellipse with a diameter ratio,  $a/b$ , equal to unity (Liu, 1998). Many researchers have reported a value of 0.85 for diameter ratio, where stress intensity factor values at different points along the crack front are nearly the same (Ravichandran, 1997).

In brittle homogenous materials under the action of uniform stresses, surface cracks follow this semi-circular pattern during their growth. In ductile materials, plastic deformation occurs mostly at the crack tip and the crack is under lower constraint. As a

result, the growth at the surface tip experiences retardation and the crack front shape becomes closer to a circular shape with a diameter ratio of  $a/b = 1.0$  (Ravichandran, 1997). Therefore, as long as the material microstructure remains homogeneous and the stress distribution remains uniform, the crack shape can be assumed to follow a semi-circular pattern.

When the crack front shape is circular or semi-circular, the stress intensity will have the same magnitude along the crack front, leading to a constant propagation rate along the crack tip. Having the same propagation rate along the crack front is a guarantee for the crack tip to keep its circular form through the rest of the fatigue life of the component (Broek, 1989). In cases where the out-of-plane bending takes place, stress gradient may cause a decrease in the stress intensity factor at the center point of the crack front (point A in Figure 3.2). In such cases, ellipse to circular shape translation may not be reached during the fatigue crack propagation through the material.

In many cases, part-through cracks are assumed to have a circular shape, leading to a constant magnitude for the stress intensity factor along the crack front and therefore, a constant fatigue crack growth rate. With such an assumption for the initial flaw, the crack is assumed to have started its growth from a circular shape, thus keeping its shape constant till the end of its growth. On the other hand, real flaws, which initiate in the structural components during their service life, are very small and gradually advance through the material. It can further be argued that these small flaws would change their shape into a circular form at the very first stages of their propagation process. In other words, the “real” flaws that initiate and further propagate in a pipe under the action of pure bending moment, or a plate under the action of pure tension, can be assumed to have a circular shape from the initiation phase of the flaw till the end of the service life of the component. In general, crack growth retardation or acceleration is mostly governed by the ratio of the stress intensities in successive cycles. The above concept is still admissible when retardation or acceleration is assumed to take place due to over-load or under-load peaks of the stress time history applied to the structural component.

To validate this concept, experimental investigations were conducted and the crack propagation rates were measured along the small and large diameter of elliptical crack

fronts in a plate. In a study done by Song *et al.* (2002), the Sih energy approach was used to investigate the growth of a semi-elliptical surface crack and the results were compared against those obtained based on the Paris law and experimental tests. The initial flaw had a crack depth ratio of  $a/t = 0.25$  and a diameter ratio  $a/b = 0.95$ . Both the Paris law and Sih's energy approach led to a good prediction of the fatigue crack growth for both directions along the small and large diameter of the elliptical crack front. The relation between the crack diameter ratio and depth ratio was introduced as (Song *et al.* 2002):

$$a/b = -0.48(a/t)^2 + 0.048(a/t) + 0.99 \quad (3.5)$$

Figure 3.10 shows the measured and predicted shape variations using the above equation, extracted from Song *et al.* (2002). It is illustrated that for a crack depth ratio lower than 0.7, the ellipse aspect ratio is higher than 0.78, which represents a crack front with a semi-circular shape. Moreover, this diagram shows different crack growth rates for surface and depth directions, as the shape of the crack front does not exactly follow a circular form during its growth through the material.

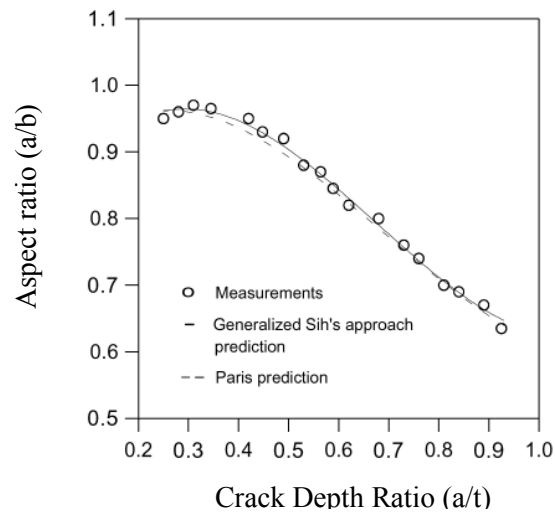


**Figure 3.10.** The relation between diameter aspect ratio and crack depth ratio for a plate with circular initial flaw under the action of pure tension (Song *et al.* 2002)

Based on the experimental test data, the Paris equation coefficients have been reported by some researchers for growth along the depth and surface direction of

elliptical surface flaws. Corn (1971) and Yen and Penndleberry (1962) have suggested the following relation for crack growth rate in depth and surface direction of an elliptical crack in plates:

$$C_{Surface} = (0.9)^m C_{Depth} \quad (3.6)$$

where  $C_{Surface}$  and  $C_{Depth}$  are the coefficients used in the Paris equation for crack growth rate along the depth and surface directions, respectively, and  $m$  is the material constant. This relation has been used by many researchers to study the crack propagation rate in both crack depth and surface directions (Newman and Raju 1981). Based on the surface crack tension and bending test results for a wide range of aspect ratio, Kim and Hwang (1997) suggested a value of 0.904 rather than 0.9 for the above equation (Kim and Hwang, 1997). The difference between the  $C_{Surface}$  and  $C_{Depth}$  values is believed to be due to the difference between the stress intensity factors and changes in the state of the stress from plane stress on the front surface to the plane strain at the deepest point on the crack front (Burande and Sethuraman, 1999). Experimental research (Wu, 1985) indicates that the crack front propagates toward having a semi-circular shape in a plate under tension, almost regardless of the initial configuration of the surface flaw. The smaller the initial surface flaw, the sooner the crack front changes its shape to a semi-circular one and follows the same trend towards the end of the fatigue life of the structural component. As the crack depth approaches the plate back surface or the inside surface of pipe, the crack at the deepest point may become shallow. This phenomenon is due to the bending component, which even in a plate under pure nominal tension, occurs at small net section sizes. This bending moment is introduced due to the specimen rotation with respect to loading axis as crack advances (Ravichandran, 1997).

The analytical solution of the shape change equation for a plate under tension loading has been presented by Wu (1985). The solution has also been verified against a considerable number of experimental data available in literature. It was shown that a small semi-circular surface crack tends to remain semi-circular at the initial stages of their growth. The shape change equation has been introduced as (Wu, 1985):

$$db/da = \left\{ (a/b)^{1/2} \left[ 1 + 0.3182(a/t)^2 \right] \right\}^m \quad (3.7)$$

The accurate solution for this equation has been presented for  $m = 2, 3$  and  $4$ , and a linear interpolation has been suggested for values between 2 to 4. It has been shown that the shape of the crack front during its propagation depends on the initial crack front shape (Wu, 1985). Moreover, as the crack propagates through the material, the crack front shape changes to an almost semi-circular one with a diameter ratio of  $a/b = 0.8$ .

Regarding the shape change of any initial surface flaws to a semi-circular form, one would expect the ellipse diameter ratio to have a value greater than 0.8, where the dimensionless stress intensity factor ratio,  $K_{I,Plate}^* / K_{I,Pipe}^*$ , shows negligible variations as the crack grows through the material (see Figures 3.8 and 3.9). Details of a computational simulation approach to study the shape change of a surface flaw during its propagation are discussed in the next section. Once the surface flaw is shown to have a semi-circular shape during its growth, one may compare the crack growth rate in a pipe under bending moment with that of an equivalent plate under pure tension. As will be seen, this would provide a more cost-effective means of characterizing fatigue crack growth in pipes.

### **3.8. Computational Simulation of Crack Front Shape**

A computer code in the MATLAB language was developed to further verify the results of the above studies. The program enables us to compare the crack growth in a plate under tension and a pipe under bending. The stress intensity factors for a plate under tension and a pipe under bending moment with two  $R/t$  ratios of 10.0 and 1.0 were calculated by the computational method. The simple analytical expressions for the stress intensity factors for a pipe under bending moment are not available in the literature. Therefore, a cubic form interpolation function was used to interpolate the values for desired  $a/b$  and  $a/t$ . An initial crack shape was assumed and the loading was changed accordingly so that the stress intensity factor would be greater than the threshold value along the crack front. The following general crack laws were used for depth and surface crack growths, respectively (Broek, 1989):

$$\frac{da}{dN} = C_{Depth} \frac{(\Delta K_{I,Depth})^m}{(1-R)K_{I,C_{Depth}} - \Delta K_{I,Depth}} \quad (3.8.1)$$

$$\frac{db}{dN} = C_{Surface} \frac{(\Delta K_{I,Surface})^m}{(1-R)K_{I,C_{Surface}} - \Delta K_{I,Surface}} \quad (3.8.2)$$

where  $da/dN$  and  $db/dN$  are the crack growth rates for both into the depth and surface directions, respectively,  $\Delta K_{I,th}$  is the threshold stress intensity factor range for fatigue crack growth in mode  $I$ ,  $K_{I,C}$  is the fracture toughness,  $\Delta K_I$  is the stress intensity factor range, and  $R$  is the stress ratio. The  $(1-R)$  term accommodates the termination point, where  $K_{max}$  exceeds the fracture toughness,  $K_{I,C}$ . It should be noted that this term does not govern the relation between  $d/dN$  for different  $R$  ratios.

By dividing Equations 3.8.1 and 3.8.2, one may use the following to calculate the relation between the crack growth rate in depth and surface direction.

$$\frac{da}{db} = \frac{C_{Depth}}{C_{Surface}} \left( \frac{\Delta K_{I,Depth}}{\Delta K_{I,Surface}} \right)^m \frac{(1-R)K_{I,C_{Surface}} - \Delta K_{I,Surface}}{(1-R)K_{I,C_{Depth}} - \Delta K_{I,Depth}} \quad (3.9)$$

Using Equation 3.6 and assuming a small increase in  $da$ , the increase in  $db$  can be calculated accordingly. The new crack shape diameters  $a_{new} = a + da$  and  $b_{new} = b + db$  are further used to re-calculated the stress intensity factor of the new crack front. These values are used subsequently to calculate the crack growth within the next loading cycle. This procedure is continued until the stress intensity factor at the crack depth or that of the crack surface is greater than the fracture toughness of the material, which is assumed to cause an unstable fracture. Such a computational approach has been used by other researchers to trace the shape change of surface cracks in plates or pipes under either axial or bending cyclic forces (Carpinteri, 1993; Burande and Sethuraman, 1999 and Kim and Hwang 1997). Using this approach, the specifics of a series of initial surface flaws were implemented into the computer code. The associated fatigue crack growth and changes in the associated crack front shape were monitored up to the end of

the fatigue life of the component. Figure 3.11 shows a typical surface flaw, monitored during its propagation through the wall thickness of a pipe.

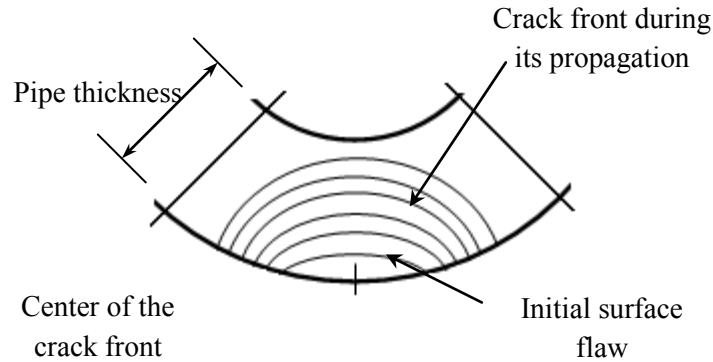


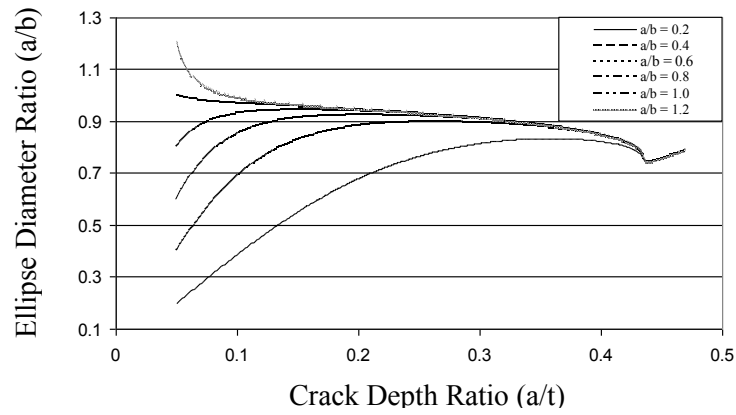
**Figure 3.11.** Computational monitoring of a typical surface flaw during its propagation through the wall thickness of a pipe

For the computational simulations of the various initial surface flaws, the properties listed in Table 3.2 were used. Figure 3.12 shows the ellipse diameter ratio as a function of crack depth ratio for a rectangular plate under pure tension with various initial crack front shapes. As illustrated in the figure, the crack front tends to change its shape to a semi-circular form. The crack fronts with ellipse diameter ratio of 0.2 to 0.4 show a slower trend in reaching a semi-circular shape. However, even for these initial surface flaws, the crack shape changes its form to a semi-circular form at a crack depth ratio of less than 0.1 to 0.2. As the crack propagates through the wall thickness of the material, the ellipse diameter ratio remains between a value of 0.8 to 1.0, hence, representing a semi-circular shape for the crack front. This interesting concept is also observed in Figures 3.12b and 3.12c, for pipes with the radius to thickness ratio,  $R/t$ , of 1.0 and 10.0, respectively. These results are consistent with those produced by other researchers, both numerically and experimentally (Newman and Raju, 1981; Carpinteri, 1993, Kim and Hwang, 1997). Furthermore, showing that the crack front follows a semi-circular shape during its propagation for these two structural components with different loading conditions, one may refer to Figures 3.8 and 3.9 to see the variation of their dimensionless stress intensity factor as the crack propagates through the material.

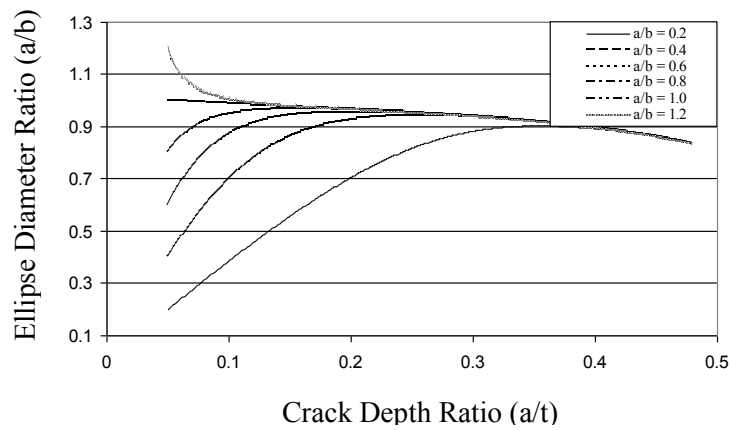
**Table 3.2.** Material property used in the computational simulation of crack growth

$\sigma_{\min}$	10.0 MPa
$\sigma_{\max}$	50.0 MPa
$K_{I,C_{Surface}} = K_{I,C_{Depth}}$	50.0 MPa
$\Delta K_{I,th}$	6.6 MPa
$da$	0.001
$C_{Depth}$	6.9E-12
$C_{Surface}$	5.0301E-12
$m$	3.0

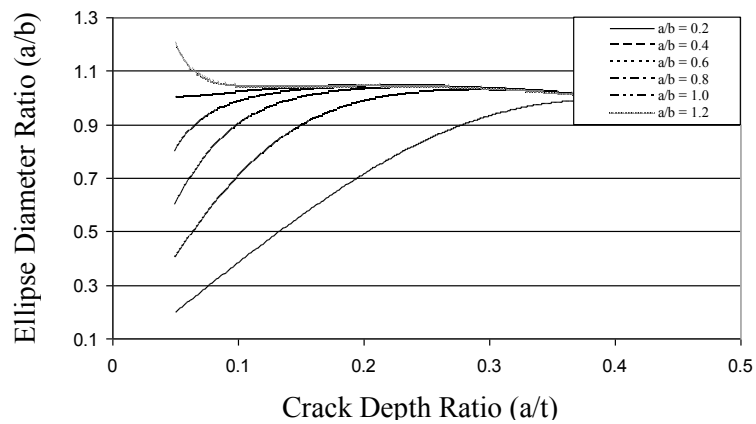




(a)



(b)



(c)

**Figure 3.12 (a, b and c).** Variation of ellipse diameter ratio,  $a/b$ , as a function of crack depth ratio (a) for a rectangular plate subject to tensile load, (b) for a pipe with  $R/t = 1.0$  under pure bending and (c) for a pipe with  $R/t = 10.0$  under pure bending

### 3.9. Experimental Investigation

An experimental investigation was carried out to verify the results obtained from the computational. Figure 3.13 shows the test apparatus and set up. The 4-point bending setup subjects the pipe under pure bending moment in the mid-segment of the pipe. The tests were performed using a computer controlled Instron Servo-hydraulic Universal Testing Machine model 8500<sup>+</sup>. The machine has a load cell capacity of  $\pm 100kN$  under dynamic or  $200kN$  under static loading conditions. The top and bottom fixtures, on which the plate specimen was mounted, were connected to the load cells.

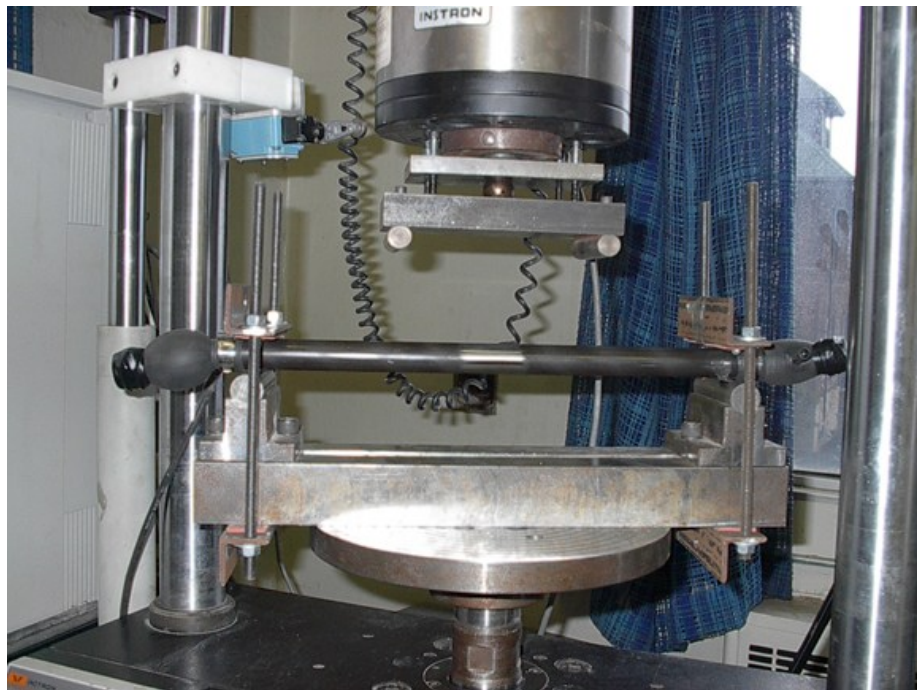


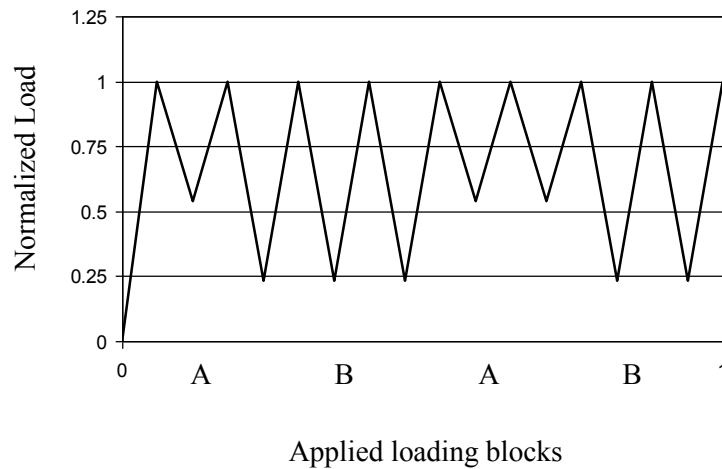
**Figure 3.13.** Test apparatus

The tests were done at room temperature in air, under constant amplitude loading. The surface of the specimen was polished with a wide range of sand papers, starting from coarse ones (No. 120) to fine ones (No. 600). This helped the crack tip and its propagation to be clearly visible on the outer surface of the pipe. To monitor the crack growth, fractography technique was used. In this technique failure surfaces' appearance is correlated to the cause of the failure. The fracture surface usually contains lines

referred to as “beach marks”. The cause of such markings on the fracture surface is attributed to gradual failure (sudden crack propagation) over a length of time, or due to the application of different blocks stress cycles with different  $\Delta K$  (Hertzberg, 1996). The beach marking bands represent different periods of crack growth, not the growth due to each individual load excursions. The center of the beach marks are at the crack origin, which makes it practical to understand the point where the crack initially started. The dark and light bands on the fracture surface represent the difference in the magnitude of the prevailing  $\Delta K$  associated with that loading block.

In this paper, the above-noted marking bands were used to characterize size and shape of the crack during its propagation. It should be noted that crack growth delays may occur in cases where low level  $\Delta K$  blocks follow a high  $\Delta K$  block. The influence of such over-load and under load peaks has been investigated in various studies (Rushton and Taheri, 2005 and Taheri et al. 2002). To avoid the interaction effects, different loading blocks were selected to maintain a constant  $K_{\max}$  during the test (Ragazzo *et al.* 1995). Experimental results have shown that the contrast changes in the crack surface is dependent on  $\Delta K$  and does not show any dependency on  $K_{\max}$ . When the magnitude of  $K_{\max}$  is held constant during the test, no load interaction effects take place between different blocks of applied loads (Hertzberg, 1996). Figure 3.14 shows the normalized load applied to the specimen. Block A includes 100,000 cycles, while block B only covers 10,000 cycles.

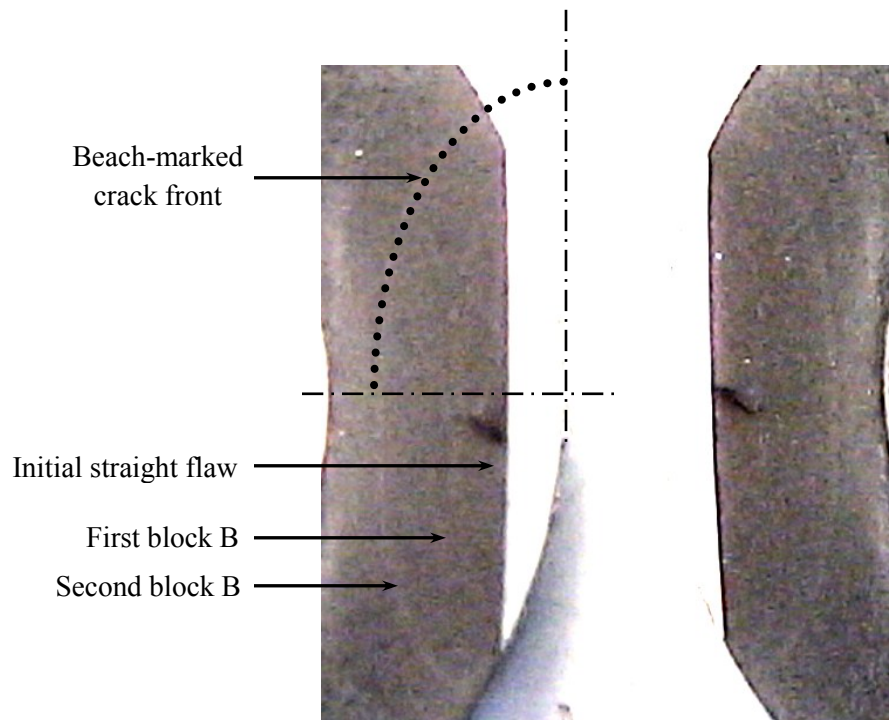
As discussed previously, accurate measurement of the crack front profile is often difficult and expensive. As a more cost-effective solution, periodic beach marking is used by researchers to reveal the crack front and trace its propagation through the material (Shin and Cai, 2004).



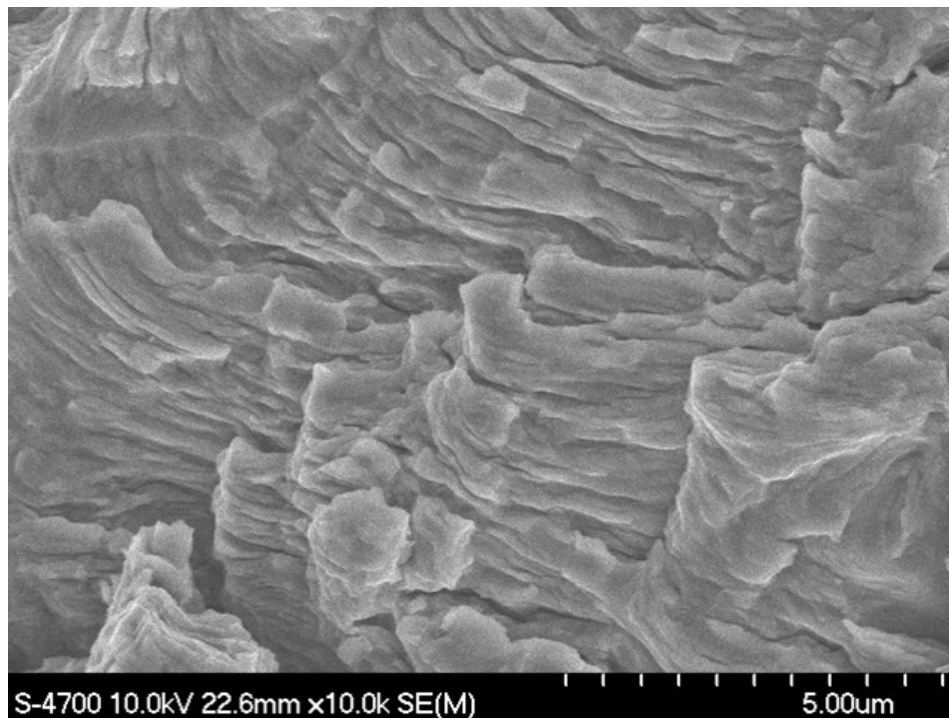
**Figure 3.14.** Typical normalized applied load

Figure 3.15 shows the photos of the fracture surface after the specimen was failed under the applied cyclic load blocks. As it is illustrated in this figure, there are two bands (the second band is more clear than the first one), representing block B of the applied loading cycle. This band clearly shows size and shape of the crack front during its progress through the wall thickness of the pipe. This figure illustrates a straight initial flaw, which gradually changed its shape to an elliptical form during its propagation. The test results are well verified against the computational simulation of a crack front with the same initial flaw.

Figure 3.16 is a Scanning Electron Microscope (SEM) image, showing the marker band associated with block B of the applied load. The distinct markings illustrated in this figure represent the cyclic stresses applied to the fracture surface. Although beach marks are sometimes more clearly visualized by SEM as opposed to those visible in surface photos, it is not practical to trace a band from one end of the crack front all the way to the other end under the microscope. Therefore, a high resolution digital camera was used in this research to study the fracture surface (Figure 3.15).



**Figure 3.15.** Fracture surface showing two beach-marked bands on the cross section of the pipe



**Figure 3.16.** Beach-marks under Scanning Electron Microscope (SEM)

### 3.10. Summary and Discussion

Based on this study and the fact that crack propagation starts from very small initial flaws, one would expect the crack front to grow towards having a semi-circular shape at the very initial stages of its growth, regardless of its initial shape. Moreover, in an experimental investigation, where initial surface flaws of any shape could be made on the test specimen, this consistency between the response of pipes and plates can be of interest. One can therefore test a plate under tension rather than a pipe under bending moment. This equivalency would considerably simplify the test setups for crack growth propagation studies. In such a case, a relatively low cost conventional microscope can be used to monitor the crack growth instead of the more sophisticated and costly instruments required for monitoring the crack growth of a surface flaw in pipes.

To further support the admissibility of the suggested simplified test methodology, the following explanations are offered. It was observed that for such a semi-circular shape crack front, where ellipse diameter ratio has a value of 0.8 to 1.1, the normalized stress intensity factor ratio,  $K_{I,Plate}^* / K_{I,Pipe}^*$ , would follow the trend illustrated in Figures 3.8 and 3.9.

As illustrated in those figures, the normalized stress intensity factor ratio,  $K_{I,Plate}^* / K_{I,Pipe}^*$ , attains almost constant value along the crack front, further rationalizing the proposed simplified equivalent testing approach. Figure 3.17 shows the dimensionless stress intensity factor ratio,  $K_{I,Plate}^* / K_{I,Pipe}^*$ , for circular crack fronts in both thick and thin wall pipes with different penetration ratios,  $a/t$ , along the middle region of the crack front. It is clearly observed that the dimensionless stress intensity factor ratios exhibit almost a constant value along this region of the crack front, with a maximum deviation of not more than five percent. This deviation increases as the crack depth ratio,  $a/t$ , increases; however, this increase seems to be negligible.

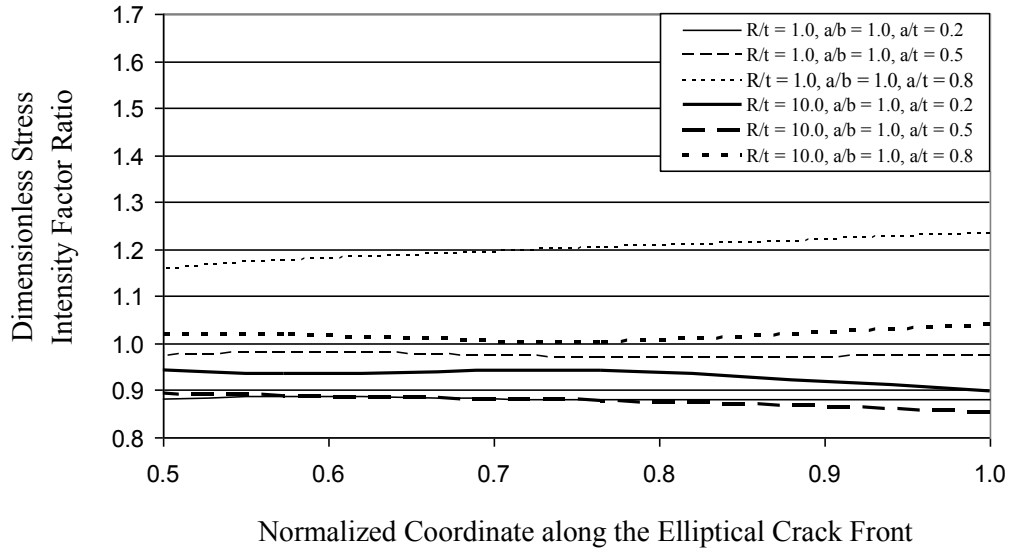


**Figure 3.17.** Comparison of the dimensionless stress intensity factor ratio of plates and pipes with an elliptical crack with different penetration ratio through the wall thickness

Figure 3.18 shows the variation of the normalized stress intensity factor ratio,  $K_{I,Plate}^* / K_{I,Pipe}^*$ , at the center of the crack front (point A in Figure 3.2), as a function of different crack depth ratios,  $a/t$ , for circular and semi-circular crack shapes with a diameter ratios of 1.0 and 0.8, respectively. As the crack propagates through the wall thickness of the pipe, the stress intensity factor ratio decreases at a crack depth ratio of 0.25 and 0.40, for the thick and thin wall pipes, respectively. Beyond these points, the stress intensity factor ratio increases as the crack depth ratio increases and the crack propagates through the wall thickness. It is observed in the figure that for cases with higher  $R/t$  ratios, where the pipe wall thickness is small compared to the pipe diameter, the dimensionless stress intensity factor ratio shows less variation in its magnitude as the crack propagates. In other words, as  $R/t$  ratios increase, the crack growth propagation response in a pipe subject to bending moment becomes even more consistent with a plate subject to tension.

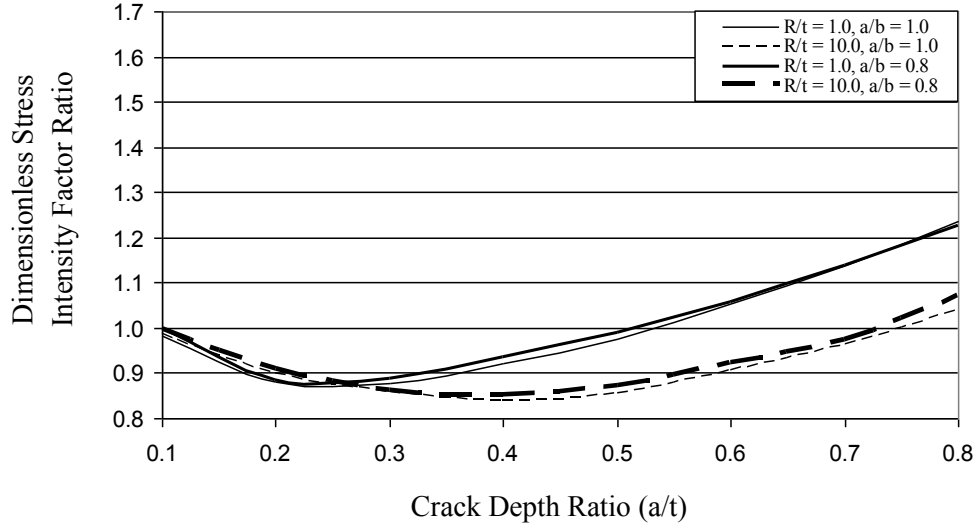


**Figure 3.18.** Variation of stress intensity factor ratio,  $K_{I,Plate}^* / K_{I,Pipe}^*$ , at the center of a circular crack front as a function of crack depth ratio  $a/t$  for various  $R/t$  and  $a/b$  ratios

As seen, the dimensionless stress intensity factor ratio shows negligible difference for cases with a crack front diameter ratio of 1.0 and 0.8. It may be seen that for a semi-circular crack growing through the wall thickness, the changes in the dimensionless stress intensity factor ratio follows a certain trend for a penny shape crack in a pipe under pure bending moment and a plate under pure tension. Using this concept, expressions are introduced for evaluating the dimensionless stress intensity factor ratio as a function of only the crack depth ratio,  $a/t$ , for two different ratios of  $R/t$ :

$$\frac{K_{I,Plate}^*}{K_{I,Pipe}^*} = 6.2\left(\frac{a}{t}\right)^4 - 13.6\left(\frac{a}{t}\right)^3 + 11.3\left(\frac{a}{t}\right)^2 - 3.6\left(\frac{a}{t}\right) + 1.2 \quad \text{for } R/t = 1.0 \quad (3.10.1)$$

$$\frac{K_{I,Plate}^*}{K_{I,Pipe}^*} = 0.5\left(\frac{a}{t}\right)^4 - 1.7\left(\frac{a}{t}\right)^3 + 3.0\left(\frac{a}{t}\right)^2 - 1.7\left(\frac{a}{t}\right) + 1.1 \quad \text{for } R/t = 10.0 \quad (3.10.2)$$

It should be noted that these relations are valid for cases where the diameter ratio,  $a/b$ , varies between 0.8 to 1.1. This range of ratio can be easily assured by making a semi-circular initial surface flaw when conducting experimental investigations. In real



cases, where the crack propagates from very small initial flaws, it has been observed that the semi-circular shape was attained at the initial stages of the crack growth, regardless of the shape of the initial flaw. This concept makes the use of Equations 3.10 practical and convenient for relating the fatigue crack growth rate of pipes with initial surface flaws under bending moment with plates under tension, either for those tested in a laboratory or in the field, such as pipelines and risers.

### **3.11. Conclusions**

This paper studied the admissibility of replacing a pipe subject to bending moment with an equivalent plate subject to tension. This equivalency provides a means for avoiding the complexity and significant costs that are usually associated with conducting experimental investigation on pipes with an advancing initial surface flaw.

A series of finite element analyses was performed to verify the values of the stress intensity factor of a pipe with elliptical crack front reported in literature, as well as those interpolated during the computational simulation in this study. This simulation was done by a MATLAB code, which could monitor the shape of an advancing crack front during its propagation through the wall thickness of the material. In addition, the results from the computational simulations were compared to those from experimental investigation, either done in this research, or those found in literature. The simulation illustrated that the crack front follows a semi-circular shape during its propagation for these two structural components subjected to different but equivalent loading conditions.

Furthermore, a dimensionless relationship between the stress intensity factor of a pipe under bending moment and that of a plate under pure tension was introduced. It was further illustrated that the dimensionless stress intensity factor ratios would exhibit almost a constant value along a large portion of the crack front. The semi-circular crack was observed to grow through the wall thickness of the material. The resulting changes in the dimensionless stress intensity factor ratio followed a specific trend. This was observed for both the penny shape crack in a pipe under pure bending moment and in the case of the plate under pure tension. Based on this observation, expressions were

introduced for evaluating the dimensionless stress intensity factor ratio as a function of only the crack depth ratio,  $a/t$ , for two different ratios of pipe inside radius to its wall thickness. As one would expect, this approach becomes even more rational as the ratio of pipe inside diameter to its thickness increases. The validity of the proposed relations is based on the fact that crack propagation starts from very small initial flaws and attains a semi-circular shape at very initial stages of its growth. For experimental studies, where initial surface flaws of almost any shape can be made on the material tests in the laboratory, a circular shape is recommended for the initial flaw.

### **3.12. Acknowledgements**

The financial support of Natural Sciences and Engineering Council of Canada (NSERC) in the form of a partnership agreement grant to the second author in support of this work is gratefully acknowledged.

## Chapter 4

### Structural Life Assessment of Oil and Gas Risers under Vortex-induced Vibration

Mohammad Iranpour†, Farid Taheri† and J. Kim Vandiver‡

† Department of Civil and Resource Engineering, Dalhousie University, 1360 Barrington Street, Halifax, Nova Scotia B3J 1Z1, Canada

‡ Department of Mechanical Engineering, Massachusetts Institute of Technology, 77 Massachusetts Avenue - Room 5-222, Cambridge, MA, USA 01239

Published in the Journal of Marine Structures, 2008, vol. 21, pp. 353-373

#### 4.1. Abstract

Estimating the fatigue damage due to Vortex Induced Vibration (VIV) is an important issue when considering oil and gas risers used in the offshore industry. In severe current profiles, especially in very deep waters, the VIV-induced fatigue damage could result in a relatively short life for risers. As water depth increases, the riser requires thicker wall to keep the stresses within the allowable limit of the material. Moreover, risers may interfere with each other in deep waters, which is not acceptable to the current design guidelines. Therefore, the current design philosophy prevents the riser clashing, which results in very expensive systems. As an alternative approach, such as the one recommended by the new provisions of DNV, interference and collision of risers are allowed. However, such an approach is only recommended for a riser that has been designed based on full consideration of VIV and a state-of-the-art fatigue analysis.

In this research, the field data on multimodal vibration of a long flexible riser is used to conduct a series of experimental tests for fatigue life estimation of risers. The resulting VIV imposes a variable amplitude loading (VAL) on the riser, which makes the evaluation of its fatigue life difficult. Moreover, the influence of load interaction effects

is also investigated through experimental tests. Lastly, influence of different frequency harmonics in the VIV-induced time-history is also studied. The experimental results from this study indicate that the higher harmonics cause significant fatigue damage and cannot be ignored.

**Keywords:** Risers, Fatigue, Vortex-induced vibration (VIV), Variable amplitude loading, Paris model, Walker model, Barsom model, Hudson model, Rainflow

## 4.2. Introduction

With the increasing demand for oil and gas products in the world and the new offshore discoveries, the offshore industry has moved into deep and ultra deep waters. This has resulted in many challenges in analysis and design of the offshore platforms and risers. One such problem is the fatigue characterization of the risers in those waters due to vortex-induced vibration (VIV). With the increasing speed of the current profile, the complex nature of VIV causes great uncertainties in predicting the VIV-induced stresses, making the accumulated fatigue damage in the riser of significant concern. Many studies have been conducted to predict the risers' VIV response; however, an accurate prediction of the results of such VIV phenomenon is still a topic requiring more in-depth attention. In deep waters, understanding the dynamics of risers in sheared current profiles and their vibration in higher modes becomes even more challenging. When a riser is excited in its higher mode of vibration, the estimation of fatigue damage becomes even more difficult due to the complexity of the vibration and the resultant variable amplitude stress-time history.

A review of the available methods for riser VIV fatigue life estimation (Iranpour and Taheri 2006a) has revealed that the calculated fatigue life can be grossly overestimated, which is not desirable. A riser's VIV-induced fatigue life is greatly dependent on various parameters, and any small change in these parameters could significantly influence the predicted fatigue life. Moreover, long flexible risers have the ability to respond simultaneously to several modes of vibrations, causing even more complexity in the VIV-induced stress-time history. The assessment of the fatigue response of such risers under

such a variable amplitude loading (VAL) becomes accordingly more complex when compared to those subjected to constant amplitude loading (CAL). Many models have been proposed to date that suggest an equivalent constant amplitude loading that could replace a variable amplitude loading scenario and create the same fatigue response. This is done so because the performance of several of CAL models (such as those of Paris, Walker and Forman) are fully investigated and their limitations have been established through many experimental investigations. However, the applicability of such models is highly dependent on the nature of the stress time-history that is imposed on the component due to the VAL scenario. In a VAL scenario, the resulting crack growth in the structure is a function of the stress amplitude, the stress ratio (i.e., ratio of minimum to maximum applied stresses), and the frequency and the nature of the stress-time history. This complexity has resulted in the development of numerous VAL models over the last few decades; however, no universal model exists to date. Most of these models are developed for a specific case or application, incorporating some of the main influencing parameters (Taheri *et al.* 2002). In general, the riser designers incorporate the fatigue models that are based on the constant amplitude loading assumption. It has been shown that the overload and underload stress spikes and their sequence could significantly influence the fatigue response of a component (Taheri *et al.* 2002; Rushton and Taheri, 2003). The resultant crack tip plasticity caused by an overload could significantly influence the material response at the crack tip region, hence influencing crack propagation within the subsequent load cycles (Yuen and Taheri, 2004). Tension overloads are observed to cause considerable decrease in the fatigue crack growth rate, while compression underloads are shown to accelerate the growth rate of the crack (Taheri *et al.* 2002; Yuen and Taheri, 2004). Such irregularities in the loading scenario make it very difficult to estimate the VIV-induced fatigue damage of the riser and to understand the underlying physics of the phenomenon.

The main focus of the most recent studies has been to examine the underlying complexity of VAL scenarios and the resultant crack growth rate retardation or acceleration (Rushton and Taheri 2003; Yuen and Taheri, 2004). The crack tip blunting, strain hardening of the material, crack deflection, residual stresses, time history of the applied loads and the crack closure are the other significant factors known to affect crack

growth under VAL (Sadananda *et al.* 1999). Although much effort has been expended in extending the constant amplitude loading fatigue models to assess VAL scenarios, the accurate characterization of fatigue crack growth under VAL remains a challenge. This becomes even more critical in deep waters due to the complexity of the structural vibration at the higher modes. More specifically, most of the abovementioned experiments have used hypothetical loadings (especially when considering the influence of semi-random or variable loading). It is therefore prudent to investigate the influence of actual variable loadings, obtained from actual field data, on the fatigue response of structures like risers.

In this study, the data obtained from a series of field tests on multimodal VIV of a long flexible model riser have been used to conduct an experimental crack propagation investigation. The strain-time histories recorded during the field tests were used to calculate stresses, which were subsequently applied to the fatigue test specimens. In the first stage of the study, the exact VIV-induced stress-time histories were applied to a number of specimens and the crack growth was monitored accordingly. The results are compared with those obtained through analytical approaches used in the offshore industry for fatigue life estimation of risers under VIV-induced vibrations. It is observed that the available methods may significantly underestimate the fatigue damage of risers, which is not acceptable for design purposes. This may justify the high safety factors that are used in the offshore industry for estimating the fatigue life of risers.

In the next stage of the study, the VIV-induced stress-time history was filtered for a certain portion of the frequency range, so that the influence of different VIV harmonics on the overall fatigue damage of the riser could be investigated. Currently, the fatigue design of risers is generally based on the assumption that the VIV-induced stress-time history is a narrow-banded random process, centered on the vortex shedding frequency. The presence of higher harmonics is overlooked. In 1988, Vandiver and Chung (1988) reported the existence of higher harmonic components in low mode number VIV response of flexible cylinders at three and five times the fundamental vortex shedding frequency. In 2006 new high mode number experiments revealed that the third harmonic (at three times the frequency of the first) may cause fatigue damage at a rate exceeding

that of the first harmonic, and should not be ignored when estimating the fatigue life of the structure under high mode VIV (Vandiver *et al.* 2006).

In the present study, in the analytical simulation of the fatigue crack growth, first the VIV-induced VAL was transformed to equivalent constant amplitude loading using the Hudson and the Barsom methods. At the next stage, the Paris and Walker fatigue models were used to calculate the fatigue crack growth due to the equivalent constant amplitude loading. It is demonstrated that these models may significantly underestimate the fatigue damage of risers; hence the use of more sophisticated approaches is recommended. The results from the experimental tests are explained in detail in this study, and direction for future research in this area is proposed accordingly.

### **4.3. Long Flexile Tensioned Risers in Deep Waters**

As stated, due to the recent explorations in deeper waters by the oil and gas industry, the risers have become very long and flexible. Therefore, the risers now have the potential to vibrate in high modes. This has prompted the investigators to conduct extensive investigations in order to understand the high mode VIV response of long flexible risers in deep waters (see for example: Li *et al.* 2005; Vandiver *et al.* 2006). In the following paragraph, the recent work by Vandiver *et al.* (2006), which forms the foundation of the loading scenario used in the present study, is summarized.

In a recent series of studies by Vandiver *et al.* (2006), a densely instrumented carbon-glass fiber-reinforced composite pipe with a length of 147.9m and an outside diameter of 35.5mm was tested in the Gulf Stream in offshore of Miami, Florida (see Figure 4.1). The research was aimed at understanding the VIV response of a long riser at high mode numbers and to determine the relative contribution of damage rate arising from in-line and cross-flow VIV. The length and diameter of this pinned-pinned model riser were chosen such that the riser would be excited at high mode numbers. Table 4.1 summarizes the specifics of the model riser, which had a length to diameter ratio of 4160. The current profiles encountered by the towed model riser were recorded using an acoustic doppler current profiler (ADCP). Sending an acoustic ping and recording the returned sounds, the

ADCP measured the current speed and direction from the surface to a depth greater than 500 feet (152.4m). Mechanical current meters suspended beneath the surface vessel and 2 m below the weight at the bottom of the towed riser, provided independent current speed measurements at the top and bottom of the riser. Riser inclination angle at the top, top tension and the signals from two conventional current meters were recorded using a laptop controlled SigLab data acquisition system. Both static and dynamic components of tension were measured using a load cell.

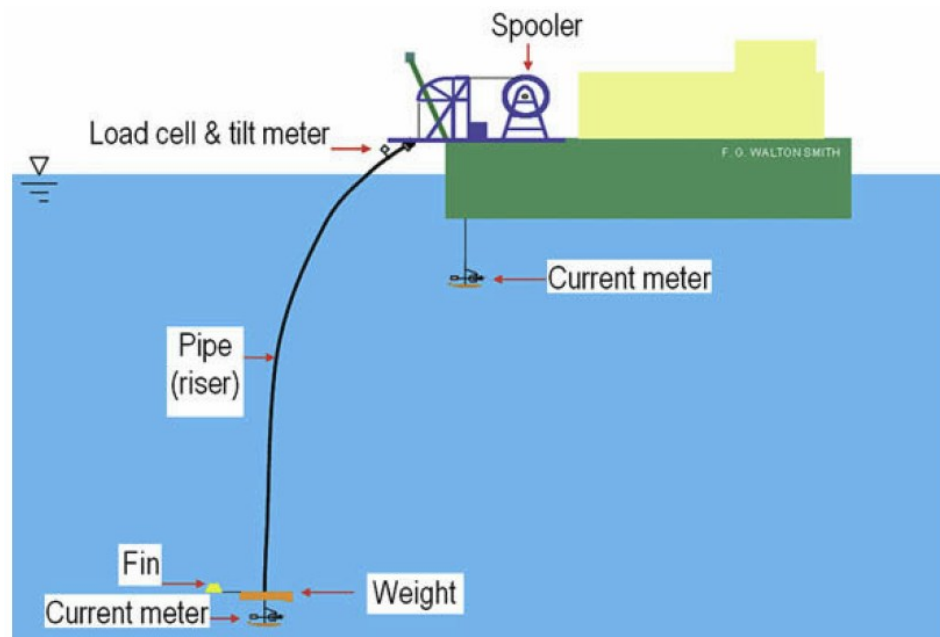


**Fig. 4.1.** Schematics of the VIV test (from Vandiver *et al.* 2005).

To monitor the vibration of the riser and calculate the strains over its length due to VIV, the riser was instrumented with fiber optic strain gauges. More details on this investigation can be found in Vandiver *et al.* 2006.

The measured strains in the pipe were a result of both tension force acting along the longitudinal direction of the riser at any point, and the bending moment due to cross-flow and/or in-line VIV. To calculate the net bending strain, the strain due to the tensile force must be decoupled from that created in the pipe by the bending action. This approach could not be used for the whole riser’s length in the riser tested by Vandiver and his coworkers, because a great number of “paired” strain gauges used to record the strains in



their experiment encountered mechanical failures (Vandiver *et al.* 2006). As an alternative approach, the bare data could be filtered to eliminate the low frequency tension variation caused by vessel motions.

**Table 4.1.** Material and physical properties of the carbon-glass fiber-reinforced composite riser (Vandiver *et al.* 2006)

Outer diameter	35.5 mm
Optical fiber diameter	33.0 mm
E	15858 MPa
EA	3780988 N
Weight in seawater	0.179 kg/m
Weight in air	1.237 kg/m
Density	1.47 (g/cc)

It is noted that the VIV-induced VAL strain-time history from the tests on the carbon-glass fiber-reinforced composite riser explained above can be used to calculate the stresses in a riser made of a different material, so long as the risers exhibit *similar* natural frequency and VIV response. The fundamentals used in this approach and the requirements to ensure the ‘*similarity*’ are explained later in detail in this chapter. It should be noted that in this study the fatigue tests are done on an aluminum alloy, and not on the carbon-glass fiber-reinforced composite that was used to form the riser used to measure the strain-time history. The reasons for choosing the alloy for performing the fatigue tests in this study are explained later in detail.

Once the data was appropriately high pass filtered to remove the high frequency components arising from instrument noises and prevent aliasing, the dynamic stress at any point along the model riser could be determined by multiplying the strain values by the Young’s modulus of the material. Figure 4.2 shows a typical graph of the strain

recorded due to the cross-flow vibration near a region with the maximum RMS response along the model riser. The sampling frequency was 51.1658 Hz. and this particular sensor was almost perfectly aligned with the cross-flow direction.

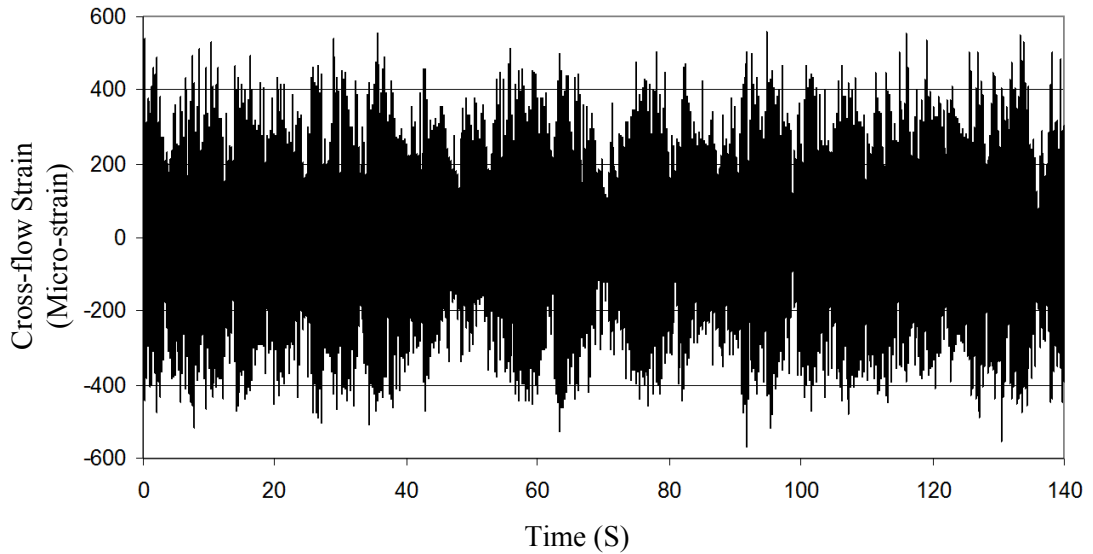


**Figure 4.2.** Cross-flow strain-time history for the 485.3 foot long model riser

Figure 4.3 shows the power spectral density (PSD) of the cross-flow strain time history obtained from a single fiber optic strain gauge. As shown in this figure, the dominant frequency for the cross-flow vibration is approximately 4.5 Hz., which is known as the Strouhal response frequency. This figure also illustrates that a considerable amount of energy is imposed on the structure at a higher frequency range, herein referred to as the third harmonic (being actually the second harmonic resulting from the cross-flow vibration). Such a high frequency shows that the fatigue of a riser is mainly due to low stress amplitude, high frequency stress cycles; rather than high-amplitude stresses. Vibrating with such a high frequency, the riser may face severe fatigue problems during its service life, even at low stress amplitudes. Assuming an average vibration frequency of 5.0 Hz., this model riser would undergo more than two billion stress cycles during a service life of 10 years. At points where the riser experiences higher stress levels, such as touch down point or upper parts of the structure, the fatigue damage becomes even more

likely and severe. Due to both the broadband range and the high frequency content of the third harmonic, it is expected that load cycles related to this frequency range would significantly affect the fatigue life of the riser. This third vibration harmonic is approximately three times the Strouhal frequency. At such a high frequency, this harmonic could cause up to more than 6 billion additional stress cycles on the riser in a 10-year period, resulting in even more fatigue damage than that induced by the first harmonic. Investigation of the fatigue response of risers due to this third harmonic is the primary objective of our study, since the available riser design software packages do not directly consider this third harmonic.

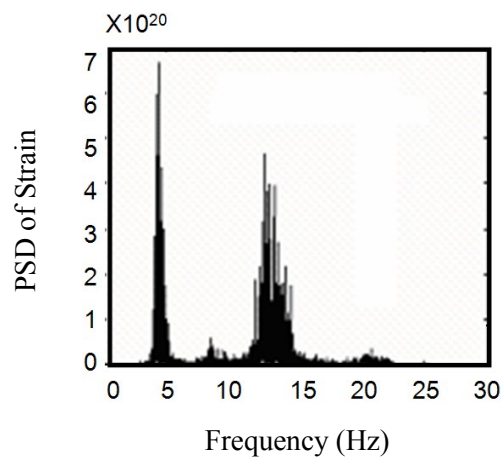


**Figure 4.3.** Power spectral density of the cross-flow strain time history of a 485.3 foot long model riser

#### 4.4. Experimental Set up

The fatigue life assessment of the riser was conducted based on fatigue tests performed in the laboratory, using equivalent specimens and load sequences that would basically represent the actual in-service performance of risers in deep waters. A representative load sequence was selected from the field data. It should be noted that a load spectrum does not necessarily contain information on the variation of the applied load that contributes to the overall fatigue damage of the component (Reis *et al.* 2004). Therefore, in the present

work, the authors used the actual strain-time history data measured during the field tests, and transformed it to a stress-time history to be applied to the test specimens. Although it was somewhat difficult and time consuming to apply such a detailed stress-time history to the specimen, this strategy was vital for understanding the basic physics of the VIV-induced fatigue response of riser, and for future direction of our research.

The nature of riser VIV-induced stress-time history is very close to the stress history associated with the wings of an aircraft. For such components, the damage is usually calculated by a cycle-by-cycle or flight-by-flight crack growth approach (Pantelakis *et al.* 1997). To simplify the complex VIV load history, some codes allow the application of the linear elastic fracture mechanics (LEFM). The LEFM concept focuses on the fatigue crack growth and does not consider the fatigue crack initiation life of the component. This concept can be justified for structural analysis by studying the influence of load interaction effects on the overall fatigue life of a component (Pantelakis *et al.* 1997, Yuen and Taheri, 2004 and Iranpour and Taheri, 2006b), or where defects are assumed to exist in material (DNV-OS-F201 2001). Moreover, the results from a crack growth analysis can be used to correlate the influence of history-sensitive residual stresses to the nonlinearity resulting from cumulative fatigue damage under VAL (Sunder, 2003).

The concept of linear elastic fracture mechanics has been recommended by DNV for evaluating the fatigue crack growth life of risers, and establishing effective inspection criteria (DNV-OS-F201 2001). Since this approach does not include the number of cycles consumed for the crack initiation, shorter fatigue life is expected when using this approach. As recommended by DNV, only the stress components normal to the propagation plane need to be considered and the effect of compressive stresses are ignored. However, recent studies have illustrated the significant influence of compression underload on the crack growth rate of metallic components (see for instance Yuen and Taheri 2004). In this study, the initial representative stress-time history has been further filtered for a specific frequency range, so that the influence of different VIV related harmonics on the overall fatigue damage of the component could be investigated.

For the experimental program, the stress-time history was applied to test specimens via a computer program. Due to some limitations of the computer software package, the

entire VIV stress-time history could not be applied to the specimen in one block. Selecting a representative VIV time history block seemed to be a reasonable approach for reducing the number of data points down to the level that could be handled by the software. Based on the frequency content of different selected regions of the recorded field data, a period of 151.23 seconds was selected, which was considered to be a very good representation of the data set. The Rainflow algorithm, based on the ASTM standard (ASTM E 1049-85, 1999) was used to count the loading cycles within this period, which resulted in 1,824 cycles in each block. This block of loading was then repeatedly applied to the test specimen and the relevant crack growth rate was measured. Therefore, instead of plotting crack length versus number of cycles ( $da/dN$ ), as done conventionally, here the results are presented in the format of crack length versus number of blocks (each block being 151.23 sec.)

The following paragraphs will provide details for the stress-time history, and other pertinent information regarding the material and testing scheme followed in this study.

#### 4.4.1. Loading (stress-time) History

As stated earlier, the carbon-glass fiber-reinforced composite riser was densely instrumented with fiber optic strain gauges. The measured strains were multiplied by the modulus of elasticity of the riser's material to obtain the resultant VIV-induced stresses. As will be explained later, the fatigue tests in this study are performed on aluminum plates with a different modulus of elasticity than the tested carbon-glass fiber-reinforced composite model riser. Therefore, it was necessary to relate the magnitude of the strains measured for the model riser to the aluminum plate specimens tested in this study. This equivalency was based on the actual dynamic response of the model riser tested in the field.

Equation 4.1 shows the natural frequency of a tensioned riser with pinned boundary condition (Vandiver and Peoples 2003; Harrison and Nettleton 1997):

$$f_n = \frac{1}{2\pi} \left( \left( \frac{n\pi}{L} \right)^2 \frac{T}{m} + \left( \frac{n\pi}{L} \right)^4 \frac{EI}{m} \right)^{1/2} \quad (4.1)$$

where  $f_n$  is the natural frequency of the  $n^{\text{th}}$  mode (Hz.),  $n$  is the mode number,  $L$  is the length of the riser ( $m$ ),  $m$  is the mass per unit length ( $kg/m$ ),  $T$  is the tension in the riser ( $N$ ),  $E$  is the modulus of elasticity of the material ( $N/m^2$ ) and  $I$  is the area moment of inertia of the riser's cross section ( $m^4$ ). The first term on the right hand side of Equation 4.1 is related to the tension in the beam, while the second term accounts for the bending rigidity of the structure. In cases where the tension-related term is much larger than the bending term (such as in the case in hand), the riser can be considered as a tension-dominated structure. In such a case, the natural frequency would be primarily a function of the tension force, the length of the riser, and its mass per unit length. In other words, as long as two tension-dominated long risers with two different materials have identical dimensions and mass per unit length, their natural frequencies will be the same.

In summary, this equivalency makes it possible to multiply the measured strain field data by the modulus of elasticity of another material (e.g., aluminum), and apply the resultant stresses to that material (i.e., aluminum plate test specimens), using an appropriate test machine. It should be noted that this equivalency procedure is admissible so long as the tension term is significantly larger than the bending term. Vandiver and Peoples (2003) estimated the tension term to be approximately 13 times larger than the bending term in the riser tested.

It should be noted that once a crack initiates and grows further through the wall thickness of the pipe, the natural frequency of the system remains unchanged. This is due to the fact that none of the parameters that govern the natural frequency of a tensioned structure would significantly change after the crack grows through the material. This is also supported by a series of experimental researches performed by Odahara and his co-workers in 2005, where a small pipe was tested under the action of very high frequency in-line VIV. Even in their bending-dominated response case, it was observed that neither the vibration amplitude and the resultant strain history, nor the natural frequency of the pipe changed as the crack grew through the material. In fact, all these parameters remained constant almost up to the failure stage of the specimen. This implies that a cracked riser would undergo the same VIV and strain-time history as that of an uncracked one. This supports the equivalency idea stated earlier, indicating that the

available field data could be directly used to perform fatigue tests on aluminum or steel plates.

#### **4.4.2. Material Selection**

##### 4.4.2.1. Preamble

In risers, fatigue occurs at low stresses, in the order of giga-cycles, with most of the cycles being near the endurance stress limit of the material. Therefore, the resulting fatigue response would be different from that commonly experienced by most structures that become subjected to relatively high stress cycles.

The low stress, high cycle fatigue in risers result in near-threshold fatigue crack growth, which is a function of many parameters such as the material properties, the environmental conditions, stress ratio, crack closure, microstructure and the nature of the stress time history (Antolovich, 1997). Due to the lack of crack closure in small surface cracks, the threshold value decreases with decreases in the crack length. This results in a crack growth at a stress intensity factor below the threshold value of the material for macroscopic cracks (McEvily, 1997). The length of such a short surface crack is usually in the order of 0.005 mm. This process is referred to as anomalous fatigue crack growth behavior (McEvily, 1997). The values reported for the endurance limit are based on constant amplitude tests, where *all* cycles of the stress-time history are required to be lower than the endurance limit (Dowling, 1988). In a VAL scenario, no damage is assigned to stress cycles with an amplitude lower than the endurance limit. However, studies have shown that stress cycles below the endurance limit become damaging in VAL scenarios, where the endurance limit is often exceeded (Veers, 1997).

A literature review revealed that Miner's accumulation fatigue damage rule is being widely used for fatigue life estimation of risers under VIV-induced stress time history (Iranpour and Taheri, 2006a). Many researchers have investigated the applicability of Miner's rule for fatigue life estimation of components under VAL scenarios. These experiments have shown that the Miner's sum is rarely equal to unity under VAL scenarios (Wirshing and Wu, 1985). Under such a loading scenario, they demonstrated Miner's sum to be within a range of 0.792 to 1.72, having a COV range of 0.16 to 0.98.

For cross-flow variable amplitude VIV-induced stress time history, a value between 0.2 to 0.8 has been reported for Miner's sum by Odahara *et al.* (2005). However, the same authors stated that as the time history approaches a constant amplitude loading scenario under very high frequency in-line VIV (e.g. in the case of fast breeder reactors in nuclear power plants), the Miner's sum becomes closer to unity. Such a large scatter in Miner's sum for VAL causes significant errors in fatigue life calculation of the component. One of the reasons for such a high scatter is explained to be the complexity of the material response and its behavior at the endurance limit under VAL scenarios (Veers, 1997).

It should be noted that the threshold value decreases due to the decrease in the crack length, increase in the stress ratio, and the presence of the corrosive seawater environment. Note that changing the environment from air to salt water usually tends to reduce the crack growth threshold, while accelerating the fatigue crack growth rate in any stress intensity factor range (Radon, 1979). The influence of such a corrosive environment has shown to become even more pronounced at relatively low values of stress intensity factors (Radon, 1979). Moreover, due to its effects on the crack closure, debris in salt water has shown to exert significant influence on near-threshold growth (Soboyejo and Knott, 1990).

Moreover, compressive underloads and periodic tensile overloads in a variable amplitude stress-time history decrease the threshold stress intensity factor. It was also illustrated that microscopic short surface fatigue cracks may grow at a stress intensity factor below the threshold value of the material. This becomes even more pronounced under the action of a corrosive environment such as seawater. This fact has encouraged the authors to conduct the tests on a material, other than steel, which shows a lower endurance limit. By using such an approach (which includes the influence of all stress cycles and also masks the influence of some of the parameters, such as sea water), one can better investigate the influence of VIV-induced stress-time history on fatigue response.

#### 4.4.2.2. Material selected for this investigation

For materials that do not show a specific endurance limit (i.e. aluminum), the stress-life response of the structure can be more correctly described by the fatigue strength at a



given number of cycles (Cameron *et al.* 1997). The endurance limit does not exist for high strength steel or nonferrous metals such as aluminum alloys (Mitchell, 1997). The ratings for the fatigue endurance that is reported for aluminum alloys are for a certain number of cycles and are based on rotating-beam tests (Bucci *et al.* 1997). Such a test setup creates constant amplitude loading, not accounting for the effect of periodic overload cycles on the fatigue limit. Study shows that a single large overload that is usually applied to the component during its service life causes the endurance limit to decrease, if not become totally eliminated at all (Mitchell, 1997; Brose *et al.* 1974). Moreover, no well-defined quantitative relationship is observed between the fatigue limit and the static strength of aluminum alloys.

Fatigue behavior of aluminum alloys has shown significant directionality effects, especially in the threshold region (Antolovich, 1997). In the L-T orientation, the crack can propagate intergranularly, resulting in a more flat fracture surface with no closure effect. In such cases, the whole stress range of a cycle is considered responsible in the growth of the crack and the threshold value would not be affected. For a crack growing in the S-T direction, the crack surface is rougher and the resultant crack closure leads to lower threshold values compared to the L-T direction (Antolovich, 1997). However, such ranking for the aluminum alloys is not presented when the alloy is under the action of VALs or components are under the action of constant amplitude loads combined with periodic overloads (Antolovich, 1997). This is due to the overloads and their influence on debonding large particles and the subsequent reduced constraint during lower stress cycles (Antolovich, 1997).

The above facts were the motivations for the authors to use aluminum alloys for the experimental program in this research. Using an alloy with lower threshold value (if any at all), allows one to account for the influence of all stress cycles in the VIV-induced stress-time history. Therefore, there would be more similarity between the experimental tests in this study and the actual conditions experienced by risers, where the threshold value of material decreases due to the corrosive effects of seawater.

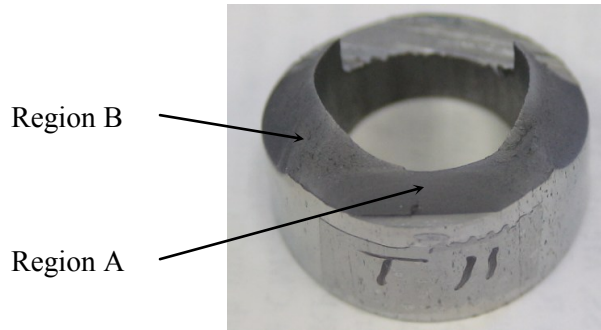
The test specimens were cut from a 6061-T651 aluminum alloy commonly used to fabricate many structural components. Dimensions and other physical properties of the specimens are given later.

#### **4.4.3. Equivalency Testing Preamble**

To study the fatigue crack growth rate of a riser structure under multimodal VIV in a uniform current profile, a series of experimental tests were performed at the Materials Testing Laboratory of Dalhousie University, in Canada. Although the model riser tested in the Gulf Stream offshore of Miami was a pipe under the action of bending moments arising from cross-flow and in-line vibrations, the authors decided to perform the tests on plate specimens rather than a pipe. The use of an equivalent plate subject to tension instead of a pipe subject to bending has also been tried by other researchers (Chen and Lambert, 2005). The reason for this simplification is to avoid the complexities that are usually involved with the experimental crack growth monitoring in pipes. This approach minimizes the use of more sophisticated and expensive monitoring instruments. The details and justification of the equivalency is reported by the authors in a different publication (Iranpour and Taheri, 2006b; see Chapter 3 of this dissertation). In that study, a dimensionless relationship between the stress intensity factor of a pipe under bending moment and that of an equivalent plate under pure tension was proposed.

To observe the mode of the crack growth and its shape during its propagation through the wall thickness of the pipe, a series of preliminary tests were conducted on pipe specimens. In this series of tests, a 4-point bending test setup subjected the pipe to pure bending moment as induced by VIV. It was observed that the crack grew under mode I fracture, where stress intensity factors for the modes II and III are zero. Figure 4.4 shows a typical crack surface of a pipe specimen under VIV-induced bending moment. As illustrated in this figure, the crack grows in mode one before it reaches the inside surface of the pipe. This is shown as Region A in Figure 4.4. After the crack reaches the inside surface, stable crack growth region is terminated and the crack grows in an unstable mode with a much faster speed (Region B in Figure 4.4). This represents the growth in region three of a typical  $da/dN$  versus  $\Delta K$  graph (where  $da$  being the crack length

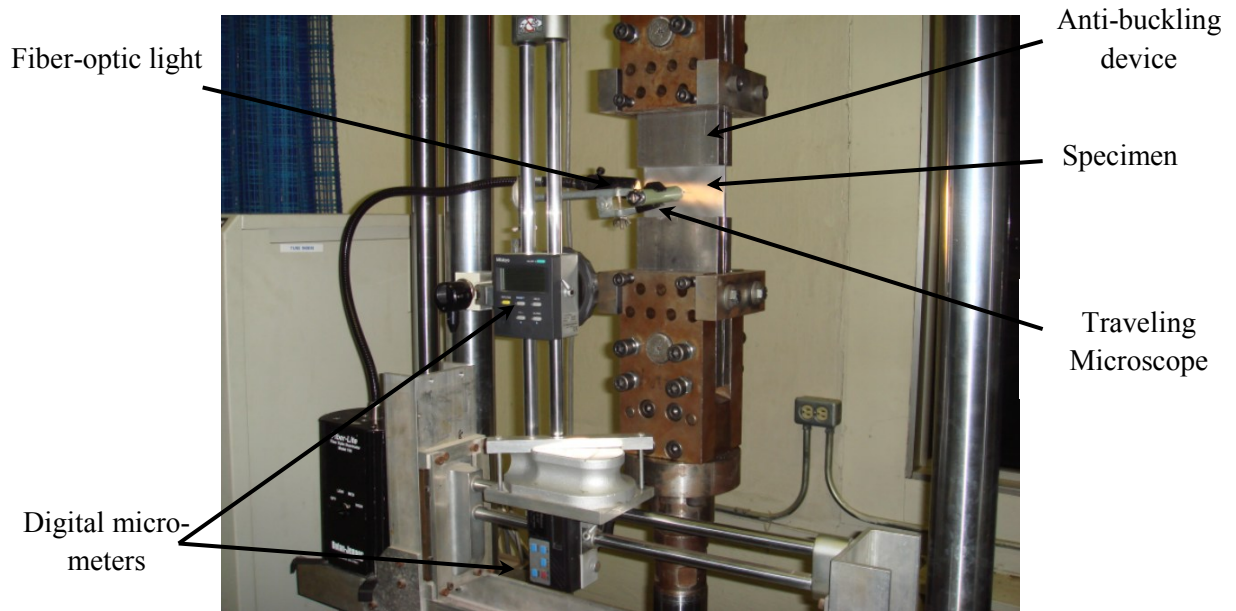
increment,  $dN$  being the increment of cycles and  $\Delta K$  being the range of stress intensity factor). The focus of this study is on the crack growth accruing in a stable mode (i.e. Region A), before it reaches the inside surface of the pipe and causes leakage.



**Figure 4.4.** A typical crack surface of a pipe under VIV-induced stress-time history

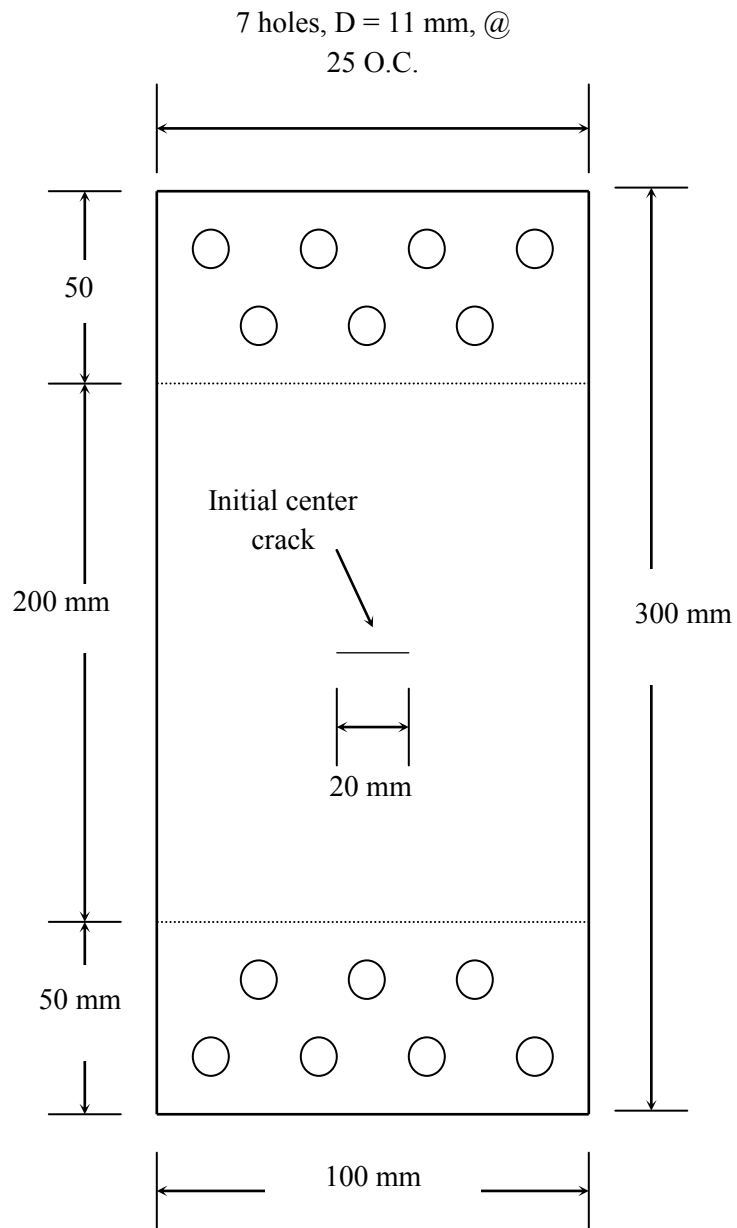
#### 4.4.4. Testing Apparatus

Figure 4.5 illustrates the test set up. A digitally-controlled Instron Servo-hydraulic Universal Testing Machine model was used to apply the VIV load time history to the test specimen. The VIV load was applied to the plate specimen through a special purpose software package. The machine was equipped with a load cell with a capacity of  $\pm 100KN$  under dynamic or  $200KN$  under static loading conditions. To monitor the growth of the crack tip after applying a certain number of blocks of VIV load history, a Mitutoyo traveling microscope with a magnification of 50X controlled by two traveling micrometers with a resolution of 0.01mm were used to record the crack growth increment. A fiber optic light was used to illuminate the crack tip region.



**Figure 4.5.** Test setup

Figure 4.6 shows the rectangular test specimen with the center crack and its dimensions. The tests were performed per ASTM E 8M, Standard Test Methods for Tensile Testing of Metallic Materials (ASTM E 8M, 2001). This standard requires that acceptable geometric correction factors be available for the specimen configuration. Moreover, as a means to ensure that LEFM holds, this standard suggests that the specimen be large enough to promote predominately linear elastic conditions during testing. The plates were cut so that the length of the specimen had the same direction as the rolling direction of the original plate. This caused the fatigue crack to grow transverse to the rolling direction, which is similar to the case for a surface crack growing through the wall thickness of a riser. The surface of the specimen was polished with a wide range of sand paper grits, starting from coarse (No. 120) to very fine (No. 1200). This enabled the crack tip to be clearly visible on the outer surface of the plate.



**Figure 4.6.** Specimen layout and dimension

The top and bottom fixtures, by which the plate specimen was gripped, were connected to the load cell and the actuator, respectively. The fixtures were designed with the capability of aligning the specimen in order to eliminate any unwanted bending due to misalignment. Since the loading sequence consists of tension and compression stress

cycles, small slips of the plate were observed during the first set of tests on plates. This resulted in unequal crack growth rate on the left and right hand side of the center crack. This problem was modified to some extent by re-aligning the specimen during the test procedure and after applying a certain number of load cycles. However, the results were not yet satisfactory, because the crack growth rates were found to be quite sensitive to re-aligning the specimen during the test. Therefore, the grips were modified for the next set of tests to both decrease the slippage and to increase grip capability for better alignment accuracy. Sheet buckling, which occurs at the top and bottom of the crack surface, causes lateral compressive stresses at the crack tip. Moreover, some additional normal stresses may be induced at the crack tip to maintain the balance of the state of the stress of the system (Shows *et al.* 1983). Although the applied compression load to the specimen was lower than its elastic buckling load, anti-buckling devices were created on the grips to prevent any probable buckling in order to eliminate any additional normal stress.

An electric discharge machine (EDM) machine was used to create a 20 mm notch in each plate using. The notch was then pre-fatigued so that sharp crack tips could be obtained. The resulting crack length in each specimen, before the actual VIV-induced loading was applied, was therefore  $2a=24$  mm. This was done to remove the effects of a blunt starter notch and to provide a sharper fatigue crack of adequate straightness and size. The tests were done at room temperature in air. The magnitude of the applied pre-cracking fatigue load was selected to be low enough to prevent any load sequencing effect on the crack growth rate due to the subsequent VIV-induced stress-time history. After the pre-cracking, a specified number of blocks of the VIV-induced stress-time history were applied to the specimen and the crack growth was measured. This procedure was followed until the plates failed (fractured across the width). The crack length was measured by the traveling microscope at specific numbers of elapsed cycles, trying to have a crack growth increment of less than 5.0 mm between each measurement. To compensate for any probable misalignment in the test setup, the crack length was calculated by averaging the measurements of the left and right cracks.

## 4.5. Experimental Results and Discussion

The experiments involved testing three specimens for each VIV-induced stress-time history data set. As stated earlier, during the first stage of the investigation, the stress-time history obtained from the field data was applied to a number of specimens and the crack growth rates were measured. In the subsequent stages, the VIV stress-time history was filtered for a certain portion of the frequency range. This was done to investigate the influence of different vibration harmonics on the fatigue crack growth under VIV load. Each *block* of the VIV-induced stress-time history contained 4,000 data points (2,000 cycles), representing 151.23 seconds of the measured field data. Using the Rainflow counting method, a total of 1,824 cycles were counted for each block. The Rainflow algorithm was based on the ASTM standard (ASTM E 1049-85, 1999). Considering that the data was sampled at a frequency of 51.1658 Hz, one would expect more data points for the selected time period of 151.23 Sec. However, only the local maximum values of each cycle were used for conducting the fatigue tests. This resulted in a decrease in the number of data points required for the tests. It should be noted that none of the stress spikes in the stress-time history were eliminated. The machine frequency was set between 4.0 to 5.0 Hz, so that it could exactly trace the input load history.

As explained earlier, the crack length was measured at both sides of the center crack after a certain number of VIV-induced loading blocks were applied to the test specimen. Figure 4.7 shows a typical crack length versus the number of applied stress blocks. As illustrated in this figure, the crack growth rates on both sides of the started notch are almost equal, demonstrating that the far field stresses were uniform along the width of the plate. This was also used as a technique to check the results from each test for any probable misadjustments or misalignments.

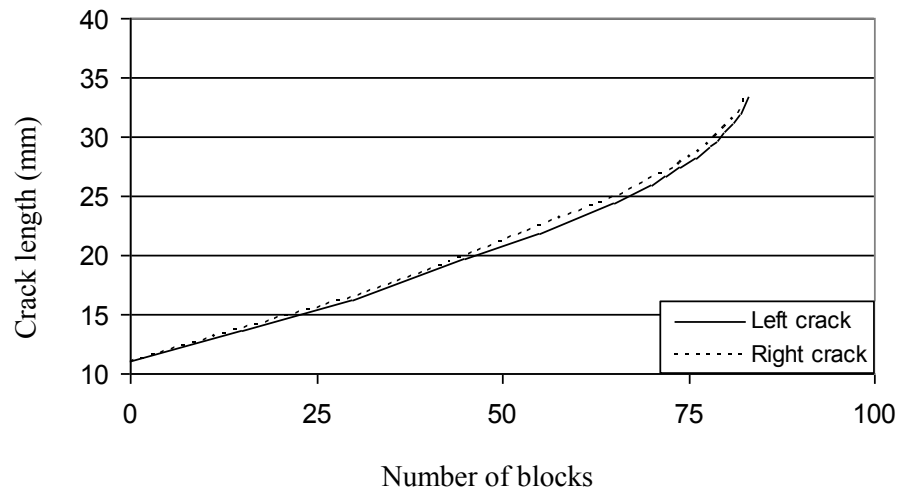


**Figure 4.7.** Typical crack growth versus the number of VIV-induced stress blocks

#### 4.5.1. Actual VIV-Induced Stress-Time History

In this series of tests, the real VIV-induced stress-time history was applied to the specimens and the crack growth rate was measured accordingly. As explained earlier, the measured strains were multiplied by the modulus of elasticity of the tested specimens to calculate the stresses. The resultant stress-time history was then transformed to a load-time history and applied to the specimens. This transformation was based on the cross-sectional area of the uncracked portion of the plate specimen along the crack plane. Figure 4.8 shows the crack length versus the number of the applied cross-flow VIV-induced stress blocks.



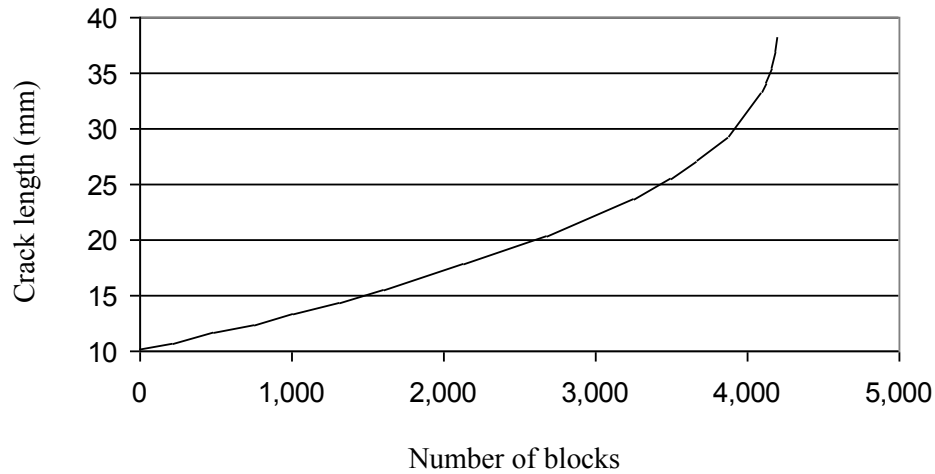


**Figure 4.8.** Crack length versus the number of applied VIV-induced stress blocks (note: each block consists of 2,000 cycles)

#### 4.5.2. Influence of the Third Harmonic

Due to the low frequency and small magnitude of the applied stress, it took a very long time (i.e. weeks) to conduct each test when the exact magnitude of the VIV-induced stress was applied to the specimen. For cases where a certain portion of the vibration frequency was filtered out from the stress-time history, the magnitude of stresses would become even smaller, resulting in even longer times for each test (i.e. over a month). Therefore, the load was increased by a certain multiplier to accelerate the crack growth and shorten the testing time to a reasonable level. For that, in the next testing stage, the VIV-induced stress-time history was multiplied by 2.25. Figure 4.9 shows a typical response in the form of crack length versus the number of applied VIV-induced stress blocks. As illustrated in this figure, the specimens failed after approximately 73.85 to 83.75 stress blocks, representing 147,700 to 167,500 stress cycles, respectively. It should be noted that this approach was only used for studying the influence of different vibration harmonics on the overall fatigue damage of the material.

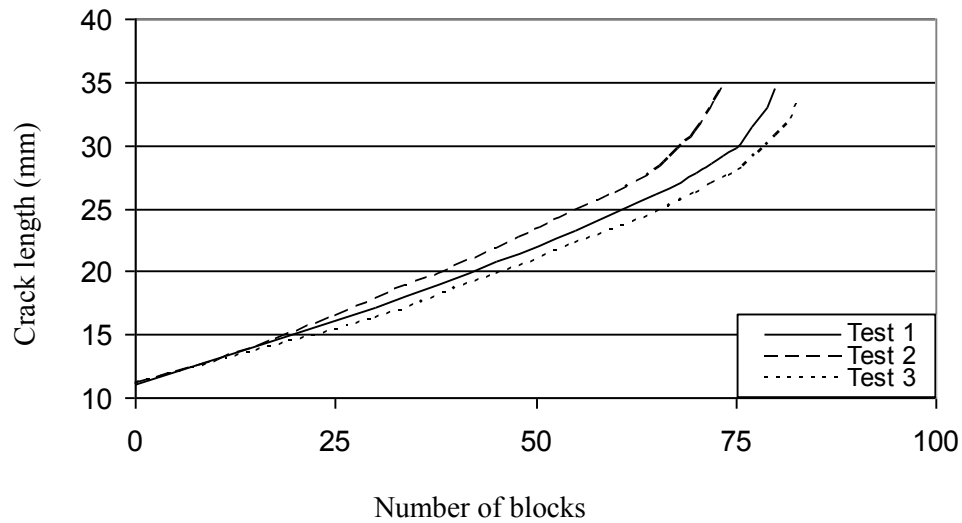


**Figure 4.9.** Crack length versus the number of applied VIV-induced stress blocks (stresses multiplied by 2.25)

In the subsequent set of tests, the cross-flow stress-time history was filtered for the frequency range corresponding to the third harmonic of the cross-flow VIV (those corresponding to  $\sim 13$  Hz as shown in Figure 4.3). The filtered stress-time history was then applied to a number of specimens with the same geometry and initial pre-crack. After filtering the stress-time history, the number of cycles in each *block* decreased to 1,912, compared to 2,000 cycles in each *block* of the unfiltered data. Figure 4.10 shows the filtered strains. A comparison between Figures 4.2 and 4.10 illustrates a reduction in the magnitude of the strains, hence decreasing the resulting fatigue damage.

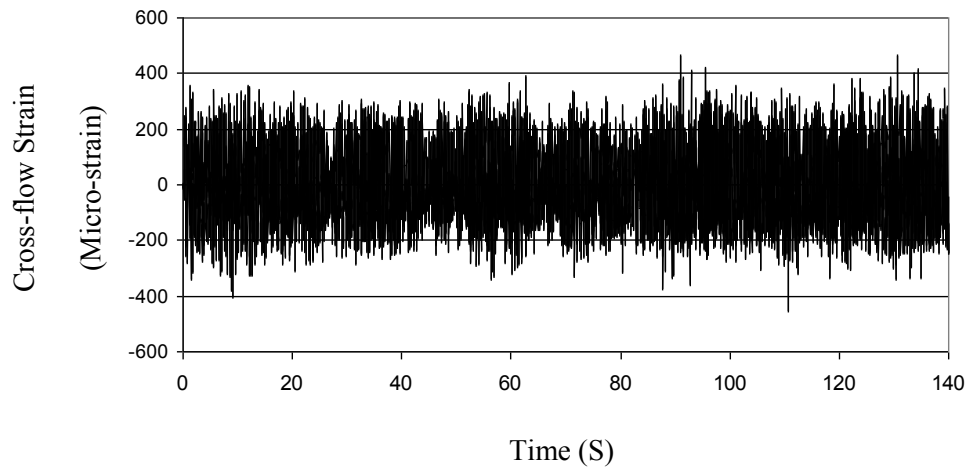


**Figure 4.10.** Cross-flow strain time history of the filtered data

The power spectral density (PSD) of the filtered data is plotted in Figure 4.11, clearly illustrating the elimination of the frequency range from 12.0 to 16.0 Hz. As explained earlier, this harmonic is referred to as the third harmonic in this paper. This vibration harmonic is believed to contain a great amount of energy, which is expected to have a significant contribution to the overall fatigue damage of the riser.

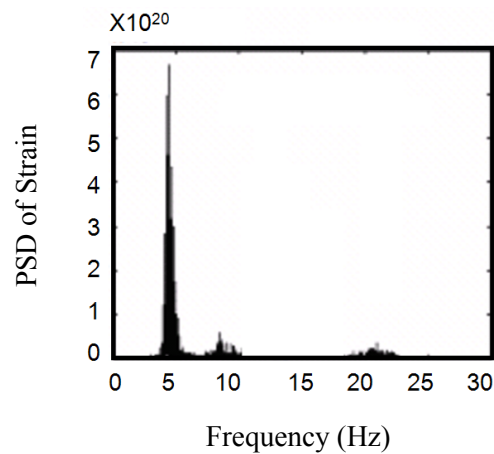


**Figure 4.11.** Power spectral density of the cross-flow filtered strain time history

The filtered strain-time history was multiplied by the modulus of elasticity of the material and then by the 2.25 multiplier before being applied to the test specimens. These specimens failed after approximately 284.7 to 291.1 stress blocks (i.e. 544,346 to 556,600 stress cycles), a range which is approximately three to four times greater than the number of stress cycles required to fail the specimens under the unfiltered cross-flow VIV stress-time history. This indicates the significant contribution of the third harmonic on the overall fatigue damage of risers. Figure 4.12 shows the average crack length versus the number of applied blocks for both filtered and unfiltered stress-time histories for a number of test specimens in each case.

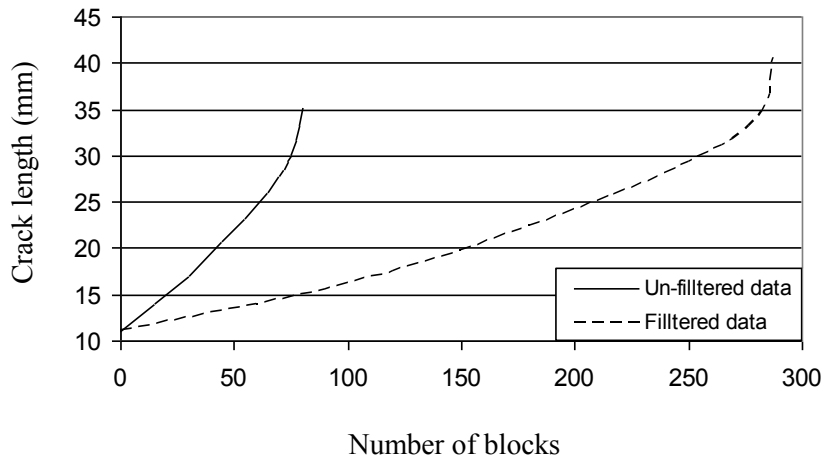


**Figure 4.12.** Crack length versus the number of applied VIV-induced stress blocks for both filtered and unfiltered data (stresses multiplied by 2.25)

As stated, in both the filtered and un-filtered data, the magnitude of stresses was multiplied by a factor of 2.25 to accelerate the crack growth. As illustrated in this figure, the crack growth rate of the filtered data is almost 30% of the unfiltered one. This shows the significant damaging effect of the third harmonic in the cross-flow VIV, a fact that is usually overlooked in the design of such structures. The third vibration harmonic has a frequency range of about 10.5 to 16 Hz., which is three times the Strouhal frequency.

## 4.6. Analytical Simulation of Crack Growth

A computer code was developed in the MATLAB environment to validate the applicability of the most commonly used VAL analytical crack growth models for estimating the fatigue life of risers under VIV-induced stresses. The analytical fatigue life estimation involves the growth of the crack from its initial length after pre-cracking to the intermediate length or the final stage of fracture, where the specimen fails under the applied load. The fatigue crack growth calculation for a VAL should at least consider the stress intensity factor, the stress ratio and the history of the applied load. The nature of the applied loads; that is, whether overloads or underloads exist in the load spectrum, can significantly affect the crack growth in subsequent cycles. In the next paragraphs, the shortfalls of the block-by-block and cycle counting approaches will be discussed, followed by outline of the stress intensity factor-based methodology used by us to evaluate the crack propagation in our specimens.

In the block-by-block approach (based on the Rainflow methodology), the applied load history is divided into a certain number of different blocks and fatigue crack growth from each block is calculated accordingly. With this approach, the total fatigue damage of the component would then be the cumulative sum of the damage from all loading blocks. In the second approach (the cycle counting approach), the crack growth due to each load cycle is calculated and added sequentially to those obtained from the other cycles. These approaches have worked satisfactorily for cases where the applied load is highly irregular, so long as the frequency of the applied overloads in both tension and compression are similar (Stephens *et al.*, 2001).

The cycle counting in the block-by-block approach is based on the Rainflow method, which is widely used in the offshore industry and provides better fatigue life prediction than other methods such as the level-crossing or the peaks-and-valleys methods (Johannesson, 2002). This method is used to reduce a huge set of data to a manageable set of arrays (Nagode *et al.* 2001). Extensive efforts have been made to modify the Rainflow algorithm so that load sequencing effects can be taken into account (Anthes, 1997). However, any improvement to this method should be based on experimental tests that implement the specific time-history for which the method needs to be improved. In

the block-by-block approach and the Rainflow algorithm, the fatigue crack propagation rate,  $da/dN$ , is assumed to be constant. Therefore, to obtain the best results, one should divide the stress time-history into a large number of small blocks. On the other hand, the sequence effect can be better traced if each block contains a large portion of the stress-time history. This conflict can be considered as one of the main disadvantages of the block-by-block approach and the Rainflow algorithm. This highlights the importance of conducting experimental tests, in which a large stress-time history is applied to the specimen and the results are compared with those from such analytical approaches.

To estimate the crack growth in the specimens, the approach based on the stress intensity factor is used, which basically predicts the state of the stress at the crack tip caused by remote loading. The approach, which is applicable under the condition of linear elastic fracture mechanics (LEFM), amplifies the magnitude of the applied stresses near the crack tip and accounts for geometry related parameters of the component. The stress intensity can be calculated by:

$$K = S\phi\sqrt{\pi a} \quad (4.2)$$

where  $S$  is the nominal far field stress normal to the crack,  $\phi$  is a dimensionless geometric parameter (i.e. function of crack length to specimen width ratio) and  $a$  is the crack length. Although empirical equations are available for calculating the stress intensity factor of a rectangular plate with through-the-thickness center crack, one may use the following formulation, which is based on finite element analysis and offers a more accurate relation (Anderson, 1991):

$$K = S\sqrt{\pi a} \left[ \sec\left(\frac{\pi a}{2W}\right) \right]^{1/2} \left[ 1 - 0.025\left(\frac{a}{W}\right)^2 + 0.06\left(\frac{a}{W}\right)^4 \right] \quad (4.3)$$

where  $W$  is the width of the plate. Once the stress intensity factor is calculated, the fatigue life of the component could be estimated using an appropriate fatigue model, such as the Paris or Walker models as examples. When the applied load has a repeating load history pattern, or in cases with block load spectra, one may use an equivalent stress intensity factor for fatigue life estimation of the component (Stephens *et al.*, 2001). This approach simplifies the analysis and is considered to be admissible for cases where the

crack growth rate is relatively low (such as the case under the study). This is the approach that is used in this study and coded into the Matlab program. In other words, the variation of the crack tip stress-strain field is described in terms of the root-mean-square value of stress intensity factor range,  $\Delta K_{rms}$ , written as:

$$\Delta K_{rms} = \Delta S_{rms} \times \phi \sqrt{\pi a} = \sqrt{\frac{\sum_{i=1}^N \Delta S_i^2}{N}} \times \phi \sqrt{\pi a} \quad (4.4)$$

where  $\Delta S_{rms}$  is the nominal root-mean-square stress range of the variable amplitude load history,  $\Delta S_i$  is the nominal stress range in the  $i^{\text{th}}$  cycle, and  $N$  is the total number of cycles. The root-mean-square stress intensity factor is known to be the characteristic of the load distribution curve and is independent of the order of the cyclic load fluctuation (Barsom and Rolfe, 1999). The same crack growth rate has been reported for descending, ascending and random-sequence loadings (Barsom and Rolfe, 1999). Once the root-mean-square stress intensity factor for a loading block is calculated, one may use it to calculate the fatigue crack growth rate of that loading block.

The above approach was coded into the MATLAB. The stress-time history of the loading block and the geometrical properties of the tested plate specimen (e.g. plate width and thickness, modulus of elasticity, initial crack length, etc.) were input to the MATLAB code and the crack growth rates were calculated accordingly. Both the Paris and Walker equations were used for calculating the fatigue crack growth. The Paris equation is expressed (Stephens *et al.* 2001):

$$\frac{da}{dN} = A(\Delta K)^n \quad (4.5)$$

where  $da/dN$  is the crack growth rate, and  $A$  and  $n$  are material constants that are determined from experimental tests for each material. For aluminum 6061-T651, these constants are reported in literature as  $A = 1.743 \times 10^{-11}$  and  $n = 2.82$  (Sheu and Song, 1995). As a more advanced fatigue model, in which the effect of stress ratio is taken into account, one may use the Walker's model (Stephens *et al.* 2001):

$$\frac{da}{dN} = \frac{A(\Delta K)^n}{(1-R)^{n(1-\lambda)}} \quad (4.6)$$

where  $R$  is the stress ratio equal to  $R = K_{\min} / K_{\max} = S_{\min} / S_{\max}$ . It is well known that the influence of the stress ratio on fatigue crack growth is material dependent. Therefore, it is necessary to determine the material constant  $\lambda$ . For components under VAL, in which a wide variety of stress ratios exist, one may use a typical value of 0.5 for  $\lambda$  (Stephens *et al.* 2001). For cases with block loading, the root-mean-square values for stress intensity factor and stress ratio were used to calculate the related crack growth rate.

The fatigue crack growth versus the number of applied stress blocks were illustrated in Figures 4.8 and 4.12, for both real and factored VIV-induced stress-time histories, respectively. The experimental results in this research were compared with those from the analytical monitoring of crack growth. Figures 4.13 and 4.14 show this comparison for both the real and factored VIV-induced stress-time histories, respectively.

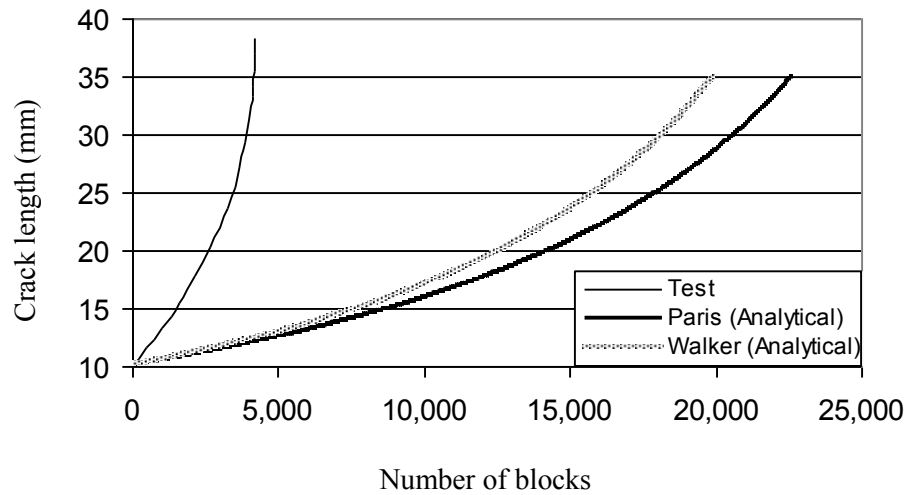


**Figure 4.13.** Crack length versus the number of applied VIV- induced stress blocks (for actual VIV-induced stress-time history with un-factored stresses)



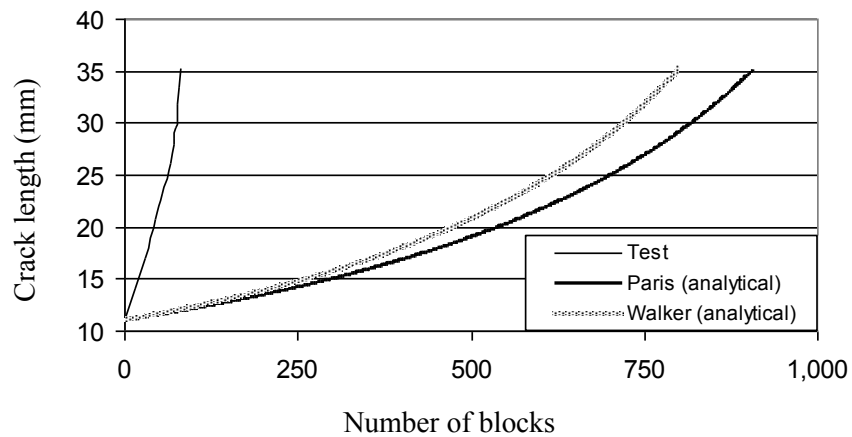


**Figure 4.14.** Crack length versus the number of applied VIV-induced stress blocks (stresses multiplied by 2.25)

As observed in these figures, both the Paris and Walker models highly underestimate the fatigue crack growth of the specimen under the applied VIV-induced stress-time history. One of the disadvantages of these models is that they ignore the crack growth deceleration or acceleration due to overload or underload stresses in a given stress-time history. As studies have shown, the compressive stresses accelerate the rate of the crack growth (Rushton and Taheri, 2003; Yuen and Taheri, 2004). The influence of compressive portion on the crack growth rate of a component under a VAL scenario is reported in detail in a different publication (Iranpour and Taheri, 2006b). In that study, it was explicitly shown that omitting the compressive portion of the stress-time history could result in as much as 60 to 70% increase in the fatigue life of the component, which is alarmingly non-conservative.

The crack growth rate computed based on the Walker model happens to be closer to the real crack growth rate based on the test results. This is due to the fact that the Walker model takes into account the influence of the mean stress, while Paris' model does not. Nonetheless, the growth rates from both models are still alarmingly non-conservative. This explains the reason for using large safety factors that are used by the offshore industry for fatigue design of risers.

## 4.7. Equivalent Constant Amplitude Load

Although Barsom's approach (Equation 4.4) has been reported to be effective for estimating the fatigue crack growth of components under VAL scenarios (Barsom and Rolfe, 1999), when applied to the experimental data of this investigation, as shown in Figures 4.13 and 4.14, it does not seem to be an appropriate approach for estimating the fatigue crack propagation of risers due to VIV-induced variable loads. This may be due to the nature of the VIV-induced stress-time history of risers. The Barsom model is primarily suited for cases where the component is under a random variable amplitude scenario. However, VIV-induced stresses cannot be considered as a complete random loading. In a random loading scenario, the stress overloads or underloads are spread out in a completely random manner in the time history, resulting in a random trend in the Power Spectral Density (PSD) of the applied load. However, the VIV-induced stress-time history cannot be considered as a complete random process. This is shown in Figure 4.3, where the PSD of the VIV-induced stress-time history is plotted. As illustrated in that figure, this stress-time history is not a completely random sequence of loads, since there is a clear repeated trend in the frequency ranges.

To check the applicability of the root mean square approaches for the VIV-induced stress-time history, the numerical results produced by the application of Equations 4.7 were used to generate an equivalent constant amplitude loading, based on the factored VIV stress-time history, in which the stresses were multiplied by 2.25. Moreover, only the tensile portion of the VIV loading was used (i.e., the compressive portion of the VIV-induced stress-time history was ignored). Then, another series of tests were conducted using the calculated equivalent tension-only constant amplitude load. The objective was to determine whether the equivalent constant amplitude load, as determined based on the root mean square approach, could show the same crack growth rate as that produced by the VIV stress-time history. Note that the minimum and maximum loads were determined based on the Hudson model, which implements a root-mean-square approach (Stephens *et al.* 2001):

$$S_{\min(rms)} = \left[ \frac{1}{N} \sum_{i=1}^N (\Delta S_{\min(i)})^2 \right]^{1/2} \quad (4.7.1)$$

$$S_{\max(rms)} = \left[ \frac{1}{N} \sum_{i=1}^N (\Delta S_{\max(i)})^2 \right]^{1/2} \quad (4.7.2)$$

where  $S_{\min(i)}$  and  $S_{\max(i)}$  are the minimum and maximum stresses of each cycle, respectively. Before using Equations 4.6, the stresses in the stress-time history were counted by the Rainflow cycle counting method. The stress ratio of the resultant constant amplitude loading was calculated by:

$$R = S_{\min(rms)} / S_{\max(rms)} \quad (4.8)$$

This method provides an average fatigue crack growth rate and is considered to be an effective approach for cases where the influence of the load interactions is small (Hudson, 1981). When the loading is random in nature, the load interactions would offset each other.

The resultant tension-tension constant amplitude load was applied to a number of specimens with the same geometry as the specimens tested under VIV-induced VAL described earlier. If the Hudson approach was applicable for the VIV-induced stress-time history, one would expect the crack growth rate of the equivalent tension-tension constant amplitude load to be close to that for the VIV-induced stress time-history. However, the results of the tests conducted on the specimens under the equivalent constant amplitude load did not support the applicability of the Hudson model in this case. Figure 4.15 compares the tests result from the equivalent constant amplitude load with the test results from factored VIV-induced stress-time history and the analytical approaches. The curve that represents the tension-tension constant amplitude load is identified in this figure as ‘Hudson’.

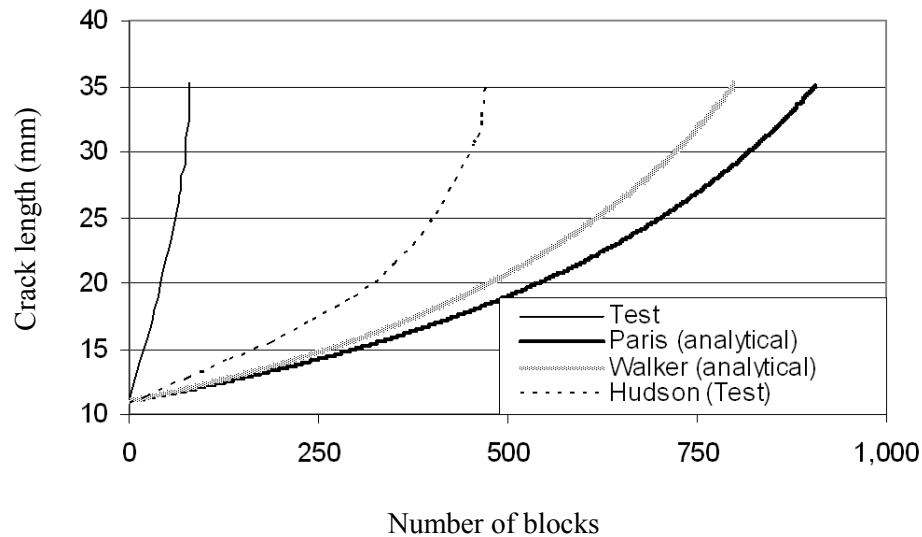


**Figure 4.15.** Crack length versus the number of applied VIV-induced stress blocks (stresses multiplied by 2.25)

As illustrated in this figure, the specimen tested under the equivalent constant amplitude loading failed after applying 471.5 stress blocks. This is about six times greater than the number of the factored VIV-induced stress-time history blocks (i.e. 79.85) that caused similar specimen to fail. As explained earlier, some portion of this difference is due to omitting the compression stress cycles in the equivalent constant amplitude loading. The remaining portion of the difference may be due to the inapplicability of Hudson's model for transforming the VIV-induced stress-time history to an equivalent constant amplitude load. In other words, the Hudson model does not seem to be very suitable for calculating the fatigue crack growth of components under VIV-induced stress-time history.

At this juncture we wondered whether the observed difference between the experimental and analytical results was due to inadmissibility of the root mean square based approaches when applied to VAL scenario, or to the third VIV-induced vibration harmonic. To clarify this issue the authors conducted another experimental investigation using a series of VIV-induced stress-time histories that had been generated in the laboratory, and only consisted one vibration harmonic (see Iranpour and Taheri, 2012b;

see Chapter 5 of this dissertation). The test results from that study demonstrated that the root mean square based approach is inadmissible to such VIV-induced stress-time histories, even if only one vibration harmonic is observed in the PDS of the stress-time history. Additional information can be found in Iranpour and Taheri (2007).

As explained earlier, the inapplicability of the root mean square based approaches to VIV-induced stress-time histories may be due to the fact that such VAL scenarios cannot be considered as a complete random loading. Moreover, most of the tests on risers use a constant amplitude loading scheme. However, this study illustrates that approaches used by the offshore industry for computing the equivalent constant amplitude load may not result in an accurate prediction of the fatigue damage. This highlights the necessity of using more sophisticated fatigue crack models, which have been developed based on experimental tests using actual VIV-induced stress-time histories. VAL scenarios in risers are not a fully random process, and therefore, the influence of load sequencing effects could play an important role and should be taken into account.

#### **4.8. Summary and Conclusions**

The field data from a long flexible model riser was used to study the fatigue crack growth due to the stresses generated by high mode VIV. Long risers in deep waters undergo multimodal vibration with two different harmonics clearly illustrated by the PSD of the field data shown in this paper. In this research, the measured strain field data was directly transformed to stress and then applied to a number of specimens to investigate the fatigue crack growth rate.

The tests indicated that the crack growth rate under the real VIV-induced stress-time history is very slow, in the order of about  $2.5E-6$  mm per cycle. This is due to the low amplitude stress cycles that are imposed on the riser due to the cross-flow vibrations, which cause the crack to grow at the threshold region. It was also illustrated that the third harmonic, which imposes a considerable amount of energy on the structure at a higher frequency range, had a significant influence on the VIV-induced fatigue crack growth rate. For specimens where the influence of third harmonic was not taken into account, a

decrease of about 70 % in the fatigue crack growth rate was observed. This is due to the fact that the stresses due to the third harmonic get superimposed onto the stresses from the first harmonic, resulting in an increase in the stress ratio. Moreover, the higher frequency of the third harmonic generates more stress cycles to the riser during its service life, hence increasing the VIV-induced fatigue damage.

The experimental results of this research were compared to the results obtained from our analytical simulation. The cycles in the stress-time history were first counted using the Rainflow counting method. The Barsom approach was then used to calculate the root-mean-square of the applied stresses, followed by the application of the Paris and Walker fatigue models to calculate the crack growth rate. It was observed that these two models significantly underestimated the crack growth rate of the specimen subjected to the applied VIV stresses.

In this study, the Hudson and the Barsom approaches were also used to check the applicability of an equivalent constant amplitude load that could replace the variable amplitude VIV-induced loading scenario imposed on a riser. The fatigue life of specimens tested under the equivalent tension-tension constant amplitude load was six times greater than the fatigue life of the specimens under the tension-compression VIV-induced variable amplitude load. As discussed earlier, about 30 to 40 percent of this difference seems to be associated with ignoring the presence of the compressive stresses in the equivalent tension-tension constant amplitude load. The remaining large portion of the difference could be associated with the inapplicability of the root mean square approaches to the VIV-induced stress-time history. This may be due to the fact that the VIV-induced stress-time history is not a fully random loading. Therefore, the influence of load-sequencing effects, an important parameter, should be taken into account. This highlights the fact that more sophisticated fatigue models should be used by the offshore industry for evaluating the fatigue life of risers under variable amplitude VIV-induced load. This illustrates the need for more research in this area, so that a more accurate and robust fatigue model could be developed.

## **4.9. Acknowledgments**

The financial support of the Natural Sciences and Engineering Council of Canada (NSERC) in the form of a partnership agreement grant to the second author in support of this work is gratefully acknowledged. The VIV field data was provided by the DEEPSTAR Consortium.

## Chapter 5

# Applicability of Equivalent Constant Amplitude Loading for Assessing the Fatigue Life of Pipelines and Risers and the Influence of Compressive Stress Cycles

Mohammad Iranpour and Farid Taheri

Department of Civil and Resource Engineering, Dalhousie University, 1360 Barrington Street, Halifax, Nova Scotia B3J 1Z1, Canada

Accepted for Publication in the Journal of Pressure Vessel Technology

### 5.1. Abstract

Fatigue life assessment of pipelines and risers is a complex process, involving various uncertainties. The selection of an appropriate fatigue model is important for establishing the inspection intervals and maintenance criteria. In offshore structures, the vortex-induced vibration (VIV) could cause severe fatigue damage in risers and pipelines, resulting in leakage or even catastrophic failure. The industry has customarily used simple fatigue models (such as the Paris or Walker's), for fatigue life assessment of pipelines and risers; however, these models were developed based on constant amplitude loading scenarios. In contrast, VIV-induced stress-time history has a variable amplitude nature. The use of the simplified approach (which is inherently non-conservative), has necessitated the implementation of large safety factors for fatigue design of pipelines and risers.

Moreover, most of the experimental investigations conducted to date with the aim of characterizing the fatigue response of pipelines and risers have been done based on incorporation of constant amplitude loading (CAL) scenarios (which is unrealistic), or converting the variable amplitude loading (VAL) scenarios to an equivalent CAL. This study demonstrates that the use of such approaches would not be applicable for accurate



assessment of the fatigue response of risers subject to VIV-induced VAL. The experimental investigation performed in this study will also clarify the underlying reasons for the use of large safety factors by the industry when assessing the fatigue life of pipelines and risers. In addition, an experimental investigation was also conducted to highlight the influence of the compressive portion of VIV stress-time history on the fatigue life of such components. It is shown that the compressive stress cycles significantly influence the fatigue crack growth response of risers, and their presence should not be ignored.

**Keywords:** Fatigue, Riser, Pipeline, Vortex-induced vibration (VIV), Compressive stress, Variable amplitude loading, Equivalent constant amplitude load, Barsom model, Paris and Walker models, Rainflow.

## 5.2. Introduction

In addition to the first and second order floating platform motions, vortex-induced vibration (VIV) creates serious fatigue damage in risers used in the offshore industry. In deep waters, where risers undergo severe VIV-induced stresses and encounter multi-modal vibration, the VIV-induced fatigue becomes an even more significant contributor to the overall damage. Therefore, prediction of the fatigue damage becomes more challenging due to the complexity of a riser's vibration due to the resultant stress-time history. Many attempts have been made by researchers to better predict the fatigue damage under such a severe condition by the available analytical formulations. However, due to the lack of realistic experimental data, it has not been possible to fully verify such schemes; the present study attempts to do that.

A review of the available methods for fatigue analysis of risers indicates that constant amplitude fatigue models are customarily used to estimate the fatigue life of risers (Iranpour and Taheri, 2006). However, due to the nature of the VIV, risers are primarily subjected to variable amplitude loading (VAL). Moreover, the irregularities inherent in such loading scenarios create tensile overloads and compressive underloads. Taheri *et al.* (2002) and Yuen and Taheri (2005) demonstrated that overloads and underloads have

significant influence on the fatigue life of structural steel, and provide robust models to account for such variability. Such irregularities in the loading scenario cause severe degree of plasticity at the tip of the crack, leading to inconsistency in the material response to the subsequent loading cycles following an over-load or underload. This, in turn makes the estimation of the fatigue life of the material and understanding of the underlying physics of the phenomenon very complicated. In all, because of the complexity in the VIV-induced loads, which are generally stochastic in nature, and vary greatly depending on the riser's surrounding environment, the associated fatigue assessment can be very challenging and complicated.

To date, many researchers have conducted studies with the aim of understanding the basics and underlying complexity of fatigue crack growth under variable amplitude loadings. The early research in this area goes back to 1970, when tensile overloads were observed to result in significant retardation in crack growth rate (Jones and Wei 1971). In recent years, however, the focus has been on understanding the fundamentals of the retardation mechanism. For example, researchers have observed that compressive underloads also have significant influence on accelerating the crack growth rate of the material (Rushton and Taheri 2003). In addition, variations in the crack growth rate are attributed to several other mechanisms, including the crack deflection, crack tip blunting, strain hardening of the material, residual stress ahead of the crack tip, crack closure and the stress-time history (Sadananda *et al.* 1999). Investigators have proposed several methods that consider the changes in the crack growth rate due to overloads or underloads. Most of the works have focused on extending the Paris fatigue model to account for the influence of such retardations or accelerations in the crack growth rate (for example, see Taheri *et al.* 2002). This has encouraged the offshore industry to use the same approach for calculating the fatigue damage of risers. However, actual experimental data for fatigue life estimation of risers under VIV-induced loads are very scarce in the public domain literature.

The work in this area goes back to decades ago, when the influence of tensile overloads on the fatigue crack growth of components became more understood (Pook and Greenan, 1979; Cheng, 1985; Barsom, 1973). Although numerous works have lately targeted the examination of the influence of overloads and underloads, the combined

influence of these irregularities still deserves more attention. As stated earlier, most of the studies conducted thus far have considered CAL scenarios involving only a few periodic overloads or underloads, thus, not taking account of the actual variable amplitude nature of the stress-time history. For instance, in a study conducted by Wu and Huang (1993), it was demonstrated that depending on the configuration (irregularity) of the VAL stress-time history, an *equivalent* stress history of the VAL can be obtained by applying the rain-flow cycle counting method, by considering the power Spectral Density Function (PSD) of the VAL. The use of *equivalent* CAL in place of a VAL has also been suggested in respected textbooks (e.g., Barsom and Rolfe 1999). However, despite the fact that some researchers have argued against the use of an *equivalent* CAL for fatigue life assessment of materials subjected to VAL, nonetheless, due to the relative simple algorithm, the approach has been widely used by the industry for fatigue life assessment of offshore components subject to VAL scenarios. The inapplicability of the simplified approach has also been demonstrated by several experimental studies (see for instance, Iranpour *et al.* 2008). Another example is the study that was conducted to examine the fatigue response of aluminum alloys subject to random loading (Wu *et al.* 1997). The study demonstrated that the use of the Palmgren-Miner rule resulted in non-conservative results, and Morrow's plastic work interaction damage rule should be used for more accurate fatigue life assessment. Moreover, Wu and Ni (2007) also showed that the fatigue life estimated based on the *equivalent* CAL can be non-conservative by a factor of two.

It should also be noted that almost all of the tests reported in the literature have been conducted on specimens subjected to tensile stress cycles, and the influence of compressive portion of the stress-time history has been generally ignored. This seems to be due to the notion that fatigue cracks would not grow under compressive stress cycles. For example, the ASTM recommends that for negative stress ratios, the compressive portion of the stress cycles could be ignored (ASTM E647-95a, Silva 2004 and Silva 2005). However, studies have shown that even under a fully compressive alternating external loading conditions, a fatigue crack could be initiated and grow nearly to the point of failure (Kasaba *et al.* 1998). This is believed to be due to the tensile residual stress field that could be produced by excessive compressive pre-loads. In a recent

research by Silva (2005), it has been shown that the compressive portion of the loading scenario would have a significant influence on the fatigue crack growth, and should not be ignored.

### **5.3. Motivation and Problem Definition**

The above facts were the motivation for the authors to conduct a series of experimental investigations on the fatigue crack propagation of risers under a real VIV-induced variable amplitude loading scenario. The experimental data from a series of tests on the multimodal VIV of a tensioned riser are used in this investigation to conduct the fatigue tests. The VIV-induced stress time history is directly applied to a number of metallic specimens and the resulting crack growth rates are recorded. The influence of the compressive portion of the VIV-induced stress-time history on the overall fatigue damage of the component is also investigated. It is shown that compressive stresses have significant influence on the fatigue crack growth of risers, and should not be ignored. The test results are compared with the fatigue crack growth results obtained through the analytical models. It is illustrated that the fatigue models commonly used by the offshore industry may significantly underestimate the fatigue damage of risers subject to such random loading scenarios; hence the use of more sophisticated approaches is recommended.

### **5.4. Experimental VIV Data**

In research done by Li *et al.* (2005), a highly flexible tensioned (rubber-hose) riser with a length of 8.5m and outside diameter of 0.04m was tested in uniform current profile to study its multimodal VIV response. The tests were performed in the ice tank of the Institute for Ocean Technology, the National Research Council of Canada, Saint John's, Newfoundland. A total of 16 accelerometers were mounted on the model riser to measure the accelerations due to both cross-flow and in-line vibration. This significant number of accelerometers facilitated accurate measurement of the riser's higher mode response.

Previous tests done by other researchers had implemented a very limited number of accelerometers mounted on their model risers; consequently, the higher mode response of the risers could not be accurately traced. The riser, horizontally fixed on a supporting frame below the tank carriage, was tested in a water depth of 1.0 m. For more information on test setup, measurement devices, experimental program and test outputs, please refer to Li *et al.* 2005 or Li, 2005.

Using two different scale factors for riser length and diameter, a model riser was designed to account for the small dimensions of the model riser as opposed to the real ones. The modal response of a riser is a function of five different parameters including the modal amplitude of vortex shedding, the frequency of vortex-shedding, the modal natural frequencies, the modal mass and the modal damping (Li, 2005). These main modal characteristics form the basis of the non-dimensional parameters. Reynolds number does not explicitly appear as a non-dimensional parameter; however, it is implicitly included in these non-dimensional parameters. Establishing that all non-dimensional parameters were equal for both the model and the prototype risers, a complete similarity was assumed between the two systems, except for the similarity between the current velocity and riser diameter, as explained later in this paper (Li, 2005). The term prototype refers to a sample riser in the ocean under the action of current profile. For more information, one may refer to Li 2005 and Li *et al.* 2004.

In Li's study (2005), the hydrodynamic mass and damping were estimated based on Morison's formula, assuming an uncoupled motion between the cross-flow and in-line vibrations. This led to a sinusoidal wave form solution for both the cross flow and in-line vibrations along the riser length. As it will be discussed later, having a sinusoidal waveform is the fundamental assumption on which the measured accelerations could be transformed to stresses. The Reynolds number was the same for both the prototype and the model riser. Therefore, the added mass coefficient, drag coefficient, lift coefficient and the Strouhal number were approximately the same for both models. The model riser length and diameter were selected based on the tank dimensions and the available instrumentation. Table 5.1 shows the main properties of the model and the prototype riser.

**Table 5.1.** Main Properties of the Model and the Prototype Riser

	Unit	Model riser	Prototype riser
Length	$m$	8.5	1000
Outside diameter	$m$	0.04	0.30
Weight per unit length in air	$N / m$	16.8	944
Bending stiffness	$N \times m^2$	1.52	0.360E5

The length of the model riser was shown to influence only the modeling of the frequency ratio (Li, 2005). Matching the Reynolds number of the model riser to the prototype risers required higher currents velocity for the model riser; however, the similarity in the risers' diameter ratio reversed the situation. In other words, due to the similarity in risers' diameter, a smaller current velocity was required for the model riser compared to the prototype riser (Li, 2005). Therefore, it was not actually possible to design a model riser fully similar to the prototype riser (Li *et al.*, 2005). To resolve this issue, the criterion of similarity between the current velocity and riser diameter was omitted. This led to a model riser with partial similarity to the prototype riser, where the model riser's current velocity was selected so that the Reynolds number of the two risers would be similar (Li, 2005). Since it was not possible to test a riser with a high Reynolds number in the tank, a Reynolds number of  $R_e = 0.6 \times 10^5$  was selected, which corresponded to a current velocity of 0.2 m/s for the prototype riser. The structural mass, damping and tension in the model riser were therefore calculated based on this similarity condition. This tension force was kept constant during the test.

A considerable number of current velocities were tested for two pretension forces of 200 N and 600 N. Although there was a relatively large fluctuation in the frequency range, the in-line VIV was observed to have lower vibration amplitude than the cross-flow VIV (Li, 2005). Increasing the current velocity resulted in an increase in the dominant mode number (Lie *et al.*, 2001). However, it did not cause any increase in the

amplitude of vibration for either the cross-flow, or the in-line VIV (Li *et al.*, 2005). Therefore, only the VIV test data corresponding to a current velocity of 1.5 m/s is used in our fatigue tests. Moreover, no obvious peaks were observed over the whole current velocity range. This indicates that a strong resonance was not observed in the experimental VIV tests.

When fluid flows around a solid object, the resulting vortex shedding creates both in-line and cross-flow vibrations. Any structure with sufficiently bluff trailing edge sheds vortices in the flow. As the flow velocity is increased or decreased, the shedding frequency approaches the natural frequency of the structure and suddenly “locks” into structure’s frequency. The lock-in resonant oscillations of the near wake input energy to the structure, causing large amplitude vibration response. The broad response peaks of the vibration amplitude versus fluid velocity diagrams are indicative of the lock-in vortex shedding resonances. In the tests done by Li (2005), no lock-in phenomenon was observed as the result of the VIV experiments. This observation was consistent with the results reported by other researchers (e.g., Lie *et al.* 2001).

In the modal analysis, modal components of up to the tenth mode were observed for both the in-line and cross-flow vibrations. Comparing the results from the two different pretension forces of 200 N and 600 N demonstrated that the pretension force did not show much influence on the fluctuation of the average peak amplitudes (Lie *et al.* 2001). This led to the conclusion that multimodal VIV response of flexible risers did not seem to be sensitive to the magnitude of the pretension force, which is also confirmed by others (Lie *et al.* 2001). Therefore, only the VIV test data corresponding to a pretension force of 600 N is used for the fatigue tests in this study.

#### **5.4.1. Acceleration-time History**

As stated earlier, the measured accelerations of the riser subject to a current velocity of 1.5 m/s and a pretension force of 600 N were used to perform the fatigue tests. In order to exclude the end-effects, and considering the geometric symmetry of the model riser, the VIV data at the mid-span of the riser was used for our fatigue tests. Figure 5.1 shows the magnitude of the cross-flow accelerations at this location for a time period of 28 seconds.

No selected portion of the time history could be considered as a good representative of the whole data set, as it does not cover the entire frequency range of a typical VIV-induced acceleration-time history. Therefore, the whole acceleration-time history was applied to the fatigue tests specimens rather than selecting a representative portion of the data.

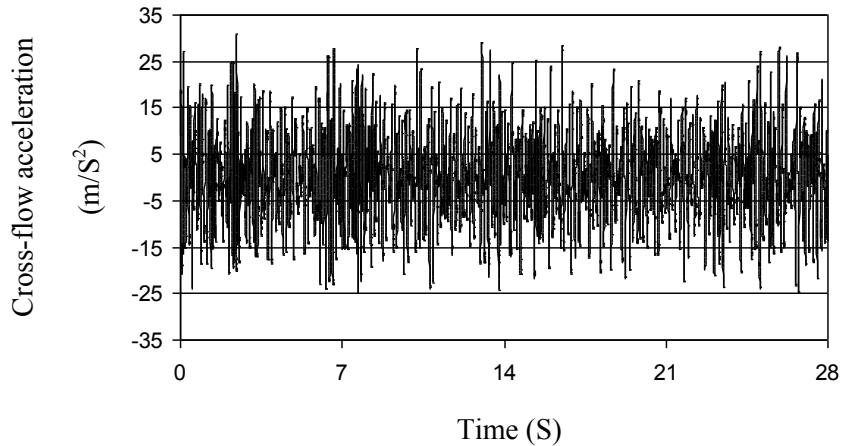


**Figure 5.1.** Cross-flow acceleration-time history of the 8.5m long model riser at the riser's mid-span, associated with a pretension force of 600N

It is clear that this VIV cross-flow acceleration-time history imposes variable amplitude stresses on riser's cross-section, thus making the use of the available CAL fatigue models for predicting the fatigue life of risers unsuitable. In a study by Iranpour and Taheri (2006), it was demonstrated that most of the available methods used for fatigue life estimation of risers employ the Paris fatigue model. The Paris model is known to provide accurate prediction for the mid-range of a given fatigue crack growth diagram. Moreover, to predict the fatigue life for various stress ratios, this model requires introduction of a family of parallel straight lines corresponding to the different stress ratios (Taheri *et al.* 2002). However, the large number of tension overloads and compressive underloads resulting from a VIV would significantly affect the fatigue crack growth rate, and would be untraceable by the Paris model, even in its revised form as used by Taheri *et al.* (2002). Some of the constant amplitude fatigue models have been



modified for predicting fatigue damage under variable amplitude loading scenarios. An example would be the modified Foreman model (see Barsom and Rolfe 1999). This approach is used to more accurately predict the influence of a large number of closely spaced random cycles.

Due to the application of the overloads, the crack growth rate in a variable amplitude loading shows a sudden change in magnitude, by an amount dependent on the magnitude of the overload (Rushton and Taheri, 2003). The ratio between the over-load and underload is a good identifier to quantify the crack growth retardation or acceleration, with greater influence for higher ratios (Rushton and Taheri, 2003). However, regardless of the level of effort in the modified constant amplitude models, it is observed that they are inadequate for predicting crack growth in VAL scenarios. To account for the retardations and accelerations in crack growth developed due to overloads or underloads, Yuen and Taheri (2005) proposed a number of modifications to the Wheeler fatigue crack retardation model. These modifications enabled the model to account for overload and underload interactions. However, when the number of overload and underload ratios become larger, the model produced significant errors in the predicted fatigue life of the component. Moreover, most of the previously conducted investigations have used time-histories that are basically a constant amplitude load scenario with a few overload or underload stress spikes added to them. Therefore, it is very difficult to extend the result of such tests to a VIV-induced loading history, where the loading scenario has an entirely variable amplitude nature.

The above discussion briefly highlights the limitations of the available fatigue models used by the offshore industry for estimating the fatigue life of pipelines and risers. For the fatigue analysis in this investigation, the VIV acceleration-time history is first transformed into a stress-time history. This is performed based on the wave propagation theory applied to a tensioned string, as explained in the next section.

#### **5.4.2. Stress-time History**

Due to the nature of the loads applied to the riser, the riser behaves as a beam. Using the elementary beam theory, the stresses at any point along the length of a beam can be

directly calculated by using the applied bending moment and geometric characteristics of the beam:

$$\sigma_{\max} = \frac{MR}{I} \quad (5.1)$$

where  $\sigma_{\max}$  is the maximum stress at the outer layer of the pipe,  $M$  is the bending moment,  $R$  is the outer radius and  $I$  is the area moment of inertia of the pipe. The bending moment is related to the curvature by the following equation:

$$M = EI \frac{\partial^2 u}{\partial x^2} \quad (5.2)$$

where  $E$  is the modulus of elasticity of the material and  $u$  represents the displacement transverse to the longitudinal axis of the pipe. Combining the above equations, one may calculate the flexural stresses resulting from bending at any point along the pipe using the following equation:

$$\sigma_{\max} = ER \frac{\partial^2 u}{\partial x^2} \quad (5.3)$$

Based on the wave propagation theory of non-dispersive transverse waves, which travel at a constant speed of  $c$  along the longitudinal direction of an elastic medium without any change in its shape, the transverse acceleration can be related to the curvature using the following equation (Harrison and Nettleton 1997):

$$\frac{\partial^2 u}{\partial t^2} = c^2 \frac{\partial^2 u}{\partial x^2} \quad (5.4)$$

where  $\partial^2 u / \partial t^2$  is the acceleration. The wave propagation speed can be written as  $c = \omega / k$ ; where  $k$  is the wave number and  $\omega$  is natural angular frequency of the vibration. The above relation basically applies to cases such as the longitudinal or torsional waves in a uniform bar, and to small-amplitude waves in a stretched string. In cases where the shape of the transverse wave continually changes, a constant speed cannot be assumed for propagation of the wave. In such cases, different wavelengths would travel at different speeds. Recognizing that the riser is a long and slender pre-

tensioned structure, its curvature could be assumed to be in a sinusoidal shape. In short risers, the tension may slowly vary along the structure and the transverse deflections could be assumed to have a series of localized sinusoidal mode shapes. Vandiver and Peoples (2003) showed that Equation 5.4 can still be used to relate the acceleration to curvature for risers that experience sinusoidal deformed mode shapes or those risers where waves travel along their length. By combining Equations 5.3 and 5.4, one may calculate the stresses using:

$$\sigma_{\max} = ER \frac{1}{c^2} \frac{\partial^2 u}{\partial t^2} \quad (5.5)$$

Equation 5.6 can be used to evaluate the natural frequency of a tensioned pipe with pin ends (Vandiver and Peoples 2003; Harrison and Nettleton 1997):

$$f_n = \frac{1}{2\pi} \left( \left( \frac{n\pi}{L} \right)^2 \frac{T}{m} + \left( \frac{n\pi}{L} \right)^4 \frac{EI}{m} \right)^{1/2} \quad (5.6)$$

where  $f_n$  is the natural frequency of the  $n^{\text{th}}$  mode (Hz.),  $n$  is the mode number,  $L$  is the length of the riser ( $m$ ),  $m$  is the mass per unit length ( $kg/m$ ),  $T$  is the tension in the riser ( $N$ ),  $E$  is the modulus of elasticity of the material ( $N/m^2$ ) and  $I$  is the area moment of inertia of the riser's cross section ( $m^4$ ). The first term on the right hand side of Equation 5.6 is related to the tension in the pipe, while the second term accounts for the bending rigidity of the structure. In cases where the tension-related term is much larger than the bending-related term, the riser can be considered as a tension-dominated structure (Vandiver and Li 2005; Vandiver and Peoples 2003). In such cases, the natural frequency is primarily a function of the tensile force, the length of the riser and its mass per unit length. In tension dominated cases, the speed of the wave propagation is constant. Therefore, one may use Equation 5.5 to calculate the magnitude of the stresses directly from the accelerations. To verify the tension-dominated behavior of the riser, Vandiver and Peoples (2003) suggest that the following relation be calculated:

$$P = \frac{T}{EI(n\pi/L)^2} \quad (5.7)$$

When  $P$  has a value much greater than 1.0, the riser behavior is dominated by the tensile stiffness, rather than the bending stiffness. The mode number of a sinusoidally vibrating cable can be found by  $k = n\pi/L$ , with the natural frequency of  $f_n = nc/2L$ . In cases where the riser vibration is tension dominated, the following equation can be used to calculate the speed of the wave propagation along the structure (Vandiver and Peoples 2003):

$$c = \sqrt{T/m} \quad (5.8)$$

where  $m$  is the mass per unit length of the riser structure. Combining Equations 5.5 and 8, leads to the following relation, which enables us to calculate the maximum stresses for any position along riser's length, when the accelerations data are available (Vandiver and Peoples 2003):

$$\sigma_{\max} = ER \frac{m}{T} \frac{\partial^2 u}{\partial t^2} \quad (5.9)$$

The magnitude of the stresses can therefore be directly calculated from the acceleration-time history by Equation 5.9. In doing so, the mass of the riser per unit length,  $m$ , should also include the added mass of the submerged structure. Having this total mass and the tension in the riser, one can calculate the stress-time history for both in-line and cross-flow vibrations. The calculated stress-time history is presented in Figure 5.2. In general, the shape of the stress-time history plot is similar to the acceleration-time history plot shown in Figure 5.1.

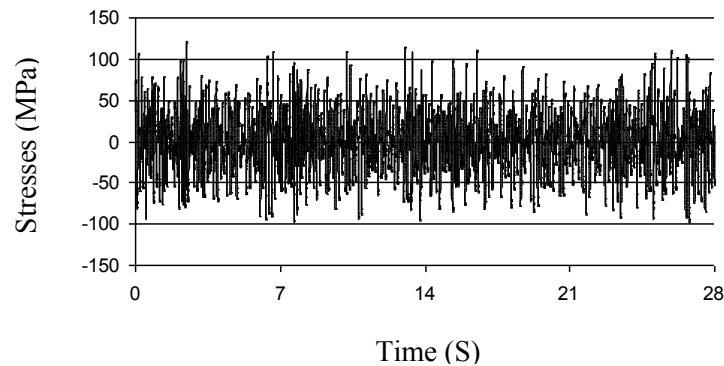


**Figure 5.2.** Stress-time history applied to the test specimen

As observed in Equation 5.6, for the riser under consideration, the natural frequency is primarily a function of the tensile force, the length of the riser and its mass per unit length. In other words, as long as two risers with different materials have identical dimensions and mass per unit length, their natural frequency should also be the same, which in turn, results in identical acceleration time-history. Therefore, the VIV-induced acceleration time-history recorded for the rubber-hose riser tested in the lab can be used for an equivalent steel or aluminum pipe having the same dimensions and identical VIV response, along with their related material properties. Therefore, as long as the stress-time history is concerned, the tested rubber-hose riser can be assumed to be an aluminum pipe, with the same dimensions, tensile force and mass per unit length. This equivalency was the primary assumption for using the VIV test data obtained from testing the rubber-hose model riser to perform the fatigue tests on aluminum plates in this study. This procedure is widely accepted and has been used by many other researchers (Vandiver and People, 2003, Vandiver *et al.* 2006).

## 5.5. Experimental Setup

The experimental fatigue tests were performed at the Materials Testing Laboratory of Dalhousie University, in Canada. To simplify the test apparatus and decrease the

experimental costs, the tests were performed on equivalent rectangular plate specimens rather than pipes. This simplification helps to avoid the complexities involved with fatigue testing of pipes, and eliminates the use of more sophisticated and expensive monitoring systems. The validity and justification for the equivalency is reported in detail by the authors in a different publication (Iranpour and Taheri, 2007).

The fatigue tests were conducted using an Instron Servo-hydraulic Universal Testing Machine with a capacity of  $\pm 100$  kN under cyclic or 200 kN under static loading conditions. The stress-time history was applied to the specimen through a special-purpose software. A fiber optic light was used to illuminate the crack tip region. To monitor the growth of the crack tip and record the crack growth increment, a Mitutoyo traveling microscope with a magnification of 50X mounted on a pair of micrometers with a resolution of 0.01mm were used. The tests were performed per ASTM E647 Standard, using plate specimens with dimensions of 300mm (L)  $\times$  100mm (W)  $\times$  4.8mm (T) hosting a central notch of  $2a=20$ mm. For the crack growth to be consistent with the direction of crack growth through the wall thickness of a pipe, the plates were cut so that the length of the specimen had the same direction as the rolling direction of the original plate. To get a better vision of the crack tip during its monitoring throughout the test, the surface of the specimen was polished with a wide range of sand paper grits, starting from coarse ones (No. 120) to a very fine one (No. 1200). Figure 5.3 shows the general overview of the test apparatus. Figure 5.4 shows the rectangular test specimen with the center crack and its dimensions. As per ASTM E 8M standard, acceptable geometric correction factors should be available for the specimen configuration. Moreover, as a means to ensure that linear elastic fracture mechanics (LEFM) holds, this standard suggests that the specimen be large enough to promote predominately linear elastic conditions during testing. The material used for this study is 6061-T651 aluminum alloy, with mechanical properties and compositions listed in Tables 5.2 and 5.3, respectively.

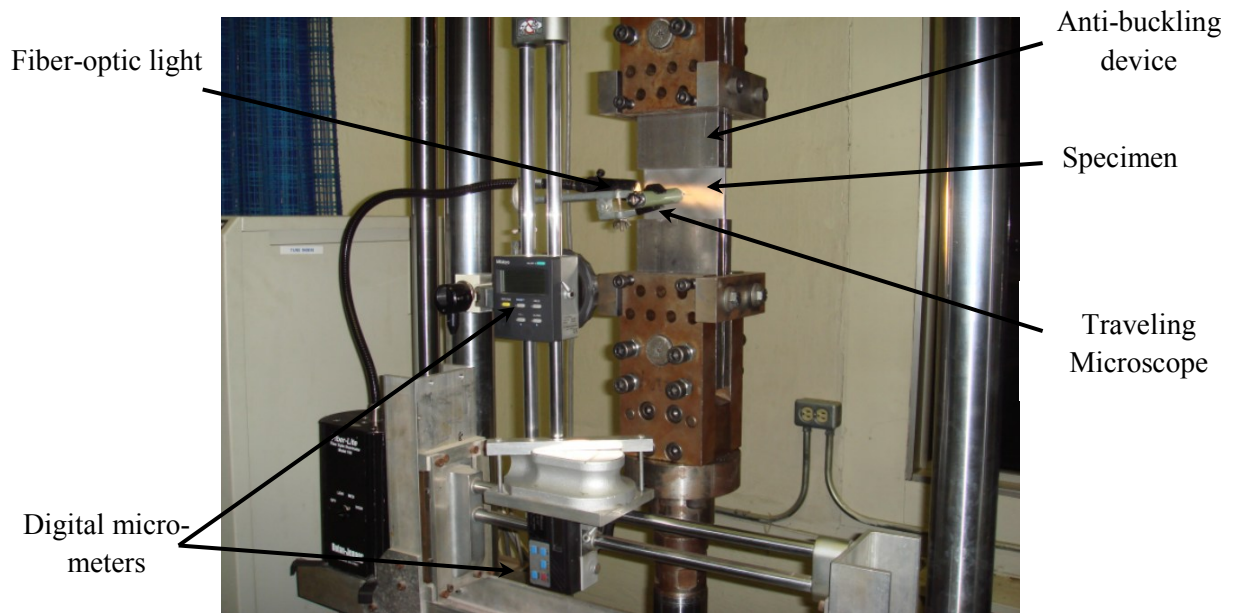


**Figure 5.3.** Test setup

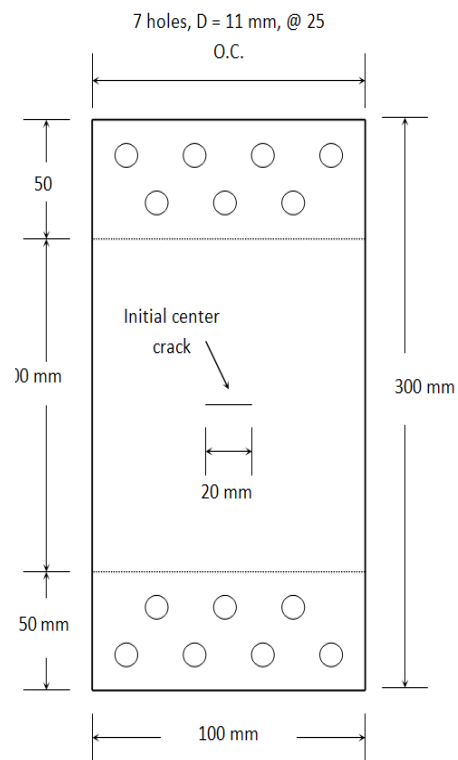


**Figure 5.4.** Specimen layout and dimensions

**Table 5.2.** Mechanical Properties of the 6061-T651 Aluminum Alloy

Modulus of Elasticity (GPa)	0.2% Yield Stress (MPa)	Ultimate Tensile Stress (MPa)
68.9	275.4	330.6

**Table 5.3.** Compositions (%) of the 6061-T651 Aluminum Alloy

Fe	Cu	Mn	Ni	Si	Mg	Zn	Ti	Cr
0.201	0.198	0.41	0.006	0.528	0.961	0.004	0.014	0.202

## 5.6. Experimental Results and Discussion

The specimen has an initial center notch with a length of  $2a = 20$  mm. After pre-cracking to a length of  $2a' = 24$  mm, a certain number of VIV-induced stress-time history *blocks* was applied to the specimen and the crack growth was measured during the test, after applying a certain limited number of *blocks*. Figure 5.2 shows one *block* of the applied load. This procedure was continued to the end of the test, with the qualification that crack growth rate between each measurement would remain within 5.0 mm. Each new incremental crack length was measured at both sides of the initial center crack. This was done to ensure that the crack growth rates were equal at both ends of the initial notch and that there was no misalignment in the test setup. The machine frequency was set between 4.0 to 5.0 Hz, so that the input load history could be accurately traced.

Due to some limitations of the computer software, the entire VIV stress-time history could not be applied to the specimen in *one* block. Selecting a *representative* VIV time history block seemed to be a reasonable approach for reducing the number of data points down to the level that could be handled by the software. However, it should be recognized that no selected portion of the VIV time history could cover the entire frequency range of the original lab data. Therefore, it was decided to break the entire



VIV-induced stress-time history to several *sub-blocks* and apply them sequentially to the specimen. Note that each *block* contained 1754 data points, resulting in a total of 877 stress cycles in each block. This loading scenario was then applied to the test specimen and the resulting crack growth rate was monitored.

Figure 5.5 shows the average of the response of three specimens in the form of crack length versus the number of applied VIV-induced stress cycles. In this paper, each curve or data point represents the results of at least three tests. The test results of the three specimens for each stress-time history were usually so close that there was no need to plot them all separately in one figure. The specimens failed after applying 227 to 231 VIV-induced stress blocks, representing 199,079 to 202,587 stress cycles, respectively.

A computer code was developed in MATLAB to monitor the fatigue crack growth in the specimens under the applied variable amplitude stress-time history. The analytical fatigue life estimation involves the growth of the crack from its initial length after the pre-cracking throughout the intermediate crack length, up to the final fracture stage.

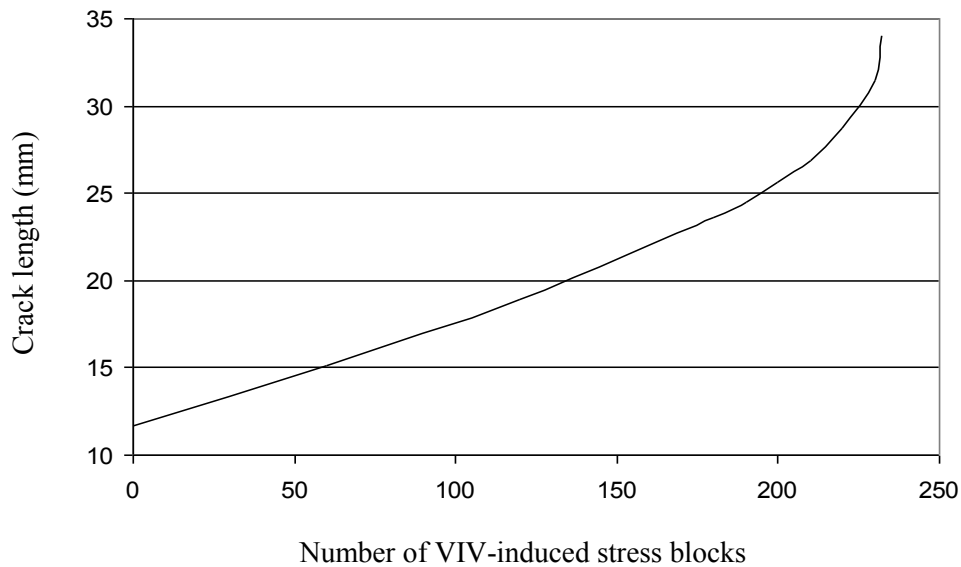


**Figure 5.5.** Crack length versus the number of applied VIV-induced stress blocks

### 5.6.1. Analytical Estimation of Crack Growth

There are two main approaches for analytical estimation of fatigue crack growth in component under variable amplitude loading. In one approach, the fatigue crack growth of each *block* of the time history is calculated individually and added to the growth of the previous blocks. In this approach, a cycle counting method (i.e. the Rainflow algorithm) is used to calculate the cycles in each block, and to determine the corresponding stress ranges for each cycle. In the second approach, the crack growth due to each load cycle is calculated and added to those from the previous cycles. Both approaches have reported to generate satisfactory results for cases where the applied load is highly irregular and the frequency of the applied overloads in both tension and compression are similar (Stephens *et al.*, 2001). In this study, the block-by-block approach is used to perform the analytical evaluation. The approach is based on the concept of LEFM, which amplifies the magnitude of the applied stresses and accounts for the geometry of the component.

It should be noted that in the block-by-block approach, it is possible to use an equivalent stress intensity factor for fatigue life estimation of the component in each block. This approach simplifies the analysis and is considered to be admissible for cases where the crack growth rate is relatively low (Stephens *et al.*, 2001). The variation of the crack tip stress-strain field is described in terms of the root-mean-square value of  $\Delta K$ , expressed by (Stephens *et al.*, 2001):

$$\Delta K_{rms} = \Delta S_{rms} \times \phi \sqrt{\pi a} = \sqrt{\frac{\sum_{i=1}^N \Delta S_i^2}{N}} \times \phi \sqrt{\pi a} \quad (5.10)$$

where  $\Delta S_{rms}$  is the nominal root-mean-square stress range of the variable amplitude load history,  $\Delta S_i$  is the nominal stress range in the  $i^{\text{th}}$  cycle,  $\phi$  is a dimensionless geometric parameter (i.e. function of crack length to specimen width ratio), and  $a$  is the crack length. This approach, which has been introduced for fatigue crack growth calculations under descending, ascending and random-sequence loadings (Barsom and Rolfe, 1999), is being widely used by the offshore industry for fatigue life estimation of risers under VIV-induced VAL. This is due to the hypothesis that the root-mean-square

stress intensity factor is a characteristic of the load distribution curve and is independent of the order of the cyclic load fluctuation (Barsom and Rolfe, 1999).

Once the stress cycles in each block are counted using a cycle counting method (i.e. the Rainflow algorithm), one may use the corresponding root-mean-square stress intensity factor to calculate the fatigue crack growth rate of that loading block. In this study, both the Paris and Walker fatigue models were used to evaluate the fatigue life. The Paris equation is expressed by (Stephens *et al.* 2001):

$$\frac{da}{dN} = A(\Delta K)^n \quad (5.11)$$

where  $da/dN$  is the crack growth rate, and  $A$  and  $n$  are constants that are determined from experimental test results for a given material. Paris's model does not account for the influence of stress ratio. For that, one may use Walker's model represented by (Stephens *et al.* 2001):

$$\frac{da}{dN} = \frac{A(\Delta K)^n}{(1-R)^{n(1-\lambda)}} \quad (5.12)$$

where  $R$  is the stress ratio (i.e.,  $R = S_{\min} / S_{\max} = K_{\min} / K_{\max}$ ), with  $S$  being the applied stress), and  $\lambda$  is an imperial material constant.

The material constants  $A$ ,  $n$  and  $\lambda$  used for the analytical estimation of crack growth in this paper are calculated based on various CAL fatigue tests performed on the aluminum material used for this study (Iranpour *et al.* 2008). These material constants are  $A = 1.743 \times 10^{-11}$ ,  $n = 2.82$  and  $\lambda = 0.5$ , which corroborates well with those reported in literature (Sheu and Song, 1995).

As anticipated and shown in Figure 5.6, the results obtained from the above-mentioned methods do not compare well to the experimental results. As seen from the figure, both the Paris and Walker models grossly underestimate the fatigue crack growth of the specimen. This is because both models ignore the influence of stress irregularities and the presence of compressive cycles in the stress-time history. The presence of the compressive cycles have been shown to accelerate the rate of the crack growth (Rushton and Taheri, 2003; Yuen and Taheri, 2004). As shown in Figure 5.6, the crack growth rate

computed based on the Walker model is relatively closer to the original crack growth rate obtained through experiment. This is basically due to the fact that the Walker model is capable of considering the influence of the mean stress, while the Paris model does not consider this effect. For the stress-time history block applied to the specimen during the tests, a root-mean-square stress ratio of about 0.5 was calculated based on the Barsom approach. Having such a high stress ratio, one would expect a significant difference between the results from the Walker model and that from the Paris model, as illustrated in Figure 5.6. Nevertheless, both models still grossly underestimate the crack fatigue growth rate, which is un-conservative and not desirable for design purposes.

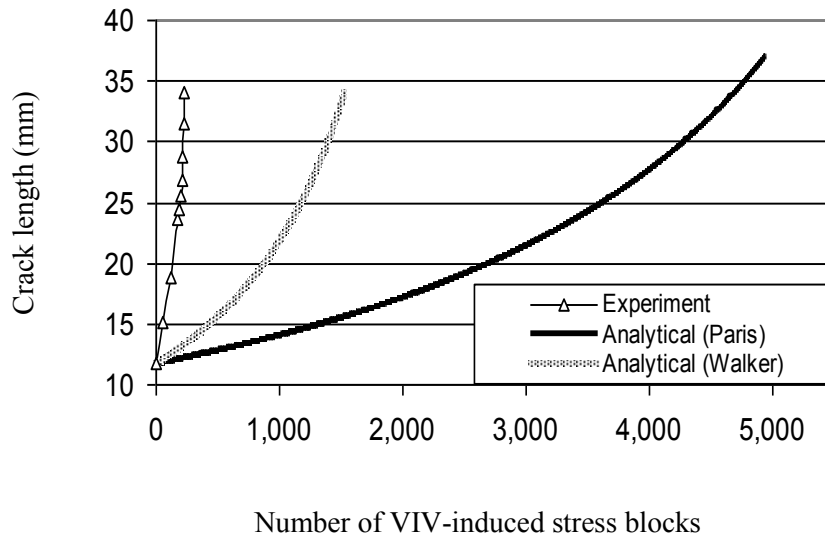


**Figure 5.6.** Crack length versus the number of applied VIV-induced stress blocks

Barsom’s approach (Equation 5.10) has been reported to be effective for estimating the fatigue crack growth of components under variable amplitude loading scenarios (Barsom and Rolfe, 1999). However, based on our experience and the results from this research, this approach does not seem to be a suitable one for estimating the VIV-induced fatigue crack growth of risers. This may be attributed to the nature of the stress-time history of risers, which is not an entirely random process, as it has some specific trends. In other words, the VIV-induced stresses cannot be considered as a complete random loading scenario. In a random loading scenario, the stress overloads or underloads are

distributed in a completely random manner in the time history, resulting in a random trend in the Power Spectral Density (PSD) of the applied load. However, the VIV-induced stress-time history does not exhibit such a behavior. This is shown in Figure 5.7, where the PSD of the VIV-induced stress-time history is plotted. As illustrated in that figure, this stress-time history is not a complete random sequence of loads, since there is a clear repeated trend in the frequency ranges. This may explain, to some extent, the substantial difference between the results obtained by the analytical methods and tests.

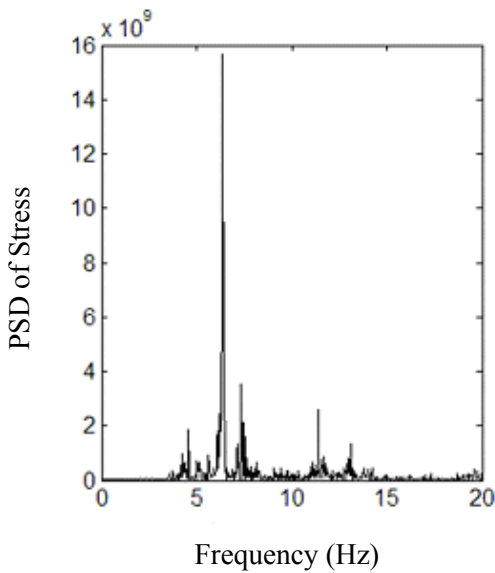


**Figure 5.7.** Power spectral density of the cross-flow stress-time history

### 5.6.2. Influence of Compressive Stresses

In the second series of tests, the compressive portion of the VIV-induced stress-time history was omitted (see Figure 5.8). This was done to investigate the influence of the compressive underloads on the fatigue crack growth rate of the component. Although compressive stress cycles do not generally produce any crack in the specimen, their combination with tension overloads could make a significant contribution in reducing the fatigue life of the component. Therefore, a higher fatigue life is expected for cases where the compressive underloads are omitted from the stress-time history. This was supported

by the results from the second set of tests. The three specimens tested during the second set of tests failed after applying 507 to 519 VIV-induced stress blocks. Note that each *block* in the second set of tests was equal to the block in the first set of tests, and the only difference was omitting the compressive stresses. However, omitting the compressive stresses resulted in a considerable decrease in the total number of stress cycles in each block. When the compressive stresses are omitted, the total number of stress cycles in one block reduced to 534 stress cycles, compared to 877 stress cycles for tension-compression stress-time history. Therefore, for comparison purposes, one should refer to the number of *blocks* that have been applied to the specimens, and not the number of stress cycles. In other words, each *block* in the tension-tension tests is exactly equal to each block in the tension-compression tests (i.e., the original recorded data), with the only difference being the omission of the compressive portion of the cycles. This means that all the compressive stresses in the block are replaced with zero stresses. This is the actual method used to convert the original tension-compression blocks into tension-tension (or basically tension-zero) blocks.

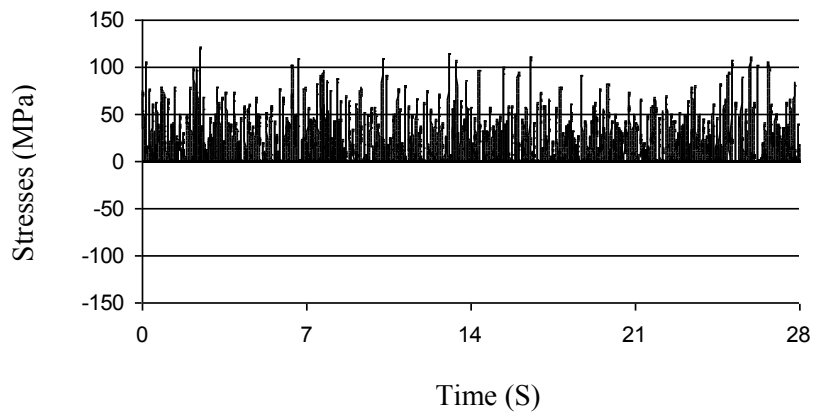


**Figure 5.8.** Stress-time history applied to the test specimen with the compression portion omitted

Figure 5.9 compares the crack growth rates for tension-tension and tension-compression VIV-induced stress-time history, as well as the results predicted by the

analytical approaches. As it is clearly illustrated in this figure, omitting the compressive stress cycles results in a considerable increase in the fatigue life of the component. This is of significant interest for application in the offshore industry, where compressive forces are customarily ignored when calculating the fatigue life of the riser, which leads to unconservative fatigue life estimation. As shown in this figure, the fatigue life of the component is about 2.5 greater for cases where the influence of compressive overloads is ignored, which is a very alarming finding.

In cases where the compressive underloads are omitted from the stress-time history, the results from the experiment are closer to the results obtained analytically. This is due to the fact that both the Walker and Paris fatigue models ignore the presence of compressive stresses. However, the calculated fatigue crack growth based on the Walker model is once again three times less than that obtained experimentally.

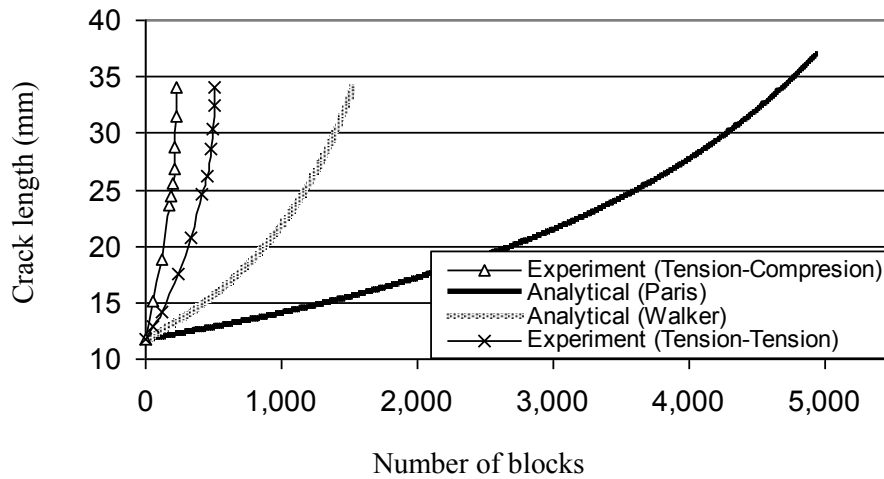


**Figure 5.9.** Comparison of the fatigue crack growth rates under tension-compression and tension-tension VIV-induced stress-time histories

### 5.6.3. Tests with the Equivalent Constant Amplitude Load

As stated earlier, it has been widely accepted that Barsom’s approach may be used to establish a constant amplitude load that is equivalent to a variable amplitude loading.

This method has been used for a long time by the offshore industry to estimate the fatigue life of risers and perform the tests on the *equivalent* CAL, rather than the original VIV-induced VAL. However, the analytical calculations in this study do not support this equivalency for VIV-induced VAL stress-time history used in this research. To further examine the applicability of the Barsom approach for VIV-induced stress-time histories, this approach is used to calculate a CAL that is *equivalent* to the VIV-induced VAL data used in this research. This *equivalent* CAL was calculated based on the main assumption of the Barsom approach, which calculates the equivalent root-mean-square stress intensity factor range for VAL (i.e. Equation 5.10). This *equivalent* CAL was then applied to a number of specimens and their resulting fatigue crack growth were compared to those obtained by applying the *original* VIV-induced VAL lab data. This procedure directly checks the applicability of Barsom’s approach for fatigue life estimation of risers, and any uncertainties arising from the empirically established material constants  $A$ ,  $n$  and  $\lambda$  (i.e., those used in Paris or Walker fatigue models) were eliminated. In other words, these set of tests directly focus on the applicability of the Barsom’s approach for fatigue life estimation of risers under high speed ocean current profiles, and eliminates any uncertainties or errors arising from material properties for analytical calculations of the fatigue crack growth rate.

As a common approach, the influence of the compressive portion of the VIV-induced stress-time history was ignored and the tests were conducted using a tension-tension constant amplitude load applied to the specimen. The minimum and maximum loads were determined based on the Hudson model, which implements a root-mean-square approach (Stephens *et al.* 2001):

$$S_{\min(rms)} = \left[ \frac{1}{N} \sum_{i=1}^N (\Delta S_{\min(i)})^2 \right]^{1/2} \quad (5.13.1)$$

$$S_{\max(rms)} = \left[ \frac{1}{N} \sum_{i=1}^N (\Delta S_{\max(i)})^2 \right]^{1/2} \quad (5.13.2)$$

where  $S_{\min(i)}$  and  $S_{\max(i)}$  are the minimum and maximum stresses of each cycle, respectively. Before using Equations 5.13, the stresses in the stress-time history were



counted by the rainflow cycle counting method. The stress ratio of the resultant constant amplitude loading is calculated by:

$$R = S_{\min(rms)} / S_{\max(rms)} \quad (5.14)$$

This method provides an average fatigue crack growth rate and is considered as affective for cases where the influence of the load interactions is small (Hudson, 1981). When the loading is random in nature, the load interactions offset one another.

The resultant *equivalent* tension-tension CAL was applied to a number of specimens with the same geometry as the specimens tested under the *original* VIV-induced described earlier. If Barsom's approach is to be deemed applicable to the VIV-induced stress-time history at hand, and the influence of compressive stress cycles on the fatigue crack growth could be ignored, one would expect the crack growth rate of the *equivalent* tension-tension CAL to be close to that generated by the *original* VIV-induced VAL lab data. Figure 5.10 compares the tests results obtained from the *equivalent* CAL with the test results obtained by applying the original VIV-induced time-history and those resulting by the analytical approaches. As shown in this figure, the results of the series of tests conducted on the specimens with the *equivalent* tension-tension CAL do not support the applicability of the Barsom's approach in this case. The curve that represents the tension-tension CAL is identified in this figure as "Barsom-Walker". This is because after applying Barsom's equivalency procedure, the Walker model was used to estimate the fatigue crack growth cycles.

As mentioned earlier, each VIV-induced stress-history *block* contained a total of 877 stress cycles. However, when counted by the Rainflow counting method, each block contains 534 stress cycles. Therefore, each block of the *equivalent* CAL used to establish the results shown in Figure 5.10 contains 534 stress cycles.

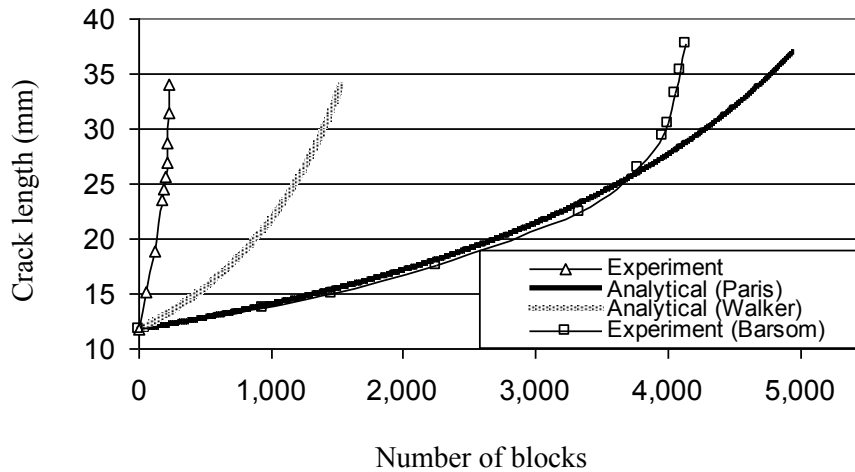


**Figure 5.10.** Comparison between the fatigue crack growth under variable amplitude VIV-induced stress-time history and the equivalent constant amplitude load

As illustrated in Figure 5.10, the specimen tested under the *equivalent* CAL failed after applying 2,213,615 stress cycles. This is equivalent to 4,137 stress blocks, if the cycles are counted by the Rainflow algorithm. This is about 18 times greater than the number of the original VIV-induced VAL stress-time history blocks (i.e. 232), that caused the specimen to fail. As explained earlier, some portion of this discrepancy is due to omitting the compressive stress cycles in the *equivalent* CAL. The remaining portion of the difference may be due to the inability of Barsom's model for transforming the VIV-induced VAL stress-time history to an *equivalent* CAL. In other words, the Barsom model does not seem to be suitable for calculating the fatigue crack growth of components under VIV-induced VAL stress-time history. As explained earlier, this may be due to the fact that VIV-induced stress-time history is not entirely random. It should be noted that most of the tests conducted on risers by other researchers have been done by implementing a constant amplitude load that is equivalent to the VIV-induced variable amplitude loading scenarios. However, this study illustrates that such an approach, which is widely used by the offshore industry for computing the *equivalent* CAL from the original VIV-induced VAL, may not result in an accurate prediction of the fatigue

damage. This is the main focus of this research, which shows when evaluating the fatigue life of risers, the use of the *equivalent* CAL calculated based on the Barsom's approach would not be a good representation of the original VIV-induced VAL stress-time history established by either field/lab tests or complex numerical analysis that could account for the fluid-structure interaction. In other words, one should use the actual VIV-induced VAL scenario instead of the equivalent CAL. This also highlights the requirement for using more sophisticated fatigue models. As also stated, the VAL scenario that risers experience is not a complete random process; as a result, the load sequencing could play an important role and should be taken into account.

## **5.7. Summary and Conclusions**

In this study, the experimental data from a model riser tested in the lab was used to examine the fatigue crack growth of pipelines and risers under the action of uniform ocean current profiles. The focus of the study was on the cross-flow vibration of the model riser, tested in the lab, as it causes severe stress fluctuations during the service life of such components. Since the model riser was tension-dominated, the recorded acceleration time history could be transformed into an equivalent stress-time history based on the theory of wave propagation of a tensioned-string. The stress-time history was then transformed into a load-time history and was applied to a number of test specimens.

As explained in the manuscript, the analytical approaches used for calculating the fatigue crack growth of the material used in this study are those directly used by the industry in design of risers for oil and gas offshore platforms. The main objective of this investigation was to demonstrate that these widely used approaches produce alarmingly non-conservative results.

The experimental results established in this study were compared to the analytical results obtained through the use of the Paris and Walker fatigue models as commonly used by the offshore industry for establishing the VIV-induced fatigue life cycles of risers. The cycles in the VIV-induced loads were counted by the Rainflow algorithm. The

Barsom's approach was used to find the constant amplitude load that is equivalent to the VIV-induced variable amplitude loading. The Barsom's approach calculated the root-mean-square of the variable amplitude stress-time history to establish the equivalent CAL. The output results obtained from using Barsom's approach were then used in the Paris and Walker fatigue models to analytically calculate the fatigue crack growth of the test specimens. It was observed that both the Paris and Walker models significantly underestimated the crack growth rate of the specimens subjected to the VIV-induced stress-time history. In fact, the calculated fatigue crack growth rate from the Walker model was six times less than that observed from experiments, which is alarmingly un-conservative and not desirable for design purposes.

The experimental results established in this study were compared to the analytical results obtained through the use of the Paris and Walker fatigue models, two commonly models used by the offshore industry for establishing the VIV-induced fatigue life cycles of risers. The cycles in the VIV-induced loads were counted by the Rainflow algorithm. Barsom's load equivalency approach was used to establish the equivalent constant amplitude load. The applicability of this *equivalent* CAL was examined using both numerical and experimental investigations. In the numerical investigation, the equivalent CALs were used in conjunction with the Paris and Walker fatigue models to estimate the fatigue crack growth of the test specimens. It was observed that both the Paris and Walker models significantly underestimated the crack growth rate of the specimens subjected to the VIV-induced stress-time history. In fact, the calculated fatigue crack growth rate produced by Walker's model was six times less than that observed experimentally, which is alarmingly un-conservative and undesirable for design purposes. In the experimental investigation, the *equivalent* CAL calculated by Barsom's approach was directly used to perform fatigue tests, thus minimizing the uncertainties that could arise by the use of the empirical material constants in the numerical method. Both investigations demonstrated that Barsom's load equivalency approach is not applicable for VIV-induced stress-time history.

Most of the experiments on VIV-induced fatigue of pipelines and risers have implemented a constant amplitude loading that is meant to be equivalent to the original VIV-induced VAL. To calculate such constant amplitude loading, many researchers use

methods such as the Barsom's approach. Once the equivalent constant amplitude loading is calculated based on such approaches, it is used to perform the fatigue tests on any desired material. To check the applicability of the Barsom's approach to a typical VIV-induced stress-time history, another series of tests were conducted in this research. This series of experiments directly tests the applicability of the Barsom's approach for calculating a CAL that is equivalent to the VIV-induced VAL, and eliminates any uncertainties arising from empirical material constants. If the Barsom's approach was applicable to components under VIV-induced stress-time history, one would expect the crack growth rate of the equivalent tension-tension constant amplitude load to be close to that produced by the original VIV-induced stress time history. However, the results of the tests on the specimens under the equivalent constant amplitude load did not support the applicability of the Barsom's approach to VIV-induced stress-time history. This may be due to the fact that VIV-induced stresses are not an entirely random loading.

One of the primary reasons for such a significant difference is believed to be due to the influence of the compressive loading cycles, which are commonly ignored when predicating the fatigue life of such structures. This was verified through a series of experimental tests, in which the compressive loading cycles due to underloads were omitted from the stress-time history. It was then observed that omitting the compressive underloads from the stress-time history resulted in a significant decrease in the fatigue crack growth of the component. This observation further emphasizes the importance of including the influence of compressive underloads when calculating the fatigue life of risers.

## **5.8. Acknowledgments**

We gratefully acknowledge Drs. N. Bose and X. Li who provided us with the VIV test data. The financial support of the National Science and Engineering Research Council of Canada (NSERC) is also gratefully appreciated.

## Chapter 6

### **On the Effect of Stress Intensity Factor in Evaluating the Fatigue Crack Growth Rate of Aluminum Alloy under the Influence of Compressive Stress Cycles**

Mohammad Iranpour and Farid Taheri

Department of Civil and Resource Engineering, Dalhousie University, 1360 Barrington Street, Halifax, Nova Scotia B3J 1Z1, Canada

Published in the International Journal of Fatigue, 2012, vol. 43, pp. 1-11

#### **6.1. Abstract**

To date, most of the studies conducted on fatigue life estimation of structural components have focused on the Constant Amplitude Loading (CAL) scenarios. However, very few structures in the real world experience such a loading condition, and most structural components undergo a Variable Amplitude Loading (VAL) during their service life. It is also observed that most of the available fatigue crack growth (FCG) models ignore the influence of the compressive stresses, despite the fact that recent studies have highlighted the detrimental effect of compressive stress cycles (CSC) on the FCG of materials.

In this paper, a VAL stress-time history is used to study the fatigue response of 6061-T651 aluminum alloy, with a focus on the compressive portion of the stress time history. An experimental investigation is conducted to assess the influence VAL, in particular, the influence of the CSC on FCG of the material. In the tests, the tensile portion of the stress-time history was kept unchanged, while the compressive portion of the stress-time history were varied by various scaling factors. The experimental results demonstrate that the compressive stress portion of the applied load has a significant influence on the overall fatigue life of the material. It is observed that even introducing a few number of

small CSC into the stress-time history can significantly decrease the fatigue life of the material.

In addition, the influence of the CSC is also examined by means of a microscopic evaluation of crack surfaces' roughness.

**Keywords:** Fatigue, crack growth, Variable Amplitude Loading (VAL), Compressive stress cycles, Tensile Overload, Compressive Underload.

## 6.2. Introduction

In the classical theory of fracture mechanics and fatigue, the influence of the compressive portion of the stress-time history is completely ignored. In other words, the CSC are assumed to have no influence on the FCGR of materials. This theory is based on the fact that under a compressive loading cycle, the crack is fully closed and no stress concentration occurs at the crack tip. Therefore, the crack is believed not to grow when it is subjected to a compressive stress.

Ignoring the compressive portion of the stress-time history is widely accepted in both academia and industry. Once the compressive portion of the stress-time history is ignored, one may use any appropriate fatigue model to calculate the fatigue life of the component. Based on such an approach, the stress intensity factor range is considered to only cover the tensile portion of the stress-time history. In other words, the stress intensity factor range is assumed to be equal to the maximum stress intensity factor for each cycle (applicable for  $R \leq 0$ ).

Ignoring the presence of the CSC is even recommended by many design guidelines and standards. For example, ASTM E647-95a suggests that the compression portion of the stress cycles could be ignored. The presence of such recommendations in design guidelines has motivated the designers to completely ignore the presence of the compressive portion of stress-time histories when evaluating the FCG of engineering components.

Although the influence of CSC on FCG of materials have been demonstrated since a few decades ago (e.g. Suresh 1985; Fleck *et al.* 1985), the research in this area has not received much attention. It should be noted that only a few recent works address this issue and present the data that clearly demonstrate the substantial influence of CSC on the crack growth rate (Silva 2005; Shabanov 2005). These researchers have demonstrated that the presence and magnitude of the CSC could have a significant influence on the overall fatigue life of materials. Moreover, it has been demonstrated that even under fully compressive alternating external loading conditions, a fatigue crack could be initiated and grow nearly to the failure (Newman *et al.* 2005; Kasaba *et al.* 1998; Hermann 1994; Vasudevan and Sadananda 2001). This is believed to be due to the tensile residual stress field that could be produced by the application of excessive compressive pre-loads. In such cases, the crack would grow under full compressive load, with a decreasing trend in the growth rate, until crack arrest occurs.

Noroozi *et al.* (2005) studied the influence of the mean stress and applied compressive stress on FCG using an elastic-plastic crack tip stress-strain history. Their study demonstrated that the FCG was controlled by a two parameter driving force, which was a function of the total maximum stress intensity factor and total stress intensity factor range. In their investigation, the difference in the stress-strain concentration at the crack tip associated with the compressive part of the loading cycle was taken into account. This was done using two different approaches; one accounting for the tensile part and the other accounting for the compressive part of the load history. This was done based on the assumption that the stress response at the crack tip to a tensile loading cycle (with no contact between the crack surfaces) would be different from that experienced under compression (Noroozi *et al.* 2005). In a recent study on aluminum alloy 7075-T6, Noroozi *et al.* (2008) demonstrated that the detrimental effect of the compressive part of a loading cycle can be taken into account using a two-parameter driving force, combining the effect of the maximum stress intensity factor and the stress intensity factor range.

Mikheevskiy and Glinka (2009) studied the load-interaction effect under variable amplitude loading scenarios, focusing on the residual compressive stresses produced by the reverse plastic deformation in the crack tip region. It was observed that the FCG rate depended on both the residual stresses produced by the previous loading cycle and all the



stress fields generated by the previous loading history. Their study suggested a procedure for combining the residual stress fields generated by all preceding loading cycles into a single resultant minimum stress field, which would affect the current fatigue crack growth rate. Their experimental results supported their proposed fatigue model for simulating the load–interaction effect for a variety of variable amplitude loading spectra (Mikheevskiy and Glinka, 2009).

In a study by Kujawski and Stoychev (2010), it was shown that the compressive loads decreased the fatigue life of their test specimens by about 300%, and that the influence of the compressive loads was just as important as that of the tensile overloads. Their study demonstrated that the influence of the compressive loads in a load spectrum on the fatigue life was equivalent to a 34% increase in the applied load. Their study concluded that the role of compressive stress cycles are very important in a spectrum loading, and cannot be treated as stipulated by the ASTM recommendation for constant amplitude loading, by which the stress intensity factor range is assumed to equal the maximum stress intensity factor due to the positive load ratios (Kujawski and Stoychev, 2010).

The scarcity of experimental data in relation to the influence of compressive stresses on the crack growth rate of materials has prompted researchers to pay more attention to the presence of compressive stress in a given cyclic loading scenario. Several researchers have studied the influence of single tensile overload or compressive underload stress spikes on the FCG of materials (Sadananda *et al.* 1999; Taheri *et al.* 2002). It has been demonstrated that any sudden change in the stress intensity factor range could result in substantial changes in the FCGR of materials. The early research in this area goes back to the 1970s, when tensile overloads were observed to result in significant retardation in crack growth rate (Jones and Wei 1971). The resultant crack tip plasticity due to an overload could significantly influence the material response at the crack tip region, hence influencing the crack propagation rate within the subsequent load cycles (Taheri *et al.* 2002; Yuen and Taheri 2005). Such tensile overloads are observed to cause considerable decrease in the FCGR. However, compression underloads have been shown to accelerate the growth rate of the crack (Taheri *et al.* 2002; Rushton and Taheri, 2003 and Yuen and Taheri, 2005).

It has also been observed that under a VAL scenario, the crack growth is a function of the stress amplitude, the stress ratio and the nature of the stress-time history (Iranpour *et al.* 2008). This complexity has resulted in the development of numerous models over the past decades; however, to the best of our knowledge, there exists no universal model that could predict the FCG under such realistic loading scenarios. Indeed, most of the available models have been mainly developed for a specific case or application, incorporating some of the main influencing parameters (see for example Taheri *et al.* 2002). Furthermore, a majority of the available studies have focused on understanding the fundamentals of the crack growth retardation or acceleration mechanism resulting from the application of a single (or a few) tensile overload(s) and compressive underload(s). A real life VAL usually contains a large number of tensile or compressive stress peaks (see Iranpour *et al.* 2008). Even a ball-bearing, which is generally considered as the best example of a component under a constant amplitude loading scenario, would be essentially subject to a variable amplitude stress-time history during its service life. Therefore, it would be more realistic to study the influence of compressive underloads by conducting experiments on specimens under a VAL stress-time history.

The major reasons that the focus of the previous studies has been basically on CAL with a few single tensile overloads or compressive underloads are as follows:

- a) In general, a CAL scenario with only a few stress spikes provides the researcher with a very convincing set of data by which the influence of a stress spike can be easily highlighted. This also facilitates the understanding of the underlying physics of the crack growth and the associated retardation/acceleration mechanisms.
- b) Furthermore, in comparison to VAL scenarios, conducting an experiment with a CAL scenario is much easier, and the tests results can be easily analyzed and interpreted. Moreover, subjecting a specimen to tension-tension loading cycles require no anti-buckling device, which in turn makes the tests setup simpler. In addition, there would be less chance of slippage or misalignment in a test with tension-tension CAL. The other factor that has basically confined researchers to

CAL tests is the requirement for specialized software for controlling the test machines, in order to impose VAL loading scenarios (often an expensive option).

The influence of a single overload or an underload stress spike is well documented for a wide range of materials. However, some researchers have demonstrated that the retardation effect experienced after a number of consecutive tensile overloads would be larger than that observed after only a single overload. This has been explained to be due to the adaptation of the material yield surface to the tensile overloads (Prommier, 2003). In general, however, the combined effect of the overload and underload on the subsequent stress spikes generates a complex influence on the crack growth rate, mainly depending on their sequence and other dominant mechanisms. It should also be noted that almost all the available studies investigating such an influence have mainly considered CAL scenarios with positive stress ratios (Silva 2005; Taheri *et al.* 2002); in other words, there is a clear lack of data in consideration of the influence of the overload/underloads and the CSC in loading scenarios with negative stress ratios. As a result, more works on this area have been pursued in recent years (see for example, Silva 2005; Shabanov 2005; Iranpour and Taheri 2007.)

In the present study, a VAL stress-time history is used. The scenario is typical of the loading scenario that is experienced by a structural component that is subjected to flow of air or fluid (such as pipelines under ocean current profiles or wings of an aircraft). Some recommendations are offered for improving the accuracy of fatigue life prediction of components under VAL scenarios, by focusing on the CSC.

### **6.3. Problem Definition and Objectives**

The motivation for the authors to conduct a series of experimental investigation into the influence of the compressive portion of a VAL stress-time history on the fatigue crack propagation was outlined above. In the experimental investigation, a realistic VAL stress time-history is directly applied to a number of specimens and the resulting crack growth rates are recorded. It is illustrated that ignoring the presence of the compressive portion of the stress-time history would result in significant underestimation of the FCGR, which

is non-conservative and is not acceptable for design purposes. A series of finite element analysis is also performed to understand the physics of the phenomenon and explain the test results. The fundamental concept of CTOD is used to relate the crack growth rate of the material to the CSC.

The main goal of this part of the research is to study the detrimental influence of the CSC on the FCGR and understanding of its underlying physics.

#### **6.4. VAL Stress-time History**

Figure 6.1 shows the stress-time history of the VAL scenario used in this study (for more detail on this stress-time history, see Iranpour and Taheri 2007). As seen in the figure, there exist numerous numbers of tensile and compressive stress spikes (also referred to as overloads and underloads, respectively) in the stress-time history. This makes it very difficult to predict the fatigue life of the component based on the classical fatigue models that only consider the presence and the influence of a few single overload and/or underload stress spike (see Iranpour *et al.* 2008). According to most of the fatigue design guidelines and standards, one is encouraged to completely ignore the presence of all CSC (Newman *et al.* 2005). Therefore, the compression-tension stress-time history is often converted to a zero-tension stress-time history. At the next step, one may use any of the available approaches (such as Barsom's approach) to find a CAL that is *equivalent* to the real VAL applied to the component. Once the *equivalent* CAL is established, an appropriate fatigue model (i.e. the Paris model) can be used to estimate the fatigue life of the component.

In this paper, the stress-time history shown in Figure 6.1 is referred to as one *block*. Due to some limitations of the computer software used for the tests, the entire VAL stress-time history could not be applied to the specimen in one setting. This is because the maximum number of data points that could be accommodated by the computer software used to control the testing machine was limited to 200 points; therefore, the entire VAL stress-time history had to be subdivided into several *sub-blocks* (see Figure 6.1). These *sub-blocks* were then applied to the specimens, sequentially. Therefore, the

*block* shown in Figure 6.1 was divided into a total of nine *sub-blocks*. Note that each *block* contained 1754 data points, resulting in a total of 877 stress cycles in each *block*.

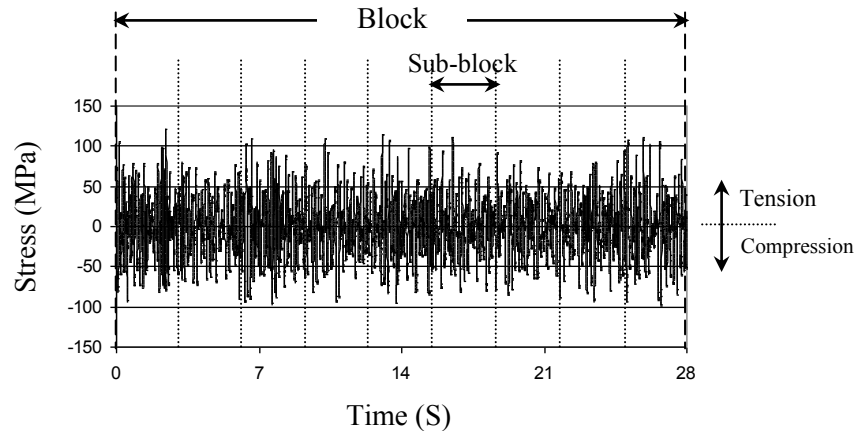


**Figure 6.1.** The VAL stress-time history *block* and its 9 *sub-blocks*

As stated earlier, there exist a very few design standards that takes into account the influence of the CSC. For example, API recommends that for cases where the stress range is entirely tensile, the stress range for the fatigue life assessment should be considered as the total stress range. However, for cases where the stress range is partially compressive, the stress range for the fatigue life estimation should be taken as the entire tensile stress range plus 60% of the compressive stress range (API 2RD, 1998). The above is recommended when assessing the fatigue response of parent material or welded joint in the post-weld heat-treated conditions. For the welded-joints in the as-welded conditions, the stress range to be used for the fatigue life analysis should be based on the entire stress range, regardless of whether the stress range is partly or entirely compressive (API 2RD, 1998).

Although API suggests that 60% of the compressive stress range could be taken into account, it does not provide any further explanation on the fundamental basis used in arriving at such recommendation. Such a provision recommended by API, however, indicates that the detrimental influence of the CSC is well recognized by this code of practice.

## 6.5. Tests with Various Levels of Compressive Stress cycles

To better understand the influence of CSC on the FCG of materials subject to VAL, a comprehensive series of experimental tests were conducted, subjecting centre-cracked specimens using various levels of CSC within a given time-history. Two main parameters were taken into considerations in the test series: (i) the *magnitude* of the compressive stresses and (ii) the *intervals* (or the number of tensile stress cycles (TSC)) emerging in between two compressive stress spikes). The tests performed in this study are categorized into four different series:

- 1) Test Series No. 1- in this series of tests, the entire compression-tension VAL stress-time history *block*, as shown in Figure 6.1, was applied to a number of test specimens and the resulting crack growth rate was recorded.
- 2) Test Series No. 2- in this series, the magnitude of all compressive stresses of the entire VAL stress-time history *block* (Figure 6.1) was multiplied by different scaling factors (i.e., 0.0, 0.3, 0.6 and 0.8). A scale factor of 0.0 would therefore indicate that all the CSC within the stress-time history block were nullified, resulting to a zero-tension stress-time history. Figure 6.2 shows the VAL stress-time history block with a scale factor of 0.3. As it is illustrated in this figure, compared to Figure 6.1, the CSC of the stress-time history have been *shrunk* to 30% of their original values.
- 3) Test series No. 3- in this series of tests, all the CSC were omitted from the stress-time history, except for the maximum CSC within each *sub-block*.

Test Series No. 3 was further subdivided into two main sub-series, as follows:

- 3.1) *Sub-block*: in this sub-series, all the CSC in each *sub-block* were set equal to zero, except for the maximum compressive *stress* spike within that *sub-block*. The magnitude of the original maximum compressive stress spike in each *sub-block* was kept unchanged.
- 3.2) *Block*: in this sub-series, all the CSC in each *block* were set equal to zero, except for the maximum compressive stress of the *block*.

In other words, in test sub-series No. 3.1, there exist a total of 9 maximum compressive stress spikes in the entire *block*; while test sub-series No. 3.2 only contains a single CSC, that being the maximum compressive stress spike that appears within the entire *block*.

- 4) Test series No. 4: in this series of tests, a certain number of entirely zero-tension stress-time history *blocks* (that is Test Series No. 2, with a compressive stress multiplier of 0.0), were followed by one *block* of a stress-time history that its compressive portion only contained the maximum compressive stress spike of the entire block (i.e., similar to Test Sub-series No. 3.2). For example, the test with designation of 2Mult-0.0/1Max-B would indicate that the specimen is subjected to two blocks of Test Mult-0.0 (corresponding to zero-tension stress-time history), followed by one block of a stress-time history in which all the CSC were set equal to zero, except for the maximum compressive stress spike within the entire block.

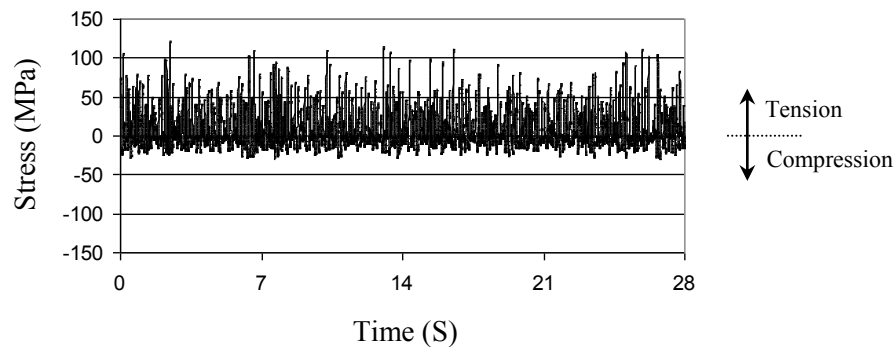


**Figure 6.2.** The VAL stress-time history (one *block*) with all the original values of its CSCs Scaled by 30% (for test Mult-0.3)

Table 6.1 summarizes the different series of tests that were conducted in this study. It should be noted that each graph or test result reported in this study represents the average of at least three test specimens. The results of the three specimens for each test were usually so close that there was no need to plot the results of each test individually, since the differences would be indistinguishable.

**Table 6.1.** Summary of the Various Test Series and their Descriptions

Test Series No.	Identifier	Test description	
1	Mult-1.0	The entire VAL stress-time history shown in Figure 6.1 is applied to the specimen	
2	Mult-0.0	The magnitude of all CSC is multiplied by the scale factor shown in the next column:	0.0
	Mult-0.3		0.3
	Mult-0.6		0.6
	Mult-0.8		0.8
3.1	Max-SB	All CSC are omitted, except the cycle having the maximum compressive stress value within each <i>sub-block</i> .	
3.2	Max-B	All CSC are omitted, except for the cycle having the maximum compressive stress magnitude within the entire <i>block</i> .	
4	2Mult-0.0/1Max-B	2, 5, 10 or 40 blocks of test series “Mult-0.0”, respectively, are followed by one block of test series “Max-B”. This trend is repeated until the specimen’s failure.	
	5Mult-0.0/1Max-B		
	10Mult-0.0/1Max-B		
	40Mult-0.0/1Max-B		

In summary therefore, the results of test series 1 and 2 would enable us to investigate the influence of the *magnitude* of the CSC on the FCG response of the material, while the results obtained from test series 3 and 4 would help us to better understand the importance of the *presence* and *interval* of CSC on the FCG response of the material. As it will be seen later in detail, the compressive portion of a VAL stress-time history has a detrimental influence on the fatigue of materials, and should not be ignored.



## 6.6. Test Setup and Material

The fatigue tests were conducted using an Instron Servo-hydraulic Universal Testing Machine with a capacity of  $\pm 100$  kN under dynamic or 200 kN under static loading conditions. The stress-time history was applied to the specimen through a special-purpose software. A fiber optic light was used to illuminate the crack tip region. To monitor the growth of the crack tips, a Mitutoyo traveling microscope with a magnification of 50X mounted on a pair of micrometers with a resolution of 0.01mm were used to record the crack growth increment. The tests were performed per ASTM E 8M Standard, using rectangular plate specimens with dimensions of 300 mm (L)  $\times$  100 mm (W)  $\times$  4.74 mm (T) with a central notch of  $2a = 20$  mm. The plates were cut in such a way that the length of the specimen was in the same direction as the rolling direction of the material (see Iranpour *et al.* 2008 for more info). To get a better perspective of the crack tip during testing, the surface of the specimen was polished with various grits of sand papers, starting from coarse (No. 120) to a very fine one (No. 1200). Figure 6.3 shows the rectangular test specimen configuration and dimensions, followed by the test set up. As per ASTM-E-8M standard, acceptable geometric correction factors should be considered for the specimen configuration. Moreover, as a means of ensuring that LEFM would be applicable, this standard suggests that the specimen be large enough to promote predominately linear elastic conditions during testing. The loading cycle frequency was set between 4.0 to 5.0 Hz, so that the input load history could be accurately traced.

The tests were conducted in air and at room temperature. The 20 mm notch of each specimen was pre-cracked to sharp crack tips, to a length of approximately  $2a' = 22.0$  (mm), before undergoing the actual VAL stress-time history. Hence, the reported crack growth rates under the VAL stress-time history were measured from the sharp pre-crack tips, rather than the initial EDM starter notch tips. After the pre-cracking, a specified number of blocks of the VAL stress-time history were applied to the specimen and the crack growth was measured. This procedure was followed until the specimen fully fractured across its width. The mechanical properties and composition of the alloy are reported in Tables 6.2 and 6.3, respectively.

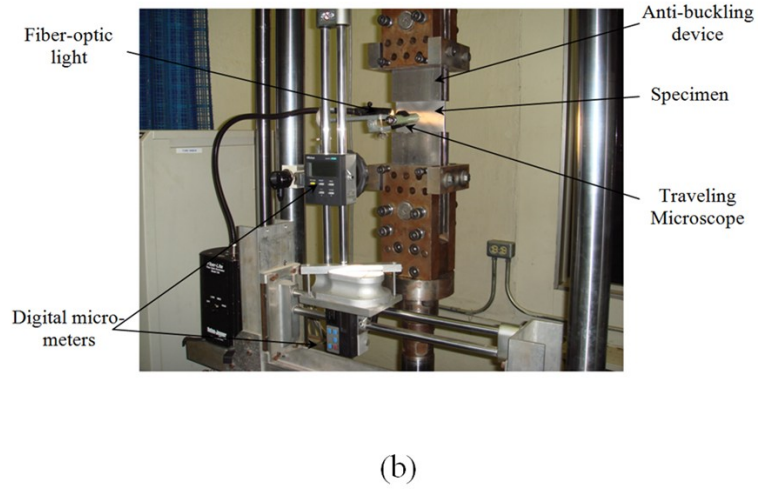
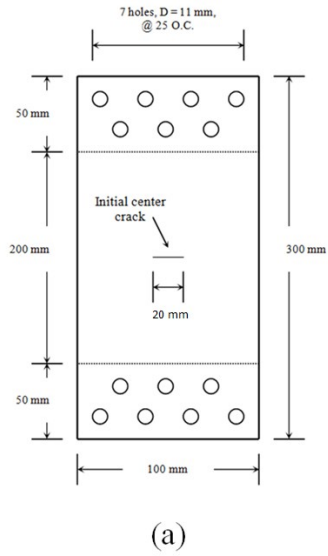


**Figure 6.3.** (a) Specimen configuration and dimensions, (b) test set up

**Table 6.2.** Mechanical Properties of the 6061-T651 Aluminum Alloy

Modulus of Elasticity (GPa)	0.2% Yield Stress (MPa)	Ultimate Tensile Stress (MPa)
68.9	275.4	330.6

**Table 6.3.** Compositions (%) of the 6061-T651 Aluminum Alloy

Fe	Cu	Mn	Ni	Si	Mg	Zn	Ti	Cr
0.201	0.198	0.41	0.006	0.528	0.961	0.004	0.014	0.202

## 6.7. Experimental Observations and Results

This section presents the experimental observations and results from the four test series explained earlier.

### 6.7.1. Results of Test Series No. 1

In Test Series No. 1, as stated, the entire compression-tension VAL stress-time history (see Figure 6.1) was applied to a number of specimens. Figure 6.4 shows the average values of crack length (average of three test specimens), versus the number of applied blocks. The specimens failed after applying 227 to 231 VAL stress time-history blocks, representing 199,079 to 202,587 stress cycles, respectively. The results of this series of experiments are used as the baseline, to which the results of the other test series will be compared.

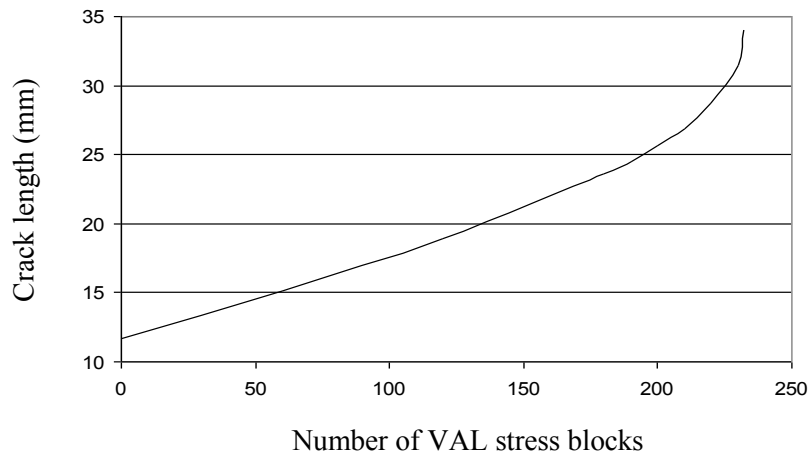


**Figure 6.4.** Crack length versus the number of applied VAL stress-time history blocks (the blocks include all the original CSCs)

### 6.7.2. Results of Test Series No. 2

In the second series of tests, the magnitude of all stresses in the compressive portion of the VAL stress-time history was multiplied by different multipliers (see Table 6.1). This was done to investigate the influence of the *presence* of the compression underloads on

the FCGR of the component. Although CSC do not generally extend the crack in a specimen, the combination of CSC with tension overloads, however, could impose significant contribution in reducing the fatigue life of the component. Therefore, a higher fatigue life could be expected for the cases in which the compressive underloads are omitted from the stress-time history, or are multiplied by a factor smaller than unity. This was supported by the results of Test Series No. 2. In this series of tests, at the first stage, the compressive portion of the VAL stress-time history was omitted entirely (i.e., scaling the CSC to zero). The three specimens tested under a zero-tension stress-time history failed after applying 485 to 494 stress blocks, which show a considerable increase in the total number of stress cycles required to fail the specimen. Note that in the cases where all the CSC were omitted, the total number of stress cycles in each block was reduced to 534 stress cycles, compared to 877 stress cycles in the original tension-compression stress-time history. Therefore, for comparison purposes in this study, we refer to the number of the applied *blocks*, as opposed to the number of stress cycles. In other words, one *block* in the zero-tension tests (test series Mult-0.0 in Table 6.1) is exactly equal to one block in the tension-compression tests (test series Mult-1.0 in Table 6.1), with the only difference being omitting the entire compressive portion of the stress-time history. That is exactly how the actual tension-compression block was converted into a zero-tension block.

Figure 6.5 compares the crack growth rates of the specimens subjected to zero-tension (test series Mult-0.0) and compression-tension (test series Mult-1.0) VAL stress-time histories. As it is clearly illustrated in this figure, omission of the CSC results in a considerable increase in the fatigue life of the component. This should be of significant importance when considering the current analytical FCG calculation approaches that usually disregard the compressive stress cycles of a given load-history, thus resulting in non-conservative fatigue life estimation. As shown in this figure, the fatigue life of the component subjected to compression-tension loading cycles is approximately 2.5 shorter than the case when the CSC are omitted, which could be very alarming.

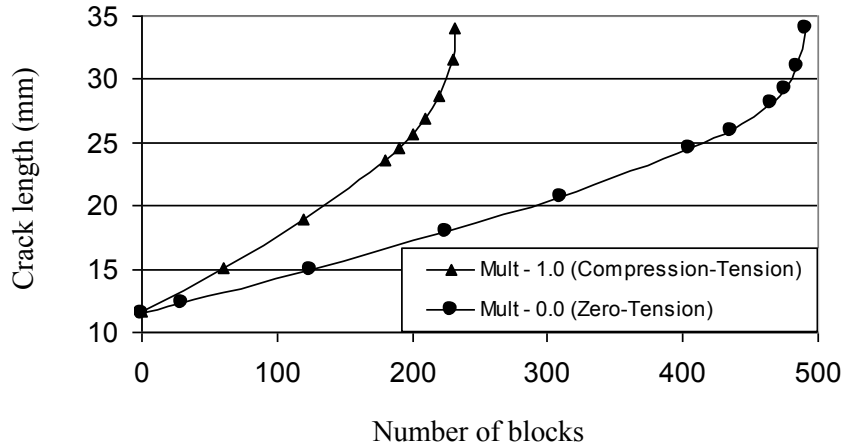


**Figure 6.5.** Comparison of the FCGR under the compression-tension and zero-tension stress-time history

In the subsequent tests of Test Series No. 2, the magnitude of all stresses in the compressive portion of the stress-time history was multiplied by factors of 0.3, 0.6 and 0.8. These tests were done to study the influence of the *magnitude* of CSC on the fatigue life of the component. Figure 6.6 compares the results of all the specimens tested in Test Series No. 2. It can be seen that the CSC have a significant detrimental influence on FCGR response of the material.

As it is illustrated in Figure 6.6, the application of the CSC with only 30% of the original CSC' magnitude (i.e., test Mult-0.3) increased the fatigue life of the specimen by almost 50% compared to the case where the magnitude of CSC was unaltered (test Mult-1.0). It is also observed that the detrimental rate of the compressive stresses increases as the magnitude of the CSC increases (that is increasing the multiplier from 0.0 to 1.0). For example, increasing the multiplier by 40% (i.e., from 0.6 to 1.0), results in only about 25% of decrease in the fatigue life. This leads to the observation that the *presence* of CSC has more influence on the fatigue response of the alloy than does their *magnitude*. In other words, the detrimental influence of the CSC decreases as their magnitude approaches a critical value. This is illustrated in Figure 6.7, where the total number of applied stress-time history blocks consumed to fail the specimen is plotted versus the scale multiplier applied to the compressive stress portion of the stress-time history. The results are also in concert with the results reported by Makabe *et al.* (2004) and Lee *et al.*

(2009), who considered VAL loading with a few overload/underload stress spikes. Again, three tests were done for each case, and the curve presents the average of the results. The results from these tests are also in concert with those reported by other researchers' works considering similar materials (e.g., Zhang *et al.* 2007).

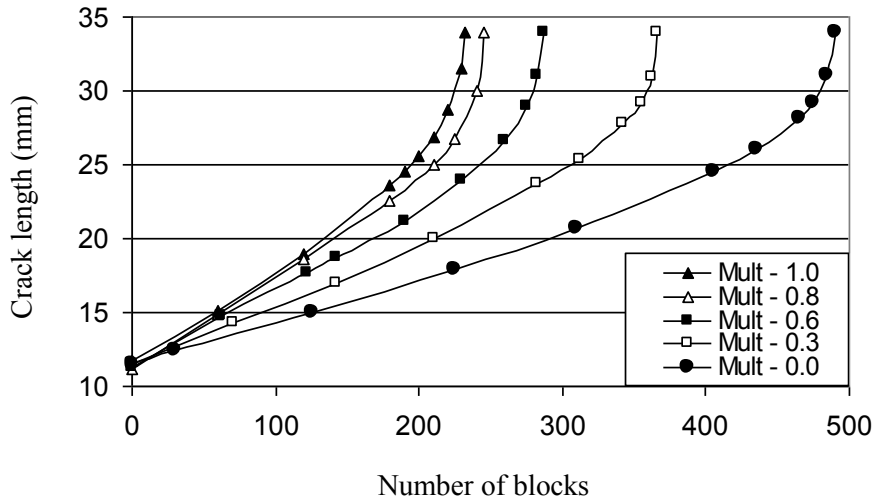


**Figure 6.6.** Comparison of FCG under compression-tension VAL with various multipliers on the compressive portion of the stress-time history (each curve is the average of at least three tests)

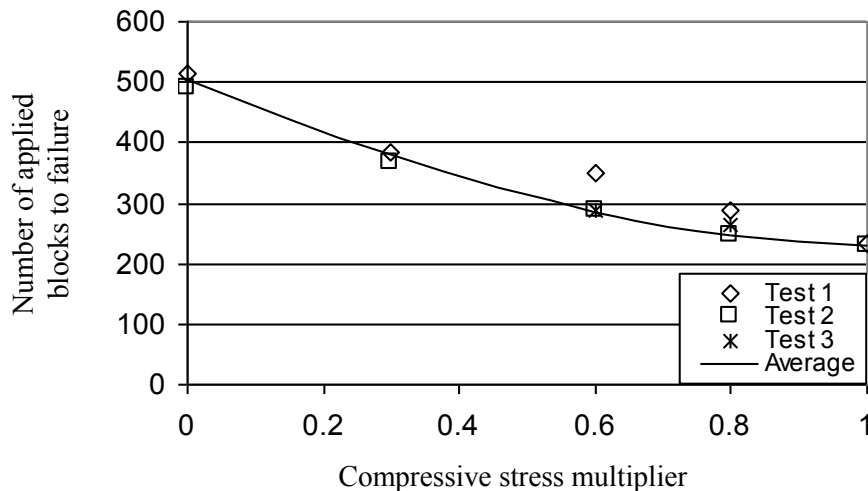


**Figure 6.7.** Plot of the number of the applied VAL blocks to failure versus the scale multiplier applied to the compressive portion of the stress-time history (Test Series No. 3)

In the investigation conducted by Lee *et al.* (2009) on aluminum alloys, it was shown that subjecting aluminum alloys to a similar stress-time history with significantly lower tensile and higher compressive stress values could result in a FCG almost twice that of the case with higher tensile and lower compressive stress values. This difference was attributed to both the retardation effect due to the tensile overloads and acceleration effects due to the compressive underload. Both the tensile overloads and compressive underloads in that research were changed within their two stress-time histories; thus, it was not possible to declare a conclusive statement on the influence of each mechanism separately. In our research, however, the tensile portion of the stress-time history was kept unchanged. Therefore, the changes in the fatigue life of the component arose only due to the accelerating effect resulted from the compressive underloads.

### **6.7.3. Results of Test Series No. 3**

One of the main goals for conducting Test Series No. 3 was to study the influence of the maximum compressive stress spikes within the entire loading block in comparison to the results obtained from Test Series No. 2. In this series of tests, all the CSC were nullified, except a certain number of the maximum compressive stress spikes (or overloads).

As explained earlier, the VAL stress-time history *block* shown in Figure 6.1 was divided into a total of nine *sub-blocks*. In the first sub-series of Test Series No. 3 (see “Max-SB” in Table 6.1), all the CSC in each *sub-block* were nullified, except the maximum compressive stress within that *sub-block*. This significantly reduced the number of the CSC of the entire VAL *block*. In other words, the number of compressive stress spikes reduced from a few hundred cycles to only 9 cycles within each *block*. The resultant stress-time history was applied to a number of specimens and the crack growth rate was measured.

Figure 6.8 illustrates the resulting crack growth rates. From the two curves on left of the figure, one corresponds to test “Mult-1.0” defined earlier (also noted in Table 6.1), and shows the baseline, where the original time-history was applied (as in Figure 6.1). The other curve on the left of the figure shows the test results from a compression-tension stress-time history, in which all the compressive stresses in each *sub-block* were nullified,

except the maximum compressive stress spike within each *sub-block* (i.e., Max-SB in Table 6.1). The third curve shows the results of the tests in which all the CSC were nullified (i.e., Mult-0.0 in Table 6.1).

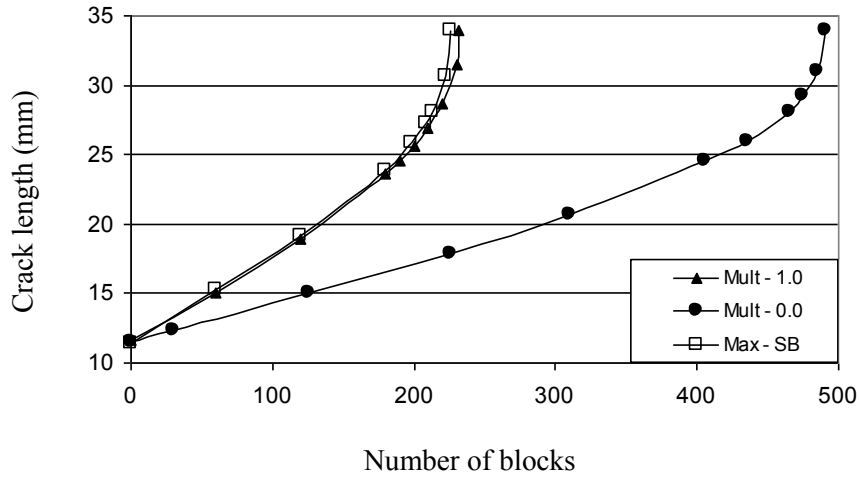


**Figure 6.8.** Comparison of the FCG for three loading scenarios

As seen from the figure, the response of specimens subject to “Mult-1.0” and “Max-SB” loading cases are very similar. It is evident that it is the maximum compressive stress of a given *sub-block* that imposes its influence on the FCG of the material. In other words, it is the largest compressive stress within a sub-block that would have the most detrimental effect. It may be concluded that when considering the influence of the CSC within a given VAL time-history, one may only consider the largest compressive stress within the loading *sub-block* and ignore the presence of all other CSC of that *sub-block*. If one ignores the presence of the limited number of maximum compressive stress spikes in the entire time-history block (here a total of 9), the FCGR would completely change as evident by the results of test “Mult-0.0” shown in the figure. The results illustrate that it would be extremely non-conservative to completely ignore the presence of the compressive portion of a VAL stress-time history.

To further study the influence of omitting all the CSC except the maximum ones, more of the compressive stress spikes were omitted in the next set of tests. As such, in the second sub-series of the tests, the maximum compressive stress spike in each *sub-block*



was also omitted, and only the maximum compressive stress spike of the entire *block* was maintained. This is identified as test “Max-B” in Table 6.1. Figure 6.9 compares the results from this series of tests with the other results illustrated earlier in Figure 6.8. It is clearly evident that the influence of a compressive loading spike cannot be ignored, and that there exists a *threshold* for the *number* of compressive stress cycles above which all other the CSC could be omitted.

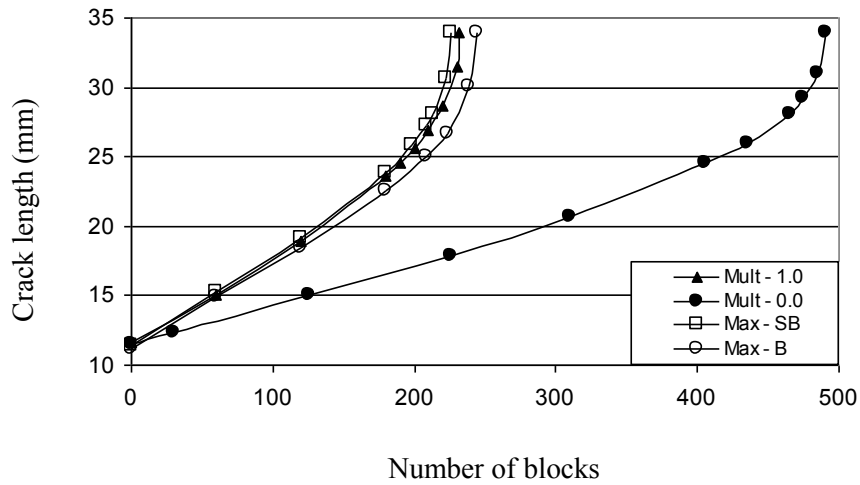


**Figure 6.9.** Further illustration of the influence of the presence of the CSCs within a VAL time-history

As stated earlier, the secondary aim of this test series was to determine whether there would be a justification for considering the stress intensity factor range covering the entire tension-compression portion of the stress range for each loading cycle. This is because most approaches used to establish the FCGR of materials consider only the stress intensity range corresponding to the tensile portion of the stress-time history. In other words, the compressive portion of the stress range is completely ignored. This is due to the notion that a crack is closed when subject to a compressive stress, and therefore, no stress intensity factor is associated with it. On the other hand, some researchers argue that one should include the entire compressive portion of the stress cycles in the calculation of the stress intensity factor range, which results in larger stress variation, thus leading to

higher crack growth rates. This is based on the observation that the application of compressive loading cycles generally increases the crack growth rate of the material.

The results shown in Figure 6.9 indicates that so long as the entire stress-time history is divided into a certain number of smaller sub-blocks, one may ignore the presence of all the CSC within the stress-time history, except for the maximum compressive stress spike within each sub-block, and yet expect to attain more or less the same FCG in a given component as if it was subject to the full compression-tension stress time history. As a result, it can be concluded that there is no justification for considering the entire compressive portion of the stress-time history when evaluating the stress intensity factor range, but should include the maximum spikes within the sub-blocks.

#### **6.7.4. Results of Test Series No. 4**

In this series of tests, a certain number of zero-tension stress-time history blocks (test “Mult-0.0”), were followed by one block of a stress-time history which only contains the maximum compressive stress spike of the entire *block* (tests “Max-B”). This loading was continued till specimens failed. A total of four groups of tests were conducted within this test series, each containing at least three specimens. The groups are differentiated by the number of Mult-0.0 loading blocks applied prior to the application of the Max-B loading block.

Figure 6.10 shows the FCGR versus the number of the applied stress blocks for Test Series No. 4, and compares it with the FCG results obtained from the zero-tension (test “Mult-0.0”) and the compression-tension (test “Mult-1.0”) loading scenarios that were discussed earlier. It can be observed that as the total number of the compressive stress spikes reduces, the FCGR decreases and the fatigue life of the specimen approaches that of the specimen group subjected to the VAL whose CSC were nullified. The results from these series of tests further help us to gain a better understanding of the influence of dismissing the CSC when evaluating the fatigue life of materials.

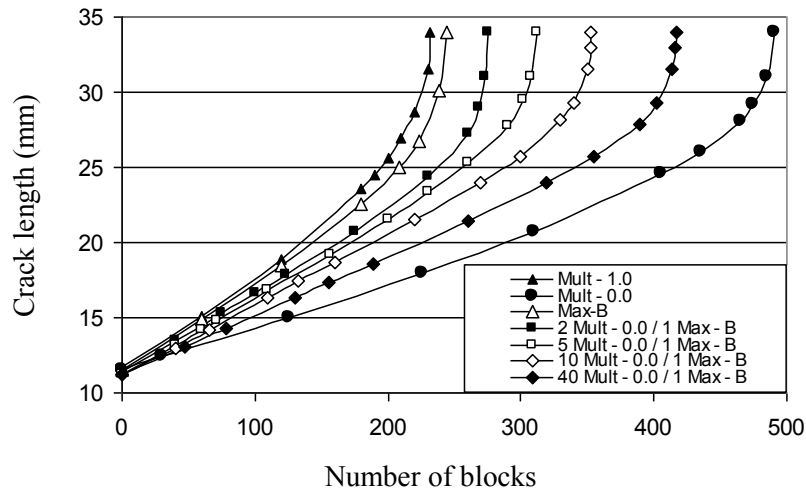


**Figure 6.10.** Evidence of the pronounced influence of the maximum compressive stress spike within the VAL *block*

It should be emphasized that tests “Max-B” only contains one compressive stress spike, which is the maximum compressive stress spike within the entire *block*; while, in tests “2Mult-0.0/1Max-B”, the maximum compressive stress spike is repeated in every third block (note that “2Mult-0.0” does not include any CSC).

It can be observed that as expected, as more compressive stress spikes are omitted from the full compression-tension stress-time history, the crack growth rate moves towards that produced by the zero-tension stress-time history (i.e., the VAL scenario that contains no compressive load cycles at all). These results further confirm that it is both the *magnitude* and *interval* (relative position) of compressive stress underloads that have a significant influence on the fatigue response of the material; and that these important factors should be considered *simultaneously* when estimating the FCG.

## 6.8. Roughness-induced Crack Closure

Since Elber (1970) explained the importance of crack closure on the crack growth rate, many investigators have conducted research in this area with the aim of better

understanding the crack closure and its influence on the fatigue of materials. The crack closure concept studies the fatigue process based on what happens behind the crack tip. In recent years, researchers have studied the relationship between the influence of CSC and the crack growth rates, with focus on the closure effects (Pommier 2003; Silva 2004 and 2005). Among all the mechanisms resulting from crack closure, the plastic-induced crack closure (PICC) and roughness-induced crack closure (RICC) are known to be of most important in explaining the influence of CSC on the crack growth rate of materials (Silva 2005). The influence of the load interaction effects and plastic-induced compressive stresses was first studied by Schijve (1962) and later by Jacoby (1966). Their work demonstrated that FCG retardation (or acceleration) was governed by the compressive stress gradient ahead of the crack tip. The influence of RICC was first noted by Walker and Beevers (1979). In general, FCG in aluminum alloys and titanium alloys are considered to be sensitive to RICC, while that of steel alloys is more dependent on the PICC (Silva 2005).

To study the influence of the roughness-induced crack closure on the FCGR of the aluminum alloy tested in this study, the surface roughness was measured for two test specimens Mult-0.0 and Mult-1.0. It is noted that the only difference between the various test performed in this study is the changes made in the compressive portion of the stress-time history, while the tensile portion was kept unchanged. Figure 6.11 shows the fracture surface of these two specimens. The fracture surface shown at the top of this figure corresponds to test Mult-1.0 (described in Table 6.1), where all the CSC were entirely included in the stress-time history applied to the specimen. The fracture surface shown at the bottom of this figure corresponds to test Mult-0.0, where all the compressive stresses were omitted. As observed in this figure, the fracture surfaces look very similar for both cases.

To study the difference between these two fracture surfaces at the microscopic level, roughness measurements were done according to standard DIN 4768, using laser profilometry and 3D microscopy techniques. Figure 6.12 shows a typical 3D roughness profile of the entire area of the fracture surface. Figure 6.13 shows a typical roughness profile measured along two parallel lines over the fracture surface.

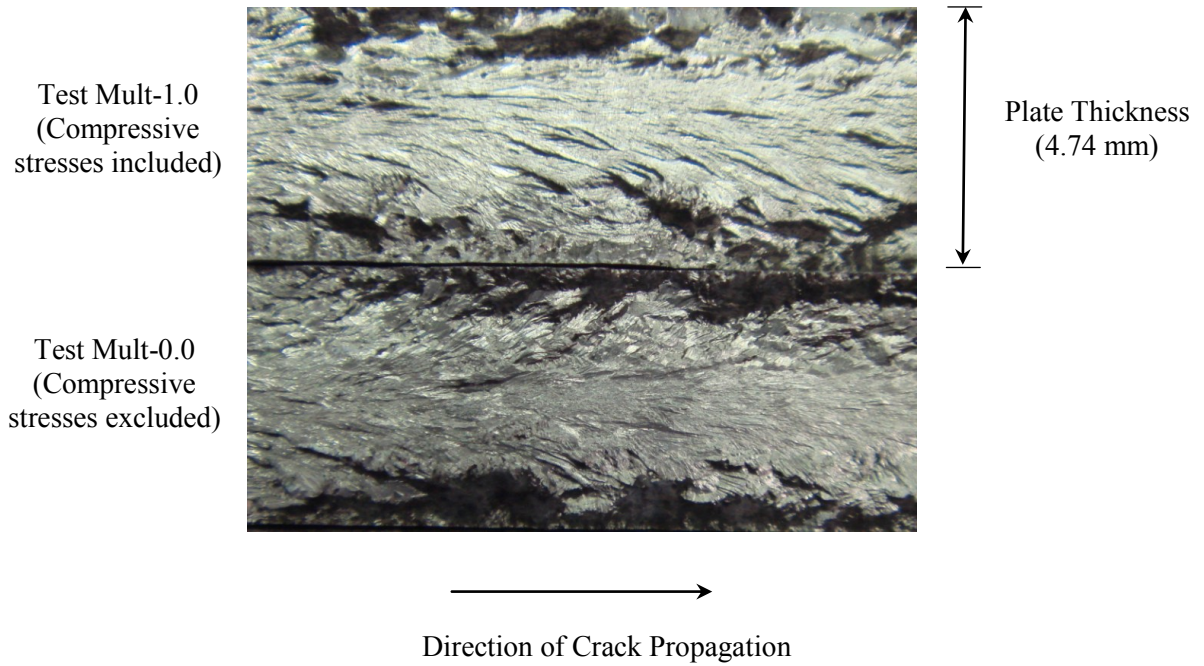


**Figure 6.11.** Comparison of the fracture surfaces for cases with (Tests Mult-1.0 at top) and without (test Mult-0.0 at bottom) the CSC

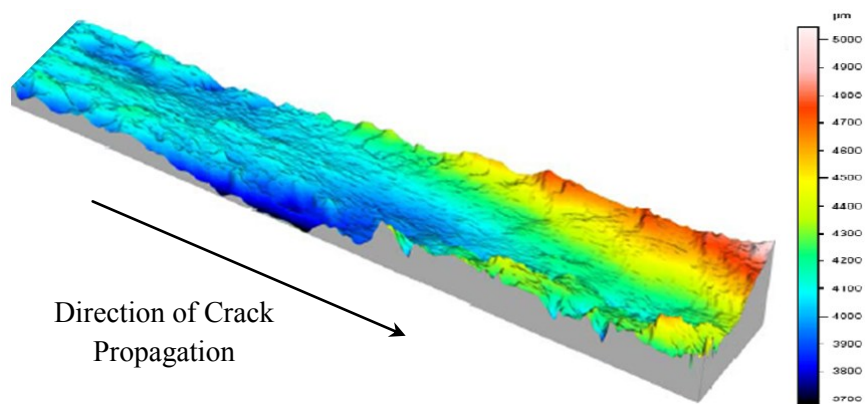
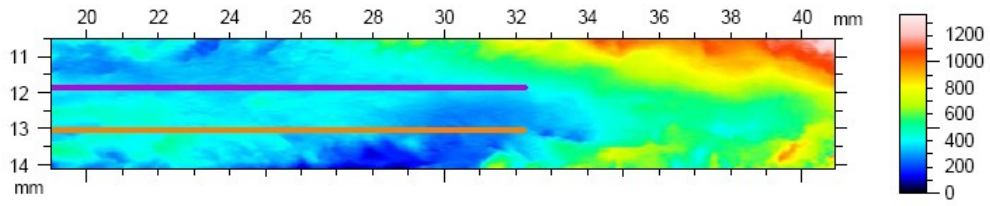
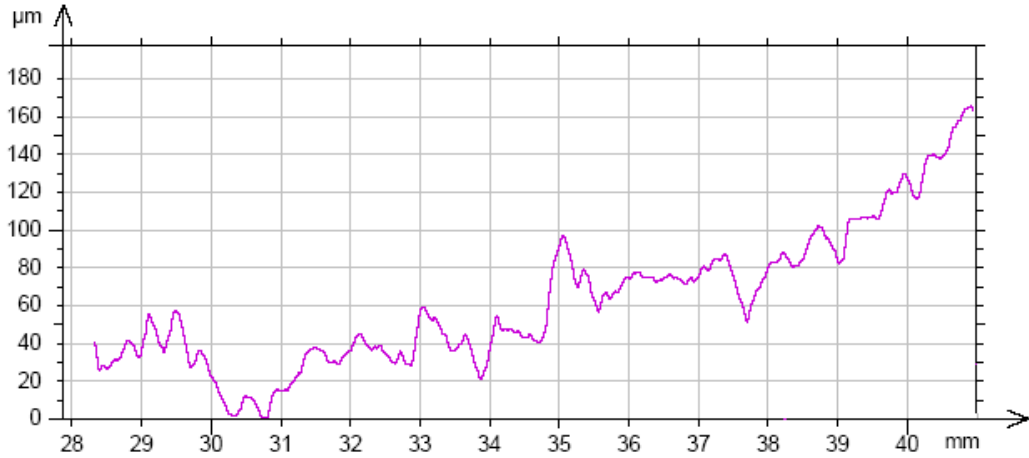



**Figure 6.12.** A typical 3D roughness profile of the fracture surface



(a)



(b)

  
 Direction of Crack Propagation

**Figure 6.13.** Typical roughness profile along the fracture surface: a) roughness measured along two parallel lines (purple and orange lines); b) roughness profile of the purple line

The Arithmetic Mean Deviation of the roughness profile,  $R_a$ , was calculated to quantify the roughness of the fracture surface by the following equation:

$$R_a = \frac{1}{l_m} \int_0^{l_m} z dx \quad (6.1)$$

where  $z$  is the value of surface profile and  $l_m$  is the reference length. The arithmetic mean deviation of the roughness profile for tests Mult-0.0 and Mult-1.0 were measured as  $2.7 \mu m$  and  $3.4 \mu m$ , respectively. Figure 6.14 shows the roughness profile of a typical

surface. The arithmetic mean deviation of the ‘surface’ for tests Mult-0.0 and Mult-1.0 were measured as  $11.7 \mu\text{m}^2$  and  $21.4 \mu\text{m}^2$ , respectively.

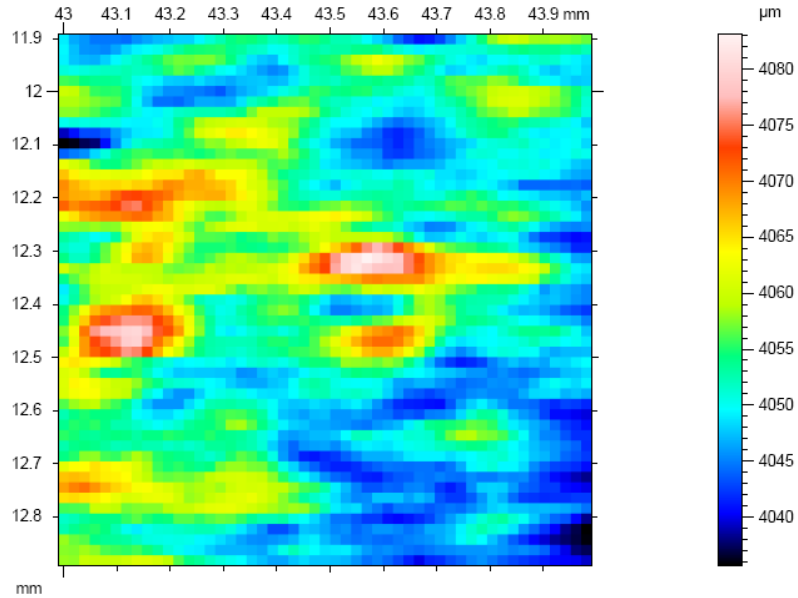


**Figure 6.14.** Typical roughness profile of the fracture surface

It is observed that for the aluminum alloy under study, omitting the compressive stresses of the VAL stress-time history results in a decrease in the surface roughness. In other words, inclusion of compressive stress cycles would not necessarily result in a decrease in the roughness of the fracture surfaces. This observation corroborate with the observations made by other researchers investigating various materials. Silva (2004 and 2005) considered the influence of compressive stresses on the crack surface roughness of a few materials such as low carbon steel Ck45, Aluminum alloy Al7175 and Titanium alloy Ti6A14V. He observed that for the aluminum alloy, the roughness increased as the value of the applied compressive stress increased. Silva (2005) concluded that the surface roughness is a material dependent extrinsic property, and does not depend solely on the value of the stress ratio,  $R$ . In general, according to the basic concepts of the RICC, an increase in the surface roughness results in a decrease in the crack growth rate of the material. It is, therefore, concluded that if the roughness was the reason for increasing the crack growth rate for test Mult-1.0 (in which all the compressive stresses are included),

one would have expected the roughness to have decreased, rather than increased as the crack propagated, when compared to crack growth of test Mult-0.0. This leads to the conclusion that the increase in the crack growth rate due to introducing the compressive stresses is not because of the decreases in the surface roughness and RICC. This verifies with the results reported by other researchers, demonstrating that in stress-time histories that include CSC, roughness effect is not the dominant mechanism resulting from the crack closure (Chen and Lawrence 1997; Silva 2005).

## **6.9. Summary and Conclusions**

In this chapter, the influence of compressive stress cycles (CSC) existing within a realistic variable amplitude loading scenario on the fatigue crack growth of Al6061-T651 aluminum alloy was studied. Both experimental and computational approaches were used to conduct the study. Moreover, analytical crack growth analyses were also carried out; the analytical and computational approaches will be presented in another publication. The VAL stress-time history used in this research represents the type of loading scenario usually expected in a structure due to interaction with fluid, such as aircrafts and offshore structures. The stress-time history consisted of both tensile and compressive loading cycles. The magnitude of the applied CSC of the stress-time history varied among the different tests, while the tensile stress cycles were kept unchanged from test to test.

The work presented in this paper concentrated on various tests that were conducted on plate specimens having a central crack (mode I). Furthermore, the influence of CSC on the crack mating surfaces asperity was also examined by means of microscopic analysis.

The outcome of the experimental investigation can be summarized as follows:

- CSC was found to significantly affect the fatigue crack growth rate (FCGR), thus CSC should not be ignored when calculating the response of structures subject to VAL.



- The mere presence of CSC within a VAL would have a more pronounced effect on the resulting fatigue life than the magnitude of the CSC.
- Even the presence of a few CSC within the VAL could significantly affect the fatigue life of the material.
- In order to effectively and efficiently account for the influence of CSC within a VAL loading scenario, one may divide the applied stress-time history into shorter intervals (*sub-blocks*), and then apply only the maximum value of the compressive stress spike present within the sub-block. This scheme would produce a similar fatigue crack propagation result compared to the case when all the CSC present within the original time-history are applied onto the specimen.
- It appears that calculation of the stress intensity factor could be effectively accomplished by considering only the tensile portion of the stress range, and that the influence of compressive stresses could be more effectively accounted for by using other approaches (e.g., by its crack growth accelerating effect through the consideration of the resulting crack closure).
- In future, the use of a new form for establishing the stress intensity factor range should be explored, so that the influence of the compressive stresses could be more effectively considered. An approach is currently being investigated in our research group on the results obtained from an investigation conducted to examine the FCGR of a magnesium alloy using a wide range of stress ratios (both negative and positive). The preliminary results have revealed that by incorporating a new expression for stress intensity factor range in the Walker model, one could more effectively and accurately predict fatigue crack growth of materials.
- The influence of CSC on adversely affecting the fatigue life of the material under the study seems to be independent of the roughness-induced crack closure.

## **6.10. Acknowledgments**

The financial support of the National Science and Engineering Resource of Canada (NSERC) is gratefully appreciated.

## Chapter 7

# **Analytical and Computational Investigations of the Influence of the Compressive Stress Cycles on Crack Growth under Variable Amplitude Loading using CTOD**

Mohammad Iranpour and Farid Taheri

Department of Civil and Resource Engineering, Dalhousie University, 1360 Barrington Street, Halifax, Nova Scotia B3J 1Z1, Canada

Submitted for Publication in the Journal of Fatigue and Fracture of Engineering Materials and Structures

### **7.1. Abstract**

Fatigue crack growth rate (FCGR) of 6061 T651 aluminum alloy centre-cracked plates, subject to the variable amplitude loading (VAL), is estimated using a coupled analytical/computational approach. The Willenborg's retardation model in conjunction with the Walker model is used, with several of the models' parameters obtained through nonlinear finite element analyses. A two-parameter approach is used in this study relating the fatigue crack growth rate (FCGR) of the material resulting from a VAL stress-time history to the Crack Tip Opening Displacement (CTOD). In addition, nonlinear finite element approach is used to further assess the FCGR of the material, particularly under the influence of the compressive stress cycles (CSC), tensile overloads and underloads. More specifically, the crack closure concept is used to explore into the retardation effect of the tensile overloads, as well as the detrimental influence of the compressive underloads. The finite element analysis results are compared to the experimental results reported in our earlier study. It is observed that the CTOD provides adequate information for calculating the FCGR under the VAL stress-time history applied to a material.

The results further demonstrate two important phenomena, i.e., (i) the influence of FCG retardation effects due to the tensile overloads, and (ii) the acceleration effect due to the applied compressive underloads of a VAL stress-time history.

**Keywords:** Fatigue, crack growth, Variable Amplitude Loading (VAL), Compressive stress cycles, Tensile Overload, Compressive Underload, Willenborg Model, Plasticity-induced Crack Closure, Roughness-induced Crack Closure, Finite Element Analysis

## 7.2. Introduction

The scarcity of experimental data in relation to the influence of compressive stresses on the crack growth rate of materials has prompted several researchers to more carefully consider the influence of presence of compressive stress cycles within a given cyclic loading scenario. Consequently, in the past two decades, several researchers have investigated the influence of single tensile overload or compressive underload (UL) stress peaks on the FCG of materials (Sadananda *et al.* 1999; Taheri *et al.* 2002). It has been demonstrated that any sudden change in the stress intensity factor range could result in substantial changes in the FCGR of materials. However, most studies have revolved around constant amplitude loading and consideration of a few compressive spikes (or ULs) within the loading scenario. The lack of experimental data in consideration of the effect of compressive cycles within a realistic random loading motivated the authors to conduct a comprehensive experimental investigation into the influence of the compressive portion of a Variable Amplitude Loading (VAL) stress-time history on the fatigue crack propagation (Iranpour and Taheri, 2012a and Iranpour and Taheri, 2012b). In the recent experimental investigation conducted by the authors, a realistic VAL stress time-history was directly applied to a number of specimens and the resulting crack growth rates were recorded. It was demonstrated that ignoring the presence of the compressive portion of the stress-time history would result in a significant underestimation of the FCGR, which is non-conservative and is not acceptable for design purposes.

The main goal of this phase of the research is to further examine the detrimental influence of the CSC on the FCGR and understanding its underlying physics. To further clarify, the compressive stress cycles are the compression portion of cycles appearing in most real-life variable amplitude loading scenarios, as illustrated in Figure 7.1, which consist of both tensile and compressive loading portions. The current study's objectives also include further examination of the stress distribution in the vicinity of the crack tip, as well as investigating the influence of various scales of CSC on the crack tip opening displacement (CTOD) by the use of nonlinear finite element method. There are several reasons for incorporating the CTOD in analyzing the response of the crack body to the VAL scenario. For example, the CTOD is one of the only standardized fracture toughness test methods that can be used to evaluate the entire range of fracture toughness in metals. Moreover, it produces consistent results for both shallow and deep notches. In addition, it is less sensitive to dimensions of the specimen being evaluated. It is also related to the J-integral, which can better describe the nonlinear fracture behavior of metals.

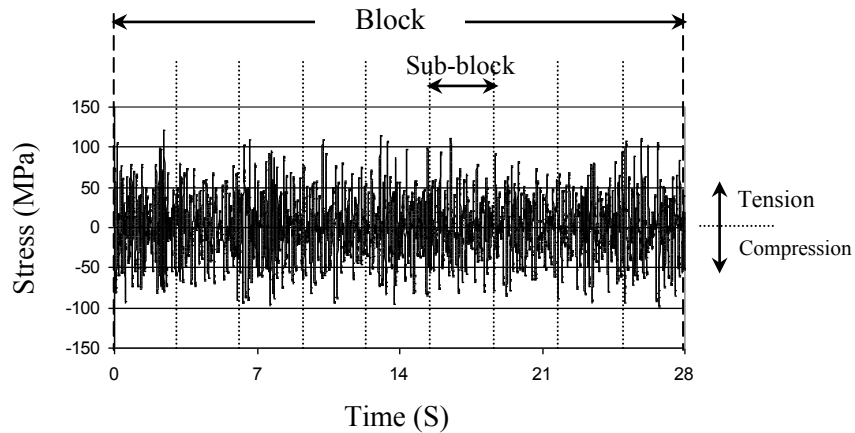


**Figure 7.1.** The VAL stress-time history *block* and its 9 *sub-block*

The work will also explore the predictive capability of two commonly used fatigue crack growth models and provide a few insights for tuning the models. More specifically, the capability of the Walker (1970) and Willenborg (1971) retardation models for accounting the influence of CSC, the overloads (OL) and the underloads (UL), will be investigated. In particular, it will be demonstrated how the computational

simulation could be effectively utilized for establishing the so-called “shutoff overload ratio”, an important input parameter used in Willenborg’s model.

### **7.3. Finite Element Analysis**

#### **7.3.1. Finite Element Mesh**

The finite element analysis (FEA) was performed using the commercial package ABAQUS (2010), suitable for the most challenging and highly nonlinear problems. The finite element mesh of the plate specimens was constructed with the aim of evaluating the radius of the plastic region and the state of the stresses at the crack tip. The dimensions are as shown in Figure 7.2, with a crack length of  $2a = 30$  mm. Due to the symmetry in geometry and boundary conditions, only one-half of the specimen was modeled. The model was constructed by 1,950 8-node bi-quadratic quadrilateral plane stress element with reduced integration (elements CPE8R of the ABAQUS), connected by 6,091 nodes.

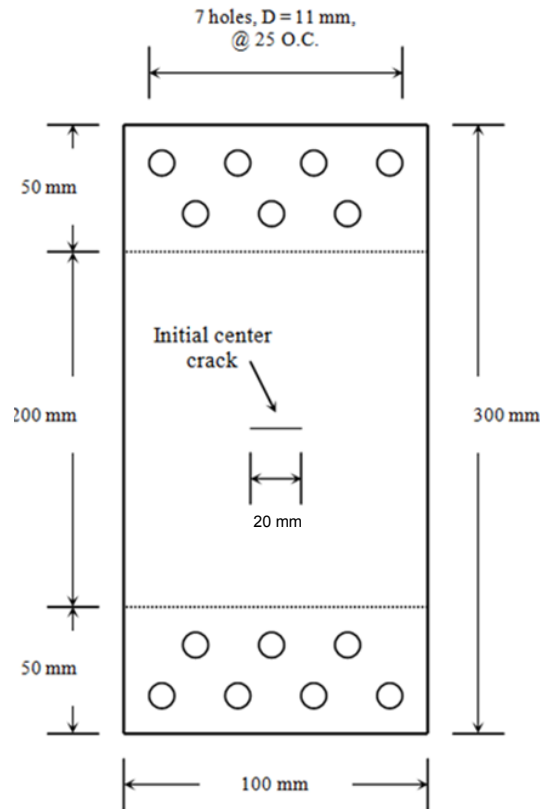


**Figure 7.2.** Specimen configuration and dimensions

The crack length was taken larger than that used in the experimental study, merely to generate larger plastic zone for better visualization and comparison. The results of the finite element analysis were compared to those obtained experimentally. Later on, it will also be revealed that the initial crack length would not have any bearing on the produced results, so long as the comparison of the results are done on the compatible crack length.

The crack face separation at the centre of the plate (on the plane of symmetry in Figure 7.3) was taken as 0.254 mm, equal to the width of the EDM notch of the test specimen. The model was restrained at its lower end, and subjected to a uniform axial compression-tension stress VAL time-history at its top edge.

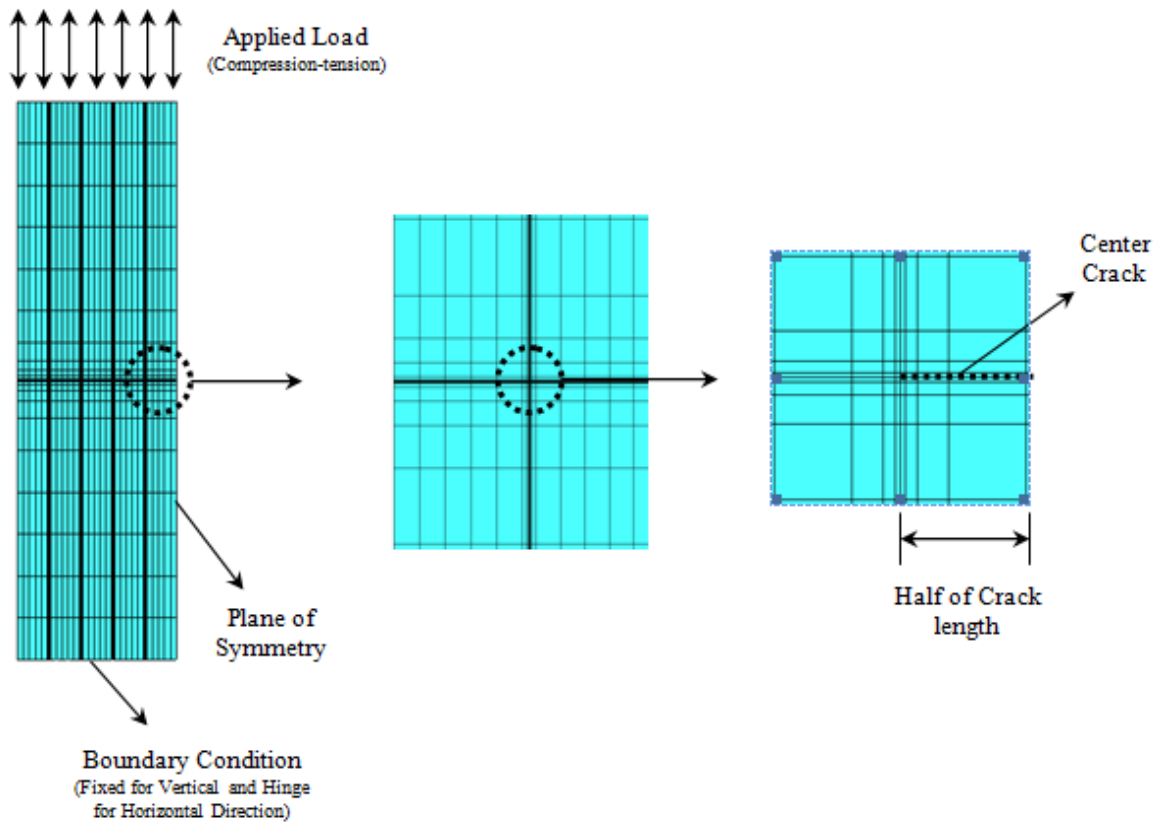


**Figure 7.3.** Finite element model of the test specimen

**Table 7.1.** Mechanical Properties of the 6061-T651 Aluminum Alloy

Modulus of Elasticity (GPa)	0.2% Yield Stress (MPa)	Ultimate Tensile Stress (MPa)
68.9	275.4	330.6

### 7.3.2. Loading Scenarios

To better understand the influence of CSC on the FCG of materials subject to VAL, a comprehensive series of experimental tests were conducted, subjecting centre-cracked specimens to various levels of CSC within a given stress time-history. The base loading history used in the investigation is illustrated in Figure 7.1. Two main parameters were



taken into considerations in the experimental investigation: (i) the *magnitude* of the compressive stresses and (ii) the *interval* (or the number of tensile stress cycles (TSC)) emerging in between two compressive stress peaks. The tests performed in this study are categorized into four different series. Details of various scenarios considered in our experimental study can be found in Iranpour and Taheri (2012b).

### 7.3.3. Material Model and Crack Tip Singularity

In the case of a plate with a sharp center crack, the strain zone at the crack tip is localized, thus the small-strain assumption would be applicable (Hertzberg 1995), thereby reducing the computational time. To simulate the singular field at the crack tip, the so-called “¼ node crack tip element” strategy was used, which was done by moving the mid-side nodes of the elements surrounding the crack tip (only those nodes nearest the crack tip) to the quarter point location (Anderson 2005; ABAQUS 2010). To maximize the accuracy of the contour integrals, the size of the crack-tip elements were kept quite small. Based on the results of a mesh convergence study, it was concluded that the element dimensions at the crack tip should be kept within 0.05% to 0.1% of the crack depth (Iranpour and Taheri, 2006).

To model the cracked body, one may use the linear elasticity, plasticity, or power-law material models. Our analysis used the power-law model that can be represented by the following mathematical relationship (ABAQUS, 2010):

$$E\varepsilon = \sigma + \alpha \left( \frac{|\sigma|}{\sigma_0} \right)^{n-1} \sigma \quad (7.1)$$

where  $\sigma$  is the stress,  $\varepsilon$  is the strain,  $E$  is the modulus of elasticity,  $\alpha$  is the yield offset,  $\sigma_0$  is the yield stress and  $n$  is the hardening exponent of the plastic term. The values of parameters  $n$  and  $\alpha$  were taken as 25 and 0.5, respectively. The other material properties are reported in Table 7.1. The plastic yield surface is assumed to obey the von Mises criterion and the associated flow rule, as it is most commonly used for isotropic ductile metals. Note that the results for pure power-law nonlinear elastic materials in a body under traction loading are proportional to the applied load to some power.

Therefore, the fracture parameters obtained for a given geometry under a particular load can be scaled to obtain its value for other loads, so long as the loading distribution is the same (ABAQUS, 2010).

As for modeling the influence of material hardening, we should first explore the hardening models commonly available in the finite element codes. The simplest hardening model is the isotropic hardening, which accounts for the change in the size of the yield surface. But in most real-life loading conditions, the magnitude of the yield stress is reduced upon load reversal, after the plastic deformation has occurred during the initial loading (also known as the Bauschinger effect). Therefore the isotropic hardening model is not suitable for modeling a material that undergoes cyclic loading.

On the other hand, the kinematic hardening, accounts for the translation of the yield surface in the deviatoric stress space (Araújo, 1998). In other words, the kinematic hardening model simulates the translation of the yield surface in the stress plane. In essence, in the kinematic hardening model, the yield surface is “dragged” in the direction of increasing stress, hence more accurately modeling the strain hardening response of the material. Therefore, the kinematic hardening model is a pressure-independent plasticity model, where the yielding of the material is independent of the equivalent pressure stress. This model is often used to simulate the inelastic behavior of the materials that are subjected to cyclic loading (ABAQUS, 2010). There is also the so-called mixed hardening model, by which both the Bauschinger effect and plasticity shakedown can be accurately accounted for. In this analysis, we used the mixed hardening model.

#### **7.3.4. Modeling of Crack Surface Interaction**

To simulate the response of the specimens hosting a crack to compression loadings, several researchers have used the gap-friction approach to transfer the load from one crack surface to the other one (see for example, Rushton and Taheri 2003, Yuen 2007). These gap/friction elements are supposed to be behaving very stiff under a compressive load (relative to the bodies they are attached to), but their stiffness is considerably reduced when they experience a tensile stress state (i.e., when the crack surfaces are forced to open). The rationale for providing a small stiffness to the elements is to prevent

the rigid body motion that may occur initially upon loss of contact or during sliding of the contacting surfaces. The compressive stiffness of the gap element is recommended to be set at approximately 10 times the axial stiffness of the adjacent elements (EMRC, 1998).

In the present study, however, another approach was used to model the contact between the fatigue surfaces under compression stresses. In the ABAQUS, two main approaches are available to define the contact between two deformable bodies: (i) surface-based contact, and (ii) element-based contact. For two deformable bodies with small or finite sliding interactions, or for cases where two separate surfaces need to be tied together during an analysis, one may use the surface-based contact (ABAQUS, 2010). This applies to the case of a center cracked fatigue specimen, in which the cracked surfaces would be in contact when the specimen undergoes the far-field compressive stresses. When the far field compressive stresses are reversed to tensile stresses, then the contact algorithm enables the fatigue surfaces to be separated, hence the surfaces are not tied up together anymore. Using this algorithm, once the crack surface elements experience contact, the surfaces are tied to one another (however, slippage is allowed), and the compressive stresses could be transferred from one surface to another.

## **7.4. Finite Element Analysis Results**

### **7.4.1. Effect of CSC on the Crack Front Stresses**

The results from this nonlinear FEA were used to calculate the radius of the plastic zone at the crack tip. Figures 7.4 and 7.5 show the distribution of the longitudinal (i.e., the stresses normal to the crack surface) and von Mises stresses, respectively, for various scale of CSC. Note that the noted scale values on the figures correspond to those noted on Table 1 in our recent work (Iranpour and Taheri 2012b). In brief, a scale factor of 0.0 would indicate that all the CSC within the stress-time history block were nullified, resulting to a zero-tension stress cycles, while 0.8 scale factor would indicated that 80% of the actual magnitude of the CSC within each block was applied to the specimen. It should be noted that the crack tip is at 15 mm ( $2a= 30$  mm). The graphs show the state of

the residual stress when the external load reaches a zero value, after a certain portion of the stress-time history shown in Figure 7.1 was applied to the plate.

It should be noted that the nonlinear analysis performed in this study accounted for all the sources of nonlinearities (i.e., material, geometry and boundary conditions). Performing a complete nonlinear analysis of the specimen subject to the entire VAL stress-time history block shown in Figure 7.1 would, however, be an unfeasible task (runtimes would exceed tens of days!). Therefore, it was decided to conduct the analysis considering only a portion of the block. For that, a portion of the stress-time history was selected so that it included the maximum tensile and compressive stress peaks of the entire block. A sensitivity analysis was also performed to compare the results of the FEA under this selected portion of the stress-time history with that under a larger selected portion of the entire block. This comparison showed that the selected portion of the stress-time history (with the maximum tensile and compressive stress peaks included) was a good representative of the entire block for calculating the plastic region at the crack tip. For our finite element analysis, this portion was selected from 0 to 1.0 second of the stress-time history data (see Figure 7.1), which also included the maximum tensile and compressive stress peaks of the entire block.

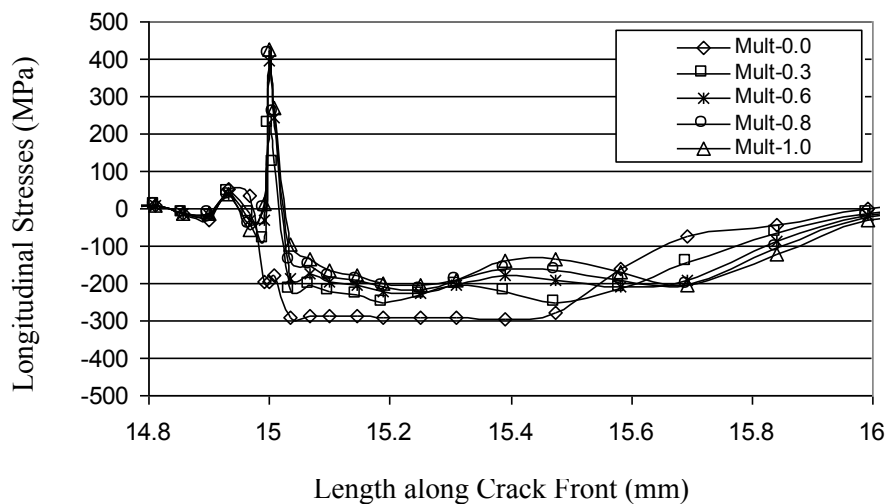


**Figure 7.4.** Distribution of the longitudinal residual stress at the crack front for various scales of compressive stress cycles (the crack tip is at location 15.0 mm)

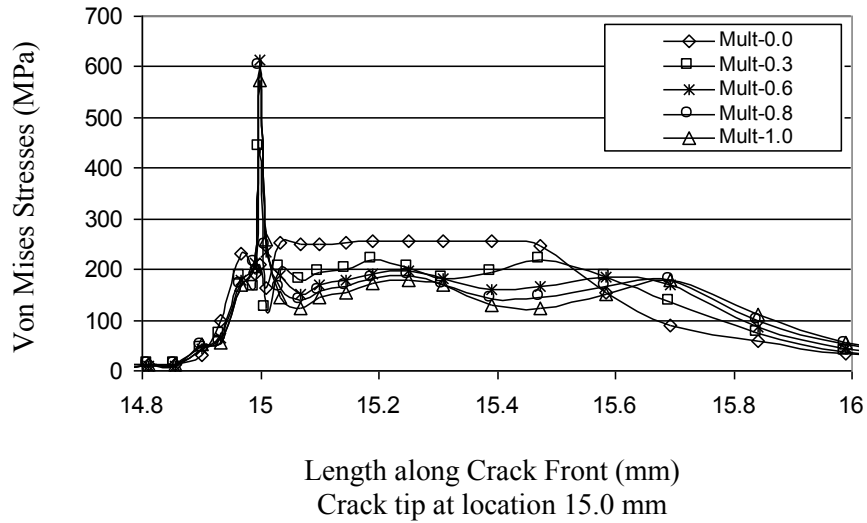


**Figure 7.5.** Variation of the von Mises residual stresses at the crack front for various scales of CSC (the crack length is at location 15.0 mm)

The influence of the CSC can be seen through the distribution of the longitudinal and the von Mises stresses behind and ahead of the crack tip, as illustrated in Figures 7.4 and 7.5. As observed, as the magnitude of the CSC decreases, the values of the longitudinal and von Mises stresses at the crack front increase. It is also observed that for all loading cases, except in the case in which no CSC was considered (i.e., test Mult-0.0), both the longitudinal and von Mises stresses exceed the yield stress of the material near the crack tip (15 mm). It is also noted that as the magnitude of the CSC increased, the stress fluctuation ahead of the crack tip increased (i.e., more variation in the magnitude of the near crack tip residual stresses), and the residual stresses extended further along the crack front. This would indicate a larger damage zone ahead of the crack tip, thus increasing the fatigue crack propagation. This increase in the plastic zone size is mainly caused by non-zero near crack tip opening displacement (CTOD), which acts as a stress concentration location (Zhang *et al.* 2007). This illustrates that the size of the yield zone depends on the relative magnitude of compressive stresses, which in turn affects the FCGR (Rushton and Taheri, 2003; Zhang *et al.* 2007). This phenomenon will be further investigated and discussed in the subsequent section.

Results in Figures 7.4 and 7.5 can also be considered as an indication of the extent of the plastic zone size ahead of the crack tip in the specimens. As can be seen, the extent of the plastic zone becomes greater as soon as a compressive stress is applied to the specimen. This is supported by the fact that the extent of the plastic zone from test Mult-0.0 to test Mult-0.3 is considerably large. Interestingly, the plastic zone size does not significantly grow as the compressive stress multiplier increases to values higher than 0.3. Similar results have also been reported by other investigators for similar materials (e.g., Zhang *et al.* 2007). It should be stated again that the stress irregularities occurring under VAL stress-time history makes the use of the analytical models that have been developed mainly based on CAL tests, somewhat impractical.

It is also seen that as expected, upon the removal of the CSC from the applied stress time-history (i.e., test Mult-0.0), the magnitude of the longitudinal stress at the crack tip location (see the value of the stress presented in Figure 7.4 at 15.0 mm), changes from a lower state of compression to a higher state. The tensile stress generated around the crack tip due to a tensile overload (OL), would however generate a compressive stress field right at the crack tip upon unloading, which would in turn retard the crack growth rate developed by the subsequent stress cycles. However, if the tensile OL is followed by a compressive UL, the stress field right at the crack tip after unloading changes from compression to tension, thereby accelerating the crack growth. This change from a tensile to a compressive stress zone at the crack tip illustrated in Figure 7.4 is in concert with the FEA results reported by other researchers (Rushton and Taheri, 2003, Makabe *et al.* 2004). It is also noted that as the value of the CSC increases (i.e., the increase depicted by the compressive stress multipliers), the magnitude of the residual tensile stress right at the crack tip (at the 15.0 mm location) also increases.

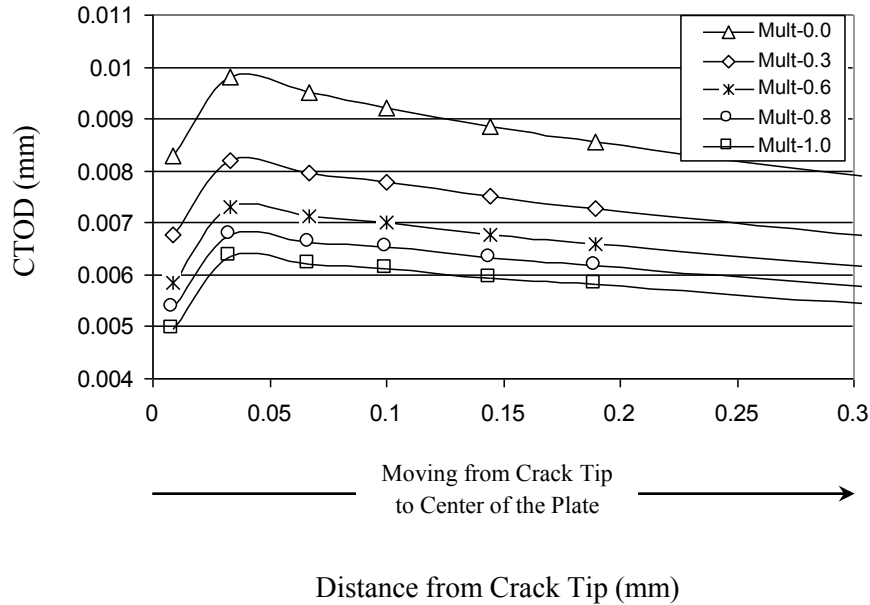
#### **7.4.2. Effect of CSC on CTOD**

Figure 7.6 shows the magnitude of the CTOD at various distances from the crack tip, when the crack front is subjected to only tensile stress cycles of the time-history (i.e., 0% CSC), as well as to some other combinations of the time-history (i.e., full tensile cycles and a certain scale of the CSC). Note that the crack tip is at location 0.0 mm in the figure.

As explained earlier, all the results from FEA presented here are for an external load of zero (the plate is at rest), and *after* the selected portion of the stress-time history is applied entirely to the model. As seen, when the value of the externally applied load is at zero, the crack remains open. This observation is also corroborated with the reported observations of several other investigators (i.e., Makabe *et al.* 2004; Zhang *et al.* 2007). As one moves from the crack tip (location 0 mm in Figure 7.6) to the center of the plate, the deformation magnitude increases, reaching its highest value at approximately 0.035 mm from the crack tip, after which it gradually decreases.

Moreover, it can be seen that the growth in the CTOD is inversely proportional to the compressive stress scaling factor (the multiplier). This is also observed in the test results reported by other investigators, in which similar materials were subject to CAL with different negative stress ratios (e.g., Zhang *et al.* 2007; Makabe *et al.* 2004). It has also been shown by Kasaba *et al.* (1998) that even when a material is subjected to full compression-compression stress cycles, the CTOD increases as the magnitude of the CSC decrease.

It can also be concluded that the observed reduction in the CTOD would in turn decrease the influence of the CTOD as a stress raiser within the plastic zone. The same conclusion was made by Zhang *et al.* (2007), who conducted experiments on similar material subject to CAL with different stress ratios. Therefore, as also confirmed by Kasaba *et al.* (1998), when evaluating the FCG under realistic time-histories, one should account for the influence of crack tip residual stresses that emanate as a result of the application of the CSC.



**Figure 7.6.** Variation of the CTOD along the crack surface for various scales of CSC after unloading (the crack length is at location 15.0 mm)

Figure 7.7 shows the variation of the CTOD versus the compressive stress multiplier at different locations along the crack. In general, the CTOD is regarded as a measure of the plastic strain at the crack tip (Shukla 2005). The results from our FEA indicate that the CTOD can be related to the FCGR of the material. The same conclusion has been reported by others (e.g., Hammouda *et al.* 1998). It is observed that as one gets closer to the crack tip, the variation of CTOD as a function of the compressive stress multiplier becomes greater. In other words, the two bold solid lines in Figure 7.7 represent CTOD's variation at the two closest locations to the crack tip (i.e., 0.0083 mm and 0.033 mm). Moreover, as also seen, the highest variations in the gradient of the CTOD are observed at these locations. The figure illustrates that the variation of CTOD at the vicinity of the crack front is a function of the compressive stress multiplier, which in turn directly affects the crack growth rate, as observed in our experimental investigation (see Figure 7.6 of Iranpour and Taheri (2012b)).



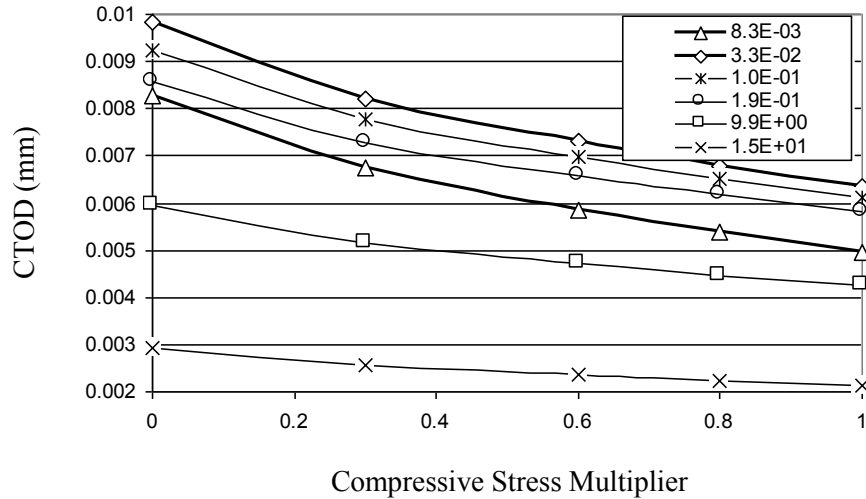


**Figure 7.7.** Plot of the CTOD versus the compressive stress multiplier at various distances (in mm) ahead of the crack tip (as identified in the legend)

In the nonlinear finite element analyses presented above, the crack length was assumed to be  $2a = 30$  mm. Since the CTOD is proportional to the crack length (Rose and Wang 2001), the same slope and ‘rate of change’ as in Figure 7.7 is observed for any crack length other than  $2a = 30$  mm. This concept was verified with a series of FEA with crack lengths varying from  $2a = 20$  mm to  $2a = 40$  mm. It was observed that the ‘rate of change’ of the CTOD versus the compressive stress multiplier was the same for any crack lengths. Figure 7.8 shows the length of the plastic region ahead of the crack tip for different crack lengths. As seen, the length of the plastic zone ahead of the crack tip is almost linearly proportional to the crack length, illustrating more or less a linear variation of the size of the plastic zone as a function of the crack lengths. Our FEA results also indicated that the shape of the plastic region remained more or less unchanged, with a similar stress gradient, for all the crack lengths studied. This fact enables us to establish the stress gradient, using the existing analytical methods or by the use of computational analysis, thereby relating the value of the CTOD to FCG under loading scenarios with different amplitudes. This is further explained in the next section.

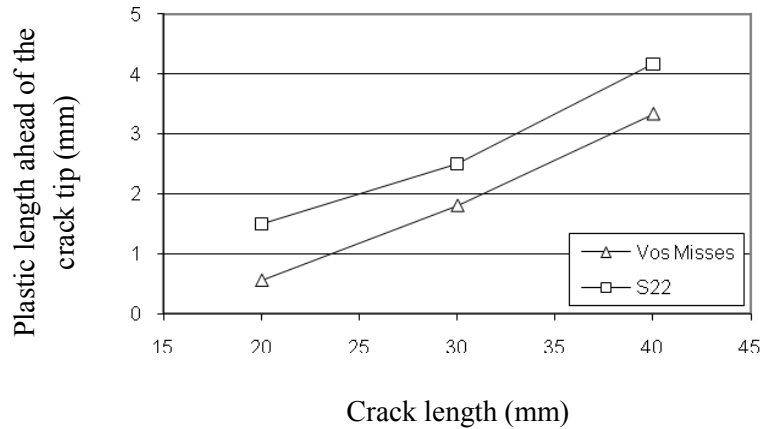


**Figure 7.8.** Length of the plastic region ahead of the crack tip

## 7.5. Further Discussion

### 7.5.1. CTOD Related Relationships

The results obtained from our earlier experimental investigation (Iranpour and Taheri 2012b; refer to Chapter 6 of this dissertation) are shown alongside of the results obtained through our nonlinear FE analysis in Figure 7.9. The trend in the variation of the CTOD and fatigue life of the test specimens as a function of the compressive stress multiplier can be clearly seen in the figure. As observed, the variation in the trend is quite similar.

As seen for the results, the influence of the compressive stress multiplier on the FCGR decreases as the compressive stress multiplier increases. In other words, the influence of the CSC on the FCGR is more pronounced at lower compressive stress multipliers. It can be further observed that the introduction of a relatively small level of compressive stresses into the stress-time history would generate a considerable influence on accelerating the crack growth in the material. It can also be seen that an increase in the compressive stress multiplier from 0.5 to 1.0 results in a lower crack growth rate when compared to the resulting crack growths for the stress multipliers less than 0.5. In other words, as the magnitude of the compressive stress increases, its influence on both the

FCGR of the component and variation of CTOD becomes less pronounced. This might be the reason for the API recommendation (API 2RD, 1998); the recommendation states that for loading scenarios with an entirely tensile stress range, one should consider the entire stress range when assessing the fatigue life of the material. On the other hand, if the loading cycles include compressive loading, then the stress range used for assessing the fatigue life should include all the tensile stress cycles plus only 60 percent of the amplitude of the compressive loading cycles (API 2RD, 1998). The recommendation indicates that there exists a relationship among the CTOD, the crack growth rate and the magnitude of the CSC.

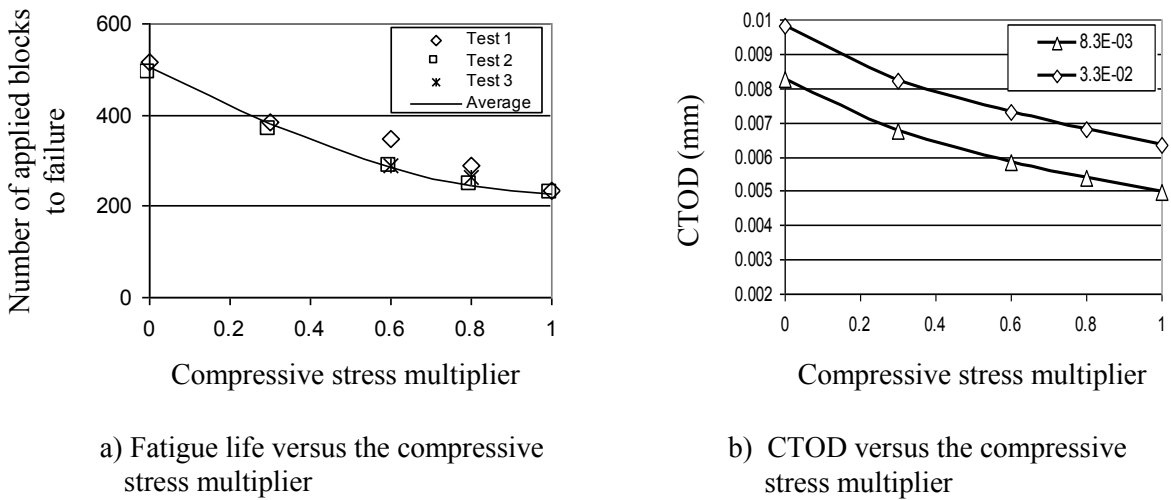


**Figure 7.9.** A comparison of the variation of the CTOD and fatigue life of the component as a function of the compressive stress multiplier

Since the initial work of Wells (1961) on crack propagation of materials, many researchers have related the fatigue life of a component to the CTOD. For instance, the strip-yield-model analysis proposed by Dugdale (1963) can be used to relate the CTOD to the applied stress and crack length. Panontin *et al.* (2000) presented a formula for calculating the CTOD using the Ramberg-Osgood material model, which employed various hardening coefficients, and then predicted the FCGR. The CTOD concept has also been used to predict the onset and direction of the crack growth for mixed-mode

fracture (Sutton *et al.* 2000). Using the boundary value method, Radayev and Stepanova (2001) presented an exact equation for calculating the CTOD based on the plastic strain localization parameters, also accounting for the crack closure effects.

### **7.5.2. The use of Stress Intensity Factor for Estimation of FCG**

The use of the CTOD concept for calculating the crack growth rate of materials offers many advantages. One such advantage is that the changes in the thickness of the plastic wake along the crack length can be captured by measuring the CTOD. Furthermore, one of the important parameters that affects the FCG of materials is the crack closure, which considers the difference between the effective value of the stress intensity factor range,  $\Delta K_{eff}$ , and the nominal value of the stress intensity factor range  $\Delta K_{nom}$ . Based on this concept, the effective stress intensity factor range ( $\Delta K_{eff}$ ) controls the crack growth, rather than the nominal stress intensity factor range ( $\Delta K_{nom}$ ). As one of its main assumptions, this concept considers a uniform thickness for the plastic wake along the crack surface, which demonstrates a constant stress intensity factor. However, a fatigue crack generally grows under the condition of constant stress, rather than constant stress-intensity factor. In other words,  $\Delta K_{nom}$  increases as the crack length increases, and therefore, the assumption of a uniform thickness wake would no longer be valid. It has been demonstrated that the width of the plastic wake would increase linearly as a function of crack length (Wang *et al.* 2001; Rose and Wang, 2001). This is referred to as steady state or self-similar crack growth. It should be noted, however, that the traditional crack closure concept is not capable of accounting for this effect; nevertheless, a nonlinear FEA, as used in this study, can account for the varying thickness of the plastic wake along the crack surface, which has been shown to affect the CTOD. This is another advantage of using the concept of CTOD (as calculated by the nonlinear FEM), for measuring the crack growth rate of materials.

Another advantage of the CTOD concept is its applicability beyond the limitations of the small scale yielding (SSY) that generally applies to the traditional stress intensity factor approaches. It is recognized that the crack tip stress level may considerably exceed

the values beyond which the small-scale yielding applies. Therefore, the stress intensity factor does not provide an adequate characterization of the crack-tip deformation. In such cases, the CTOD can be used to calculate the crack growth rates where the crack tip region is within or beyond the small-scale yielding. This approach has been demonstrated by many researchers to be a reliable method for calculating the crack growth rate based on the CTOD calculations, which also considers the influence of compressive stresses (Rose and Wang, 2001; Wang and Rose, 1999 and Tanaka and Nakai, 1983). In a study conducted by Guo *et al.* (1999) on three aluminum alloys, it was shown that for both CAL and VAL, the crack growth rate was independent of the plate thickness and stress ratio when plotted against the cyclic CTOD (Guo *et al.* 1999). It was claimed that the increase in the plate thickness causes the condition shift towards the Large Scale Yielding (LSY) as opposed to Small Scale Yielding (SSY). Their study also demonstrated that the CTOD can be used to calculate the FCGR even beyond the limit of application of SSY and CAL.

Such advantages have recently motivated some of the researchers to further study the relationship between the CTOD and FCG of materials. In a study conducted by Vasudevan and Sadananda (2001) on characterization of FCG under compression-compression loading, it was demonstrated that there exists two driving forces governing the FCG of materials; they are: the stress intensity factor range,  $\Delta K$ , and the maximum stress intensity factor,  $K_{\max}$ . In their approach, the influences of both the applied external stresses and the resultant internal stresses were included in the FCGR estimation. They also demonstrated that the entire regime of FCG can be represented by a unique internal stress gradient. The next section discusses the crack tip deriving forces and the relation between the stress state at the crack front and the CTOD.

As stated in the above, one of the two main parameters affecting the crack growth of materials is demonstrated to be the stress intensity factor range,  $\Delta K$ , which is a function of the maximum and minimum stress intensity factors. As elaborated by Vasudevan and Sadananda (2001), the maximum and minimum stress intensity factors are both affected by the presence of the internal stresses. Therefore,  $\Delta K$  is unaffected by the internal stresses and normally remains unchanged. In brief, the internal stresses can vary from a

short to a long range stress field. Short range stress fields result from point defects (such as vacancies and interstitials) that do not affect  $K_{\max}$ ; therefore, the long range stress fields are said to markedly affect the  $K_{\max}$ . These long range stresses have lesser effect on the  $\Delta K$ , since both  $K_{\max}$  and  $K_{\min}$  are simultaneously affected, thus leading to the same difference (i.e.,  $K_{\max} - K_{\min}$ ). Therefore, the total crack-tip driving force for both  $\Delta K$  and  $K_{\max}$  must exceed the threshold values of the two parameters in order for a crack to advance.

On the other hand, the influence of the internal stresses is included in the second main parameter, the maximum stress intensity factor ( $K_{\max}$ ). This quantity must exceed a critical limit for the crack to grow. In this two-parameter approach, the influence of the internal and external stresses, both, which affect the crack growth rate and the CTOD, can be captured. The internal stress gradient contributes to the crack tip driving force when the component is subjected to either a far field tensile or compressive load, which in turn affects the value of the CTOD. The internal stresses affect the driving force,  $K_{\max}$ ; as a result, it either retards, or accelerates the crack growth (Vasudevan and Sadananda, 2001).

It has been demonstrated that while the variation in the sources of the internal stresses could be significant, however, their stress gradient seem to follow a similar trend (Sadananda and Vasudevan, 1999; Vasudevan and Sadananda, 2001, Rushton and Taheri, 2003; and Yuen 2007). Therefore, the finite element method can be effectively used to calculate both the CTOD and internal stress gradients. Once the CTOD is accurately calculated, one can then calculate the FCGR under any stress-time history applied to a material. In the present study, this concept is used to relate the influence of the applied compressive stress (in terms of its magnitude, via the compressive stress multiplier), to the FCGR based on the value of CTOD. Vasudevan and Sadananda (2001) have demonstrated that the influence of internal stresses on the maximum stress intensity factor,  $K_{\max}$ , holds for all types of fatigue damage.

It should be noted that the two-parameter approach stated above has also been applied and verified by other researchers as well. For instance, in a study conducted by Toribio

and Kharin (2009), it was demonstrated that the influence of loading on FCG (including crack closure), can be related solely to the stress-strain field ahead of the crack tip, with no contribution from that present behind the crack. In concert with the findings of Vasudevan and Sadananda (2001), Toribio and Kharin demonstrated that the FCG can be represented by the two parameters  $\Delta K$  and  $K_{\max}$ , whether or not the loading scenario includes the tensile OLs or compressive ULs. They also presented the size of the stationary loop patterns at the crack tip solely in terms of  $\Delta K$  or CTOD range, by relating the range of CTOD to  $\Delta K^2$  (i.e.,  $\Delta\delta_t = \delta_{\max} - \delta_{\min} \propto \Delta K^2$ ), where  $\delta_{\max}$  and  $\delta_{\min}$  are the maximum and minimum CTOD, respectively.

The difference between the influence of a single and multiple consecutive tensile OLs on the resulting FCG was illustrated by Pommier (2003). He showed that both the degree and type of material hardening and the model by which hardening is represented by (i.e., kinematic or isotropic), were of key importance in predicting the crack growth rate, especially for components subject to VAL stress-time histories. As briefly alluded earlier, the kinematic hardening describes the translation of the yield surface in the stress space, while the isotropic hardening describes the evolution of the size of the yield surface (Araújo, 1998). The crack closure is associated with the kinematic hardening (Pommier 2003). The OLs in a VAL stress-time history result in the development of some residual plastic strain gradient (kinematic hardening). The resulting residual stresses, as explained earlier, directly affect CTOD. As explained earlier, the residual stresses directly affect the CTOD, which can be calculated using the analytical or computational approaches (such as nonlinear FEM analysis). The crack closure's effect manifest itself mainly through the kinematic hardening effect.

Using the finite element method, Pommier (2003) showed that under the applied tensile OLs with magnitudes over a certain value, the crack opening level  $K_{op} / K_{\max}$  at the crack tip increases as the number of the applied OL increases (where  $K_{op}$  is the opening threshold stress intensity factor). This finding is in concert with our FEM results, thus demonstrating how stress irregularities affect the CTOD. It is noted that tensile OLs increase the CTOD, while compressive ULs (the focus of our study) decrease the CTOD.

The above study shows that the applied stress-time history affects the internal stress under either tension or compression loading. On the other hand, any change in the internal stress affects the CTOD. Therefore, the applied stress-time history directly affects the CTOD, as evident by the comparison of our experimental and nonlinear FEA results, as shown in Figure 7.9. Furthermore, since the CTOD and the fatigue life of the component are related to the magnitude of the applied compressive stress (via the multipliers illustrated in Figure 7.9), it can be concluded that the relationships developed to calculate the CTOD can be used to study the influence of compressive stresses on the crack growth rate of the material.

### 7.5.3. The use of CTOD for Estimation of FCG

As explained earlier, the cyclic crack tip opening displacement,  $\Delta CTOD$ , can be used as a unified aggregate parameter for calculating the crack growth rate for both cases when the material undergoes both small-scale yielding and beyond.  $\Delta CTOD$  is defined as the difference between the stretch in the crack tip,  $\delta_M$ , occurring due to the applied maximum load, and that resulting from the crack tip residual stress,  $\delta_R$ , which results due to the minimum value of the applied load (Rose and Wang, 2001; Wang *et al.* 2003); it can be represented by:

$$\Delta CTOD = \delta_M - \delta_R \quad (7.2)$$

where:

$$\delta_M = \delta_{\max}(x = a), = \frac{8\sigma_0 a}{\pi E} \ln \left[ \sec \left( \frac{\pi \sigma_{\max}}{2\sigma_0} \right) \right] \quad (7.3.1)$$

$$\delta_R = \delta_{res}(x = a) = \theta_R a \quad (7.3.2)$$

In the above equations,  $\sigma_0$  is the characteristic stress at the crack tip, normal to the crack plane,  $E$  is material's modulus of elasticity,  $a$  is the crack length and  $\sigma_{\max}$  is the maximum applied stress. The parameter  $\theta_R$  is a non-dimensional constant that is unknown and should be determined in such a way that certain self-consistency conditions are satisfied (Rose and Wang, 2001).



In the Dugdale model, the characteristic stress,  $\sigma_0$ , is interpreted as the tensile yield stress  $\sigma_y$ , along with the use of the Tresca yield criterion. For cases where the remote axial loading exceeds the yield strength,  $\sigma_y$ , the characteristic stress,  $\sigma_0$ , is taken as the ultimate tensile strength of the material,  $\sigma_U$  (Tomkins 1975). In general, the characteristic stress,  $\sigma_0$ , is regarded as an adjustable parameter that represents a limiting stress that should not be exceeded at any location within the body (Rose and Wang, 2001). Some researchers have used the average of the yield and ultimate strength as the characteristic stress,  $\sigma_0$ ; that is  $\sigma_0 = (\sigma_y + \sigma_U)/2$  (Newman 1984).

Equations 7.3.1 and 7.3.2 also show that both  $\delta_M$  and  $\delta_R$  depend on the crack length,  $a$ , the fundamental non-dimensional parameter  $\sigma_0/E$  in Dugdale's model, and also on the ratio of the maximum stress to the characteristic stress  $\sigma_{\max}/\sigma_0$ . The influence of loading on the crack tip residual stress at the minimum load,  $\delta_R$ , is through the parameter  $\theta_R$ . Moreover, the crack tip residual stress at the minimum load,  $\delta_R$ , also depends on the load ratio  $R = \sigma_{\min}/\sigma_{\max}$ . Using a conventional approach, the crack growth rate can be related to the stress range  $\Delta\sigma = \sigma_{\max} - \sigma_{\min}$ . Therefore, one may use  $\Delta\sigma/2\sigma_0$  rather than  $\sigma_{\max}/\sigma_0$ , and re-write the above equations as (Rose and Wang, 2001):

$$\delta_R = \frac{2\sigma_0 a}{\pi E} f(\sigma_{\max}/\sigma_0; R) \quad (7.4.1)$$

or:

$$\delta_R / \delta_M = g(\sigma_{\max}/\sigma_0; R) \quad (7.4.2)$$

where  $f$  and  $g$  are unknown functions to be determined from a detailed analytical investigation. Combining equations 7.2, 7.3 and 7.4, the cyclic crack tip opening displacement,  $\Delta CTOD$ , can be written as (Rose and Wang, 2001):

$$\Delta CTOD = \frac{2\sigma_0 a}{\pi E} h(\Delta\sigma/2\sigma_0; R) \quad (7.5.1)$$

or, alternatively as:

$$\frac{\Delta CTOD}{\delta_M} = 1 - g(\sigma_{\max} / \sigma_0; R) \quad (7.5.2)$$

where  $h$  is a function to be determined using a numerical analysis. This problem was solved analytically by Rose and Wang (2001), using the complex potential technique by which the problem was reduced to that of a Reimann-Hilbert type problem, which involves an auxiliary complex function. The solution shows that the logarithmic plot of the normalized cyclic crack tip opening displacement,  $\Delta CTOD/2\varepsilon_0 a$ , versus the normalized stress range,  $\Delta\sigma/2\sigma_0$ , would follow an approximately linear trend, thereby describing a power-law relation (where  $\sigma_0 = \varepsilon_0 E$ ). The slope of this curve is referred to as the stress exponent,  $n$ , which asymptotes to  $n=2$  for  $\Delta\sigma/2\sigma_0 < 1.0$ , when the crack closure is ignored (Rose and Wang, 2001). This is consistent with the conventional fracture mechanics approach used for calculating the CTOD based on the effective stress intensity factor range,  $K_{eff}$  (Barsom and Rolfe, 1999), that is:

$$CTOD = \frac{\Delta K_{eff}^2}{E\sigma_y} \quad (7.6)$$

If the crack closure is taken into account, according to the self-similar analysis explained earlier, the stress exponent,  $n$ , would deviate from  $n=2$  and increase to a value as high as 4.5 for a stress ratio of  $R=0$  and a normalized stress range of  $\Delta\sigma/2\sigma_0 = 0.5$ . For lower stress ranges, a value of  $n=3$  has been suggested (Rose and Wang 2001), which verifies reasonably with the empirical values suggested by Frost and Dugdale (1958). For materials subject to both tensile and compressive stresses (with  $R=-1$ ), a higher value has been suggested for the stress exponent,  $n$ .

The analytical method proposed by Rose and Wang (2001) suggests that the  $\delta_R / \delta_M$  ratio (that is the ratio of crack tip residual stretch at the minimum load to the crack tip stretch at the maximum load) increases as the stress ratio  $\Delta\sigma/2\sigma_0$  decreases. This means that for large scale yielding (i.e., at higher ratios of  $\Delta\sigma/2\sigma_0$ ), the importance of plasticity-induced crack closure on the FCG increases, which is consistent with the concept of self-similarity explained earlier.

In the experiments conducted in our study (see Iranpour and Taheri (2012b)), the decrease in the stress ratio  $\Delta\sigma/2\sigma_0$  is attributed to the decrease in the compressive stress multiplier, as the tensile stress portion of the stress-time history remains unchanged for all cases. This means that as the compressive stress multiplier decreases from 1.0 to 0.0, the stress ratio  $\Delta\sigma/2\sigma_0$  also decreases, which should in turn result in an increase in the residual CTOD that can be obtained by the numerical approach discussed earlier. This indeed corroborates well with our FEM analysis results presented in Figure 7.6, which shows that as the compressive stress multiplier decreases from 1.0 to 0, the CTOD increases. Based on the analytical approach presented by Rose and Wang (2001), this increase in the  $\delta_R/\delta_M$  ratio is even more evident for lower values of the load ratio ( $R = \sigma_{\max}/\sigma_{\min}$ ). This is evident in the results obtained from both our FEA and experiments, as presented in Figure 7.9. As shown in that figure, the rate of variation of the CTOD decreases as the compressive stress multiplier increases (that is, as the load ratio,  $R$ , decreases) .

Moreover, in the numerical study of Rose and Wang (2001), conducted on various stress ratios (i.e.,  $\sigma_{\max}/\sigma_0 = 0.2, 0.5, 0.7$  and  $0.9$ ), they presented their results in the form of a plot of  $\delta_R/\delta_M$  versus the load ratio,  $R$ . From their graph, the ratio of  $\delta_R/\delta_M$  is observed to be 0.86 and 0.8 for the load ratios of  $R=0$  and  $R=-1$ , respectively for  $\sigma_{\max}/\sigma_0 = 0.2$ . Their results, however, indicate that the ratio of  $\delta_R/\delta_M$  for a stress ratio of  $\sigma_{\max}/\sigma_0 = 0.5$  decreases to 0.83 and 0.56 for load ratios of  $R=0$  and  $R=-1$ , respectively. This stress ratio is very close to that used in our experiments (i.e.,  $\sigma_{\max}/\sigma_0 \approx 0.48$ ). In other words, the results indicate that at that stress ratio, the  $\delta_R/\delta_M$  ratio for  $R=0$  is approximately 1.5 times higher than the ratio of  $\delta_R/\delta_M$  corresponding to  $R=-1$ , which also corroborates with the results obtained from our FEA. As shown in Figure 7.9b, the CTOD for  $R=0$  is about 1.65 times larger than that obtained for  $R=-1$ . It is noted that compressive stress multipliers of 0 and 1 refer to load ratios of  $R=0$  and  $R=-1$ , respectively.

As explained earlier, the crack tip stretch at maximum load,  $\delta_M$ , is a function of the crack length,  $a$ , the fundamental non-dimensional parameter  $\sigma_0/E$  for the Dugdale

model and the ratio of the maximum stress to the characteristic stress  $\sigma_{\max} / \sigma_0$ . For any crack length, all these parameters are constant for the various test series reported in Table 1 of Iranpour and Taheri (2012b), regardless of the compressive stress multiplier. It leads to the conclusion that  $\delta_M$  is not affected by the changes that were made to the compressive portion of the stress-time history, and remained unchanged for all test series. Therefore, for calculating the ratio of  $(\delta_R / \delta_M)_{R=0} / (\delta_R / \delta_M)_{R=-1}$ , one can use the ratio of  $(\delta_R)_{R=0} / (\delta_R)_{R=-1}$ , as presented in Figure 7.9b.

## 7.6. Application of some Analytical Models for Estimation of FCG

### 7.6.1. Variable Amplitude Loading FCG Estimation

A computer code was developed in the MATLAB environment to validate the applicability of some of the commonly used analytical crack growth models for estimating the fatigue life of the material subjected to the VAL stress-time history used in this study. A FCG approach for a VAL scenario should at least consider the stress intensity factor, the stress ratio and the history of the applied load. As also discussed earlier, the nature of the applied load cycles; that is, whether OLs or ULs exist in the load spectrum, can significantly affect the crack growth in spectrum loadings.

In the previous studies performed by the authors on VAL stress-time history, Barsom's approach was used to calculate the root-mean-square of the applied stresses, followed by the application of the Paris and Walker fatigue models to calculate the crack growth rate (Iranpour and Taheri 2007; Iranpour *et al.* 2008). It was observed that these two models significantly underestimated the crack growth rate of the materials subjected to the some VAL stress-time histories.

In this study, a different approach is used to calculate the crack growth rate of the material under the applied VAL stress-time history. The approach uses a series of tabular crack growth rate test data obtained from CAL tests conducted with various stress ratios to calculate the crack growth rate for VAL. The stress ratio,  $R$ , is taken into account

independently for each crack growth curve,  $da/dN$ . The point-by-point scheme is used along with the tabular data (obtained from our CAL tests) and the Walker equation to interpolate/extrapolate data for any desired value of stress ratio,  $R$ . This approach has been widely used for calculating the crack growth rate under VAL stress-time histories (Harter 1994; Harter 2008).

The walker equation is represented by:

$$\frac{da}{dN} = C[\Delta K(1-R)^{(m-1)}]^n \quad (7.7)$$

where  $C$ ,  $m$  and  $n$  are constants obtained through experimental data. For a given value of stress ratio,  $R$ , the Walker equation can be rewritten as (Harter 2008):

$$\Delta K = \Delta K_{R=0}(1-R)^{(1-m)} \quad \text{for} \quad R \geq 0.0 \quad (7.8)$$

$$K_{\max} = \Delta K_{R=0}(1-R)^{(m-1)} \quad \text{for} \quad R < 0.0 \quad (7.9)$$

As can be observed,  $\Delta K$  is replaced with  $K_{\max}$  for negative stress ratios,  $R$ . For a certain increment of crack growth, corresponding to two positive values of stress ratio,  $R$ , one can use Equation 7.8 to write:

$$\Delta K_1(1-R_1)^{(m-1)} = \Delta K_2(1-R_2)^{(m-1)} \quad (7.10)$$

By replacing  $\Delta K$  with  $K_{\max}$  for negative stress ratios,  $R$ , and solving for parameter,  $m$ , we get the value of  $m$  for three various possible cases (Harter 2008):

$$m = 1 + \left[ \log\left(\frac{\Delta K_1}{\Delta K_2}\right) / \log\left(\frac{(1-R_2)}{(1-R_1)}\right) \right] \quad \text{for} \quad (R_1 \geq 0.0 \text{ and } R_2 \geq 0.0) \quad (7.11.1)$$

$$m = 1 + \left[ \log\left(\frac{K_{\max 1}}{\Delta K_2}\right) / \log((1-R_1) \times (1-R_2)) \right] \quad \text{for} \quad (R_1 < 0.0 \text{ and } R_2 \geq 0.0) \quad (7.11.2)$$

$$m = 1 - \left[ \log\left(\frac{K_{\max 1}}{K_{\max 2}}\right) / \log\left(\frac{(1-R_2)}{(1-R_1)}\right) \right] \quad \text{for} \quad (R_1 < 0.0 \text{ and } R_2 < 0.0) \quad (7.11.3)$$

From the physical perspective, parameter  $m$  controls the shift in the crack growth data as a function of stress ratio,  $R$ , on a point-by-point basis.

The calculation procedure is as follows:

- i) As the first step, the parameter  $m$  is calculated from the above equations based on  $\Delta K$  values that were obtained for two values of  $R$ .
- ii) In the second step, the tabular values of  $m$  are used to calculate the crack growth rate,  $da/dN$ , for any desired value of  $\Delta K$  and  $R$ .
- iii) The Matlab code then calculates the crack growth rate based on  $\Delta K$  until its value exceeds the current  $\Delta K$  value of interest.
- iv) In the last step, the code uses a logarithmic interpolation using the last two points in the curve to calculate the current crack growth rate.

The above approach was used to calculate the FCG, and the results were compared against those obtained from our actual tests reported in our earlier study (Iranpour and Taheri 2012b). Based on this approach, the number of stress cycles required to fail the specimen were found to be much lower than that obtained experimentally. This difference between the test results and the analytical approach explained above is believed to be due to ignoring the crack growth retardation due to the applied tensile OLs and crack closure effect. In the next section, the influence of these two mechanisms on the FCG of the material under the applied VAL stress-time history is studied.

### **7.6.2. Evaluation of Crack Growth Retardation due to Tensile Overloads**

The influence of load-sequencing in a VAL stress-time history can be summarized by three main approaches:

- (i) The yield zone model, which accounts for the retardation by considering the plastic zone size and the OL.
- (ii) The strip-yield model, which is based on Dugdale's approach for crack closure numerical relationship.
- (iii) The crack closure model, which uses the experimental data to calculate the crack opening load (Miranda *et al.* 2003).

Among the yield zone approaches, the Wheeler model (Wheeler 1972) and Willenborg model (Willenborg et al. 1971, Gallagher 1974) have been widely used by many researchers (Yuen and Taheri, 2005; Pereira *et al.* 2007).

In this study, the generalized Willenborg retardation model is used to incorporate the influence of the tensile OLs on the fatigue crack propagation of the specimens. This model uses the effective stress intensity factor, which is based on the size of the yield zone ahead of the crack tip. The Willenborg model assumes that the crack growth delay after a tensile OL is due to a reduction in  $K_{\max}$ , corresponding to the current crack length. According to the Willenborg model, the reduction in  $K_{\max}$  is defined by (Willenborg *et al.* 1971; Gallagher, 1974 and Pereira *et al.* 2007):

$$K_{red} = K_{req} - K_{\max} \quad (7.12)$$

where,  $K_{req}$  is the stress intensity factor necessary to produce a plastic crack zone that extends a distance  $\lambda$  ahead of the advancing crack tip to the far end of the plastic zone generated by the tensile OL. The effective stress intensity factors can be calculated by:

$$K_{\max,eff} = K_{\max} - K_{red} \quad (7.13.1)$$

$$K_{\min,eff} = K_{\min} - K_{red} \quad (7.13.2)$$

where  $K_{\min}$  is that obtained under a CAL. These maximum and minimum effective values can then be used to calculate the effective stress intensity factor range,  $\Delta K_{eff}$ , and the effective stress intensity factor ratio,  $R$ . It is noted that negative values of  $K_{\min,eff}$  should be taken as null, leading to the value of  $\Delta K_{eff}$  equal to  $K_{\max,eff}$  (Willenborg *et al.* 1971 and Pereira *et al.* 2007). The reduction in  $K_{\max}$  can be re-written as (Harter 2008):

$$K_{red} = \phi \left( K_{\max,ol} \times \sqrt{1 - \frac{(a - a_{ol})}{R_{y,ol}}} - K_{\max} \right) \quad (7.14)$$

where,  $a$  is the crack length and  $a_{ol}$ ,  $K_{\max,ol}$  and  $R_{y,ol}$  are the crack length, the maximum stress intensity factor and the size of the yield zone, respectively (all at overload);  $\phi$  is a parameter used in Willenborg's model, defined as (Harter 2008):

$$\phi = \left(1 - \frac{\Delta K_{th}}{K_{max}}\right) \times (\beta - 1) \quad (7.15)$$

where  $\Delta K_{th}$  is the lowest value of  $\Delta K$  that will cause the crack to grow for  $R=0$ . The material property  $\beta$  is the shutoff overload ratio, introduced into the equation to account for the effect of load history on the predicted life. It is basically the ratio of the overload's maximum stress to the subsequent maximum stress required to arrest the crack growth. In literature, a value of  $\beta=3.0$  is suggested for the grade of aluminum used in this study (Harter 2008). However, as it will be explained later in detail, a linearly varying value for  $\beta$  better fits the test results for the VAL scenario studied in this research. The yield zone size due to an OL is calculated by (Dugdale, 1963 and Irwin, 1957):

$$R_{y,ol} = \frac{1}{2} \left( \frac{K_{max,ol}}{\sigma_y} \right)^2 \quad \text{For plane stress} \quad (7.16.1)$$

$$R_{y,ol} = \frac{1}{6} \left( \frac{K_{max,ol}}{\sigma_y} \right)^2 \quad \text{For plane strain} \quad (7.16.2)$$

To account for the influence of the CSC, the absolute value of the ratio of the compressive stress to the OL ratio can be used to calculate the reduction in the size of the current OL zone (Harter 2008):

$$R_{y,ol} = \left( 1 - 0.9 \left| \left( \frac{\sigma_{comp}}{\sigma_{ol}} \right) \right| \right) \times R_{y,ol} \quad (7.17)$$

The Walker fatigue model described above, along with the Willenborg retardation model, was used in this study to predict the FCG of the material under the VAL stress-time history shown earlier. Figure 7.10 compares the results of the analytical calculation of the crack growth with those obtained from our earlier experimental investigation. It is observed that the methods used in this study provide a very good estimate of the fatigue life of the component under the VAL stress-time history presented earlier.



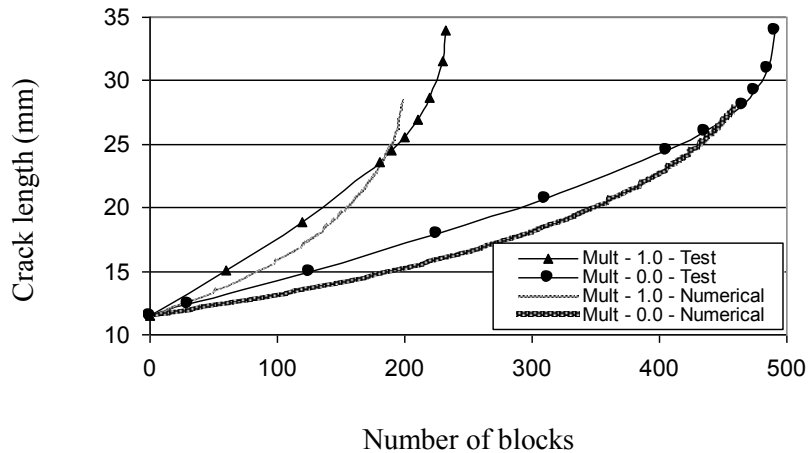


**Figure 7.10.** Comparison of the experimental and numerical/analytical results (using the point-by-point approach of Walker Model combined with Willenborg Retardation Model)

Our finite element analysis results indicated that the crack opening stresses were smaller for lower stress ratios (In other words, the crack opening stress decreases as the stress ratio decreases). This demonstrates the significant influence of the applied stress level on the fatigue crack closure, and corroborates with the results reported by other researchers (e.g. Chang *et al.* 2005; Wang *et al.* 2001; Kim and Lee 2000; Zhang *et al.* 1999). This demonstrates the influence of the compressive stresses on increasing the FCGR by affecting (decreasing) the crack closure effect.

As observed from the results shown in Figure 7.10, the Willenborg model slightly underestimates the FCG of the material during the first half portion of the loading history. In other words, the slope of the crack growth rate calculated based on the analytical/numerical approach is less than the slope of the crack growth rate obtained based on the experimental data (for the first half portion of the curve). After the crack length reaches nearly half its final length (before specimen's failure), the numerical approach tends to overestimate the crack growth rate. Overall, however, from the practical perspective, the Willenborg model used in this study seems to provide a good estimation of the fatigue life of the component under this VAL stress-time history.

As also explained earlier, a shutoff overload ratio of  $\beta = 3.0$  has been suggested by other researchers for the grade of aluminum used in this study (Harter 2008). However, we could not find any basis for this value in literature. As a result, we conducted a parametric study during our numerical investigation. The result of our study revealed that varying the value of  $\beta$  linearly (that is, from approximately  $\beta=6.0$  to  $\beta=2.9$ , as the crack propagated through the specimen), provided more compatible results to those obtained experimentally. In other words, the shutoff overload ratio,  $\beta$ , which is commonly believed to be a material property (therefore a constant value), seems to be a variable value, a function of the crack length, and its value reduces as the crack propagates through the material.

## 7.7. Summary and Conclusions

The influence of compressive stress cycles (CSC) that exist within a realistic variable amplitude loading scenario, on the fatigue crack growth of Al6061-T651 aluminum alloy was studied. Our recent experimental investigation (Iranpour and Taheri 2012b) explored the influence of various scales of CSC on the resulting fatigue crack growth (FCG) on plate specimens having a central crack (mode I). The present study continues that investigation by conducting a nonlinear finite element simulation to further examine the stress distribution in the vicinity of the crack tip, also investigating the influence of various scales of CSC on the crack tip opening displacement. The work also explored the predicting capability of two commonly used fatigue crack growth models and provided few insights for tuning the models. Moreover, a comprehensive investigation was conducted to explore the relationship among the CTOD, CSC and the number of loading cycles. The findings of this study can be summarized as follows:

- In concert with the experimental results obtained in our recent work, the results of our finite element analysis also confirmed the significant influence of CSC on the fatigue crack growth rate (FCGR). It is therefore strongly recommended that the CSCs be considered when establishing the FCGR of materials.

- Incorporation of the stress intensity factor in estimating the fatigue life of the material seems to account for the influence of only the tensile stress cycles. It is believed that if one wishes to also account for the influence of the CSC on FCG, one should then use more robust approaches that could account for the crack growth acceleration effect resulting from the crack closure.
- The CTOD is an effective and adequate parameter for calculating the FCGR, and also enable ones to account for the influence of CSC.
- The rate of variation of the fatigue crack growth and CTOD when plotted as a function of the magnitude of CSC followed a similar trend; as the rate decreased, the magnitude of the CSC increased.
- The shut-off overload ratio (that is the ratio of the maximum stress OL to the subsequent maximum stress cycle required to arrest the crack growth), appears to decrease as the crack length increases.

## **7.8. Acknowledgments**

The financial support of the National Science and Engineering Resource of Canada (NSERC) is gratefully appreciated.

## Chapter 8

### **Influence of the Peak Tensile Overload Cycles and Clipping Level on the Fatigue Crack Growth of Aluminum Alloy under Spectrum Loading**

Mohammad Iranpour and Farid Taheri

Department of Civil and Resource Engineering, Dalhousie University, 1360 Barrington Street, Halifax, Nova Scotia B3J 1Z1, Canada

Conditionally Accepted for Publication in the Journal of Materials Engineering and Performance

#### **8.1. Abstract**

Many structures, such as aircrafts, risers and offshore pipelines that are in contact with fluids, become subjected to complex variable amplitude loading (VAL) stress-time histories during their service lives. As a result, the structural life assessment and damage-tolerant analyses of such structures are considered as two important design criteria.

In this paper, a VAL stress-time history is used to study the fatigue life of 6061-T651 aluminum alloy, with focus on the retardation effect resulting from the applied peak tensile overload cycles (TOLC). Various so-called “clipping” levels are tested, and the results are compared with those obtained through an analytical method, using the Willenborg retardation approach, in conjunction with the Walker fatigue crack growth model. The results would demonstrate the significant influence of the TOLC present within variable amplitude loading scenarios (VAL) on retarding the fatigue crack growth rate of the material.

The study also investigates the influence of various clipping levels on the fatigue response of the material, also highlighting the limitations of the analytical approach in estimating the resulting crack growth rate. It is observed that the analytical method predicts a higher fatigue life for the material subjected to VAL, which is non-

conservative for design purposes. Some suggestions are provided for fatigue life estimation of the material when subjected to VAL scenarios.

**Keywords:** Fatigue, Tensile Overloads, Crack Retardation, Clipping Level, Variable Amplitude Loading (VAL) and Willenborg Model.

## 8.2. Introduction

Fatigue and damage tolerance analyses are some of the most dominating design concepts in aerospace, pipeline and offshore industries. When a fluid moves around a solid body, it may create severe vibrations in the body, which could lead to fatigue and ultimately fracture of the body. Such vibration states are random or semi-random in nature, and the resulting variable amplitude loading (VAL) stress-time histories would in turn cause difficulties when assessing the fatigue life of the material. In general, therefore, the assessment of the fatigue behavior of such components under a VAL is more complex than members subjected to constant amplitude loading (CAL).

Studies on flight simulation and fatigue life estimation of aircraft have shown that there exist several sources of VAL in aircraft components during their service lives. Among these sources are the gust load spectrum, ground-air-ground cycles, taxi loads, changes in the sequence of flights, spectrum severity and the peak load clipping levels (Wanhill 1994; Schijve and Hoeymakers, 1979). These sources can be divided into two main categories: pilot-induced (i.e., those due to the maneuvers) and gust-induced stress cycles (McColl and Phan 2007). In consideration of other structural components such as pipelines, risers and offshore structural members, the sources of vibration could be due to handling, transportation and installation, wind and wave-induced, which can be exacerbated by storm events, as well as vortex-induced vibrations (VIV) that can occur during the service life of the component (Iranpour and Taheri, 2006).

Studies on fatigue crack growth of materials under such VAL dates back to decades ago (Schijve and Hoeymakers, 1979; Jones and Wei, 1971; Tomkins, 1975; Elber, 1970). Various models have been proposed to date by many researchers with the aim of better

estimating the fatigue life of structural components under such applied loading scenarios; nevertheless, no universal model exists to date. Researchers have studied many parameters that could affect the fatigue crack growth of materials under VAL. The crack tip blunting, strain hardening of the material, crack deflection, residual stresses, time history of the applied loads and the crack closure are among the important factors that affect the crack growth under VAL (Sadananda *et al.* 1999).

A VAL, as commonly perceived, stress-time history usually consists of a large number of more or less constant amplitude loading cycles, as well as several tensile overload and compressive underload cycles. However, many of real world VAL do not contain any CAL trend, and are usually consisted of stress cycles with varying amplitudes (as in the case shown in Figure 8.1). In general, the TOLCs would decrease the crack growth rate, while compressive underload cycles would accelerate the crack growth rate of most engineering materials. The influence of a single overload or underload stress spike in a CAL is well documented for a wide range of materials. However, the influence of a large number of TOLCs that may exist in most VAL scenarios has received less attention. Having a large number of TOLCs is generally known to increase the fatigue life of the material. The main focus of recent studies has been to examine the underlying complexity of VAL scenarios and the resultant crack growth rate retardation or acceleration (Iranpour *et al.* 2008; Yuen and Taheri, 2004; Rushton and Taheri 2003; Taheri *et al.* 2002). The crack tip plasticity resulting from TOLCs could significantly influence the material response at the crack tip region, hence affecting the crack propagation rate within the subsequent load cycles. To account for the fatigue crack growth retardation effect of TOLCs in a more conservative manner, the highest peak loads of the VAL stress-time history can be clipped (truncated) at a certain level. The resulting clipped VAL stress-time history leads to an acceptable more conservative (i.e., underestimated) fatigue life for the material, which is more favored for design purposes.

For aircrafts, the test results have demonstrated that the clipping levels have more influence on the gust-induced fatigue rather than the maneuver-induced fatigue (Wanhill 1994). Due to their frequent occurrence and their corresponding peak loads, flights in severe weathers have been observed to induce more significant influence on the fatigue

crack growth of aircraft components. These frequently applied higher loads can result in crack growth retardation, and hence increase the fatigue life of the member.

Although in general the peak TOLC in a VAL scenario result in crack growth retardation, they could also cause monotonic crack extension (Wanhill 1994). Therefore, the choice of peak load clipping level must be carefully considered for both the full-scale and the laboratory scale articles. This aspect takes even more importance when considering thin-gauge damage-tolerant materials (such as 2024-T3 aluminum alloy), rather than thicker specimens or materials with inherently higher crack growth rates (Wanhill 1994). In the case of relatively thicker specimens (thicker than 5 mm) or materials with relatively high yield strength (such as the 7000 series aluminum alloys), the clipping level becomes of less importance due to the increased constraint and the resulting lower tendency of the crack tip approaching a plane stress state under the peak loads (Wanhill 2002). The clipping level is therefore varied mainly depending on the nature of the applied VAL stress-time history and the material under consideration.

In summary, the choice of the appropriate peak load clipping level has been under debate for a long period of time, especially by the experts involved in flight simulation and those evaluating other fluid-induced vibration fatigue; it therefore deserves more attention.

In this paper, the influence of the clipping level on the fatigue crack growth of 6061-T651 aluminum alloy subject to VAL stress-time history is studied through experimental and computational investigations. The VAL stress-time history used in this study is a typical time-history, usually affecting a structural component that moves through air or other fluids. The test results are compared against the results obtained analytically, using Willenborg's retardation approach and the Walker crack growth model. Some recommendations are provided for better fatigue life prediction of components under VAL scenarios and determination of the appropriate clipping level.

### 8.3. Problem Definition and Objectives

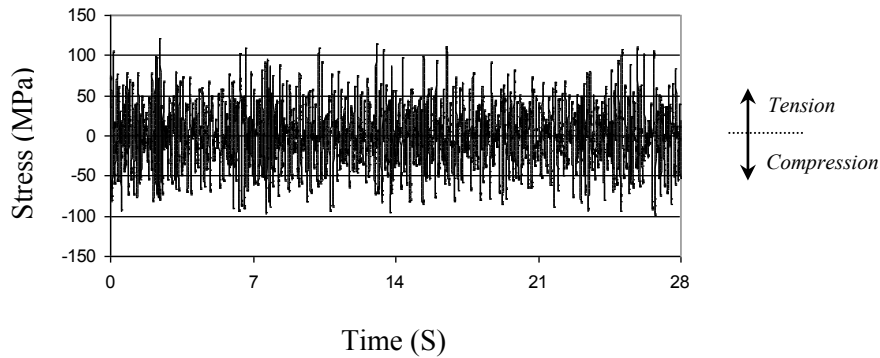
The above facts motivated the authors to conduct a series of experimental investigation into to study the influence of TOLC of the VAL stress-time history on the fatigue crack propagation of 6061-T651 aluminum alloy. In the experimental investigation, a VAL stress time-history is applied to a number of specimens, and the resulting crack growth rates are recorded. In summary, the objectives of our investigation are:

1. To study the retardation effect of TOLCs on material's fatigue crack growth rate.
2. To determine the most optimum clipping level for the VAL stress-time history used in this study.
3. To determine whether the Willenborg retardation model could accurately estimate the fatigue crack growth rate of the material.

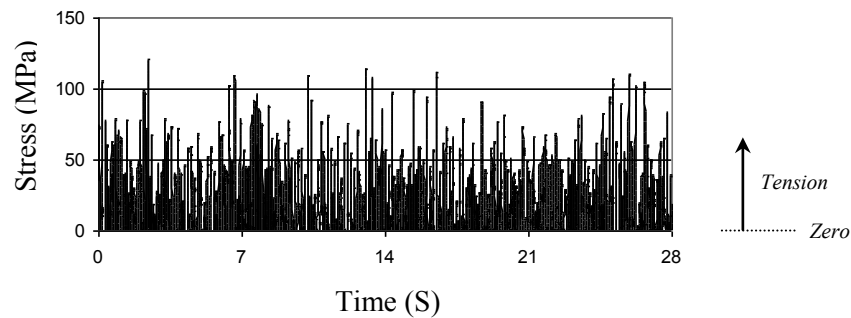
### 8.4. VAL Stress-time History

Figure 8.1 shows the stress-time history of the VAL scenario used in this study. For more detail on this VAL stress-time history, please see Iranpour and Taheri (2007). As it is illustrated in this figure, there exist a number of TOLC and compressive underload cycles stress spikes in the stress-time history. This complicates the prediction of the fatigue life of the component by the classical fatigue models that have been developed based on the consideration of the presence and influence of a few single overload and/or underload stress spikes (Iranpour *et al.* 2008). The influence of the compressive portion of the stress-time history has been previously studied by the author (Iranpour *et al.* 2008, Iranpour and Taheri 2012a, 2011, and 2007). It was demonstrated that the compressive portion of a stress-time history would have a considerable influence on the fatigue crack growth of the material, thus should not be ignored. The objective of the investigation presented in this chapter is to only assess the influence of the tensile stresses on the FCG of the material, and therefore, the compressive portion of the stress-time history is entirely omitted (see Figure 8.2).





**Figure 8.1.** A typical compression-tension VAL stress-time history observed in pipelines, risers, helicopters or airplane components



**Figure 8.2.** The zero-tension VAL stress-time history used in this study (*one block*)

In this paper, the stress-time history shown in Figure 8.2 is referred to as a *block*. Due to some limitations of the computer software, the entire VAL stress-time history could not be applied to the specimen in a single block (the maximum number of data points that could be introduced to the computer software available in our test facility was one *sub-block* with 200 points). Therefore, it was decided to break the entire VAL stress-time history to several *sub-blocks*, and then apply them sequentially to the specimen. Consequently, the *block* shown in Figure 8.2 was divided into a total of nine *sub-blocks*. Note that each *block* contained 1068 data points, resulting in a total of 534 stress cycles in each *block*.

There are essentially two main approaches for the analytical simulation of the fatigue crack propagation of a material under such complicated VAL stress-time history: (i) the block-by-block approach, or (ii) the cycle-by-cycle approach. In the block-by-block approach, the applied load history is divided into a certain number of different blocks and the fatigue crack growth from each block is calculated accordingly. In this approach, the total fatigue damage of the component is the cumulative sum of the damage from all loading blocks. In the cycle-by-cycle approach, the crack growth due to each load cycle is calculated and added sequentially to those obtained from other cycles. These two approaches have worked satisfactorily for cases where the applied load is highly irregular and the frequency of the applied overloads in both tension and compression are similar (Stephens *et al.*, 2001, Barsom and Rolfe, 1999). For such VAL stress-time history, one may use any of the available approaches (such as the Barsom's approach) to establish a CAL that is *equivalent* to the real VAL applied to the component. Once the *equivalent* CAL is calculated, an appropriate fatigue model (e.g., the Paris model) can be used to estimate the fatigue life of the component.

## 8.5. Tests with Various Maximum Tensile Stress Levels

Two sets of test were performed in this study to gain a better understanding of the influence of the maximum tensile stress peaks on the fatigue crack growth of materials subject to a VAL stress-time history:

1. Test Series No. 1: in this series of tests, the entire tensile loading cycles, as seen in Figure 8.2, were applied to a number of test specimens and the crack growth rate was recorded.
2. Test Series No. 2: in this series, all tensile stress cycles higher than a *certain level* were multiplied by a factor less than unity (i.e., were scaled down or clipped). A total of four different multipliers (factors) were used, and the tests are identified by the multiplier used for the maximum tensile stress of the entire *block*. For example, for a clipping level of 0.55, all the tensile stress cycles that are greater than 55% of the maximum tensile stress of the entire *block* were replaced by loading cycles with their

magnitude equal to the maximum tensile stress of the entire *block* multiplied by the factor (i.e., 0.55; see Figure 8.3). In the case, the maximum tensile stress of the entire *block* illustrated in Figure 8.2 (i.e., 121.47 MPa) was reduced to 66.81 MPa using the 0.55 multiplier. These clipping factors (i.e., 0.85, 0.70, 0.55 and 0.45) were also tried within this category of test.

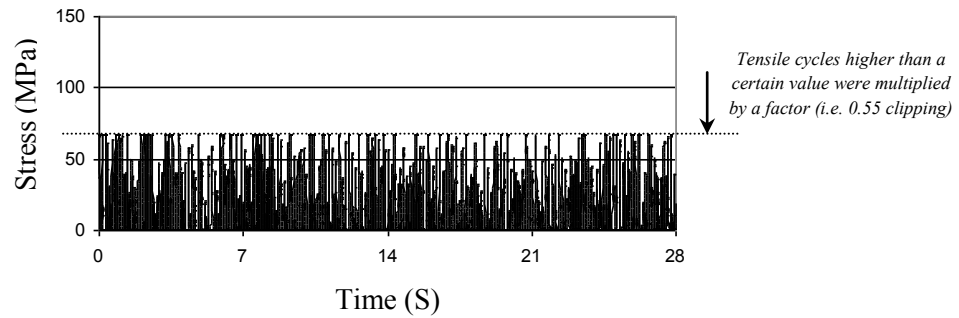


**Figure 8.3.** The VAL stress-time history of test series with a clipping level of 0.55

Table 8.1 summarizes the different series of tests. It should be noted that each graph or a set of test results reported in this study represents the mean results of at least three test specimens. Since the results of the three specimens in each set of tests were usually so close to one another, there was no need to plot them all separately in a figure.

**Table 8.1. The Summary of Various Test Series and their Descriptions**

Test Series No.	Test name	Test description	
1	No Clipping	The entire VAL stress-time history as shown in Figure 8.2 is applied to the specimen	
2	Clipping level of 0.85	All tensile stresses higher than this clipping level times the maximum tensile stress are replaced with this magnitude	0.85
	Clipping level of 0.70		0.70
	Clipping level of 0.55		0.55
	Clipping level of 0.45		0.45

## 8.6. Test Setup and Material

The fatigue tests were conducted using an Instron servo-hydraulic universal testing machine with a capacity of  $\pm 100$  kN, under dynamic or 200 kN under static loading conditions. The stress-time history was applied to the specimen through a special-purpose software. A fiber optic light was used to illuminate the crack tip region. To monitor the growth of the crack tip, a Mitutoyo traveling microscope with a magnification of 50X mounted on a pair of micrometers with a resolution of 0.01 mm was used to record the crack growth increment. The tests were performed per ASTM E-8M Standard, using plate specimens with dimensions of 300 mm (L)  $\times$  100 mm (W)  $\times$  4.74 mm (T) with a central notch of  $2a=20$ mm. The plates were cut such that the length of the specimens was oriented at the rolling direction of the original plate (refer to Iranpour *et al.* 2008 for more info). To get a better vision of the crack tip during its monitoring throughout the test, the surface of the specimen was polished with a wide range of sand paper grits, starting from coarse ones (No. 120) to a very fine one (No. 1200). Figure 8.4 shows the general overview of the test set up, and Figure 8.5 shows the rectangular test specimen with the center crack and its dimensions. As per ASTM E8M standard, acceptable geometric correction factors should be considered for the specimen configuration. Moreover, as a means of ensuring that LEFM holds, this standard suggests that the specimen be large enough to promote predominately linear elastic conditions during testing. The machine frequency was set between 4.0 to 5.0 Hz, so that it would exactly trace the input load history.

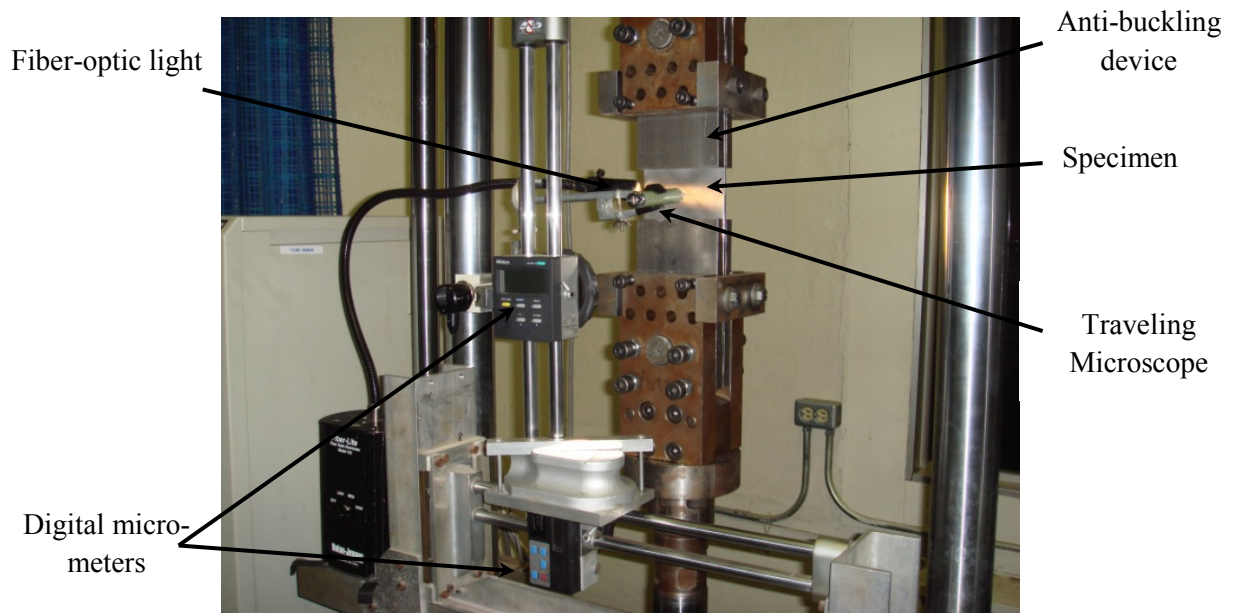


**Figure 8.4.** Test set up

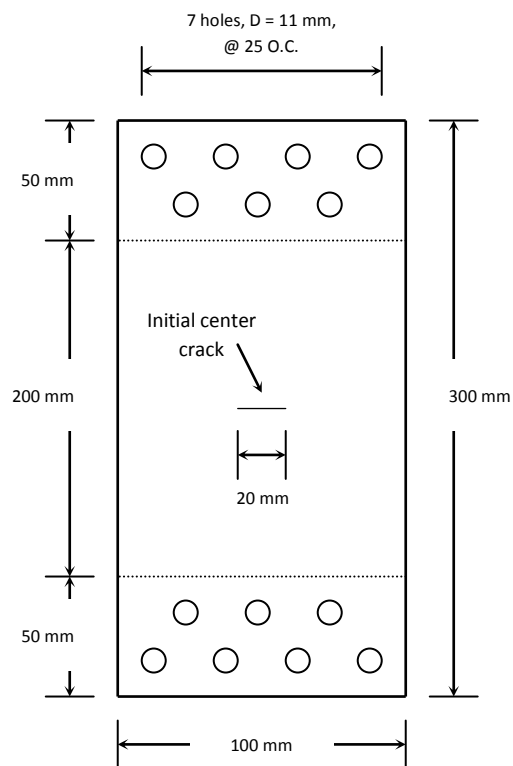


**Figure 8.5.** Test specimen configuration and dimensions (drawing not to scale)

The top and bottom fixtures, by which the plate specimen was gripped, were connected to the load cell and the actuator, respectively. The fixtures were designed with the capability of aligning the specimen in order to eliminate any unwanted bending due to misalignment. Small slips of the plate were observed during the first trials, resulting in unequal crack growth rate on the left and right hand side of the center crack. This problem was alleviated to some extent by re-aligning the specimen and after applying a certain number of load cycles. However, the results were not very satisfactory, since the crack growth rates were found to be quite sensitive to re-aligning the specimen during the test. Therefore, the grips were modified for the next tests, so to decrease the slippage and also increase grip capability for better alignment accuracy.

The tests were done at room temperature in air and the specimens were pre-cracked to a length of approximately  $2a' = 22.0$  mm before the VAL was applied to the specimen. This was done to remove the effects of the blunt starter notch, thus producing sharp fatigue crack of adequate straightness and size. Therefore, the subsequent crack growth under the VAL stress-time history was measured from the tip of this sharp pre-crack, rather than the initial EDM starter notch ends.

The magnitude of the applied pre-cracking fatigue load was selected to be low enough to prevent any load sequencing effect on the crack growth rate due to the subsequent stress-time history. After the pre-cracking, a specified number of *blocks* of the VAL stress-time history were applied to the specimen and the crack growth was measured. This procedure was followed until the plates fractured across specimen's width. The crack length was measured by the traveling microscope at specific numbers of elapsed cycles, trying to have a crack growth increment of less than 5.0 mm between each measurement. This check was done to ensure that the crack growth rates were equal at both sides of the initial notch and that there was no misalignment in the test setup. To compensate for any probable misalignment in the test setup, the reported crack lengths were based on the average of the measured crack lengths on both sides.

As stated earlier, the material used for this study was 6061-T651 aluminum alloy, with mechanical properties and compositions listed in Tables 8.2 and 8.3.

**Table 8.2.** Mechanical Properties of the 6061-T651 Aluminum Alloy

Modulus of Elasticity (GPa)	0.2% Yield Stress (MPa)	Ultimate Tensile Stress (MPa)
68.9	275.4	330.6

**Table 8.3.** Compositions (%) of the 6061-T651 Aluminum Alloy

Fe	Cu	Mn	Ni	Si	Mg	Zn	Ti	Cr
0.201	0.198	0.41	0.006	0.528	0.961	0.004	0.014	0.202

## 8.7. Experimental Observations

### 8.7.1. Test Series No. 1

Figure 8.6 shows the average response of three test specimens in the form of crack length versus the number of applied blocks. The specimens failed after applying 485 to 494 VAL stress time-history blocks, representing 258,990 to 263,796 stress cycles, respectively. The results of this series of experiments are used as the base variable amplitude loading (Base-VAL), with which the results of test series No. 2 will be compared later.

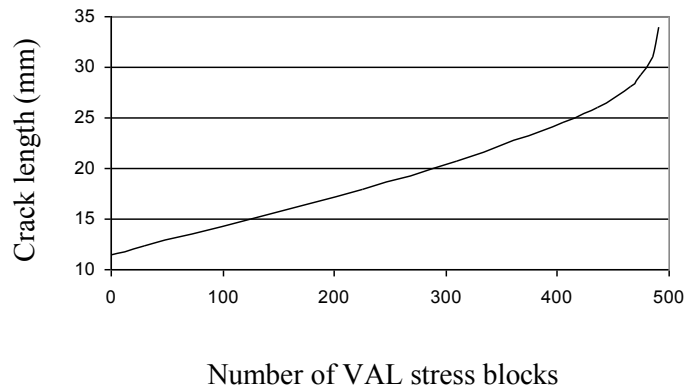


**Figure 8.6.** Crack length versus the number of applied VAL stress-time history blocks

### 8.7.2. Test Series No. 2

As explained earlier, in the second test series, the tensile stresses higher than the maximum tensile stress of the entire *block* were clipped by a certain factor. This series of tests was performed to investigate the influence of the maximum tensile stress cycles present within a VAL on the fatigue crack growth rate of the material. It has been demonstrated by several researchers that the application of TOLCs results in a reduction in the fatigue crack growth rate of steel (Yuen 2007; Rushton and Taheri 2003; Taheri *et al.* 2002; Hammouda *et al.* 1998). Therefore, it is expected that reducing the maximum tensile stress peaks of the loading *block* to a lower magnitude would increase the crack growth rate of the material under the resulting applied VAL stress-time history. In other words, it is postulated that as long as the tensile stresses higher than a certain *level* are replaced by lower values, then the fatigue crack growth rate of the material is expected to increase compared to that observed as the result of the application of the base-VAL (i.e., that with larger TOLCs). However, there should exist a certain limit below which the maximum tensile stress peaks present in the VAL stress-time history would cause no decrease in material's fatigue crack growth rate. It should be noted that in all tests, the total number of stress cycles within the loading blocks were kept identical.

Figure 8.7 compares the crack growth rates of the original base-VAL (i.e., subject to the VAL stress-time history shown in Figure 8.2), against the test series whose VAL was



altered by a clipping level of 0.85. As it is clearly illustrated in this figure, reducing the magnitude of those tensile stress spikes that are greater than 0.85 times the maximum tensile stress spike of the base-VAL increased the fatigue crack growth rate of the material by approximately 30%. This leads to the conclusion that those tensile stress cycle peaks in the original base-VAL with a magnitude greater than 0.85 times the maximum tensile stress of the entire *block* were acting as TOLCs. This is supported by the fact that decreasing the magnitude of those tensile stress peaks down to only 0.85 times the maximum tensile stress of the entire *block*, resulted in an increase in the fatigue crack growth rate of the material.

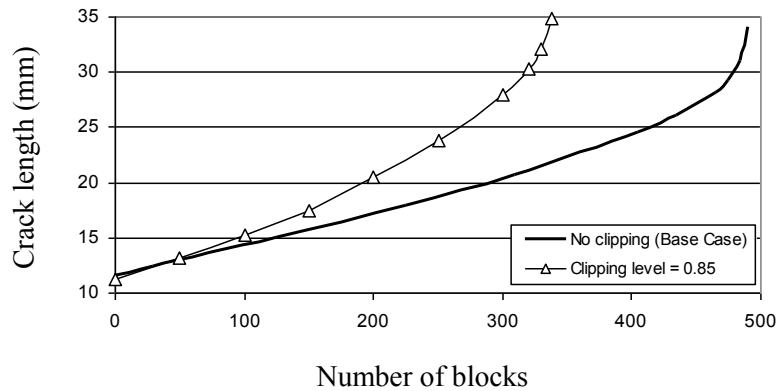


**Figure 8.7.** Comparison of the fatigue crack growth rates of the base-VAL with test series with a clipping level of 0.85

In the next tests, the clipping level was reduced to various lower scales and the related fatigue crack growth rates were monitored. Figure 8.8 shows the test result for all the cases summarized in Table 8.1. As observed in this figure, reducing the clipping level from 0.85 to 0.70 increased the fatigue crack growth rate even further. However, once the clipping level is reduced from 0.70 to 0.55, the fatigue crack growth tends to become very close to the crack growth rate observed in the specimens that were subject to the original base-VAL. In other words, replacing all the tensile stresses higher than half the maximum tensile stress peak, with half the magnitude of the maximum tensile stress peak of the entire block, would not result in any significant difference in the fatigue crack growth rate of the material. This observation leads to the conclusion that a majority of the

tensile stress peaks of the VAL stress-time history used in this study acted as TOLCs, and tend to increase the fatigue life of the material. Once the clipping level decreased from 0.55 to 0.45, the fatigue life of the material increased by approximately 30% compared to that observed when the specimens were subjected to the original base-VAL.

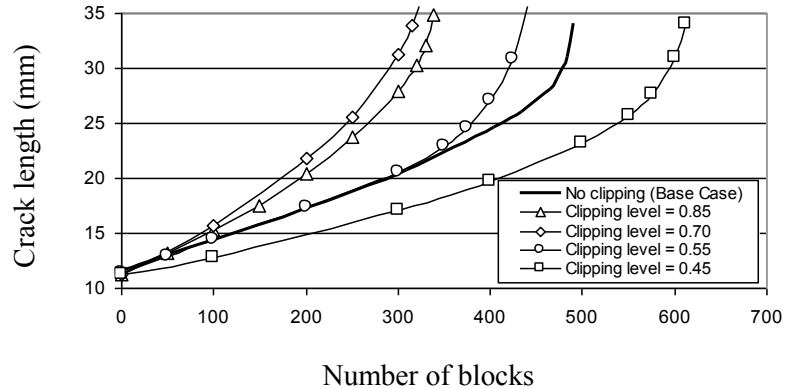


**Figure 8.8.** Comparison of the fatigue crack growth rates of the original ‘BASE-VAL’ with test results from various clipping levels

In the investigation that Lee *et al.* (2009) conducted, also on aluminum alloys, it was shown that a stress-time history with significantly lower tensile and higher compressive stress cycles could exhibit a fatigue crack growth almost twice of that with higher tensile and lower compressive stress cycles. In our previous studies, it was also shown that one of the culprits for such differences could be due to the crack growth accelerating effect induced by the compressive underloads (Iranpour and Taheri 2007 and 2011). Moreover, the present study shows that the difference in the crack growth rates as reported by Lee *et al.* in 2009 could also be attributed to the fatigue crack growth retardation effect due to the existence of the TOLC, since most of the peak tensile stress cycles present in a given VAL stress-time history could act as overloads.

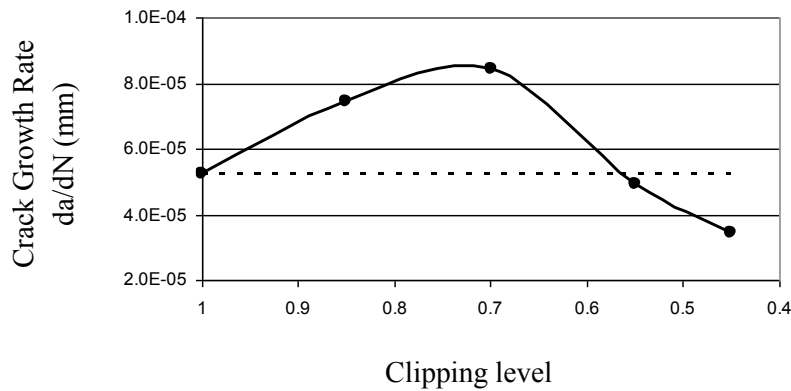
In a study by Kim *et al.* (2003), investigating the fatigue crack growth of 7050-T7451 aluminum alloy, attachment lugs were subjected to a typical flight spectrum loading. It was observed that the increase in the magnitude or frequency of the peak tensile stress cycles resulted in a significant retardation in the fatigue crack growth rate of the alloy.

The retardation in the fatigue life was believed to be the outcome of the large plastic deformation that would occur ahead of the crack tip due to the existence of large positive stress cycles within the spectrum (Kim *et al.* 2003). In their study, two clipping levels of 0.9 and 0.8 were also considered. A clipping level of 0.9 indicates that the stress cycles having a magnitude larger than 90% of the largest tensile stress cycle within the spectrum were replaced by a stress magnitude equal to 90% of the largest tensile stress cycle. It was observed that 0.9 clipping of the stress cycles decreased the fatigue life of the component by a factor of approximately two. However, when clipping of 0.8 was applied to the stress cycles, then the fatigue life of the material was increased by approximately 20% (Kim *et al.* 2003).

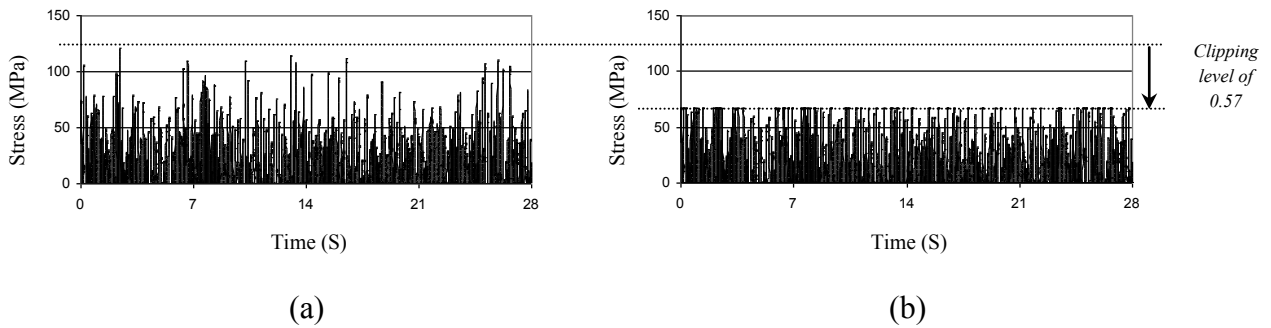
As can be observed from the results presented in Figure 8.8, the fatigue crack growth rate increased in our specimens as the clipping level was decreased from 0.85 to 0.70; however, as the clipping factor decreased below 0.7, the fatigue growth rate was decreased. It is postulated that within the relatively larger clipping levels, the influence of the observed fatigue growth retardation was as a result of the large tensile spikes present within the VAL. However, while the tensile overload cycles were clipped by a relatively lower clipping magnitude, the VAL stress-time history approached to that of a CAL, which results in lowering the overall stress intensity factor range. Under this condition, the influence of the maximum tensile stress cycles within the entire block become diluted and diminishes; as a result, the crack growth retardation effect vanishes. In other words, for clipping levels of approximately 0.70, the crack growth retardation effect due to the remaining TOLCs would essentially vanish, since additional decrease in the clipping level does not result in any more decrease in the fatigue life of the material, and the stress-time history becomes more like a CAL scenario. This demonstrates that the retardation effect of the TOLCs is more pronounced in the base-VAL scenario (see Figure 8.2).

Figure 8.9 shows the fatigue crack growth rate versus the clipping level. As observed, the fatigue crack growth rate increases as the clipping level decreased from 1.0 to approximately 0.7, after which the fatigue crack growth rate decreased with the decrease in the clipping level. The maximum fatigue crack growth rate is for the clipping level of approximately 0.7, thus indicating that the reduced maximum tensile stress cycles (the

clipped cycles at 0.7 level) of the loading block did not enact as TOLCs. As illustrated in this figure, a VAL stress-time history with a clipping level of 0.57 has the same crack growth rate as that caused by the original stress-time history for the base-VAL. In other words, the two stress-time histories, as presented side-by-side in Figure 8.10, resulted in exactly the same crack growth rate.



**Figure 8.9.** Fatigue crack growth rate versus the clipping level



**Figure 8.10.** The VAL stress-time history of: (a) the original BASE-VAL, (b) and after application of clipping level of 0.55

Figure 8.11 compares the exceedance plots (the number of exceedance versus the stress level) for the clipping levels of 1.0 and 0.55. The stress sequence used to plot the graph has been analyzed by the Rainflow cycle counting method. As it is observed, the clipping level of 1.0 (the original stress-time cycles) covers the entire stress range, while the clipping level of 0.55 only covers the peak stresses of up to approximately 63 MPa

(almost half of the maximum tensile stress cycle level present in the original base-VAL. Under the application of these stress levels, the responses are almost identical. The slight difference observed in this figure is due to the inherent nature of the Rainflow cycle counting method used in this study.

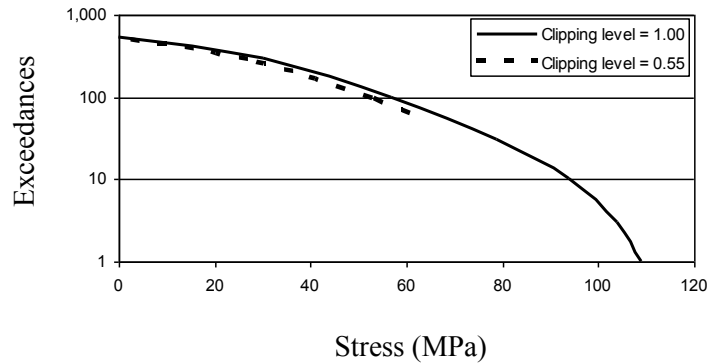


**Figure 8.11.** A comparison between the exceedances for clipping levels of 1.0 and 0.55

In the previous tests performed by the authors (Iranpour and Taheri 2007 and 2011), the full compression-tension VAL stress-time history (as shown in Figure 8.1) was applied to a number of specimens and the crack growth rate was monitored. Figure 8.12 compares the result of that study with the base-VAL (with no compressive stresses) and the test with a clipping level of 0.70. It is noted that among all tests performed in our study, the base-VAL demonstrates a case where the crack growth retardation effect of TOLCs is more pronounced, while the case with the full compression-tension loading cycles demonstrates that the crack growth acceleration effect due to the compressive underload cycles is more pronounced. As observed in this figure, the fatigue life of the compression-tension VAL stress-time history is approximately 45% of that subjected to the base-VAL (i.e., loading cycles with zero-compressive stress cycles), while the fatigue life of the test conducted with 0.7 clipping level is approximately 60% of that subject to the base-VAL. This comparison indicates that the fatigue crack growth acceleration effect due to the compressive underloads is seemingly more pronounced than the retardation effect due to the TOLCs. This observation does not corroborate with that of Kim *et al.*, who mentioned that their compressive stress cycles were not as effective in diminishing

the positive effect of their tensile overload cycles, and therefore, the overall balance in their tests was in the favor of the TOLCs, and the resulting retardation effects (Kim *et al.* 2003).

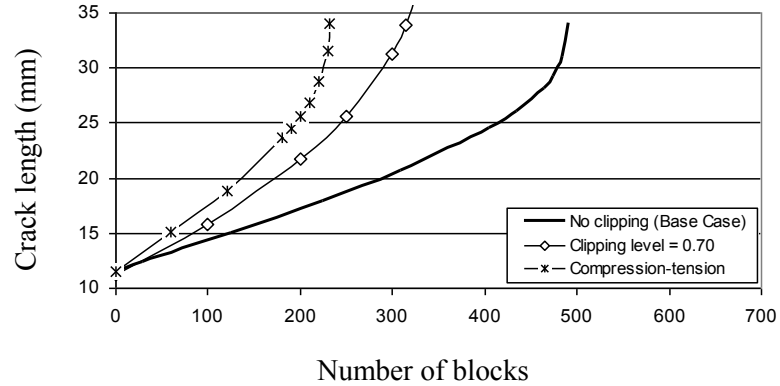


**Figure 8.12.** Comparison of the fatigue life of the alloy subjected to the original BASE-VAL with test results with the clipping level of 0.70 and the full compression-tension stress-time history

## 8.8. Analytical Analysis and Discussion

A computer code was developed, in the MATLAB environment, to validate the effectiveness of some of the commonly used analytical crack growth models for estimating the fatigue life of the material under the VAL stress-time history used in this study. The analytical fatigue life estimation involves evaluation of the total cycles taking the crack from its initial length after pre-cracking (i.e.,  $2a' = 22$  mm), to the intermediate length or the final stage of fracture of the specimen. A fatigue crack growth calculation for a VAL usually includes the consideration of the stress intensity factor, the stress ratio and the history of the applied load. The nature of the applied loading cycles (i.e., whether overload or underload cycles are present in the loading spectrum), as seen, can significantly affect the crack growth in materials.

The analytical analysis of fatigue crack growth used in this study is based on the Walker model, using a series of tabular crack growth rate test data obtained based on CAL scenarios conducted with various stress ratios. This information was then used to calculate the crack growth rate of the material that was subject to the VAL, based on a point-by-point shift basis. In this approach, the stress ratio,  $R$ , is taken into account independently for each crack growth curve,  $da/dN$ . Accordingly, first a tabular set of data (crack length vs. number of cycles) were established based on our previously conducted CAL tests. Subsequently, the Walker equation was applied on a point-by-point basis to interpolate/extrapolate data for any desired value of stress ratio,  $R$ . This approach has been widely used for calculating the crack growth rate under VAL stress-time histories (Harter 2008; Harter 1994). The walker equation is represented by:

$$\frac{da}{dN} = C[\Delta K(1-R)^{(m-1)}]^n \quad (8.1)$$

where  $m$  and  $n$  are model's parameters, established by experimental data. For a given value of stress ratio,  $R$ , the Walker equation can be written as (Harter 2008):

$$\Delta K = \Delta K_{R=0}(1-R)^{(1-m)} \quad \text{for} \quad R \geq 0.0 \quad (8.2)$$

$$K_{\max} = \Delta K_{R=0}(1-R)^{(m-1)} \quad \text{for} \quad R < 0.0 \quad (8.3)$$

As can be observed from the above equations,  $\Delta K$  is replaced with  $K_{\max}$  for negative stress ratios,  $R$ . Using the Walker's equation (as per Equation 8.1) for a certain crack growth rates for two positive values of stress ratio,  $R$ , we can write:

$$\Delta K_1(1-R_1)^{(m-1)} = \Delta K_2(1-R_2)^{(m-1)} \quad (8.4)$$

By replacing  $\Delta K$  with  $K_{\max}$  for negative stress ratios,  $R$ , and solving for parameter,  $m$ , we get three various cases (Harter 2008):

$$m = 1 + \left[ \log\left(\frac{\Delta K_1}{\Delta K_2}\right) / \log\left(\frac{(1-R_2)}{(1-R_1)}\right) \right] \quad \text{for} \quad (R_1 \geq 0.0 \text{ and } R_2 \geq 0.0) \quad (8.5.1)$$

$$m = 1 + \left[ \log\left(\frac{K_{\max 1}}{\Delta K_2}\right) / \log((1-R_2) \times (1-R_2)) \right] \quad \text{for} \quad (R_1 < 0.0 \text{ and } R_2 \geq 0.0) \quad (8.5.2)$$

$$m = 1 - \left[ \log \left( \frac{K_{\max 1}}{K_{\max 2}} \right) / \log \left( \frac{(1-R_2)}{(1-R_1)} \right) \right] \quad \text{for } (R_1 < 0.0 \text{ and } R_2 < 0.0) \quad (8.5.3)$$

The parameter,  $m$ , essentially controls the shift of the crack growth data as a function of stress ratio,  $R$ , on a point-by-point basis. As the first step, therefore the parameter  $m$  is calculated from the above equations based on  $\Delta K$  for two values of  $R$  taken for the same crack growth rate. In the second step, the tabular values of  $m$  are used to calculate the crack growth rate,  $da/dN$ , for any desired value of  $\Delta K$  and  $R$ . The crack growth rate is then calculated based on  $\Delta K$ , incrementally, until the subsequent calculated value of  $\Delta K$  exceeds the  $\Delta K$  value established in the previous step. In the last step, a logarithmic interpolation is applied to the last two points in the curve in order to establish the current crack growth rate.

The above approach was used to calculate the fatigue crack growth, and the results were compared against those obtained experimentally. Based on this approach, the number of stress cycles required to fracture the specimen were found to be much lower than that observed experimentally. This difference seems to be due to ignoring the crack growth retardation effect due to the TOLCs.

The influence of load-sequencing in a VAL stress-time history can also be considered by three commonly used approaches, namely: (i) the yield zone model, which accounts for the retardation by considering the overload and magnitude of the current plastic zone sizes; (ii) the strip-yield model, which is based on Dugdale's crack closure approach; and (iii) the crack closure model, which uses the experimental data to establish the crack opening load (Miranda *et al.* 2003). Among the yield zone approaches, the Wheeler model (Wheeler 1972) and Willenborg model (Willenborg 1971, Gallagher 1974) have been used more widely by researchers working in this field (Yuen and Taheri, 2005; Pereira *et al.* 2007).

In this study, the generalized Willenborg retardation model is used to incorporate the influence of TOLC on the fatigue crack propagation of the specimen. This model uses an effective stress intensity factor based on the size of the yield zone ahead of the crack tip. The Willenborg model assumes that the crack growth delay after a tensile overload cycle



is due to the reduction in  $K_{\max}$ , corresponding to the crack length being considered. According to the Willenborg model, the reduction in  $K_{\max}$  is defined by (Willenborg *et al.* 1971; Gallagher, 1974 and Pereira *et al.* 2007):

$$K_{red} = K_{req} - K_{\max} \quad (8.6)$$

where,  $K_{req}$  is the stress intensity factor necessary to produce a plastic crack zone that extends a distance  $\lambda$  ahead of the advancing crack tip to the far end of the plastic zone created by the applied tensile overload cycle. The effective stress intensity factors can be calculated by:

$$K_{\max,eff} = K_{\max} - K_{red} \quad (8.7.1)$$

$$K_{\min,eff} = K_{\min} - K_{red} \quad (8.7.2)$$

where  $K_{\min}$  is the stress intensity factor of the crack subject to CAL. These maximum and minimum effective values can then be used to calculate the effective stress intensity factor range,  $\Delta K_{eff}$ , and the effective stress intensity factor ratio,  $R$ . It is noted that negative values of  $K_{\min,eff}$  should be taken as null and  $\Delta K_{eff}$  becomes equal to  $K_{\max,eff}$  (Willenborg *et al.* 1971 and Pereira *et al.* 2007). The reduction in  $K_{\max}$  can be re-written as (Harter 2008):

$$K_{red} = \phi \left( K_{\max,ol} \times \sqrt{1 - \frac{(a - a_{ol})}{R_{y,ol}}} - K_{\max} \right) \quad (8.8)$$

where,  $a$  is the crack length,  $a_{ol}$  is the crack length at overload,  $K_{\max,ol}$  is the maximum stress intensity factor at overload,  $R_{y,ol}$  is the size of the yield zone at overload and  $\phi$  is a parameter in Willenborg model defined by (Harter 2008):

$$\phi = \left( 1 - \frac{\Delta K_{th}}{K_{\max}} \right) \times (\beta - 1) \quad (8.9)$$

in which  $\Delta K_{th}$  is the lowest value of  $\Delta K$  that will cause the crack to grow at zero stress ratio ( $R=0$ ). The material property  $\beta$  is a shutoff overload ratio introduced into the equation to control the effect of load history on the predicted life. It is basically the ratio of the overload maximum stress to the subsequent maximum stress required to arrest the crack growth. In literature, a value of  $\beta=3.0$  is suggested for the aluminum material used in this study (Harter 2008). The yield zone size due to overload is calculated by (Dugdale, 1963 and Irwin, 1957):

$$R_{y,ol} = \frac{1}{2} \left( \frac{K_{\max,ol}}{\sigma_y} \right)^2 \quad \text{for Plane Stress} \quad (8.10.1)$$

$$R_{y,ol} = \frac{1}{6} \left( \frac{K_{\max,ol}}{\sigma_y} \right)^2 \quad \text{for Plane Strain} \quad (8.10.2)$$

The Walker fatigue model described above, along with the Willenborg retardation model, was used in this study to predict the fatigue crack growth of the material under the VAL stress-time history shown earlier. Figure 8.13 compares the results of the analytical calculation of the crack growth with those obtained from experiments for the base-VAL and a clipping level of 0.7. It is observed that the analytical calculations provide a good estimation of the fatigue crack growth due to the BASE-VAL (i.e., the original zero compression-tension stress-time history); however, the predicted analytical crack growth results for the stress cycles with clipping level of 0.70 are approximately 30% conservative compared to the experimental results.

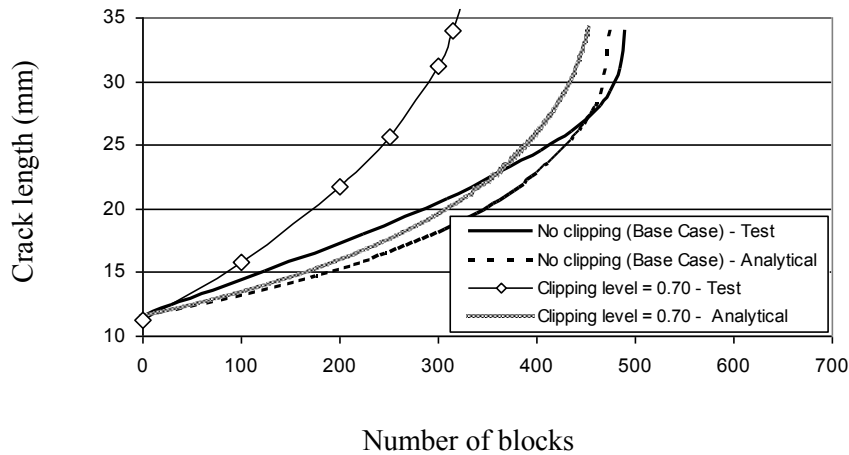


**Figure 8.13.** Comparison of the fatigue crack growth results predicted analytically for the original BASE-VAL load history and the load history clipped at 0.70 level and the experimental results

As seen in Figure 8.13, the Willenborg model slightly underestimates the fatigue crack growth of the material during the first half of specimen's life. In other words, the slope of the crack growth rate calculated from the analytical approach is less than the slope of the experimentally observed crack growth rate through the first half portion of the curve. After that stage, the analytical approach starts overestimating the fatigue crack growth rate. Overall, the Willenborg model used in this study seems to provide a good estimation of the fatigue life of the component under this VAL stress-time history.

As explained earlier, and as suggested by other researchers for the alloy used in this study (see for example Harter 2008), a shutoff overload ratio of  $\beta = 3.0$  was used in this study. Our investigation, however, showed that the use of gradually decreasing values of  $\beta = 6.0$  to  $\beta = 2.9$  could produce a better prediction of the fatigue crack growth of the material over the entire range of the loading history. In other words, the shutoff overload ratio,  $\beta$ , which is commonly known to be a material property, seems to be a function of the crack length, and is a non-stationary value, which in fact reduces as the crack propagates through the material.

The results from the above alteration to  $\beta$  is illustrated in Figure 8.14. As can be observed, the analytical results depict a non-conservative estimation of the fatigue crack growth rate, which is not desirable for design purposes. Both curves shown in the figure depict the fatigue crack growth rate at the initial stages of the growth. As the clipping level decreases from 1.0 to 0.75, both curves show an increase in the fatigue crack growth rate. However, as the clipping level decreases further from 0.75 to 0.55, the fatigue crack growth rate decreases in both the analytical and experimental results. Comparing the rather abruptly varying curve constructed by the experimental data to the smoother curve resulting from the analytical approach indicates that the fatigue crack growth rate is more sensitive to the variation of clipping level. In other words, the analytical approach cannot be considered as a reliable means for tracing the influence of TOLC on the fatigue crack growth rate of the material under the applied VAL stress-time history. However, it is interesting to note the fact that the experimental result associated with a clipping level of approximately 0.55, which generated a similar crack growth rate to that observed for the base-VAL scenario, is better corroborated by the analytical approach as well.

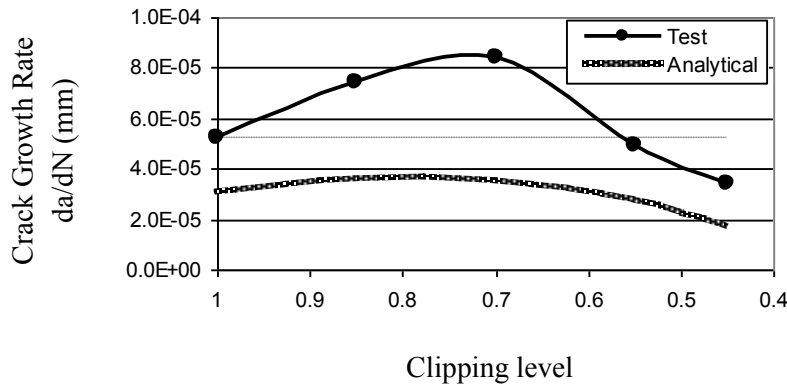


**Figure 8.14.** Comparison of the fatigue crack growth rate obtained experimentally and analytically.

Furthermore, the observation of the results in Figure 8.14 indicates that as the clipping level decreases from 1.0 to 0.70, the difference between the analytical and experimental results becomes more evidence. This observation also corroborate with that of Kim *et al.* (2003); their analytical method was based on the use of the

Willenborg retardation model combined with the weight function method and the stress intensity factor approach derived from the boundary element method by which the influence of the contact pressure on the stress intensity factor was taken into account (Kim *et al.* in 2003).

## 8.9. Summary and Conclusion

In this paper, the influence of the peak tensile overload cycles (TOLC) on the fatigue crack growth rate of 6061-T651 aluminum alloy was studied. The VAL stress-time history used in this research represents the type of loading scenario usually experienced by the structures encountering fluid-structure interactions (e.g., aircrafts and offshore structures). Tests with various clipping levels of the tensile stress cycles were performed on specimens with a through central crack in order to determine the influence of the TOLCs within a VAL scenario on material's crack growth response.

It was observed that the TOLC had a significant influence on retardation of the fatigue crack growth rate of the alloy. This retardation is believed to be as a result of the large plastic deformation formed ahead of the crack tip due to the large magnitudes of the TOLCs. Therefore, as a means for generating a conservative fatigue life for the material at the design stage, one can clip (or truncate) the relatively very large peak tensile cycles within a given variable loading scenario. The choice of the clipping level, however becomes critical, especially when considering thin-gauge materials with relatively low yield strength, as customarily used in designs employing a damage-tolerant philosophy. As a result, several researchers have been motivated to conduct experimental investigations on various metallic alloys with the aim of evaluating the influence of the clipping level on their fatigue response. For instance, experiments performed by other researchers on 7050-T7451 aluminum alloy subjected to flight spectrum loading, have demonstrated that clipping of a 10% applied to the TOLCs resulted in approximately a twofold decrease in the fatigue life of the component. However, the influencing of the clipping is not usually linear; for instance, the clipping of 20% applied to the same alloy, surprisingly increased the fatigue life of the alloy by almost 20%. In fact, it has been

shown (as also supported by our test results presented in this study) that the slope of the crack growth rate versus the clipping level curve changes from a positive value to a negative value at a clipping level of approximately 0.85 for 7050-T7451 aluminum alloy.

The results of our experimental investigation conducted on 6061-T651 aluminum alloy indicated that as the clipping level decreased from 1.0 to 0.75, the crack growth rate in the material increased. However, further decrease in the clipping level resulted in a decrease in the crack growth rate. In other words, the slope of the crack growth rate versus the clipping level diagram changed from a positive value to a negative value at a clipping level of approximately 0.75 for aluminum alloy 6061-T651. This is approximately 10-15% lower than that observed for 7050-T7451 aluminum alloy by Kim *et al.* (2003). The observed difference is believed to be essentially due to the higher yield strength of 7050-T7451 aluminum alloy, which results in more constraint on the crack tip, which in turn lowers the tendency of the crack tip to be in the state of plane stress while being subjected to a large (peak) tensile overload cycle. This corroborates with the observations made by other researchers, indicating that the influence of the clipping level becomes of less importance as the yield strength of the material increases.

An analytical method, using the Willenborg retardation approach, combined with the Walker fatigue model, was also used to estimate the fatigue life of the alloy subject to the various applied clipping magnitudes. In general, the analytical method estimated a higher fatigue life for the material, which is non-conservative, thus not desirable for design purposes. It was observed that the Willenborg model underestimated the fatigue crack growth of the material essentially during the first half of specimen's fatigue life. However, during the stage, when the crack length was approximately half of its final length till the final fracture of the specimen, the analytical approach still overestimated the crack growth, but the accuracy in predicting the rate of crack growth was improved. Moreover, the results from both the experimental and analytical investigation demonstrated that the clipping level of 0.55 induced the same fatigue crack growth rate of the alloy as did the original VAL. It was also observed that as the clipping level decreased, the Willenborg model provided a less accurate estimation of the fatigue crack growth rate of the material.

It is believed that the difference between the analytical and experimental results is basically due to the use of the shut-off overload ratio (that is the ratio of the overload maximum stress to the subsequent maximum stress required to arrest the crack growth), which is taken as a fixed value in the analytical method. The fixity of this value is based on the notion that. In general, the shut-off overload ratio has been taken as a material property. However, our experimental results indicate that the shut-off overload ratio seem to be a non-stationary parameter, with its value decreasing as the crack length increases. This corroborates with the VAL stress-time histories fatigue test results obtained by the authors in their other investigations.

Comparison of the analytical and experimental results indicates that the analytical approach is less sensitive to the change in the clipping level; therefore, the analytical approach cannot be considered as a reliable means for evaluating the influence of the magnitude of the TOLC on the fatigue crack growth response of the material.

It is hoped that the experimental fatigue crack growth data presented in this paper and the differences seen in the prediction of the fatigue life by the use of the widely-used Willenborg retardation model, would provide an incentive to researchers to further investigate the influence of the clipping level and the ensuing retardation due to the application of TOLCs present within most variable amplitude loading scenarios.

## **8.10. Acknowledgments**

The financial support of the National Science and Engineering Resource of Canada (NSERC) is gratefully appreciated.

## **Chapter 9**

### **Summary and Conclusion**

#### **9.1. Summary**

In spite of extensive research for consideration of risers' fatigue, there appears to be no consensus on a unified approach that could reliably predict the fatigue response of risers subject to VIV. The available approaches for analyzing VIV fatigue of risers mainly focus on the VIV portion of the task, and indeed less attention is paid to the actual fatigue life analysis using various models once the VIV-induced stresses are calculated. Moreover, the influence of compressive stresses in a VAL on FCGR is usually ignored.

In this research program, several real VIV test data were used to conduct fatigue tests on 6061-T651 aluminum alloy, followed by nonlinear finite element analyses and FCG calculations using analytical methods. As the first step, it was verified that the fatigue tests could be performed on a plate subject to tension rather than a pipe subject to bending. The next phase of the research focused on the influence of the second VIV harmonics on the FCGR. The influence of the compressive stresses within a VAL was also studied using different load combinations and compressive stress multipliers. Available analytical methods were investigated, and recommendations were made for a better fatigue life estimation of the material under VAL, focusing on the influence of compressive stresses. The adequacy of CTOD as an effective parameter for calculating the FCGR was also studied, with focus on the effects of compressive stresses. The influence of the clipping level on the FCGR of material was also studied, and recommendations were made for a better fatigue life estimation of the material under such loading condition.



## 9.2. Conclusions

The findings of this research program can be briefly summarized as follows:

- It is admissible to test a plate subject to tension in place of a pipe subject to bending moment.
- The crack front follows a semi-circular shape during its propagation for both a plate under tension and a pipe under bending moment, regardless of the initial shape of the flaw.
- Dimensionless stress intensity factor ratios (relating the crack in a pipe under bending moment to a plate under tension) exhibit almost a constant value along a large portion of the crack front.
- The fatigue crack growth rate under the real VIV-induced stress-time history is very slow and is close to the threshold region (in the order of about  $2.5E-6$  mm per cycle).
- The third harmonic has a significant influence on the VIV-induced fatigue crack growth, and can decrease the fatigue life up to about 70%.
- The equivalent CAL calculated using the root mean square method of Barsom and Hudson approaches significantly (about 6 times) underestimates the FCGR under real VIV-induced VAL, which is alarming and un-conservative for design purposes.
- The VIV-induced stress-time history is not a fully random loading, and the influence of load-sequencing effects should be taken into account by using more sophisticated fatigue models.
- Compressive stresses significantly reduced the fatigue life of the material under VAL, and cannot be ignored. This was verified using experimental tests, finite element analyses and analytical methods.

- The mere presence of CSC within a VAL would have a more pronounced effect on the resulting fatigue life than the magnitude of the CSC. Even the presence of a few CSC within the VAL could significantly affect the fatigue life of the material.
- In order to effectively and efficiently account for the influence of CSC within a VAL loading scenario, one may divide the applied stress-time history into shorter intervals (sub-blocks), and then apply only the maximum value of the compressive stress spike present within the sub-block. This scheme would produce a similar fatigue crack propagation result compared to the case when all the CSC present within the original time-history are applied onto the specimen.
- It appears that calculation of the stress intensity factor could be effectively accomplished by considering only the tensile portion of the stress range, and that the influence of compressive stresses could be more effectively accounted for by using other approaches (e.g., by its crack growth accelerating effect through the consideration of the resulting crack closure).
- The influence of CSC on adversely affecting the fatigue life of the material under the study seems to be independent of the roughness-induced crack closure for the material tested in this research project.
- Incorporation of the stress intensity factor in estimating the fatigue life of the material seems to account for the influence of only the tensile stress cycles. It is believed that if one wishes to also account for the influence of the CSC on FCG, one should then use more robust approaches that could account for the crack growth acceleration effect resulting from the crack closure.
- The CTOD is an effective and adequate parameter for calculating the FCGR, and also enables one to account for the influence of CSC.
- The rate of variation of the fatigue crack growth and CTOD when plotted as a function of the magnitude of CSC follows a similar trend; as the rate decreased, the magnitude of the CSC increased.

- The shut-off overload ratio (that is the ratio of the maximum stress OL to the subsequent maximum stress cycle required to arrest the crack growth), seem to be a non-stationary parameter and appears to decrease as the crack length increases.
- The slope of the crack growth rate versus the clipping level curve changes from a positive value to a negative value at a clipping level of approximately 0.75. This level varies for different materials.
- The influence of the clipping level becomes of less importance as the yield strength of the material increases.
- The clipping level 0.55 induced the same fatigue crack growth rate as did the original tension-tension VAL.
- The Willenborg retardation approach combined with the Walker fatigue model predicted a higher fatigue life for a tension-tension VAL, which is non-conservative, thus not desirable for design purposes. As the clipping level decreased, the Willenborg model provided a less accurate estimation of the FCGR.
- The analytical approach is less sensitive to the change in the clipping level, and therefore, cannot be considered as a reliable means for evaluating the influence of the magnitude of the TOLC on the FCG.

### **9.3. Recommendations for Future Work**

It is hoped that the experimental, analytical and computational results presented in this dissertation, as well as the differences observed in the prediction of the fatigue life using different approaches, would provide an incentive to researchers for further investigation.

The following future works are suggested:

- Materials other than that tested in this research program should also be investigated to provide better recommendations for fatigue life estimation under VAL scenarios.

- The focus of this research program was on the cross-flow VIV. Although the in-line VIV is known to have smaller influence on the total fatigue life of the riser, its influence should also be investigated. Moreover, the influence of the fourth harmonic (that is the second harmonic associated with the in-line VIV) deserves its own attention.
- The corrosive influence of sea water environment should also be studied and simulated in a proper test setup using the real VIV-induced stress-time history.
- As stated earlier, no attempt was made in this investigation to examine the influence of VIV induced fatigue on risers' welds. Welds usually include defects; therefore, it is important to examine the response of welds to the parameters investigated in this project. Such an investigation should also consider the influence of the residual stresses that are created due to the welding process and the resulting heat affected zone.
- The use of a new form for establishing the stress intensity factor range should be explored, so that the influence of the compressive stresses could be more effectively considered.
- More research is required to evaluate the influence of shut-off ratio on FCG to provide a better estimation for this parameter as a function of the crack length, and not just a material property.

## **Bibliography**

ABAQUS, 2010, Analysis User's Manual, Version 6.9, ABAQUS Inc.

ABAQUS, 2010, Theory Manual, Version 6.9. ABAQUS Inc.

ABAQUS, 2006, Analysis User's Manual, Version 6.6, ABAQUS Inc.

ABAQUS, 2005, Theory Manual, Version 6.5, ABAQUS Inc.

Anderson T. L., 1991, Fracture Mechanics: Fundamentals and Applications, CRC Press

Anthes, R. J., 1997, Modified Rainflow Counting Keeping the Load Sequence, International Journal of Fatigue, V. 19, N. 7, 529-535.

Anderson, T. L., 2005, Fracture Mechanics: Fundamentals and Applications, Third Edition, CRC Press

Antolovich, S. D., 1997, Alloy Design for Fatigue and Fracture, ASM Handbook, Fatigue and Fracture, The Materials Information Society, Vol. 19, 25-41.

Araújo, M. C., 1998, Nonlinear Kinematic Hardening Model for Multiaxial Cyclic Plasticity, M.Sc. thesis, Universidade Federal do Piauí, Brazil

ASTM E 1049-85, 1999, Standard practices for cycle counting in fatigue analysis, in: Annual Book of ASTM Standards, V. 03.01, Philadelphia, 710-718.

API 2RD, 1998, Design of Risers for Floating Production Systems (FPSs) and Tension-Leg Platforms (TLPs), American Petroleum Institute, Washington D.C., USA.

ASTM E647-95a, 1995, Standard Test Method for Measurement of Fatigue Crack Growth Rate, Annual Book of ASTM Standard, Vol. 11.03.

ASTM E 8M-01, 2001, Standard Test Methods for Tension Testing of Metallic Materials, Annual Book of ASTM Standards, ASTM, West Conshohocken, PA, 2001, 82-103.

Baarholm, G. S., Larsen, C. M., Lie, H., Mork, K., and Meling, T. S. 2004. Simplified model for evaluation of fatigue from vortex induced vibrations of marine risers., 799-806.

Bai, Y. 2001. Pipelines and risers. Elsevier, Amsterdam ; New York

Barsom, J. M. and Rolfe, S. T., 1999, *Fatigue and Fracture Control in Structures – Application of Fracture Mechanics*, American Society for Testing and Materials.

Barsom J. M., 1973, Fatigue crack growth under variable amplitude loading in ASTM A514-B Grade-B steel, Progress in flaw growth and fracture toughness testing, ASTM STP 536

Bian, L. and Taheri, F., 2006, Investigation of fatigue crack propagation in line pipes containing an angled surface flaw, Accepted for publication in the ASME Journal of PVT, Nov. 2006.

Bergman, M., 1995, Stress intensity factors for circumferential surface cracks in pipes, *Fatigue and Fracture of Engineering Materials and Structures*, 18 (5), 1155-1172

Broek D., 1989, *The Practical Use of Fracture Mechanics*, Kluwer Academic Publishers

Burande S. and Raju Sethuraman, 1999, Computational simulation of fatigue crack growth and demonstration of leak before break criterion, *International Journal of Pressure Vessels and Piping*, 76, 331–338

Brose, W., Dowling, N. E. and Morrow, J., 1974, Effect of Periodic Large Strain Cycles on the Fatigue Behavior of Steel, SAE, No. 740221, Automotive Engineering Congress, Detroit, MI.

Bucci, R. J., Nordmark, G. and Starke, E. A., 1997, Selecting Aluminum Alloys to Resist Failure by Fracture Mechanics, *ASM Handbook, Fatigue and Fracture*, The Materials Information Society, Vol. 19, 771-812.

Cai, C.Q. and C.S. Shin, 2005, A normalized area-compliance method for monitoring surface crack development in a cylindrical rod, *International Journal of Fatigue*, 27, 801–809

Cameron, D. W., Allegany, NY. Hoepfner, D. W., 1997, Fatigue Properties in Engineering, *ASM Handbook, Fatigue and Fracture*, The Materials Information Society, Vol. 19, 15-26.

Carpinteri A., Brighenti R. and Spangoli A., 1998, Part-through cracks in pipes under cyclic bending, *Nuclear Engineering and Design*, 185, 1-10

- Carpinteri A., Brighenti R. and Spangoli A., 2000, Fatigue growth simulation of part-through flaws in thick-walled pipes under rotary bending, *International Journal of Fatigue*, 22, 1-9
- Carpinteri A., 1993, Shape change of surface cracks in round bars under cyclic axial loading, *International Journal of Fatigue*, 15 (1), 21-26
- Chang, T., Li, G. and Hou, J., 2005, Effects of Applied Stress Level on Plastic Zone Size and Opening Stress Ratio of Fatigue Crack, *International Journal of Fatigue*, Vol. 27, 519-526
- Chen, N. and Lawrence, F. V., 1997, A comparison of two total fatigue life prediction methods. In: *Advances in fatigue crack closure measurement and analysis*, STP 1343, Philadelphia (PA): ASTM, p. 351–66
- Chen, Y. and Lambert, S. 2005, Numerical modeling of ductile tearing for semi-elliptical surface cracks in wide plates, *International Journal of Pressure Vessels and Piping* 82, 417–426
- Cheng Y. W., 1985, The fatigue crack growth of a ship steel in seawater under spectrum loading, *International Journal of Fatigue*, V. 7(2), 95-100
- Corn L., 1971, A study of cracking techniques for obtaining partial thickness cracks of pre-selected depths and shapes. *Engineering Fracture Mechanics* , 3, 45–52
- Dowling, N. E., 1973, Fatigue Life and Inelastic Strain Response under Complex Histories for an Alloy Steel, *Journal of Testing & Evaluation*, Vol. 1, No. 4, 271-287.
- Dowling, N. E., 1988, Estimation and Correlation of Fatigue Lives for Random Loading, *International Journal of Fatigue*, V. 10, N. 3, 179-185.
- DNV-OS-F201, 2001, Dynamic risers, Offshore standards DNV-OS-F201. Det Norske Veritas (DNV).
- DNV-RP-C203, 2001, Fatigue strength analysis of offshore steel structures, Det Norske Veritas (DNV).
- Dugdale, D. S., Yield of Steel Containing Slits, *Journal of Mechanics and Physics of Solids*, Wiley Interscience, New York, 1963

- Elber W., 1970, Fatigue crack closure under cyclic tension, *Engineering Fracture Mechanics*, V. 2, 37–45
- EMRC, Engineering Mechanics Research Corporation, 1998, NISA II / DISPLAY III User's Manual, EMRC, Michigan
- Fleck, N. A., Shin, C. S. and Smith, R. A., 1985, FCG under Compressive Loading, *Engineering Fracture Mechanics*, Vol. 21(1), 173-185
- Gallagher, J. P., 1974, A Generalized Development of Yield-zone Models, AFFDL-TM-74-28, Air Force Flight Dynamics Laboratory, Wright-Patterson Air Force Base, Ohio
- Guo, W., Wang, C. H. and Rose, L. R. F., 1999, The Influence of Cross-sectional Thickness on FCG, *Fatigue and Fracture of Engineering Materials and Structures*, V. 22, 437-444
- Hammouda. M. M., Ahmad, S. S. E., Sherbini, A. S. and Sallam, H. E. M., 1998, Deformation Behavior at the Tip of a Physically Short Fatigue Crack due to a Single Overload, *Fatigue and Fracture of Engineering Materials and Structures*, V. 22, 145-151
- Harrison, H.R., Nettleton, T., 1997, *Advanced Engineering Dynamics*, John Wiley & Sons, New York, USA
- Harter, J. A., 2008, AFGROW Users Guide and Technical Manual (V.4.0012.15), Technical Memorandum, AFRL-VA-WP-TR-2008, Air Force Research Laboratory, Wright-Patterson AFB, OH
- Harter, J. A., 1994, MODGRO Users Manual (V. 1.2), Technical Memorandum, AFWAL-TM-88-157-FIBE, AFWAL Flight Dynamics Laboratory, Wright-Patterson AFB, OH
- Hermann, R., 1994, Fatigue Crack Growth in Ductile Materials under Cyclic Compressive Loading, *Fatigue and Fracture of Engineering Materials and Structures*, Vol. 17(1), 93-103
- Hertzberg, R. W., 1996, *Deformation and Fracture Mechanics of Engineering Materials*, Forth edition, John Wiley & Sons Inc.



Hertzberg, R. W., 1995, Deformation and Fracture Mechanics of Engineering Materials, Fourth edition, John Wiley

Hudson, C. M., 1981, "A Root-Mean-Square Approach for Predicting Fatigue Crack Growth under Random Loading," Methods and Models for Predicting Fatigue Crack Growth under Random Loading, ASTM STP 748, J. B. Chang and C.M. Hudson, Eds., American Society for Testing and Materials, pp. 41-52.

Iranpour, M. and Taheri, F., 2012a, Applicability of Equivalent Constant Amplitude Loading for Assessing the Fatigue Life of Pipelines and Risers and the Influence of Compressive Stress Cycles, Accepted for Publication in the Journal of Pressure Vessel Technology

Iranpour, M. and Taheri, F., 2012b, On the effect of stress intensity factor in evaluating the fatigue crack growth rate of aluminum alloy under the influence of compressive stress cycles, International Journal of Fatigue, Vol. 43, pp. 1-11

Iranpour M., Taheri, F. and Vandiver J. K., 2008, Structural Life Assessment of Oil and Gas Risers under Vortex-induced Vibration, Journal of Marine Structures Vol. 21, 353-373.

Iranpour, M. and Taheri, F., 2007, An Experimental Investigation into Fatigue Characterization of Oil Platform Risers under Variable Amplitude Loading, Proceedings of PVP2007, ASME PVP 2007/CREEP 8 Conference, July 22-26, 2007, San Antonio, Texas

Iranpour, M. and Taheri, F., 2006a, The State-of-the-art Review of Riser's VIV Fatigue, OMAE2006-92636, 25th International Conference on Offshore Mechanics and Arctic Engineering, CFD and VIV Symposium, June 4-9, 2006, Hamburg, Germany.

Iranpour, M. and Taheri, F., 2006b, A Study on Crack Front Shape and the Correlation between the Stress Intensity Factors of a Pipe Subject to Bending and a Plate Subject to Tension, Journal of Marine Structures, Vol. 19, n. 4, 193-216.

Irwin, M. A., 1957, Analysis of Stresses and Strains near the end of a Crack Traversing a Plate, Journal of Applied Mechanics, V. 24, 361-364

- Jacoby, G., 1966, Application of Microfractography to the Study of Crack Propagation under Fatigue Stresses, AGARD Report 541, Paris; 1966.
- Jensen, J. C. 1999. Ultimate Strength and Fatigue Analysis of Metallic Catenary Risers. M. Sc. thesis at Stavanger University College for JP Kenny A/ S
- Johannesson, P., 2002, On Rainflow Cycles and the Distribution of the Number of Interval Crossing by a Markov Chain, Probabilistic Engineering Mechanics, V. 17, 123-130.
- Jones, O. and Wei, R. P., 1971, An exploratory study of delay in FCG, International Journal of Fracture, Vol. 7, 116-118.
- Kasaba, K., Sano, T., Kudo, S., Shoji, T., Katagiri, K. and Sato T., 1998, FCG under Compressive Loading, Journal of Nuclear Materials, Vol. 258–263, N. pt B, 2059-2063.
- Kim, J. H. and Lee, S. B., 2000, Fatigue Crack Opening Stress based on the Strip-yield Model, Theoretical and Applied Fracture Mechanics, V. 34, 73-84
- Kim, J. H., Lee, S. B. and Hong, S. G., 2003, Fatigue Crack Growth Behavior of AL7050-T7451 Attachment Lugs under Flight Spectrum Variation, Theoretical and Applied Fracture Mechanics, V. 40, 135-144
- Kim, J. H. and Hwang, I. S. 1997, Crack shape evolution of surface flaws under fatigue loading of austenitic pipes, Nuclear Engineering and Design, 174, 17-24
- Kujawski, D. and Stoychev, S., 2010, Effects of Spectrum Modification on Fatigue Crack Growth, Fatigue & Fracture of Engineering Materials & Structures, V. 33, pp 161-173.
- Landes, J., Lee, K., Bose, W. W., Ito, H. 2001. Evaluation of fatigue lives of steel catenary risers, 20<sup>th</sup> International Conference on Offshore Mechanics and Arctic Engineering - OMAE, p 111-118
- Larsen, C. M., Vikestad, K., Yttervik, R., and Passano, E. VIVANA Theory manual. 2000. Norwegian Marine Technology Research Institute.
- Lee, E. U., Glinka, G., Vasudevan, A. K., Lyyer, N. and Phan, N.D. 2009, Fatigue of 7075-T651 Aluminum Alloy under Constant and Variable Amplitude Loading, International Journal of Fatigue, Vol. 31, 1858-1864.

- Lei, Y., 2004, J-integral and limit load analysis of semi-elliptical surface cracks in plates under tension, *International Journal of Pressure Vessels and Piping*, 81, 21-30
- Li, X., Bose, N., Zhu, L. and Spencer, D., 2005, Multi-modal Vortex-induced Vibration Tests on a Flexible Model Riser, *International Symposium on Technology of Ultra Deep Ocean Engineering*, Tokyo, Japan, Feb. 1-2.
- Li, X., 2005, Identification of Linear and Non-linear Multi-Modal VIV Responses for Flexible Deepwater Risers, PhD. Thesis, Faculty of Engineering and Applied Science, Memorial University of Newfoundland, November 2005.
- Lie, H., Larsen, C. M. and Tvei, 2001, Vortex Induced Vibration Analysis of Centenary Risers, *The Proceedings of Offshore Technology Conference*, V. 2, Houston, U.S.A.
- Liu A. F., *Structural Life Assessment Methods*, The Materials Information Society, 1998
- Lugg M. C. 1992, *An Introduction to AC Potential Drop (ACPD)*, Technical Software Consultants Ltd., United Kingdom
- Lyons, G. L., Patel, M. H., Witz, J. A. 1994. *Vertical riser design manual*. Bentham Press, London.
- Maher, J., and Finn, L. 2000, A combined time-frequency domain procedure to estimate riser fatigue caused by heave-induced vortex-induced vibration. *Offshore Technology Conf.*, Paper No.11994.
- Makabe, C., Purnowidodo, A. and McEvily, A. J., 2004, Effects of Surface Deformation and Crack Closure on Fatigue Crack Propagation after Overloading and Underloading, *International Journal of Fatigue*, Vol. 26, 1341-1348.
- Matsuoka, S., Masuda, H. and Shimodaira, M., 1990, Fatigue threshold and low-rate crack propagation properties for structural steels in 3 pct sodium chloride aqueous solution, *Metallurgical Transactions A (Physical Metallurgy and Materials Science)*, Vol. 21A, N. 8, 2189-2199.
- McColl, C. and Phan, N., 2007, Measured Gust Cycle Clustering Effects and the Implications on Aircraft Fatigue and Damage Tolerance, *10th Joint FAA/DoD/NASA Conference on Aging Aircraft*

- McEvily, A. J., 1997, Fatigue Crack Threshold, ASM Handbook, Fatigue and Fracture, The Materials Information Society, Vol. 19, 134-152.
- Mikheevskiy, S. and Glinka, G., 2009, Elastic–plastic fatigue crack growth analysis under variable amplitude loading spectra, *International Journal of Fatigue*, V. 31, pp 1828–1836.
- Miranda, A. C. O., Meggiolaro, M. A., Castro, J. T. P. and Martha, L. F., 2003, Fatigue Life Prediction of Complex 2D Components under Mixed-mode Variable Amplitude Loading, *International Journal of Fracture*, V. 25, 1157-1167
- Nagode, M., Klemenc, J. and Fajdiga, M., 2001, Parametric Modeling and Scatter Prediction of Rainflow Matrices, *International Journal of Fatigue*, V. 23, 525-532.
- Newman, James, Jr., Schneider, J., Daniel, A. and Dustin, M., 2005, Compression Pre-cracking to Generate Near Threshold Fatigue-crack Growth Rates in Two Aluminum Alloys, *International Journal of Fatigue*, Vol. 27, 1432-1440.
- Newman, J. C., 1984, A Crack Opening Stress Equation for FCG, *International Journal of Fracture*, Vol. 24, R131-R135.
- Newman J. C. and Raju, I. S., 1981, An empirical stress intensity factor equation for the surface crack, *Engineering Fracture Mechanics*, 15, 185- 192
- Noroozi, A. H., Glinka, G. and Lambert. S., 2008, Prediction of fatigue crack growth under constant amplitude loading and a single overload based on elasto-plastic crack tip stresses and strains, *Engineering Fracture Mechanics*, V. 75, 188-206.
- Noroozi, A. H., Glinka, G. and Lambert. S., 2005, A two parameter driving force for fatigue crack growth analysis, *International Journal of Fatigue*, V. 27, 1277–1296.
- Odahara, S. Murakami, Y. Inoue, M. and Sueoka, A., 2005, Fatigue Failure by In-line Flow-induced Vibration and Fatigue Life Evaluation, *JSME International Journal, Series A*, Vol. 48, No. 2, 109-177.
- Panontin, T. L., Makino, A. and Williams, J. F., 2000, Crack Tip Opening Displacement Estimation for C(T) Specimens, *Engineering Fracture Mechanics*, V. 67, 293-301

- Pantelakis, Sp. G., Kermanidis, Al. Th. and Daglaras, P. G., 1997, Crack-growth analysis code for assessing fatigue life of 2219 T851 aluminum specimens under aircraft structure service spectra, *Theoretical and Applied Fracture Mechanics*, Vol. 28. N. 2, 1-12.
- Pereira, M. V. S., Darwish, F. A. I., Camarao, A. F. and Motta, S. H., 2007, On the Prediction of Fatigue Crack Retardation Using Wheeler and Willenborg Models, *Material Research*,
- Pommier, S., 2003, Cyclic Plasticity and Variable Amplitude Fatigue, *International Journal of Fatigue*, Vol. 25, 983-997.
- Pommier S., 2002, Plane strain crack closure and cyclic hardening. *Engineering Fracture Mechanics*, V. 69, 25–44
- Pommier S. And Bompard P., 1999, Bauschinger effect of alloys and plasticity-induced crack closure: a finite element analysis. *Fatigue and Fracture of Engineering Materials and Structures*, V. 23, 129–39
- Pook, L. P. and Greenan, A. F., 1979, The effect of narrow-band random loading on the high cycle fatigue strength of edge-cracked mild steel plates, *International Journal of Fatigue*, V. 1(1), 17-22
- Radayev, Y.N. and Stepanova, L.V., 2001, On the effect of the residual stresses on the crack opening displacement in a cracked sheet, *International Journal of Fracture*, Vol. 107 (4), 329-360.
- Radon, J. C., 1979, Influence of Environment on Threshold in Fatigue Crack Growth, *Metal science*, Vol. 13, No. 7, 411-419.
- Ragazzo C., Hertzberg R.W. and Jaccard R., 1995, A method for generating fatigue marker bands using a constant  $K_{max}$  test procedure, *ASTM J Test Eval.*, 23, 19–26
- Raju I. S and Newman J. C. 1979, Stress intensity factors for a wide range of semi-elliptical surface cracks in finite-thickness plates, *Engineering Fracture Mechanics*, 11, 817- 829
- Ravichandran K. S., 1997, Effect of Crack Shape on Crack Growth, *ASM Handbook, Fatigue and Fracture*, The Materials Information Society, 19

- Reis, L., Fonseca, A. and De Freitas, M., 2004, Methodology for Fatigue Life Assessment of the Structural Integrity of Fighter Aircraft, *Fatigue & Fracture of Engineering Materials & Structures*, Vol. 27, 873-877.
- Rose, L. R. F. and Wang, C. H., 2001, Self-similar Analysis of Plasticity-induced Closure of Small Fatigue Cracks, *Journal of the Mechanics and Physics of Solids*, V. 49, 401-429
- Rushton P. A. and Taheri, F., 2005, Fatigue response and characterization of 350WT steel under semi-random loading, Accepted for publication in ASME journal of PVT, Oct 2005.
- Rushton, P. A. and Taheri, F., 2003, Prediction of Variable Amplitude Crack Growth in 350WT Steel Using a Modified Wheeler Approach, *Marine Structures*, Vol. 16, N. 7, 517-539.
- Rushton, Pa. and Taheri, F., 2003, Prediction of crack growth in 350WT steel subjected to constant amplitude with over- and under-loads using a modified wheeler approach, *Marine Structures*, 16, Issue 7 , September-October 2003, 517-539.
- Sadananda, K., Vasudevan, A.K. Holtz, R.L. and Lee, E. U., 1999, Analysis of overload effects and related phenomena, *International Journal of Fatigue*, Vol. 21, 233-246.
- Saka M., Sato I. and Abe H., 1997, NDE of 3-D surface crack using magnetic field induced by DC current flow, *NDT E Int.*, 31, 325–328.
- Sarpkaya, T. 1979. Vortex-induced oscillations, a selective review. *Journal of applied mechanics* 46 241-258.
- Schijve, J., 1962, *Fatigue Crack Propagation in Light Alloy Sheet Material and Structures*, *Advances in Aeronautical Sciences*, V. 62. Oxford: Pergamon Press, 387–408.
- Schijve, J. and Hoeymakers, A. H. W., 1979, Fatigue crack growth in lugs, *Fatigue of Engineering Materials and Structures*, V. 1, 185–201
- Serta, O. B., Sphaier, S. H., Fernandes, A. C. 2000. Fatigue design of risers: An improved methodology incorporating a transverse hydrodynamic force model., *Proceedings of the 10<sup>th</sup> International Offshore and Polar Engineering Conference*, Seattle, USA, June 2000, pp 49-53.

- Shabanov, 2005, Mechanism of Fatigue-crack Growth under Compressive External Stresses, *Journal of Applied Mechanics and Technical Physics*, Vol. 46, No. 6, 861-866.
- Sheu, B. C. and Song, P. S., 1995, Shaping Exponent in Wheeler Model under a Single Overload, *Engineering Fracture Mechanics*, Vol. 51, No. 1, 135-143.
- Shin C.S. and Cai C.Q., 2004, Experimental and finite element analyses on stress intensity factors of elliptical surface crack in a circular shaft under tension and bending, *International Journal of Fracture*, 129, 239–64
- Shows, D., Liu, A. F., and FitzGerald, J.H., 1983, Application of Resistance Curves to Crack at a Hole, *Fracture Mechanics: Fourteenth Symposium*, Vol. II, Testing and Applications, STP 791, American Society of Testing and Materials, 78-100.
- Shukla A., 2005, *Practical Fracture Mechanics in Design*, Second Edition, Marcel Dekker, New York
- Silva, F. S., 2005, The Importance of Compressive Stresses on Fatigue Crack Propagation Rate, *International Journal of Fatigue*, Vol. 27, 1441-1452.
- Silva, F. S., 2004, Crack Closure inadequacy at Negative Stress Ratios, *International Journal of Fatigue*, V. 16, 241-252
- Soboyejo, W. O. and Knott, J. F., 1990, An Investigation of Environmental Effects on Fatigue Crack Growth in Q1N(HY80) Steel, *Metallurgical Transactions*, Vol. 21A, No. 11, 2977-1983.
- Song P. S., Sheu B. C. and Shieh Y. L., 2002, Prediction of semi-elliptical surface crack growth in 2024-T4 aluminum alloy, *International journal of pressure vessels and piping*, 79, 273-278
- Stephens, R. I., Fatemi, A., Stephens, R. R. and Fuchs, H. O., 2001, *Metal Fatigue in Engineering*, John Wiley & Sons, New York, USA
- Sunder, R., 2003, Spectrum Load Fatigue – Underlying Mechanisms and Significance in Testing and Analysis, *International Journal of Fatigue*, Vol. 25, 971-981.
- Suresh, S., 1985, Crack Initiation in Cyclic Compression and its Applications, *Engineering Fracture Mechanics*, 1985. Vol. 21(3), 453-463.

- Sutton, M. A., Deng, X., Ma, F., Newman, J. C. and James, M., 2000, Development and Application of a Crack Tip Opening Displacement-based Mixed Mode Fracture Criteria, *International Journal of Solids and Structures*, V. 37, 3591-3618
- Taheri, F., Trask, D., and Pegg, N., 2002, Experimental and analytical investigation of fatigue characteristics of 350WT steel under constant and variable amplitude loadings. *Marine Structures*, 16, 69-91
- Tan, C.L. and Shim, M.L. 1986, Stress Intensity factor influence coefficients for internal surface cracks in thick-walled cylinders, *International Journal of Pressure Vessel and Piping*, 24, 49-72
- Tanaka, K. and Nakai, Y., 1983, Mechanics of Growth Threshold of Small Fatigue Cracks, In: Davidson, D.L., Suresh, S., FCG Threshold Concepts, the Metallurgical Society of AIME, 497-516
- Tomkins, B., 1975, The Development of Fatigue Crack Propagation Models, *Journal of Engineering Materials and Technology*, V. 97, 289-298
- Toribio, J. and Kharin, V., 2009, Finite-deformation Analysis of the Crack-tip Fields under Cyclic Loading, *International Journal of Solids and Structures*, V. 46, 1937-1952
- Torres, L. A. L. F., Mourelle, M. M., De Siqueira, M. Q., Ellwanger, G. B., 1997, Random fatigue analysis of a steel catenary riser in frequency and time domain. *Proceedings of the International Symposium on Offshore Engineering* 361-374.
- Torres, L. A. L. F., Mourelle, M. M., Silva, R. M. C., 2001, Fatigue damage verification of steel catenary risers. *20th International Conference on Offshore Mechanics and Arctic Engineering*, Brazil, 749-759.
- Varvani-Farahani A., Topper T.H., 1997, Short fatigue crack characterization and detection using confocal scanning laser microscopy (CSLM). Nontraditional method of sensing stress, strain, and damage in materials and structures. *ASTM STP*, 1318, 43–55.
- Vandiver, J.K., Swithenbank, S.B., Jaiswal, V. , & Jhingran V., 2006, Fatigue damage from high mode number vortex-induced vibration, OMAE2006-9240, *Proceedings of the 25th International Conference on Offshore Mechanics and Arctic Engineering*, June 4-9, Hamburg, Germany.



- Vandiver J.K., Marcollo, H., Swithenbank, S., Jhingran, V., 2005, High mode number vortex-induced vibration field experiments, OTC Paper Number 17383, Offshore Technology Conference, Houston, TX, USA; 2–5 May.
- Vandiver J.K. and Li, L., 2005, SHEAR7 V4.4 Program Theoretical Manual, Department of Ocean Engineering, Massachusetts Institute of Technology.
- Vandiver, J. K., Swithenbank, S., Jaiswal, V. and Marcollo, H., 2003, The Effectiveness of Helical Strakes in the Suppression of High-Mode-Number VIV, Offshore Technology Conference, Huston, Texas, 1-4 May 2006
- Vandiver, J. K., Peoples, W. W., 2003, The Effect of Staggered Buoyancy Modules on Flow-Induced Vibration of Marine Risers, Offshore Technology Conference, Houston, Texas, U.S.A., 5–8 May.
- Vandiver, J.K., 1993, Dimensionless parameters important to the prediction of vortex-induced vibration of long, flexible cylinders in ocean currents, *Journal of Fluids and Structures*, July.
- Vandiver, J.K. and Chung, T-Y., 1988, Predicted and Measured Response of Flexible Cylinders in Sheared Flow, *Proc., ASME, Winter Annual Meeting Symposium on Flow-Induced Vibration*, Chicago, December.
- Vasudevan, A.K. and Sadananda, K., 2001, Analysis of FCG under Compression-Compression Loading, *International Journal of Fatigue*, Vol. 21, S365-S374
- Veers, P., 1997, Statistical Consideration in Fatigue, *ASM Handbook, Fatigue and Fracture*, The Materials Information Society, Vol. 19, 295-302.
- Walker, N. and Beevers, C. J., 1979, Fatigue Crack Closure Mechanism in Titanium, *Fatigue of Engineering Materials and Structure*, V. 1 (1), 135-148
- Walker, K., 1970, The Effect of Stress Ratio during Crack Propagation and Fatigue for 2024-T3 and 7075-T69 Aluminum, *ASTM STP 462*, pp. 1-14.
- Wang, C.H., Barter, S. A., Liu, Q., 2003, A Closure Model to Crack Growth under Large-scale Yielding and Through Residual Stress Fields, *Journal of Engineering Materials and Technology*, V. 125, 183-190

- Wang, C.H., Rose, L. R. F. and Newman Jr., J. C., 2001, Closure of Plane-strain Cracks under Large-scale Yielding Conditions, *Journal of Fatigue and Fracture of Engineering Materials and Structures*, V. 25, 127-139
- Wanhill, R.J.H., 2002, Flight simulation fatigue crack growth guidelines, National Aerospace Laboratory of the Netherlands, NLR-TP-2001-545
- Wanhill, R. J. H., 1994, Flight simulation fatigue crack growth testing of aluminum alloys - Specific issues and guidelines, *International Journal of Fatigue*, V. 16 (2), 99-110
- Wells, A.A., 1961, Unstable Crack Propagation in Metals – Cleavage and Fast Fracture: Cranfield Crack Propagation Symposium, V. 1, September 1961, P. 210
- Wheeler, O.E., 1972, Spectrum Loading and Crack Growth, *Journal of Basic Engineering*, 181-186
- Willenborg, J. Engle, R. M. and Wood, H. A., 1971, A Crack Growth Retardation Model using an Effective Stress Concept, Report No. AFFDL-TR71-1, Air Force Flight Dynamic Laboratory, Wright-Patterson Air Force Base, USA
- Wirshing, P. H. and Wu, Y. T. 1985, Probabilistic and Statistical Methods for Fatigue Analysis and Design, Pressure Vessel and Piping Technology Conference – 1985: A Decade of Progress, American Society of Mechanical Engineers, 793-819.
- Wu Sh.X. 1985, Shape change of surface crack during fatigue growth, *Engineering Fracture Mechanics*, 22 (5), 897-913
- Wu, W. F. and Ni, C. C., 2007, Statistical aspects of some fatigue crack growth data *Engineering Fracture Mechanics*, V. 74 (18), 2952-2963
- Wu, W. F., Liou, H. Y. and Tse, H. C., 1997, Estimation of fatigue damage and fatigue life of components under random loading, *The International Journal of Pressure Vessels and Piping*, V. 72 (3), 243-249
- Wu, W. F. and Huang, T. H., 1993, Prediction of fatigue damage and fatigue life under random loading, *The International Journal of Pressure Vessels and Piping*, V. 53 (2), 273-298

- Yen S. and Penndleberry S. L., 1962, Technique for making shallow cracks in sheet metals, *Material Research Standard*, 2 (11), 913–916
- Yuen, B. K. C., 2007, *An Investigation Into Fatigue Crack Propagation In Stiffened and Unstiffened 350WT Steel Ship Plating Subjected to Variable Amplitude Loading*, Ph.D. Thesis, Dalhousie University, Halifax, NS
- Yuen, B. K. C. and F. Taheri, 2005, Proposed modifications to the Wheeler retardation model for multiple overloading fatigue life prediction, *International Journal of Fatigue*, Vol. 28, No. 12, Sep 21, 1803-1819.
- Yuen, B. K. C. and F. Taheri, 2004, The effects of loading frequency, tensile overload and compressive underload on the fatigue crack propagation behavior of polymethyl methacrylate, *Polymer Testing*, Vol. 23, 491–500.
- Zhang, J., He. X. D. and Du, S. Y., 2007, Analysis of the Effects of Compressive Stresses on Fatigue Crack Propagation Rate, *International Journal of Fatigue*, Vol. 29, 1751-1756.
- Zhang, J. Z., Halliday, M. D., Bowen, P. and Poole, P., 1999, Three Dimensional Elastic-plastic Element Modeling of Small FCG under a Single Tensile Overload, *Journal of Engineering Fracture Mechanics*, Vol. 63, 229-251

## **Appendix A**

### **Copyright Agreement Forms**

#### A.1. Copyright Agreement Form for Chapter 2

----- Message from DarchiB@asme.org -----

Date: Tue, 11 Sep 2012 15:15:03 +0000

From: Beth Darchi <DarchiB@asme.org>

Subject: RE: RE: Request for Publication in Ph.D. Thesis

To: 'Mohammad Iranpour' <Iranpour@dal.ca>

Dear Mr. Iranpour:

It is our pleasure to grant you permission to use any part or all of the ASME paper "The State-of-the-Art Review of Risers' VIV Fatigue," by Mohammad Iranpour and Farid Taheri, Paper no. OMAE2006-92636, as cited in your letter for inclusion in a Ph.D Thesis entitled FATIGUE CHARACTERIZATION OF RISERS AND PIPELINES UNDER REALISTIC VARIABLE AMPLITUDE LOADING AND THE INFLUENCE OF COMPRESSIVE STRESS CYCLES in Structural Engineering at Dalhousie University in Halifax, Nova Scotia, Canada.

Permission is granted for the specific use as stated herein and does not permit further use of the materials without proper authorization. Proper attribution must be made to the author(s) of the materials, and no alterations of the materials is permitted in any material manner.

As is customary, we request that you ensure full acknowledgment of this material, the author(s), source and ASME as original publisher. Acknowledgment must be retained on all pages printed and distributed.

Many thanks for your interest in ASME publications.

Sincerely,  
Beth Darchi  
Permissions & Copyrights  
ASME, 3 Park Avenue  
New York, NY 10016  
T: 212-591-7700  
F: 212-591-7841  
E: [darchib@asme.org](mailto:darchib@asme.org)

## A.2. Copyright Agreement Form for Chapter 3

**ELSEVIER LICENSE  
TERMS AND CONDITIONS**

Aug 13, 2012

---

This is a License Agreement between Mohammad Iranpour ("You") and Elsevier ("Elsevier") provided by Copyright Clearance Center ("CCC"). The license consists of your order details, the terms and conditions provided by Elsevier, and the payment terms and conditions.

**All payments must be made in full to CCC. For payment instructions, please see information listed at the bottom of this form.**

Supplier	Elsevier Limited The Boulevard, Langford Lane Kidlington, Oxford, OX5 1GB, UK
Registered Company Number	1982084
Customer name	Mohammad Iranpour
Customer address	1203 - 1200 W. Georgia Street Vancouver, BC V6E 4R2
License number	2964510321657
License date	Aug 08, 2012
Licensed content publisher	Elsevier
Licensed content publication	Marine Structures
Licensed content title	A study on crack front shape and the correlation between the stress intensity factors of a pipe subject to bending and a plate subject to tension
Licensed content author	Mohammad Iranpour, Farid Taheri
Licensed content date	October 2006
Licensed content volume number	19
Licensed content issue number	4
Number of pages	24

Start Page	193
End Page	216
Type of Use	reuse in a thesis/dissertation
Intended publisher of new work	other
Portion	full article
Format	both print and electronic
Are you the author of this Elsevier article?	Yes
Will you be translating?	No
Order reference number	None
Title of your thesis/dissertation	FATIGUE CHARACTERIZATION OF RISERS AND PIPELINES UNDER REALISTIC VARIABLE AMPLITUDE LOADING AND THE INFLUENCE OF COMPRESSIVE STRESS CYCLES
Expected completion date	Sep 2012
Estimated size (number of pages)	300
Elsevier VAT number	GB 494 6272 12
Permissions price	0.00 USD
VAT/Local Sales Tax	0.0 USD / 0.0 GBP
<b>Total</b>	<b>0.00 USD</b>
<b>Terms and Conditions</b>	

#### INTRODUCTION

1. The publisher for this copyrighted material is Elsevier. By clicking "accept" in connection with completing this licensing transaction, you agree that the following terms and conditions apply to this transaction (along with the Billing and Payment terms and conditions established by Copyright Clearance Center, Inc. ("CCC"), at the time that you opened your Rightslink account and that are available at any time at <http://myaccount.copyright.com>).

#### GENERAL TERMS

2. Elsevier hereby grants you permission to reproduce the aforementioned material subject to the terms and conditions indicated.
3. Acknowledgement: If any part of the material to be used (for example, figures) has appeared in our publication with credit or acknowledgement to another source, permission must also be sought from that source. If such permission is not obtained then that



material may not be included in your publication/copies. Suitable acknowledgement to the source must be made, either as a footnote or in a reference list at the end of your publication, as follows:

“Reprinted from Publication title, Vol /edition number, Author(s), Title of article / title of chapter, Pages No., Copyright (Year), with permission from Elsevier [OR APPLICABLE SOCIETY COPYRIGHT OWNER].” Also Lancet special credit - “Reprinted from The Lancet, Vol. number, Author(s), Title of article, Pages No., Copyright (Year), with permission from Elsevier.”

4. Reproduction of this material is confined to the purpose and/or media for which permission is hereby given.

5. Altering/Modifying Material: Not Permitted. However figures and illustrations may be altered/adapted minimally to serve your work. Any other abbreviations, additions, deletions and/or any other alterations shall be made only with prior written authorization of Elsevier Ltd. (Please contact Elsevier at [permissions@elsevier.com](mailto:permissions@elsevier.com))

6. If the permission fee for the requested use of our material is waived in this instance, please be advised that your future requests for Elsevier materials may attract a fee.

7. Reservation of Rights: Publisher reserves all rights not specifically granted in the combination of (i) the license details provided by you and accepted in the course of this licensing transaction, (ii) these terms and conditions and (iii) CCC's Billing and Payment terms and conditions.

8. License Contingent Upon Payment: While you may exercise the rights licensed immediately upon issuance of the license at the end of the licensing process for the transaction, provided that you have disclosed complete and accurate details of your proposed use, no license is finally effective unless and until full payment is received from you (either by publisher or by CCC) as provided in CCC's Billing and Payment terms and conditions. If full payment is not received on a timely basis, then any license preliminarily granted shall be deemed automatically revoked and shall be void as if never granted. Further, in the event that you breach any of these terms and conditions or any of CCC's Billing and Payment terms and conditions, the license is automatically revoked and shall be void as if never granted. Use of materials as described in a revoked license, as well as any use of the materials beyond the scope of an unrevoked license, may constitute copyright infringement and publisher reserves the right to take any and all action to protect its copyright in the materials.

9. Warranties: Publisher makes no representations or warranties with respect to the licensed material.

10. Indemnity: You hereby indemnify and agree to hold harmless publisher and CCC, and their respective officers, directors, employees and agents, from and against any and all claims arising out of your use of the licensed material other than as specifically authorized pursuant to this license.

11. No Transfer of License: This license is personal to you and may not be sublicensed, assigned, or transferred by you to any other person without publisher's written permission.

12. No Amendment Except in Writing: This license may not be amended except in a writing signed by both parties (or, in the case of publisher, by CCC on publisher's behalf).

13. Objection to Contrary Terms: Publisher hereby objects to any terms contained in any purchase order, acknowledgment, check endorsement or other writing prepared by you, which terms are inconsistent with these terms and conditions or CCC's Billing and

Payment terms and conditions. These terms and conditions, together with CCC's Billing and Payment terms and conditions (which are incorporated herein), comprise the entire agreement between you and publisher (and CCC) concerning this licensing transaction. In the event of any conflict between your obligations established by these terms and conditions and those established by CCC's Billing and Payment terms and conditions, these terms and conditions shall control.

14. **Revocation:** Elsevier or Copyright Clearance Center may deny the permissions described in this License at their sole discretion, for any reason or no reason, with a full refund payable to you. Notice of such denial will be made using the contact information provided by you. Failure to receive such notice will not alter or invalidate the denial. In no event will Elsevier or Copyright Clearance Center be responsible or liable for any costs, expenses or damage incurred by you as a result of a denial of your permission request, other than a refund of the amount(s) paid by you to Elsevier and/or Copyright Clearance Center for denied permissions.

#### **LIMITED LICENSE**

The following terms and conditions apply only to specific license types:

15. **Translation:** This permission is granted for non-exclusive world **English** rights only unless your license was granted for translation rights. If you licensed translation rights you may only translate this content into the languages you requested. A professional translator must perform all translations and reproduce the content word for word preserving the integrity of the article. If this license is to re-use 1 or 2 figures then permission is granted for non-exclusive world rights in all languages.

16. **Website:** The following terms and conditions apply to electronic reserve and author websites:

**Electronic reserve:** If licensed material is to be posted to website, the web site is to be password-protected and made available only to bona fide students registered on a relevant course if:

This license was made in connection with a course,

This permission is granted for 1 year only. You may obtain a license for future website posting,

All content posted to the web site must maintain the copyright information line on the bottom of each image,

A hyper-text must be included to the Homepage of the journal from which you are licensing at <http://www.sciencedirect.com/science/journal/xxxxx> or the Elsevier homepage for books at <http://www.elsevier.com> , and

Central Storage: This license does not include permission for a scanned version of the material to be stored in a central repository such as that provided by Heron/XanEdu.

17. **Author website** for journals with the following additional clauses:

All content posted to the web site must maintain the copyright information line on the bottom of each image, and the permission granted is limited to the personal version of your paper. You are not allowed to download and post the published electronic version of your article (whether PDF or HTML, proof or final version), nor may you scan the printed edition to create an electronic version. A hyper-text must be included to the Homepage of the journal from which you are licensing at <http://www.sciencedirect.com/science/journal/xxxxx> . As part of our normal production process, you will receive an e-mail notice when your article appears on Elsevier's online

service ScienceDirect ([www.sciencedirect.com](http://www.sciencedirect.com)). That e-mail will include the article's Digital Object Identifier (DOI). This number provides the electronic link to the published article and should be included in the posting of your personal version. We ask that you wait until you receive this e-mail and have the DOI to do any posting.

Central Storage: This license does not include permission for a scanned version of the material to be stored in a central repository such as that provided by Heron/XanEdu.

18. **Author website** for books with the following additional clauses: Authors are permitted to place a brief summary of their work online only. A hyper-text must be included to the Elsevier homepage at <http://www.elsevier.com>. All content posted to the web site must maintain the copyright information line on the bottom of each image. You are not allowed to download and post the published electronic version of your chapter, nor may you scan the printed edition to create an electronic version.

Central Storage: This license does not include permission for a scanned version of the material to be stored in a central repository such as that provided by Heron/XanEdu.

19. **Website** (regular and for author): A hyper-text must be included to the Homepage of the journal from which you are licensing at <http://www.sciencedirect.com/science/journal/xxxxx>. or for books to the Elsevier homepage at <http://www.elsevier.com>

20. **Thesis/Dissertation**: If your license is for use in a thesis/dissertation your thesis may be submitted to your institution in either print or electronic form. Should your thesis be published commercially, please reapply for permission. These requirements include permission for the Library and Archives of Canada to supply single copies, on demand, of the complete thesis and include permission for UMI to supply single copies, on demand, of the complete thesis. Should your thesis be published commercially, please reapply for permission.

21. **Other Conditions**:

v1.6

**If you would like to pay for this license now, please remit this license along with your payment made payable to "COPYRIGHT CLEARANCE CENTER" otherwise you will be invoiced within 48 hours of the license date. Payment should be in the form of a check or money order referencing your account number and this invoice number RLNK500835092.**

**Once you receive your invoice for this order, you may pay your invoice by credit card. Please follow instructions provided at that time.**

**Make Payment To:  
Copyright Clearance Center  
Dept 001  
P.O. Box 843006  
Boston, MA 02284-3006**

**For suggestions or comments regarding this order, contact RightsLink Customer Support: [customercare@copyright.com](mailto:customercare@copyright.com) or +1-877-622-5543 (toll free in the US) or +1-978-646-2777.**

**Gratis licenses (referencing \$0 in the Total field) are free. Please retain this printable license for your reference. No payment is required.**

### A.3. Copyright Agreement Form for Chapter 4

**ELSEVIER LICENSE  
TERMS AND CONDITIONS**

Aug 13, 2012

---

This is a License Agreement between Mohammad Iranpour ("You") and Elsevier ("Elsevier") provided by Copyright Clearance Center ("CCC"). The license consists of your order details, the terms and conditions provided by Elsevier, and the payment terms and conditions.

**All payments must be made in full to CCC. For payment instructions, please see information listed at the bottom of this form.**

Supplier	Elsevier Limited The Boulevard, Langford Lane Kidlington, Oxford, OX5 1GB, UK
Registered Company Number	1982084
Customer name	Mohammad Iranpour
Customer address	1203 - 1200 W. Georgia Street Vancouver, BC V6E 4R2
License number	2964510074811
License date	Aug 08, 2012
Licensed content publisher	Elsevier
Licensed content publication	Marine Structures
Licensed content title	Structural life assessment of oil and gas risers under vortex-induced vibration
Licensed content author	Mohammad Iranpour, Farid Taheri, J. Kim Vandiver
Licensed content date	October 2008
Licensed content volume number	21
Licensed content issue number	4
Number of pages	21
Start Page	353
End Page	373

Type of Use	reuse in a thesis/dissertation
Intended publisher of new work	other
Portion	full article
Format	both print and electronic
Are you the author of this Elsevier article?	Yes
Will you be translating?	No
Order reference number	None
Title of your thesis/dissertation	FATIGUE CHARACTERIZATION OF RISERS AND PIPELINES UNDER REALISTIC VARIABLE AMPLITUDE LOADING AND THE INFLUENCE OF COMPRESSIVE STRESS CYCLES
Expected completion date	Sep 2012
Estimated size (number of pages)	300
Elsevier VAT number	GB 494 6272 12
Permissions price	0.00 USD
VAT/Local Sales Tax	0.0 USD / 0.0 GBP
<b>Total</b>	<b>0.00 USD</b>
<b>Terms and Conditions</b>	

#### INTRODUCTION

1. The publisher for this copyrighted material is Elsevier. By clicking "accept" in connection with completing this licensing transaction, you agree that the following terms and conditions apply to this transaction (along with the Billing and Payment terms and conditions established by Copyright Clearance Center, Inc. ("CCC"), at the time that you opened your Rightslink account and that are available at any time at <http://myaccount.copyright.com>).

#### GENERAL TERMS

2. Elsevier hereby grants you permission to reproduce the aforementioned material subject to the terms and conditions indicated.

3. Acknowledgement: If any part of the material to be used (for example, figures) has appeared in our publication with credit or acknowledgement to another source, permission must also be sought from that source. If such permission is not obtained then that material may not be included in your publication/copies. Suitable acknowledgement to the source must be made, either as a footnote or in a reference list at the end of your publication, as follows:

“Reprinted from Publication title, Vol /edition number, Author(s), Title of article / title of chapter, Pages No., Copyright (Year), with permission from Elsevier [OR APPLICABLE

SOCIETY COPYRIGHT OWNER].” Also Lancet special credit - “Reprinted from The Lancet, Vol. number, Author(s), Title of article, Pages No., Copyright (Year), with permission from Elsevier.”

4. Reproduction of this material is confined to the purpose and/or media for which permission is hereby given.

5. Altering/Modifying Material: Not Permitted. However figures and illustrations may be altered/adapted minimally to serve your work. Any other abbreviations, additions, deletions and/or any other alterations shall be made only with prior written authorization of Elsevier Ltd. (Please contact Elsevier at [permissions@elsevier.com](mailto:permissions@elsevier.com))

6. If the permission fee for the requested use of our material is waived in this instance, please be advised that your future requests for Elsevier materials may attract a fee.

7. Reservation of Rights: Publisher reserves all rights not specifically granted in the combination of (i) the license details provided by you and accepted in the course of this licensing transaction, (ii) these terms and conditions and (iii) CCC's Billing and Payment terms and conditions.

8. License Contingent Upon Payment: While you may exercise the rights licensed immediately upon issuance of the license at the end of the licensing process for the transaction, provided that you have disclosed complete and accurate details of your proposed use, no license is finally effective unless and until full payment is received from you (either by publisher or by CCC) as provided in CCC's Billing and Payment terms and conditions. If full payment is not received on a timely basis, then any license preliminarily granted shall be deemed automatically revoked and shall be void as if never granted. Further, in the event that you breach any of these terms and conditions or any of CCC's Billing and Payment terms and conditions, the license is automatically revoked and shall be void as if never granted. Use of materials as described in a revoked license, as well as any use of the materials beyond the scope of an unrevoked license, may constitute copyright infringement and publisher reserves the right to take any and all action to protect its copyright in the materials.

9. Warranties: Publisher makes no representations or warranties with respect to the licensed material.

10. Indemnity: You hereby indemnify and agree to hold harmless publisher and CCC, and their respective officers, directors, employees and agents, from and against any and all claims arising out of your use of the licensed material other than as specifically authorized pursuant to this license.

11. No Transfer of License: This license is personal to you and may not be sublicensed, assigned, or transferred by you to any other person without publisher's written permission.

12. No Amendment Except in Writing: This license may not be amended except in a writing signed by both parties (or, in the case of publisher, by CCC on publisher's behalf).

13. Objection to Contrary Terms: Publisher hereby objects to any terms contained in any purchase order, acknowledgment, check endorsement or other writing prepared by you, which terms are inconsistent with these terms and conditions or CCC's Billing and Payment terms and conditions. These terms and conditions, together with CCC's Billing and Payment terms and conditions (which are incorporated herein), comprise the entire agreement between you and publisher (and CCC) concerning this licensing transaction. In the event of any conflict between your obligations established by these terms and conditions and those established by CCC's Billing and Payment terms and conditions,



these terms and conditions shall control.

14. **Revocation:** Elsevier or Copyright Clearance Center may deny the permissions described in this License at their sole discretion, for any reason or no reason, with a full refund payable to you. Notice of such denial will be made using the contact information provided by you. Failure to receive such notice will not alter or invalidate the denial. In no event will Elsevier or Copyright Clearance Center be responsible or liable for any costs, expenses or damage incurred by you as a result of a denial of your permission request, other than a refund of the amount(s) paid by you to Elsevier and/or Copyright Clearance Center for denied permissions.

#### LIMITED LICENSE

The following terms and conditions apply only to specific license types:

15. **Translation:** This permission is granted for non-exclusive world **English** rights only unless your license was granted for translation rights. If you licensed translation rights you may only translate this content into the languages you requested. A professional translator must perform all translations and reproduce the content word for word preserving the integrity of the article. If this license is to re-use 1 or 2 figures then permission is granted for non-exclusive world rights in all languages.

16. **Website:** The following terms and conditions apply to electronic reserve and author websites:

**Electronic reserve:** If licensed material is to be posted to website, the web site is to be password-protected and made available only to bona fide students registered on a relevant course if:

This license was made in connection with a course,

This permission is granted for 1 year only. You may obtain a license for future website posting,

All content posted to the web site must maintain the copyright information line on the bottom of each image,

A hyper-text must be included to the Homepage of the journal from which you are licensing at <http://www.sciencedirect.com/science/journal/xxxxx> or the Elsevier homepage for books at <http://www.elsevier.com> , and

Central Storage: This license does not include permission for a scanned version of the material to be stored in a central repository such as that provided by Heron/XanEdu.

17. **Author website** for journals with the following additional clauses:

All content posted to the web site must maintain the copyright information line on the bottom of each image, and the permission granted is limited to the personal version of your paper. You are not allowed to download and post the published electronic version of your article (whether PDF or HTML, proof or final version), nor may you scan the printed edition to create an electronic version. A hyper-text must be included to the Homepage of the journal from which you are licensing at <http://www.sciencedirect.com/science/journal/xxxxx> . As part of our normal production process, you will receive an e-mail notice when your article appears on Elsevier's online service ScienceDirect ([www.sciencedirect.com](http://www.sciencedirect.com)). That e-mail will include the article's Digital Object Identifier (DOI). This number provides the electronic link to the published article and should be included in the posting of your personal version. We ask that you wait until you receive this e-mail and have the DOI to do any posting.

Central Storage: This license does not include permission for a scanned version of the

material to be stored in a central repository such as that provided by Heron/XanEdu.

18. **Author website** for books with the following additional clauses: Authors are permitted to place a brief summary of their work online only. A hyper-text must be included to the Elsevier homepage at <http://www.elsevier.com> . All content posted to the web site must maintain the copyright information line on the bottom of each image. You are not allowed to download and post the published electronic version of your chapter, nor may you scan the printed edition to create an electronic version.

Central Storage: This license does not include permission for a scanned version of the material to be stored in a central repository such as that provided by Heron/XanEdu.

19. **Website** (regular and for author): A hyper-text must be included to the Homepage of the journal from which you are licensing at <http://www.sciencedirect.com/science/journal/xxxxx>. or for books to the Elsevier homepage at <http://www.elsevier.com>

20. **Thesis/Dissertation**: If your license is for use in a thesis/dissertation your thesis may be submitted to your institution in either print or electronic form. Should your thesis be published commercially, please reapply for permission. These requirements include permission for the Library and Archives of Canada to supply single copies, on demand, of the complete thesis and include permission for UMI to supply single copies, on demand, of the complete thesis. Should your thesis be published commercially, please reapply for permission.

21. **Other Conditions**:

v1.6

**If you would like to pay for this license now, please remit this license along with your payment made payable to "COPYRIGHT CLEARANCE CENTER" otherwise you will be invoiced within 48 hours of the license date. Payment should be in the form of a check or money order referencing your account number and this invoice number RLNK500835087.**

**Once you receive your invoice for this order, you may pay your invoice by credit card. Please follow instructions provided at that time.**

**Make Payment To:**  
**Copyright Clearance Center**  
**Dept 001**  
**P.O. Box 843006**  
**Boston, MA 02284-3006**

**For suggestions or comments regarding this order, contact RightsLink Customer Support:**[customercare@copyright.com](mailto:customercare@copyright.com) or +1-877-622-5543 (toll free in the US) or +1-978-646-2777.

**Gratis licenses (referencing \$0 in the Total field) are free. Please retain this printable license for your reference. No payment is required.**

#### A.4. Copyright Agreement Form for Chapter 5

**Important Note:**

The Copyright Agreement Form for paper related to this chapter will have to be included in this dissertation after the paper is published by the journal.

It is noted that this dissertation cannot be distributed, used and/or published any time before the Copyright Agreement Form is obtained from the journal and subsequently included in this dissertation.

## A.5. Copyright Agreement Form for Chapter 6

**ELSEVIER LICENSE  
TERMS AND CONDITIONS**

Aug 13, 2012

---

This is a License Agreement between Mohammad Iranpour ("You") and Elsevier ("Elsevier") provided by Copyright Clearance Center ("CCC"). The license consists of your order details, the terms and conditions provided by Elsevier, and the payment terms and conditions.

**All payments must be made in full to CCC. For payment instructions, please see information listed at the bottom of this form.**

Supplier	Elsevier Limited The Boulevard, Langford Lane Kidlington, Oxford, OX5 1GB, UK
Registered Company Number	1982084
Customer name	Mohammad Iranpour
Customer address	1203 - 1200 W. Georgia Street Vancouver, BC V6E 4R2
License number	2964500966464
License date	Aug 08, 2012
Licensed content publisher	Elsevier
Licensed content publication	International Journal of Fatigue
Licensed content title	On the effect of stress intensity factor in evaluating the fatigue crack growth rate of aluminum alloy under the influence of compressive stress cycles
Licensed content author	Mohammad Iranpour, Farid Taheri
Licensed content date	October 2012
Licensed content volume number	43
Licensed content issue number	None
Number of pages	11

Start Page	1
End Page	11
Type of Use	reuse in a thesis/dissertation
Portion	full article
Format	both print and electronic
Are you the author of this Elsevier article?	Yes
Will you be translating?	No
Order reference number	None
Title of your thesis/dissertation	FATIGUE CHARACTERIZATION OF RISERS AND PIPELINES UNDER REALISTIC VARIABLE AMPLITUDE LOADING AND THE INFLUENCE OF COMPRESSIVE STRESS CYCLES
Expected completion date	Sep 2012
Estimated size (number of pages)	300
Elsevier VAT number	GB 494 6272 12
Permissions price	0.00 USD
VAT/Local Sales Tax	0.0 USD / 0.0 GBP
<b>Total</b>	<b>0.00 USD</b>
<b>Terms and Conditions</b>	

#### INTRODUCTION

1. The publisher for this copyrighted material is Elsevier. By clicking "accept" in connection with completing this licensing transaction, you agree that the following terms and conditions apply to this transaction (along with the Billing and Payment terms and conditions established by Copyright Clearance Center, Inc. ("CCC"), at the time that you opened your Rightslink account and that are available at any time at <http://myaccount.copyright.com>).

#### GENERAL TERMS

2. Elsevier hereby grants you permission to reproduce the aforementioned material subject to the terms and conditions indicated.
3. Acknowledgement: If any part of the material to be used (for example, figures) has appeared in our publication with credit or acknowledgement to another source, permission must also be sought from that source. If such permission is not obtained then that

material may not be included in your publication/copies. Suitable acknowledgement to the source must be made, either as a footnote or in a reference list at the end of your publication, as follows:

“Reprinted from Publication title, Vol /edition number, Author(s), Title of article / title of chapter, Pages No., Copyright (Year), with permission from Elsevier [OR APPLICABLE SOCIETY COPYRIGHT OWNER].” Also Lancet special credit - “Reprinted from The Lancet, Vol. number, Author(s), Title of article, Pages No., Copyright (Year), with permission from Elsevier.”

4. Reproduction of this material is confined to the purpose and/or media for which permission is hereby given.

5. Altering/Modifying Material: Not Permitted. However figures and illustrations may be altered/adapted minimally to serve your work. Any other abbreviations, additions, deletions and/or any other alterations shall be made only with prior written authorization of Elsevier Ltd. (Please contact Elsevier at [permissions@elsevier.com](mailto:permissions@elsevier.com))

6. If the permission fee for the requested use of our material is waived in this instance, please be advised that your future requests for Elsevier materials may attract a fee.

7. Reservation of Rights: Publisher reserves all rights not specifically granted in the combination of (i) the license details provided by you and accepted in the course of this licensing transaction, (ii) these terms and conditions and (iii) CCC's Billing and Payment terms and conditions.

8. License Contingent Upon Payment: While you may exercise the rights licensed immediately upon issuance of the license at the end of the licensing process for the transaction, provided that you have disclosed complete and accurate details of your proposed use, no license is finally effective unless and until full payment is received from you (either by publisher or by CCC) as provided in CCC's Billing and Payment terms and conditions. If full payment is not received on a timely basis, then any license preliminarily granted shall be deemed automatically revoked and shall be void as if never granted. Further, in the event that you breach any of these terms and conditions or any of CCC's Billing and Payment terms and conditions, the license is automatically revoked and shall be void as if never granted. Use of materials as described in a revoked license, as well as any use of the materials beyond the scope of an unrevoked license, may constitute copyright infringement and publisher reserves the right to take any and all action to protect its copyright in the materials.

9. Warranties: Publisher makes no representations or warranties with respect to the licensed material.

10. Indemnity: You hereby indemnify and agree to hold harmless publisher and CCC, and their respective officers, directors, employees and agents, from and against any and all claims arising out of your use of the licensed material other than as specifically authorized pursuant to this license.

11. No Transfer of License: This license is personal to you and may not be sublicensed, assigned, or transferred by you to any other person without publisher's written permission.

12. No Amendment Except in Writing: This license may not be amended except in a writing signed by both parties (or, in the case of publisher, by CCC on publisher's behalf).

13. Objection to Contrary Terms: Publisher hereby objects to any terms contained in any purchase order, acknowledgment, check endorsement or other writing prepared by you, which terms are inconsistent with these terms and conditions or CCC's Billing and

Payment terms and conditions. These terms and conditions, together with CCC's Billing and Payment terms and conditions (which are incorporated herein), comprise the entire agreement between you and publisher (and CCC) concerning this licensing transaction. In the event of any conflict between your obligations established by these terms and conditions and those established by CCC's Billing and Payment terms and conditions, these terms and conditions shall control.

14. **Revocation:** Elsevier or Copyright Clearance Center may deny the permissions described in this License at their sole discretion, for any reason or no reason, with a full refund payable to you. Notice of such denial will be made using the contact information provided by you. Failure to receive such notice will not alter or invalidate the denial. In no event will Elsevier or Copyright Clearance Center be responsible or liable for any costs, expenses or damage incurred by you as a result of a denial of your permission request, other than a refund of the amount(s) paid by you to Elsevier and/or Copyright Clearance Center for denied permissions.

#### **LIMITED LICENSE**

The following terms and conditions apply only to specific license types:

15. **Translation:** This permission is granted for non-exclusive world **English** rights only unless your license was granted for translation rights. If you licensed translation rights you may only translate this content into the languages you requested. A professional translator must perform all translations and reproduce the content word for word preserving the integrity of the article. If this license is to re-use 1 or 2 figures then permission is granted for non-exclusive world rights in all languages.

16. **Website:** The following terms and conditions apply to electronic reserve and author websites:

**Electronic reserve:** If licensed material is to be posted to website, the web site is to be password-protected and made available only to bona fide students registered on a relevant course if:

This license was made in connection with a course,

This permission is granted for 1 year only. You may obtain a license for future website posting,

All content posted to the web site must maintain the copyright information line on the bottom of each image,

A hyper-text must be included to the Homepage of the journal from which you are licensing at <http://www.sciencedirect.com/science/journal/xxxxx> or the Elsevier homepage for books at <http://www.elsevier.com> , and

Central Storage: This license does not include permission for a scanned version of the material to be stored in a central repository such as that provided by Heron/XanEdu.

17. **Author website** for journals with the following additional clauses:

All content posted to the web site must maintain the copyright information line on the bottom of each image, and the permission granted is limited to the personal version of your paper. You are not allowed to download and post the published electronic version of your article (whether PDF or HTML, proof or final version), nor may you scan the printed edition to create an electronic version. A hyper-text must be included to the Homepage of the journal from which you are licensing at <http://www.sciencedirect.com/science/journal/xxxxx> . As part of our normal production process, you will receive an e-mail notice when your article appears on Elsevier's online



service ScienceDirect ([www.sciencedirect.com](http://www.sciencedirect.com)). That e-mail will include the article's Digital Object Identifier (DOI). This number provides the electronic link to the published article and should be included in the posting of your personal version. We ask that you wait until you receive this e-mail and have the DOI to do any posting.

Central Storage: This license does not include permission for a scanned version of the material to be stored in a central repository such as that provided by Heron/XanEdu.

18. **Author website** for books with the following additional clauses: Authors are permitted to place a brief summary of their work online only. A hyper-text must be included to the Elsevier homepage at <http://www.elsevier.com>. All content posted to the web site must maintain the copyright information line on the bottom of each image. You are not allowed to download and post the published electronic version of your chapter, nor may you scan the printed edition to create an electronic version.

Central Storage: This license does not include permission for a scanned version of the material to be stored in a central repository such as that provided by Heron/XanEdu.

19. **Website** (regular and for author): A hyper-text must be included to the Homepage of the journal from which you are licensing at <http://www.sciencedirect.com/science/journal/xxxxx>. or for books to the Elsevier homepage at <http://www.elsevier.com>

20. **Thesis/Dissertation**: If your license is for use in a thesis/dissertation your thesis may be submitted to your institution in either print or electronic form. Should your thesis be published commercially, please reapply for permission. These requirements include permission for the Library and Archives of Canada to supply single copies, on demand, of the complete thesis and include permission for UMI to supply single copies, on demand, of the complete thesis. Should your thesis be published commercially, please reapply for permission.

21. **Other Conditions**:

v1.6

**If you would like to pay for this license now, please remit this license along with your payment made payable to "COPYRIGHT CLEARANCE CENTER" otherwise you will be invoiced within 48 hours of the license date. Payment should be in the form of a check or money order referencing your account number and this invoice number RLNK500835080.**

**Once you receive your invoice for this order, you may pay your invoice by credit card. Please follow instructions provided at that time.**

**Make Payment To:  
Copyright Clearance Center  
Dept 001  
P.O. Box 843006  
Boston, MA 02284-3006**

**For suggestions or comments regarding this order, contact RightsLink Customer Support: [customercare@copyright.com](mailto:customercare@copyright.com) or +1-877-622-5543 (toll free in the US) or +1-978-646-2777.**

**Gratis licenses (referencing \$0 in the Total field) are free. Please retain this printable license for your reference. No payment is required.**

## A.6. Copyright Agreement Form for Chapter 7

### **Important Note:**

The Copyright Agreement Form for paper related to this chapter will have to be included in this dissertation after the paper is published by the journal.

It is noted that this dissertation cannot be distributed, used and/or published any time before the Copyright Agreement Form is obtained from the journal and subsequently included in this dissertation.

## A.7. Copyright Agreement Form for Chapter 8

### **Important Note:**

The Final Copyright Agreement Form for paper related to this chapter will have to be included in this dissertation after the paper is published by the journal.

It is noted that this dissertation cannot be distributed, used and/or published any time before the Copyright Agreement Form is obtained from the journal and subsequently included in this dissertation.

----- Forwarded message from ldion@copyright.com -----

Date: Wed, 30 Jan 2013 12:12:35 -0500

From: Lee Dion <ldion@copyright.com>

Subject: FW: Permission Request for PhD Thesis for J Mat Eng and Perfmnce-GRANTED-

To: Iranpour@dal.ca

Cc: Lee Dion <ldion@copyright.com>

Dear Mr. Iranpour,

Please see below-- Springer Publishing has granted permission for you to use the article in your thesis.

All the Best,

Lee

Ms. Lee Dion  
Customer Service Representative  
Copyright Clearance Center  
222 Rosewood Drive  
Danvers, MA 01923  
ldion@copyright.com  
+1.855.239.3415 Toll Free  
+1.978.646.2600 Main  
www.copyright.com

-----Original Message-----

From: Permissions Europe/NL [mailto:Permissions.Dordrecht@springer.com]

Sent: Wednesday, January 30, 2013 9:20 AM

To: Lee Dion

Subject: RE: NOT RIGHTSLINK ENABLED- Permission Request for PhD Thesis for J Mat Eng and Perfmnc

Dear Sir/Madam,

With reference to your request to reprint material in which Springer Science and Business Media control the copyright, our permission is granted free of charge and at the following conditions:

Springer material represents original material which does not carry references to other sources (if material in question refers with a credit to another source, authorization from that source is required as well); . requires full credit [Springer and the original publisher/journal title, volume, year of publication, page, chapter/article title, name(s) of author(s), figure number(s), original copyright notice] to the publication in which the material was originally published, by adding; with kind permission from Springer Science+Business Media B.V.;

. may not be altered in any manner. Abbreviations, additions, deletions and/or any other alterations shall be made only with prior written authorization of the author and/or Springer Science + Business Media.

. may not be republished in Electronic Open Access.

This permission

a. is non-exclusive.

b. includes use in an electronic form: provided it's password protected, or on intranet or university's repository, including UMI (according to the definition at the Sherpa website: <http://www.sherpa.ac.uk/romeo/>), or CD-Rom/E-book,

c. is subject to a courtesy information to the author (address is given with the article/chapter).

d. is personal to you and may not be sublicensed, assigned, or transferred by you to any other person without Springer's written permission.

e. is valid only when the conditions noted above are met.

Permission free of charge on this occasion does not prejudice any rights we might have to charge for reproduction of our copyrighted material in the future.

Best regards,

Kind regards,

Nel van der Werf (Ms)  
Rights and Permissions/Springer

Van Godewijkstraat 30 | P.O. Box 17  
3300 AA Dordrecht | The Netherlands  
tel +31 (0) 78 6576 298  
fax +31 (0)78 65 76-377

Nel.vanderwerf@springer.com  
www.springer.com

-----Original Message-----

From: Lee Dion [mailto:ldion@copyright.com]

Sent: Thursday, January 24, 2013 06:25 PM

To: Permissions Europe/NL

Cc: Iranpour@Dal.Ca; Lee Dion

Subject: NOT RIGHTSLINK ENABLED- Permission Request for PhD Thesis for J Mat Eng and Perfmnc

Importance: High

Dear Springer Permissions Group,

Mr. Mohammad Iranpour recently submitted his manuscript to the Journal of Materials Engineering and Performance - it has been conditionally accepted. The title is "Influence of the Peak Tensile Overload Cycles and Clipping Level on the Fatigue Crack Growth of Aluminum Alloy under Spectrum Loading".

He is urgently in need of permission to use the manuscript version of the paper in his thesis that he is submitting to the Faculty of Graduate Studies at Dalhousie University, Halifax, Nova Scotia, Canada this Friday, January 25 - the extended deadline.

Here is a link to the journal for reference  
<http://link.springer.com/journal/volumesAndIssues/11665>

As you can see it is not quite an Online First article, so RightsLink is unable to process his request. Could someone kindly contact Mr. Iranpour as soon as possible? This would be greatly appreciated. If I can help further, please contact me directly at [ldion@copyright.com](mailto:ldion@copyright.com). Thanks very much in advance!

Best Regards,  
Lee

Ms. Lee Dion  
Customer Service Representative  
Copyright Clearance Center

----- Forwarded message from Iranpour@Dal.Ca -----  
Date: Wed, 23 Jan 2013 20:46:09 -0400  
From: Mohammad Iranpour <[Iranpour@Dal.Ca](mailto:Iranpour@Dal.Ca)>  
Subject: Publication Permission Request for PhD Thesis for Mat Eng and Perfmnc  
To: [ania.levinson@springer.com](mailto:ania.levinson@springer.com), [david.seidenfeld@springer.com](mailto:david.seidenfeld@springer.com)  
Cc: [iranpour@dal.ca](mailto:iranpour@dal.ca)

Dear Madam/Sir,

Please see the attached Publication Permission Request.

Please note that this paper has been conditionally accepted for publication and is under final review by the journal.

I greatly appreciate your quick response.

Many thanks and regards,

Mohammad Iranpour

----- End forwarded message -----